DEVELOPMENT OF PROCESS PLANNING TOOLS FOR EDM OPERATIONS

Wouter VANDERAUWERA

Supervisor:
Prof. dr. ir. B. Lauwers

Members of the
Examination Committee:
Prof. dr. A. Bultheel (Chair)
Prof. dr. ir. J-P. Kruth
Prof. dr. ir. J. Duflou
Prof. dr. ir. D. Reynaerts
Prof. dr.-ing. F. Klocke (RWTH-Aachen)

Dissertation presented in partial fulfilment of the requirements for the degree of Doctor of Engineering Science: Mechanical Engineering.

January 2017

Preface

It's finally there! This thesis covers the work of six years of research in the domain of electrical discharge machining (EDM). My research project ends here, but I hope it can give more insights in the topics I have studied and perhaps can be the start for new researchers to get acquainted with the complex though fascinating domain of EDM.
I highly value my time at the university as it was a time in which I had the freedom to discover new things, investigate strange phenomena and transfer knowledge to a broad audience. After having left university, it wasn't easy to finalize the work I left behind. I am happy I carried through and proud to present the results in this book. During the entire period of my PhD I've received a lot of support, advice and help. With the following I want to express my appreciation towards all persons involved.

First of all, I'd like to thank my promotor Professor Bert Lauwers. He is the initiator of this specific journey as he introduced me to the domain of EDM in the scope of a master thesis. I highly value the advice he gave me whenever difficulties occurred, his considerate and pragmatic approach and the opportunities he gave me for joining European research projects.
Making this text was a big struggle and it wouldn't have become what it is without the critical comments and advice for improvement from the members of my jury. I want to thank Professor Jean-Pierre Kruth, Professor Joost Duflou, Professor Dominiek Reynaerts and Professor Fritz Klocke for their precious time spent on this. In addition, I'd like to thank Professor Adhemar Bultheel for coordinating my defense.

During my research, I have got the opportunity to collaborate with both academic and industrial partners within the scope of the KnowEDM and Integ-micro project. In particular, the cooperation with Georg Wälder and Roberto Perez was very valuable to me. I want to thank them for the interesting technical discussions and the pleasant cooperation. Also the cooperation with academics from abroad was a very enriching experience. In particular, I value the cooperation with Miguel Garzon and Andreas Klink from RWTH Aachen University.

During my stay at the university I've got the chance to work together with talented and great personalities. I want to thank the technical staff at the

department for their technical support. More specifically I'd like to thank Dirk and Viggo for their technical advice and support and Eddy for practical tips and tricks on machining and the pleasant conversations.
I want to thank my fellow researchers of the 'magnificent view' office Amar, Amir, Denys, Ehsan, Eleonora, Goncalo, Hans, Jan, Karel, Mieke, Olivier, Vitalii, Weidong and Yansong for the nice conversations and nice atmosphere in the office. In particular Karel for introducing me to the fascinating domain of EDM and his scientific approach, Hans for being a good friend and running mate and Denys for his dedicated concern on the progress of this text. During my research, I collaborated with Tom Craeghs for the organization of social events. His enthusiasm is still an inspiration for me.

All this wasn't possible without the opportunity my parents gave me to follow this path. I want to thank them for this and for their consistent encouragement. Moreover, I want to thank my sister, family and friends for their continuing interest in the course of this work and the much needed fun distractions.
Finally, this text wouldn't have gotten completed without the unconditional support, patience and love I've received from Ineke during the ups and downs of this journey. Thanks for standing by my side and I'll be happy to start our next chapter together.

January 2017

Abstract

Electrical discharge machining (EDM) is a non-conventional manufacturing technique commonly applied in the mould and precision industry due to its ability to machine materials irrespective of their hardness, its contactless nature resulting in a high level of accuracy, and its specific surface texture. Although its widespread use, additional functionality in the domain of process planning is needed to fully exploit its potential and to streamline the EDM process with other processes. Therefore, in this study two topics related to process planning were addressed: the development of time estimation models for sinking EDM operations and the development of process planning functionality for combined micro-EDM and micro-milling operations.

Accurate estimations of the machining time is still a big issue for EDM operations since multiple influencing parameters that strongly influence each other have been identified. In common EDM time estimation methods, the influence of the flushing conditions is often neglected resulting in large estimation errors (sometimes up to 200%). Therefore, this study investigated the effect of several flushing related parameters, mainly applicable to prismatic cavities. A distinction has been made between high energetic roughing and low energetic finishing operations due to a different set of influencing factors. Machining experiments identified machining depth, frontal surface area and current density as main influencing factors for roughing operations. A clear link with the process conditions (e.g. debris density as a result of flushing conditions) could be established through pulse analysis. For finishing operations this study has demonstrated that machining length, total electrodes surface area, starting roughness of the finishing operation and electrode geometry are the main influencing factors.

The proposed time estimation concept is based on machine and material dependent reference values determined by a predefined procedure. Machine and material independent corrections, based on linear regression modelling of the determined influencing parameters and trends, are applied on these values to compensate for deviating machining conditions. This independency offers a high level of flexibility when applying the concept to other EDM machines or to new material combinations. The concept has been integrated in a standalone software tool for semi-automated machining time calculation based on the interaction between the geometrical representation

of the EDM geometries and the EDM machine software, allowing the user to compare different machining strategies. With this concept a significant increase in estimation accuracy has been achieved compared to common estimation methods. For roughing operations, an average error of 27.5% with 55% of the validated cases within an error band of +/-30% has been obtained. For finishing operations, an average error of 18.4% with 85% of the validated cases within the same error band has been achieved.

The increasing demands put on micro-components in terms of increased functionality and reduced cost are pushing the manufacturing industry towards hybridization both on process and on machine level. From that perspective, the performance of micro-EDM and micro-milling operations integrated on a micro-EDM machining platform was assessed in this study.

Machining experiments on prismatic cavities showed that for micro-EDM the depth accuracy and flatness of a cavities bottom surface is largely influenced by the effectiveness of the tool wear compensation strategy, whereas for micro-milling the dimensional accuracy in the horizontal plane is strongly influenced by the properties of the integrated high speed spindle. In addition, the higher applied feedrates for micro-milling can lead to inaccuracies due to the inability of the micro-EDM machine controller to cope with fast changes in tool direction. Furthermore, this study has shown that a depth dependency for the surface roughness exists for both processes. This study also showed that micro-milling outperforms micro-EDM in terms of machining time, although the difference between both processes becomes smaller as the cavity size decreases. Energy measurements have shown that the instantaneous power required for micro-milling is higher than for micro-EDM, but due to significant lower machining times the specific energy is lower for micro-milling. Comparison of the total machining cost between both processes showed that micro-milling is more cost effective compared to micro-EDM. Similar to the specific energy, the specific cost increases as the cavity dimensions decrease. From these findings a preferred combined machining strategy for this machining platform has been proposed, namely bulk material removal by micro-milling and finishing by micro-EDM. Based on these results a semi-automatic process planning tool (CAPP) has been developed. This CAPP tool lists for every machining feature the most suitable processing sequence and determines the optimal operation sequence by minimizing the total machining time.

Samenvatting

Vonkerosie is een niet-conventionele bewerkingstechniek die vaak toegepast wordt voor de vervaardiging van matrijzen en mechanische componenten met hoge precisie. De belangrijkste redenen hiervoor zijn de mogelijkheid om harde materialen te bewerken, de contactloze bewerking die hoge nauwkeurigheden toelaat en de specifieke oppervlaktetextuur na bewerking. Ondanks het wijd verspreide gebruik van deze techniek is bijkomende functionaliteit vereist op het vlak van procesplanning om het potentieel van dit proces volop te benutten en het proces te stroomlijnen met andere processen. Daarom werden in dit onderzoek twee onderwerpen gerelateerd aan procesplanning onderzocht: ontwikkeling van tijdsschattingsmodellen voor zinkvonkoperaties en ontwikkeling van functionaliteit voor procesplanning van gecombineerde microvonk- en microfreesoperaties.

Nauwkeurige schattingen van de bewerkingstijd vormen nog steeds een probleem door de veelheid aan complexe interagerende invloedsfactoren. Daarnaast wordt in bestaande tijdsschattingsmethoden de invloed van de spoelcondities vaak niet beschouwd, wat resulteert in grote schattingsfouten (zelfs tot 200%). Daarom werd in dit onderzoek de invloed van spoelingsgerelateerde factoren onderzocht voor de bewerking van prismatische caviteiten. Door de invloed van verschillende factoren diende een onderscheid gemaakt te worden tussen hoog energetische ruwoperaties en laag energetische finisseeroperaties. Bewerkingsexperimenten toonden aan dat de bewerkingsdiepte, de frontale elektrodeoppervlakte en de stroomintensiteit of belasting de voornaamste invloedsfactoren zijn voor de bewerkingstijd van ruwoperaties. Hierbij werd een duidelijk verband met de procescondities aangetoond d.m.v. pulsanalyses (bv. verband tussen spaandichtheid en de spoelcondities). Daarnaast werd aangetoond dat de bewerkingsdiepte, de totale elektrode oppervlakte, de startruwheid van de finisseeroperatie en de elektrodegeometrie de voornaamste invloedsfactoren op de finisseertijd zijn.
Het voorgestelde concept voor tijdsschattingen is gebaseerd op machine- en materiaalafhankelijke referentiewaarden die bepaald worden onder vooraf gedefinieerde condities. Afwijkende bewerkingscondities worden in rekening gebracht d.m.v. machine- en materiaalonafhankelijke correcties, dewelke gebaseerd zijn op een lineaire regressie modellering van de

bepaalde invloedsfactoren en hun overeenkomstige trends. Deze machine- en materiaalonafhankelijkheid maakt het concept flexibel en toepasbaar voor andere vonkmachines en materiaalcombinaties. Het ontwikkelde concept werd geïmplementeerd in een software toepassing dat een semi-automatische schatting van de bewerkingstijd mogelijk maakt door interactie tussen de geometrische voorstelling van de te bewerkingen regio's en de software van de vonkerosiemachine. Deze implementatie maakt het mogelijk om verschillende bewerkingsstrategieën te vergelijken. De ontwikkeling van het voorgestelde tijdsschattingsconcept heeft geleid tot een significante verbetering van de schattingsnauwkeurigheid t.o.v. bestaande tijdsschattingsmethoden. Zo toonde een validatie met prismatische caviteiten aan dat voor ruwoperaties gemiddeld een schattingsfout van 27.5% werd bekomen, waarbij in 55% van de beschouwde gevallen de schattingsfout binnen een foutenmarge van +/-30% lag. Voor finisseeroperaties werd er voor de beschouwde gevallen een gemiddelde afwijking van 18.4% bekomen, waarbij in 85% van de gevallen de schattingsfout binnen een foutenmarge van +/-30% lag.

De steeds strenger worden vereisten op het vlak van functionaliteit, kost en doorlooptijd duwen de vervaardiging van microcomponenten richting hybridisatie, zowel op proces- als machineniveau. Vanuit dit oogpunt werd in dit onderzoek de performantie van microvonk- en microfreesoperaties, geïntegreerd op een microvonkbewerkingsplatform, bestudeerd.

Bewerkingsexperimenten op prismatische caviteiten toonden aan dat voor microvonkoperaties de dieptenauwkeurigheid en de vlakheid van het bodemoppervlak sterk beïnvloed worden door de effectiviteit van de strategie voor compensatie van de elektrodeslijtage. Voor microfreesoperaties daarentegen wordt de dimensionele nauwkeurigheid in het horizontale vlak sterk beïnvloed door de eigenschappen van de geïntegreerde hogesnelheidsspil. Daarnaast kunnen de hoge vereiste voedingssnelheiden tijdens het microfrezen resulteren in onnauwkeurigheden doordat de aansturing van de microvonkmachine niet in staat is snelle veranderingen in bewerkingsrichting te verwerken. Verder toonde deze studie aan dat voor beide processen de ruwheid van de zijwanden afhankelijk is van de bewerkingsdiepte. Dit onderzoek toonde ook aan dat de bewerkingstijd van microfreesoperaties significant lager is in vergelijking met gelijkaardige microvonkoperaties. Toch wordt het verschil tussen beide processen kleiner naarmate de afmetingen van de caviteit

kleiner worden. Energiemetingen toonden aan dat ondanks een hoger ogenblikkelijk vermogen, het specifieke energieverbruik tijdens microfrezen lager is vergeleken met microvonken door de kortere bewerkingstijd. Een vergelijking van de bewerkingskosten tussen beide processen toonde aan dat microfrezen kostenefficiënter is in vergelijking met het microvonken. Analoog aan de specifieke energie, stijgt de specifieke kost naarmate de afmetingen van de caviteit afnemen.
Gebaseerd op voorgaande bevindingen werd een gecombineerde bewerkingsstrategie geformuleerd, nl. verwijdering van de bulk van het volume d.m.v. microfrezen gevolgd door een finisseeroperatie d.m.v. microvonken. Op basis van deze bevindingen werd een software toepassing voor procesplanning ontwikkeld waarbij op semi-automatische manier voor elke te bewerken geometrie de meest geschikte bewerkingsvolgorde wordt bepaald die resulteert in een minimale bewerkingstijd.

List of symbols

Symbol	Unit	Description
A	mm^2	Frontal surface area
A_{tot}	mm^2	Total surface area
a_p	mm	Cutting depth
a_e	mm	Cutting width
B	A/cm^2	Current density
c	$J/(kg*°C)$	Specific heat
$C_{efficiency}$		Efficiency correction factor
$C_{finishing}$		Correction on $time_{ref,j}$ for finishing operations
$C_{flushing}$		Flushing correction factor
C_m	$J^2/(m^4*s)$	Erosion resistance index
C_R		Correction on $MRR_{ref,i}$ for roughing operations
$C_{roughing}$		Correction on $time_{ref,i}$ for roughing operations
D	mm	Depth
Dc	mm	Cutting diameter
i_e	A	Discharge current
L	mm	Length
L_m	µm	Machining length
$MRR_{ref,i}$	mm^3/min	Reference value in terms of removal rate for regime i
R	mm	Roughing tool radius
r	mm	Finishing tool radius
t_d	µs	Discharge delay time
t_e	µs	Discharge duration
$time_{ref,i}$	min	Reference time determined during calibration for regime i
T_m	°C	Melting point
t_0	µs	Pulse interval time
u_e	V	Discharge voltage
$\hat{u}_i$	V	Open gap voltage
v_f	mm/s	Feedrate
Vol	mm^3	Volume
W	mm	Width
W_e	J	Discharge energy
w_i		Weighting factor for performance criterion I
λ	$W/(m*°C)$	Thermal conductivity
ρ	kg/m^3	Specific mass

Abbreviations

AECDG	Abrasive Electrochemical Discharge Grinding
AEDG	Abrasive Electrical Discharge Grinding
API	Application Programming Interface
AWEDM	Abrasion assisted Wire EDM
CAD	Computer Aided Design
CAM	Computer Aided Manufacturing
CAPP	Computer Aided Process Planning
CIM	Computer Integrated Manufacturing
ECAM	Electrochemical Arc Machining
ECDM	Electrochemical Discharge Machining
ECM	Electrochemical Machining
ECSM	Electrochemical Spark Machining
EDG	Electrical Discharge Grinding
EDM	Electrical Discharge Machining
MRR	Material Removal Rate
OEE	Overall Equipment Effectiveness
PCBN	Polycristalline cubic boron nitride
PCD	Polycristalline diamond
SACE	Spark Assisted Chemical Engraving
STL	Standard Triangle Language
WEDG	Wire Electrical Discharge Grinding
XMJ	Extensible Markup Language Journal
XTL	Extended Triangle Language

Table of contents

Chapter 1 Introduction

In the last 100 years, technology has progressed at an unseen rate, more so than any other century before. It seems that today's latest gadget becomes tomorrow's antique. However, throughout history mankind has continuously strived to improve itself. Whether it is the invention of the wheel, the compass or the printing press, all these inventions opened up new opportunities and formed the basis for further developments. However, it was until the beginning of the 19th century with the first industrial revolution, marked by developments in steam, textiles and iron, that massive steps forward were made which changed the whole society. Later on in the 19th century, the second industrial revolution, characterized by steel, electrics, petroleum products and automobiles, marked the beginning of mass production. The rise of the internet and information technology in the second half of the 20th century marked the beginning of the third industrial revolution which is often referred to as digital revolution as it heavily relies on electronics and promotes automation. Currently, a fourth industrial revolution is rising, often referred to as the internet of things. People, machines, resources, production lines, logistics networks, consumption habits, recycling flows and every other aspect of economic and social life will be connected in order to continuously provide information or Big Data to different stake holders. The incentives for these revolutions have changed and need to be placed in their respective time spirit, but a constant incentive has been an increase in productivity and efficiency. This has been mainly reflected in the broad world of the manufacturing industry. Ancient mechanical processing techniques have been further developed, mechanized, automated and controlled. At the same time other inventions or newly discovered phenomena have been applied in the manufacturing industry, giving rise to new processing techniques. One of these techniques, often referred to as non-conventional techniques, is the electrical discharge machining (EDM) process. This manufacturing technique is based on the repetitive erosive impact of controllable discharges removing a substantial amount of material from the workpiece. Due to its contactless nature, its ability to machine materials irrespective of their hardness and its specific surface texture, it has become a common manufacturing process in sectors like the mould and tool industry, precision industry, consumer industry and the medical sector.

The need for increased productivity and the ever growing technological demands have challenged the process towards its limits and have nurtured its evolution towards a fully mature manufacturing process. However, to keep up with new challenges further process optimization and extension of the application range is still needed. As the EDM process is rarely used on its own, it has to be embedded in an efficient and productive chain of processes. Indispensable in an efficient manufacturing environment is the use of a reliable and accurate process planning system as it decides how to make optimal use of the available resources and has a direct impact on the bidding process, delivery performance and financial gain or loss. Especially in the die and mould sector where small series of parts are produced, an efficient use of all needed manufacturing processes is essential. Despite its widespread use, there are still some issues that need to be tackled prior to achieving a reliable and robust process planning. Therefore, this study will elaborate two process planning tools for two distinct EDM applications. The first part of this study describes the development of a process planning tool that allows accurate time estimations for sinking EDM operations. In the second part of this study a process planning tool will be elaborated for making optimal use of a hybrid micro-EDM machining platform.

The following paragraphs will give a short overview of the content of this study.

Chapter 2 provides a general overview of the state of the art of the EDM process and process planning. The evolution of the EDM process from first observation to a fully mature manufacturing technique is described. Further, the principles of the EDM process and the most common EDM techniques with their characteristics are explained. As process planning is a key element in a manufacturing environment, its use and the different types are described. Finally, a brief overview of the state of the art about process planning for EDM operations is given. Within this perspective the general research objectives of this study are stated.

To clearly make a distinction between the two research questions, this study is divided in two parts describing their specific background, detailed objectives, plan of approach and test results.

In **Part 1** of this study the topic of time estimations for sinking EDM operations will be discussed.

Chapter 3 gives an overview of different techniques for estimating the machining time for EDM operations. In the past decades several studies have been conducted to tackle the problem of an accurate EDM time estimation, either from a theoretical, empirical or practical perspective. In general it can be stated that these methods lack generality and do not consider the whole set of influencing factors. Often, the important effect of the flushing conditions is neglected hence resulting in poor time estimation accuracy. The machining speed in EDM operations is largely determined by the density of generated debris in the sparking gap. Especially in sinking EDM operations where the flushing conditions are complex, a large impact on the debris density hence the machining speed can be noticed. In order to understand the effect of the flushing conditions, different flushing techniques used in sinking EDM are described with their effect on the machining performance. From this it is stated that a model for sinking EDM time estimation will be elaborated that considers the effect of the flushing conditions.

Chapter 4 defines the concept of sinking EDM time estimation based on reference values, in terms of material removal rate or EDM time, which are determined under specific conditions. These values need to be corrected with correction factors for deviating machining conditions compared to the reference case. An EDM operation usually consists of a volume removing roughing operation followed by a surface finishing operation, each with its own specific conditions and parameters. Hence separate models for both types of operation need to be developed. For each model, the most important factors influencing the machining time for prismatic machining features will be discussed and quantified. The developed models will be validated and compared with current EDM time estimation methods.

Chapter 5 describes the implementation of the developed models in a standalone software tool. As the EDM machining strategy can be set manually by the user or defined semi-automatically by the machine software, interaction or communication with the EDM machine software is necessary. Also geometrical information should be available as it largely represents the influence of the flushing conditions. The developed tool will provide the user with reliable information for the establishment of process plans in which sinking EDM operations are involved.

In **Part 2** of this study the development of a process planning tool for a hybrid EDM machining platform will be elaborated.

Chapter 6 describes the current trend towards hybridization of processes and machines for the manufacturing of micro-components. The ever increasing demands regarding functionality, shorter time-to-market and cost cutting operations push to the limits of existing micro-manufacturing processes. As an answer to this there is a trend towards the development of processes combining different removal mechanisms and machining platforms combining different processes. In the past decades a lot of research has been conducted to combine the strengths of the EDM process with other material removal processes. An overview of the state of the art in this field is given. The combination of a mechanical cutting process with the EDM process shows to be both complementary as well as synergetic. Therefore, the combination of micro-milling and micro-EDM onto one machining platform is studied. In order to fully deploy the capabilities of both processes onto one platform, the development of a process planning system is essential. The elaboration of such a system will be described in the following chapters.

Chapter 7 firstly describes the capabilities of micro-milling and micro-EDM for the machining of prismatic machining features. This evaluation is performed empirically for different performance criteria: dimensional and geometrical accuracy, cost and time effectiveness, energy consumption and surface integrity. This knowledge is essential for the development of a process planning system as it allows the user to select that process or combination of processes that will best suit the user needs.

Chapter 8 describes the elaboration of a Computer Aided Process Planning (CAPP) tool based on the results of the capability study. Starting from the CAD model of the micro-component, the CAPP tool defines the set of processes for each machining feature which best suit the user needs and defines the machining sequence for the entire set of machining features.

Chapter 9 closes this study with some conclusions and highlights some of the research topics for further investigation.

Chapter 2 Introduction to Electrical discharge machining, process planning and objectives

This chapter provides the general perspective from which this study has been performed in order to situate the research topics. First the evolution, state of the art, the EDM process itself, its variants and the machines used in this research are described. Secondly, the application and methods of process planning are described. In a next section, this is combined in an overview of the state of the art of process planning for EDM operations. Based on this, the general research objectives of this study are highlighted. A more detailed discussion of both research topics with a definition of the specific objectives can be found in the separate parts of this study.

2.1. Electrical Discharge Machining

2.1.1. EDM: From curiosity to an important manufacturing technique

Although the first intentional use of electrical discharges as a way to remove material dates back to the 1940s, the first observation and use of electrical discharges were made in the 17th century. One of the first reports in literature was made in 1694 by Robert Boyle who observed static discharges due to a rubbing action on diamond [1]. Benjamin Franklin discovered in 1751 that the same phenomenon leads to material removal. About the same time Musschenbroek developed the so-called 'Leyden jar' [2][3], a device that can be used to produce the same kind of discharges. The 'Leyden jar', being the first type of capacitor, consisted of a glass bottle coated at the inside and outside with a metal (usually lead) and filled with water (see Fig. 2.1). The inside plating of the bottle was connected to a sphere to allow it to be charged. On the other hand, the outside plating was connected to the ground. By connecting and disconnecting the sphere with an electrical supply, discharges could be created by connecting and disconnecting the wires. The Leyden jar became the standard device to store electrical energy and was used to conduct many experiments at that time. In 1766 Joseph Priestley discovered the erosive effect of discharges made by Leyden jars and observed the occurrence of concentric circles due to the discharges on metallic surfaces connected to it, known as Priestley's rings (see Fig. 2.2).

In 1881 Meritens was the first to use electrical discharges for practical applications. He used the heat of the generated arcs to join lead plates, a technique now known as arc welding [4]. Another application was developed by Bredig in 1897 and consisted of making colloidal metal solutions by arcing between two metal electrodes in a non-conductive fluid [5].
During the 1930s V.E. Matulaitis and H.V. Harding of Elox US developed a process to remove broken taps or drills from valuable workpiece materials like cemented carbides and high speed steel [6]. This application, carried out on so called 'disintegrators', was based on erosion by intermittent arc discharges in air, initiated by mechanical contact and interrupted by retraction of the electrode. Although very popular at that time, the small degree of controllability of intermittent arc machining led to a poor surface quality and an inefficient use of the applied energy [7].
In 1943, the Russian researchers Boris and Natalya Lazarenko discovered that electrical discharges can be more efficient than intermittent arcs when being produced by RC circuits [1].

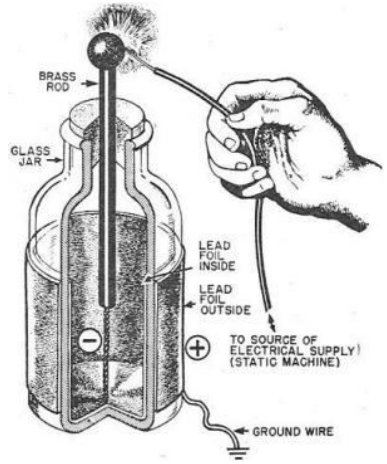

Fig. 2.1: Leyden jar[2].

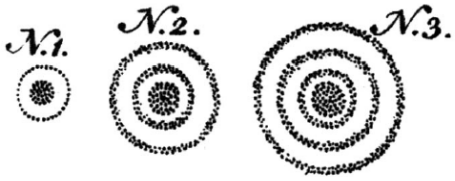

Fig. 2.2: Priestley's rings [2].

During their study on the investigation of wear on tungsten electrical power contacts, they inverted the wear effect to erode material in a controllable and efficient way [8]. For this they developed a resistor-capacitance power supply which still forms the basis of current relaxation generators. This invention meant a great breakthrough in the field of manufacturing and marks the starting point of what is now commonly known as Electrical

Fig. 2.3: First commercial EDM machine: Charmilles' Eleroda D1 [51].

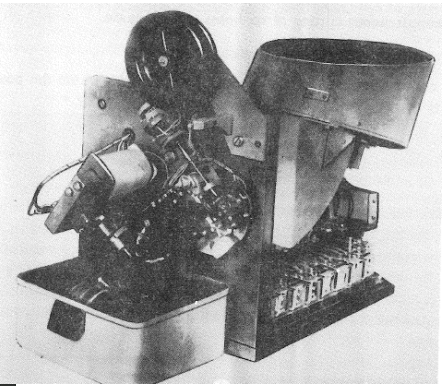

Fig. 2.4: Automated micro-EDM machine for drilling holes in injection nozzles [9].

Discharge Machining (EDM). The development of the EDM process came at the right time because at that time Russia was looking for alternative machining processes for the machining of hard metal alloys due to a shortage of diamond [7]. In the years following the invention a lot of fundamental research on EDM was performed, trying to improve the output and lowering the tool wear which led to the introduction of the first commercial EDM sinking machine in 1954: Charmilles' Eleroda D1 (see Fig. 2.3). At the same time the first demonstrations of micro-EDM were done in Russia for the production of injection nozzles for diesel engines [9]. Micro-EDM replaced the highly unreliable micro-drilling for the machining of 0.15 mm holes. Fig. 2.4 shows an example of an automatic micro-EDM drilling machine specially made for the machining of injection nozzles.

Despite all the efforts taken, many researchers in the 1950s were confronted with the limits of the relaxation type generators. The relative long charging times and short discharging times led to low removal rates and high tool wear. As an example, removal rates that could be obtained varied from 0.3 to 4.16 mm^3/min [7]. This forced the development of new types of generators. In the 1960s controlled pulse generators were introduced which are based on switching elements applying energy delivered by a DC source to the machining gap. Agie and Charmilles were the first machine tool builders to equip their EDM machines with static pulse generators [10]. This type of generator leads to higher removal rates, higher precision and lower

tool wear. However, when a good surface finish is desired relaxation generators were, and still are favorable.

A large improvement in efficiency was made with the introduction of microprocessors which enabled the development of numerical controls. In 1969 Agie introduced the first numerical controlled EDM machine (AgieCut DEM 15) and later in 1972 Seibu introduced the first CNC EDM machine. The introduction of numerical control gave a boost to the application of wire-EDM. It is also from this period that a shift was made from basic towards more applied research. Until then an important research topic was the modeling of the EDM process. Although a single discharge could be modeled very well, the modeling of multiple discharges did not yield satisfactory results due to the stochastic nature of the process [11]. Therefore the focus shifted towards specific applications and the solving of input-output problems with techniques like expert systems, fuzzy controllers and neural networks [6].

During the 1980s and 1990s EDM generators continued to be refined by controlling and monitoring the sparking gap and improved electrode movements, like planetary EDM, were introduced. This resulted in a more stable, predictable and safe process [12].

Today, industry is pushing research and EDM tool manufacturers towards a higher degree of flexibility and automation. Examples of developments that resulted from this are the large variety of electrode movements and measuring cycles, electrode and workpiece magazines, automatic wire threading systems, 3D CAD/CAM software and automated manufacturing cells (see Fig. 2.5). This increase in flexibility has been accompanied by maintaining or even surpassing the former level of performance of the process. Nowadays removal rates for sinking EDM operations are typically between 2 to 400 mm^3/min and can even go up to 1000 mm^3/min or more in roughing operations [3]. Surface roughness down to 0.09 µm Ra and holes with a diameter down to 5 µm can be machined [13].

2.1.2. The EDM process

In this paragraph the fundamentals of the EDM process and aspects related to dielectric, electrode and workpiece material are described.

Fig. 2.5: Automated cell with 2 EDM machines, tool and workpiece magazine, robot and CMM [14].

EDM principle

Electrical discharge machining is a contactless machining process based on the erosive impact of electrical discharges. Due to the electro-thermal nature of the process a large variety of conductive materials can be machined independent of their hardness and toughness.

Material removal takes place by applying a voltage ($\hat{u}_i$ in Fig. 2.6) between the tool electrode and the workpiece immersed in a dielectric fluid. As a result an electrical field arises with the highest electrical strength at locations where the distance between both electrodes is the smallest or at locations where the concentration of conductive particles is the highest. At the place of the highest electrical strength, 'primary' electrons are emitted from the cathode and collide with the neutral atoms of the dielectric fluid. Consequently these atoms split up into so called 'secondary' electrons and ions, which on their turn free electrons from the cathode. After a period of time t_d this avalanche-effect will lead to a breakdown of the dielectric accompanied by an increase of the current i_e (see Fig. 2.6). This marks the beginning of the discharge. Due to temperatures up to 20.000 °C [7] the dielectric will locally evaporate and a gas bubble and plasma channel is formed. At the contact areas of the gas bubble with both electrodes material is locally heated up by the bombardment of electrons at the anode and ions at the cathode. More material will be heated up at the cathode due to the higher mass and hence higher kinetic energy of the colliding ions. After a

certain period of time t_e the pulse is ended and is followed by an implosion of the gas bubble which results in the eruption of superheated molten material from both cathode as well as anode into the dielectric leaving a crater behind on both electrodes. The molten and evaporated material solidifies into micro-sized particles, called debris. Before applying the next pulse a certain period of time t_0 is left to ensure deionization of the dielectric. The complete cycle is repeated up to thousand times per second, or even up to a million times per second in the case of wire-EDM, and results in discharges happening randomly along the entire machining area.
The consecutive rapid heating and cooling strongly impacts the top surface of the workpiece. Only a portion of the molten material is expelled from the workpiece surface, leaving a layer of resolidified material behind (see Fig. 2.7). This layer, often referred to as recast layer or 'white layer', is characterized by micro-cracks making it very brittle. The thickness of the recast layer is dependent on the discharge energy, given by Eq. 2.1, and the material. Mostly, by choosing a proper EDM strategy the recast layer should be minimized. Nonetheless, an additional EDM finishing step with lower energy levels, mechanical finishing action or electrochemical operation may be required to remove this undesired layer. Beneath the recast layer a zone with a different metallographic structure then the core material occurs, called the heat affected zone (see Fig. 2.7). Characteristic for this zone is a difference in hardness, determined by the material and type of dielectric, and the existence of residual stresses which can cause deformations of the workpiece.

$$W_e = \int_0^{t_e} u_e(t) \cdot i_e(t) dt \qquad \text{(Eq. 2.1)}$$

With: W_e discharge energy [J];
u_e discharge voltage [V];
i_e discharge current [A];
t_e discharge duration [s].

Not only does the discharge energy affect the properties and structure of the top layer, it also affects the surface roughness. In general it can be stated that the higher the discharge energy, the larger the crater sizes resulting in a higher roughness. However, in case of ceramics there exists an optimal value of the discharge energy in terms of surface roughness [15], [16].

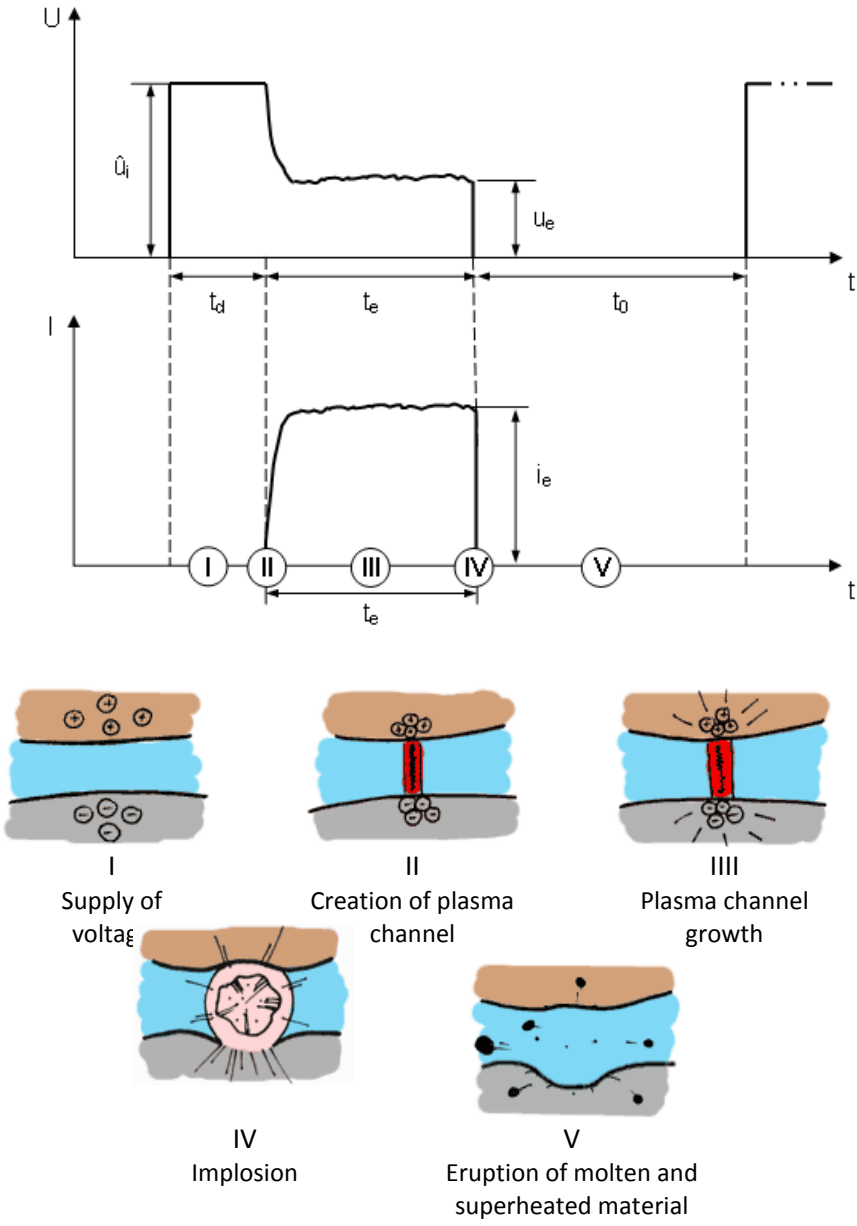

Fig. 2.6: Phases during one EDM pulse [14].

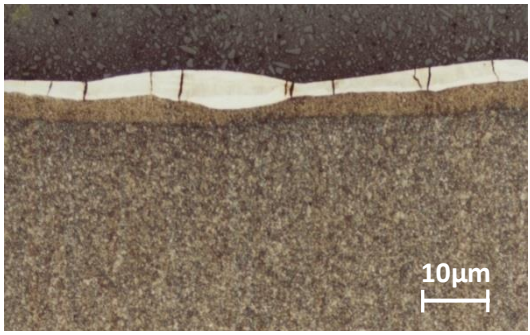

Recast layer
Heat affected zone

Core material

Fig. 2.7: Structure of EDMed surface [1].

Dielectric

Indispensable for the generation of sparks is the occurrence of a dielectric between both electrodes. In most EDM applications the workpiece is fully submerged into a dielectric fluid. In some applications (e.g. micro-EDM) the dielectric is locally supplied to the machining area. The dielectric has the following main functions:

- Concentration of energy. Due to the increase of temperature the gas bubble will try to expand, hence increasing the contact area with the workpiece surface. In order to efficiently remove material by concentrating the applied energy, the gas bubble expansion is limited by the dielectric fluid.

- Cooling of electrodes. More than 90% of the generated heat is absorbed by both electrodes [17]. To avoid excessive heating a proper cooling is needed.

- Removal of debris. Molten material solidifies as small particles into the dielectric. A good flushing action by the dielectric is necessary to avoid an accumulation of debris in the working gap that would lead to inefficient machining and would eventually result in arcing.

- Surface enhancement. Either by using powder suspended dielectrics or by using easily wearable electrodes the surface properties, like wear resistance, of the workpiece can be enhanced [18].

To achieve this functionality important fluid properties are the fluids viscosity, remaining electrical conductivity, dielectric constant and flash point. Therefore common EDM dielectrics are de-ionized water and hydrocarbon oils. In some cases gasses can be used [19] but these lack practical applications. However, the planarization and micro patterning of field emission displays by EDM in air showed to have potential [20].

Electrode material

In principle every conductive material can be used as a tool material. However the intrinsic tool wear, as a consequence of the electro-thermal nature of the process, favors especially materials with good thermal properties. Reduction of tool wear is a major concern in EDM applications because it is essential for achieving high-accuracy and cost-effective parts. The suitability of a material to be used as electrode material can be expressed by the erosion resistance index C_m [21] which is a function of thermal properties (Eq. 2.2):

$$C_m = \lambda \cdot \rho \cdot c \cdot T_m^{\,2} \qquad \text{(Eq. 2.2)}$$

With: C_m erosion resistance index [$J^2/(m^4 \cdot s)$];
λ thermal conductivity [$W/(m \cdot °C)$];
ρ specific mass [kg/m^3];
c specific heat [$J/(kg \cdot °C)$];
T_m melting point [°C].

Table 2.1 lists common electrode materials with their thermal properties (mean values) and steel as a reference material. Compared to steel all electrode materials shown in this table have either a higher thermal conductivity or a higher melting point making them suitable tool materials. This is confirmed by the erosion resistance index. Nowadays even metal-ceramic materials are tested as electrode material, e.g. ZrB_2-Cu showing lower tool wear and higher removal rate [22].

Other material properties that should be taken into account when selecting a proper electrode material are the machinability/formability, cost, smallest reachable roughness/detail and the thermal expansion coefficient.

Table 2.1: Common electrode materials and their thermal properties.

Material	Erosion resistance index C_m (10^{13})	Heat conductivity λ [W/m °C]	Specific mass ρ [kg/m³]	Specific heat c [J/kg°C]	Melting point T_m [°C]
Copper	151,5	359	8900	403	1090
Graphite (coarse grain)	150	90	1720	753 (*)	3600
Graphite (fine grain)	200	100	1880	753 (*)	3600
Graphite copper			2970		
Tungsten	521,6	146	19300	163	3370
Tungsten copper			14500		3350
Brass	30,4	109	8500	388	920
Solid carbide	151	67	14300	209	2750
Steel	33,7	45	7800	490	1400

(*) temperature dependent

Workpiece material

Whereas in conventional machining processes the machinability strongly depends on the mechanical properties of the workpiece material (e.g. hardness and toughness), the electro-erodability is not restricted by these properties. The only restriction for a material to be machined by EDM is a minimal electrical conductivity. Although there is no clear limit, it can be stated that a conductivity of at least 0.01 S/cm is required [23]. This implies that all kinds of metals irrespective of their hardness can be machined, giving EDM a big advantage compared to conventional processes.

In the early days of the development of the EDM process the main application domain was the machining of hardened steels. Due to higher demands from industry the application domain and research focus shifted to high-performance materials like hard metals and ceramics. Especially ceramics are much in favor nowadays due to their excellent mechanical, thermal and chemical properties. Although the electrical conductivity is often too low to be EDMed (like in case of Si_3N_4, ZrO_2 and Al_2O_3), efficient machining of ceramics by EDM is possible by the addition of a secondary conductive phase (e.g. TiN, TiCN, TiB_2) [24]. In some cases these additions can even further increase the hardness, strength and mechanical wear resistance of the ceramic composite [16].

The type and composition of the workpiece material has a strong influence on the process performance in terms of removal rate and surface finish. This

can be explained by the fact that different removal mechanisms occur dependent on the material type. When machining steel, material is mainly removed by the typical melting and evaporation mechanism mostly leading to a recast layer with micro-cracks and spherical debris (Fig.2.8.a.). On the contrary, for some ceramic materials (mostly those with high thermal expansion low thermal conductivity and low Young's modulus) the dominant removal mechanism is spalling, a process initiated by thermoshocks. In this case large particles or 'flakes' break out of the material due to thermal stresses and crack formation (Fig. 2.8.b.) which result in a relatively rough surface and irregular shaped debris [24]. For some ceramics the dominant removal mechanism is a chemical reaction or decomposition. For instance, the machining of Si_3N_4-TiN in de-ionized water is accompanied by an oxidation reaction resulting in a foamy and porous surface layer (Fig. 2.8.c.) [16]. In general it can be stated that different removal mechanisms occur simultaneously but there is always one which is more dominant.

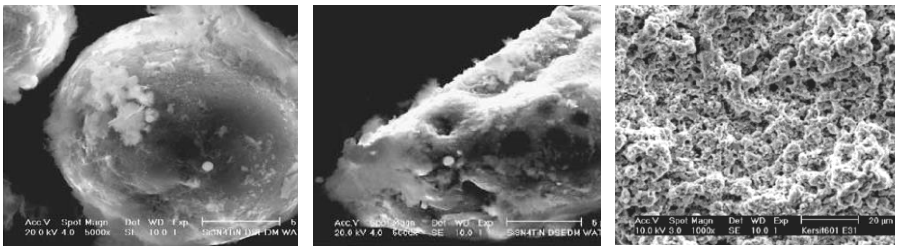

a. b. c.

Fig. 2.8: EDM removal mechanisms: (a) melting and evaporation [20]; (b) spalling [20]; (c) oxidation [21].

2.1.3. EDM techniques

EDM is a group of machining techniques which are all based on the electro-thermal principle discussed in the previous section but mainly differ in electrode and/or workpiece movement. The distinct machine setups result in a diverse range of applications. The following paragraphs give an overview of common EDM techniques with their current performances. Special attention is given to sinking and milling EDM, which formed the main focus of this research.

Sinking EDM

Among all EDM techniques, sinking EDM was the first technique to be commercialized in the mid 1950s. In this setup a 3D-preshaped tool electrode is moved along a specific direction into the workpiece (see Fig. 2.9). Mostly this is a downward movement but in some cases a lateral movement or a combination of both is applied. The result of this action is a cavity which has the negative shape of the tool electrode corrected by the working gap. The entire electro-erosion action occurs in a tank where the workpiece is fully submerged in a dielectric fluid.
Sinking EDM has especially applications in the die and mould making industry due to its ability to machine hard materials, complex 3D-shapes and the typical uniform non-shiny surface texture. Its contactless nature and the high attainable accuracy make it also a favorable technique for use in the precision sector.

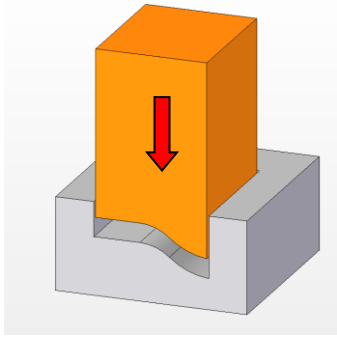

Fig. 2.9: Principle of sinking EDM.

When machining a fully enclosed cavity, the sinking EDM process cannot guarantee a uniform roughness at the side and bottom faces of the cavity due to its unidirectional movement. Therefore a variant of the sinking EDM process, called planetary EDM, has been developed in the 1970s in which the electrode is given an eccentric movement besides the downward movement (Fig. 2.10). Depending on the geometry of the final cavity the type of movement can be conical, spherical, pyramidal, star-like, etc. Besides a uniform roughness, the additional electrode movement results in a higher accuracy, a more uniform and reduced wear pattern, a reduction in the number of electrodes and an improvement of the flushing action. In practice, a sinking EDM operation consists of a sinking movement, commonly referred

to as the roughing operation, followed by a planetary movement for finishing the cavities' surfaces.

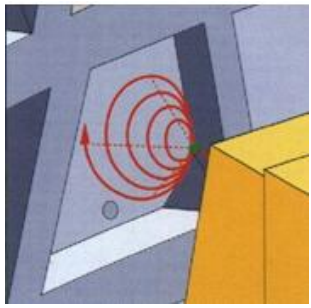

Fig. 2.10: Principle of planetary EDM.

The irregular shape of sinking EDM electrodes necessitates a good flushing of the sparking gap. For this, hydrocarbon oils are widely used, but also distilled water can be beneficial in some cases [25]. When smooth surface finishes are required, a hydrocarbon oil mixed with fine electrically conductive abrasive powder particles is often used resulting in a surface roughness down to 0.09 µm Ra [26]. Even sinking EDM in air can be performed. Kunieda et al. [19] found that die sinking EDM in dry condition can reduce the tool wear ratio significantly and can result in a thinner white layer and lower residual stresses.

A sinking EDM operation typically consists of several machining steps (e.g. roughing, semi-finishing, finishing) in which electrodes with slightly different dimensions are used to compensate for tool wear in order to obtain the desired accuracy. Here, electrode material selection plays a vital role. Common used electrode materials for sinking EDM are copper and graphite, both having their specific field of application. Copper is mainly used when smooth surface finishes are required but has the disadvantage of a relative higher tool wear. Therefore, in some cases copper tungsten is used which has beneficial wear properties and is especially used for the machining of carbides. On the other hand, graphite is used in cases where big lightweight electrodes, low tool wear, high removal rates or detailed electrode shapes are required. Nowadays a large variety of graphite grades exists, differing in grain size, to meet specific demands. For instance, fine grade graphite (grain size < 3 µm) is often used when low electrode wear is required. Moreover, the high flexural strength (up to 100 MPa) of these fine grades makes it also the preferred material for thin long rib-like electrodes as can be seen in Fig.

2.11. Another important advantage of graphite is the easiness of machining due its higher hardness (70 to 85 Shore hardness for commercial grades) compared to copper. However, special equipment is needed when machining graphite due to the generated dust. In some cases the efficiency of graphite can even be enhanced by using copper infiltrated graphite, e.g. for the machining of exotic materials like beryllium copper, titanium and tungsten carbide [27].

From the foregoing it may seem straightforward which material to apply in specific conditions. However, the choice of electrode material is due to historical reasons mainly geographically linked. For example, in the US more than 90% of the sold electrode material has been graphite for several decades whereas in Europe and Asia only more recently an increase in the use of graphite has been noticed [28], [29]. Currently there is a trend to use more graphite because more complex shapes can be made and a significant reduction in the number of electrode materials can be made [30]. Fig. 2.12 gives a comparison of the number of copper and graphite electrodes needed to machine the same mould.

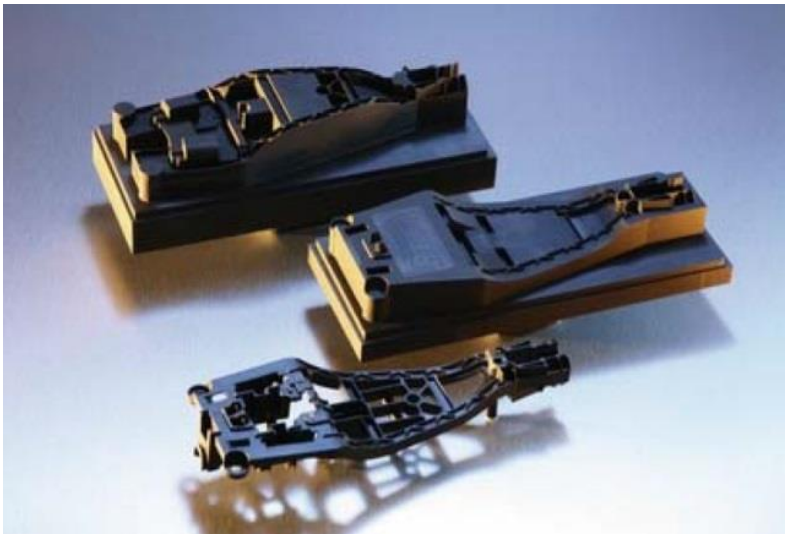

Fig. 2.11: Graphite electrode with thin ribs for the fabrication of moulds for mobile phone structures [25].

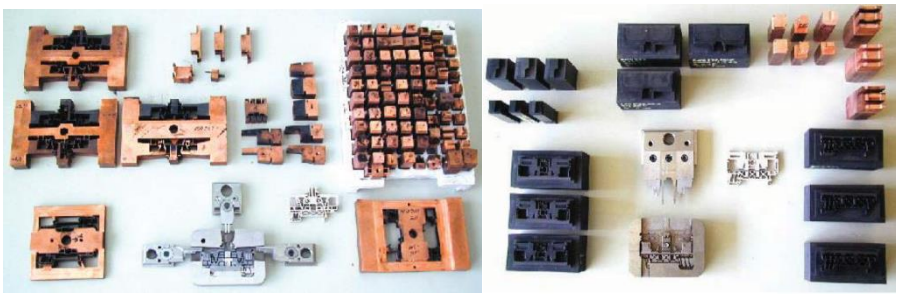

Fig. 2.12: Comparison of the number of electrodes needed to machine the same mould with only copper electrodes (left) and graphite electrodes (right) [28].

Most sinking EDM machines are equipped with both a transistor-based and a relaxation generator to cover the entire range from rough to mirror surface-like machining. Whereas the transistor-based generator is mainly used to provide high removal rates (up to several hundreds of mm^3/min), the relaxation generator mainly serves to achieve surfaces roughness values down to 0.2 µm Ra. Common EDM CNC machines have 4 axes (X, Y, Z, C) but nowadays even 7 axes machines are on the market for specific applications e.g. a corkscrew movement for the fabrication of helical closed channel geometries [31].

Wire EDM

Besides sinking EDM, wire EDM is probably the most used EDM variant in industry. The machining action is performed by a continuously travelling wire (electrode), mostly aligned vertically, which moves along a predefined path (Fig. 2.13). As the wire cuts through the workpiece, only through cavities can be machined with heights nowadays up to 700 mm [32]. In order to reach the required surface roughness and dimensional accuracy several machining passes with varying discharge energy and offset values need to be performed. During machining the wire is subject to vibrations due to small but significant process forces (e.g. pressure from gas bubbles, axial forces to straighten the wire, hydraulic flushing forces, electrostatic forces). To lower the effect of vibration on accuracy and surface quality a pre-tension is put onto the wire.
The machining mostly happens with the workpiece entirely submerged in the dielectric and flushing is supplied coaxially to the wire. Opposed to sinking EDM and milling EDM, the dielectric used in wire EDM is mostly deionized water due to its rapid cooling rate and low viscosity. Recently, there is a trend

to use oil as a dielectric to avoid oxidation of steel parts and to enable the machining of tungsten carbide without the loss of cobalt. In contrast to wet wire EDM, it has been shown that dry wire EDM can be beneficial in finishing operations by obtaining a better straightness, lower surface roughness and sharper corner radii [33]. However, further research is needed to exploit this variant.

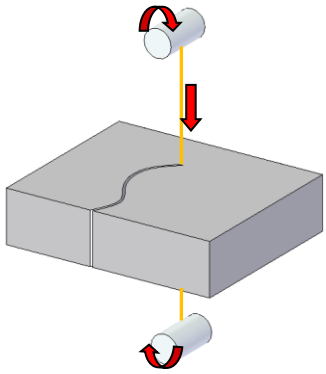

Fig. 2.23: Principle of wire EDM.

In wire EDM very short pulses with high discharge peak current are favorable as being a compromise between a good surface roughness and a relative high cutting rate. On the other hand, these pulses induce high tool wear but this is not an issue as the wire is continuously renewed. The use of these short pulses implies that the workpiece has a positive polarity, whereas the wire electrode has a negative polarity.

The wire EDM process has a broad application area, ranging from the fabrication of stamping and extrusion dies to the fabrication of high precision parts, automotive, aerospace and medical parts. This is partially due to the high degree of flexibility, as a result of having 5 or more numerically controlled axes which allow for example taper machining. Fig. 2.14 shows the machining and resulting products of a 5-axis NC wire EDM operation.

The desired precision and productivity of specific parts largely depends on the wire material used. Common wire materials are copper, brass and coated wires (often zinc coatings), each having their specific field of application. For example, when high productivity is required zinc coated wires have shown to

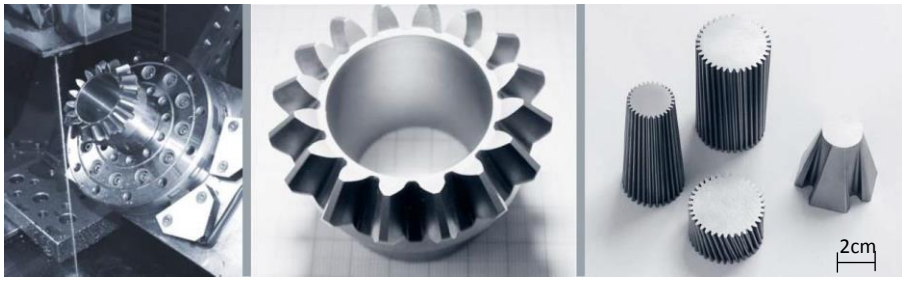

Fig. 2.14: 5-axis wire EDM of conical parts [34].

be beneficial by acting as a heat-sink protecting the core material from breakage [35]. To allow the complete machining of complex parts, 'twin wire' machines are currently available which enable the use of two different wires (e.g. rough cutting with a 0.25 mm zinc coated wire followed by cutting details with a 0.1 mm molybdenum wire).

The performance of the wire EDM process is mainly expressed by surface roughness and cutting speed. For common materials, roughness values down to 0.2 µm Ra can be obtained [36]. A further reduction down to 0.03 µm Ra is possible for tungsten carbide when using oil as a dielectric [37]. Typical cutting rates are 350 mm²/min for a 50 mm thick D2 tool steel part and 750 mm²/min for a 150 mm thick aluminium part [38].

Further improvement of the cutting rate can theoretically be obtained by adding an abrasive action onto the electro-erosive action of the wire. This is achieved in the hybrid process of **abrasion assisted wire EDM (AWEDM)** in which non-conductive abrasive grains are embedded in the outer surface of the wire (see Fig. 2.15). The kinematics are similar to the wire EDM process: the abrasive wire translates along an axis lateral to the machined surface while being continuously renewed. A gap of several micrometers is maintained between the workpiece and the wire

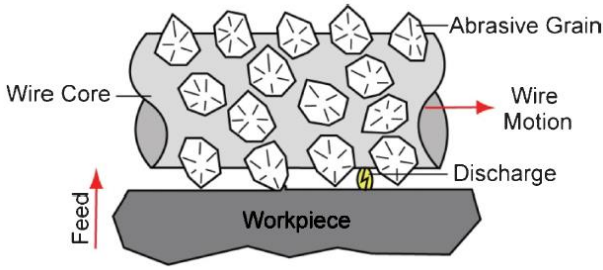

Fig. 2.15: Schematic overview of abrasive wire EDM [39].

It has been proven that the MRR significantly increases compared to normal wire EDM (increase up to 1000%) under the same conditions [39]. Moreover good roughness values can be obtained (ca. 0.9 µm Ra). However the machining accuracy is not as good compared to wire EDM due to the additional process forces caused by the abrasive action. The abrasive action also allows to obtain a machined surface with a significantly smaller recast layer, which is especially beneficial for aerospace applications where a high fatigue resistance is required. Fig. 2.16 shows the difference in recast layer (indicated as the section between the arrows) on a nickel 600 alloy machined with wire EDM and AWEDM. Despite the previously mentioned advantages of this hybrid process, still some issues regarding wear of wire guides and accuracy need to be tackled prior to commercialization.

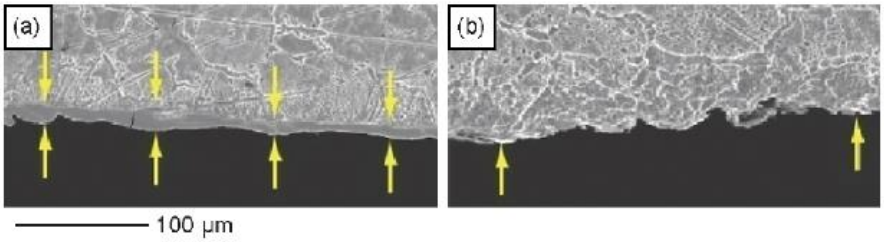

Fig. 2.16: Section view of surfaces machined with (a) wire EDM and (b) AWEDM [39].

Milling EDM

Opposed to case-specific pre-shaped electrodes in sinking EDM, milling EDM uses generic (tubular) cylindrical electrodes. In milling EDM the electrode follows a predefined path and removes material along this path. Similar to conventional milling operations, this is done in a layer-by-layer fashion (Fig. 2.17) resulting in a 3D cavity. Another similarity to conventional milling is the tool rotation which enhances flushing of the sparking gap. In most applications the workpiece is not fully submerged but dielectric is supplied either through external nozzles or through the electrode itself. The latter is used especially in case of high current densities and when machining small and deep cavities or holes. In fact, the milling EDM process is able to machine similar complex cavities as the sinking EDM process. However, a small limitation is the stair effect on non-vertical walls due to the layer-by-layer fashion of the process.

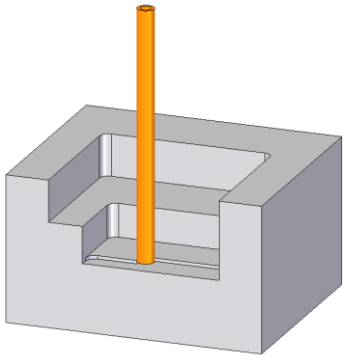

Fig. 2.17: Principle of milling EDM.

An important research topic in the field of milling EDM is the electrode wear as it strongly affects the accuracy. The electrode wear generally consists of corner wear and frontal wear. Assuming a significant volumetric wear, the tool shape will stabilize after a certain period of time making the frontal wear the dominant wear type. Fig. 2.18 shows the effect of the frontal wear on the geometrical accuracy when machining a groove. In order to reduce this geometrical inaccuracy, an additional feed movement in Z-direction is applied. Extensive research has been conducted for macro and micro machining operations to develop tool wear compensation strategies, both online methods [40][41][42] and offline methods [43][44]. The offline methods are mainly based on empirical information about the volumetric tool wear resulting in flatness values of 1 µm or less for micro-EDM milling [44]. The online methods use in addition real time pulse information resulting in a higher accuracy when machining complex shapes [45]. To increase the effectiveness of both types of tool wear compensation, intermittent electrode length measurements can be added to enable an in-process adaptation.

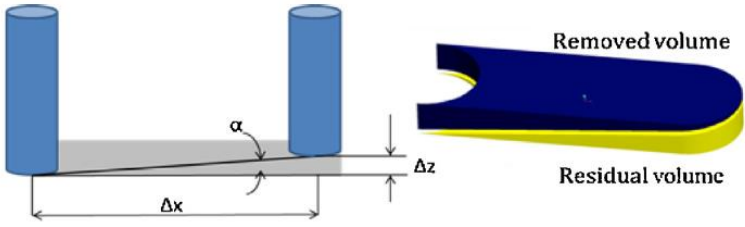

Fig. 2.18: Effect of frontal tool wear [37].

Although the potential of this EDM milling has been proven on macro-level [10][11], there has not been an industrial breakthrough of this technique. On the contrary, the milling EDM process on micro-level is already a well-established technique for the machining of micro components. Fig. 2.19 shows some typical applications of the micro-EDM milling process.

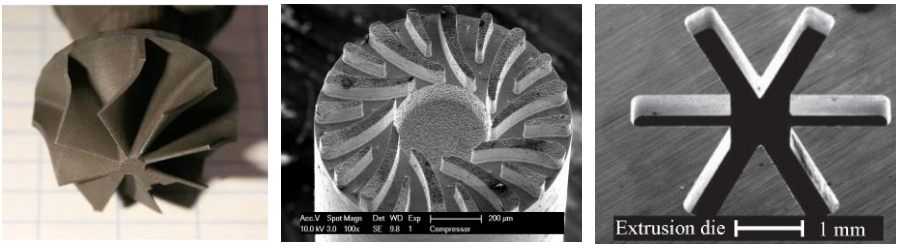

a. b. c.

Fig. 2.19: Examples of parts produced by micro-EDM milling: (a) Si_3N_4-TiN turbine impeller; (b) stainless steel compressor disc; (c) Al_2O_3-TiCN extrusion die [48].

The use of EDM milling of micro applications has several consequences regarding tool fabrication, hardware and dielectrics.

A first consequence is the need for very small electrodes. Mostly copper and tungsten carbide rods are used due to their high erosion resistance. To bring these rods to the right diameter or shape, a wire electrical discharge grinding (WEDG) operation is applied mostly directly on the milling EDM machine. Diameters of 5 µm, and even down to 2.8 µm [49], can be machined, allowing the fabrication of holes with a diameter of a few micrometers with aspect ratio up to 100 [50]. This poses a big advantage compared to mechanical drilling and laser machining where the minimal attainable hole diameter is respectively 70 µm and 40 µm [3].

Secondly, the machining of micro-components requires the removal of a minute amount of material restricting the discharge energy. The discharge voltage is typically between 10 to 40 V mainly dependent on the electrode material. Hence according to Eq. 2.1, the main control parameters for the discharge energy are the discharge current i_e and the discharge duration t_e. i_e has to be sufficiently large in order to have an effective discharge. As a consequence, t_e has to be in the nanoseconds range in order to attain discharge energies of several nanoJoules. Transistor based generators (Fig. 2.20.a.) cannot deliver such short discharges because the measuring of the occurrence of a discharge and the transistor itself have a delay time of several tens of nanoseconds to diminish the discharge current to zero [6].

Resistance-capacitance (RC) based circuits (Fig. 2.20.b.) better suit the need for a short t_e by using the discharge of capacitors with very small capacitance (less than 1 nF). The use of short pulses furthermore implies that the workpiece should have a more positive polarity than the tool electrode.

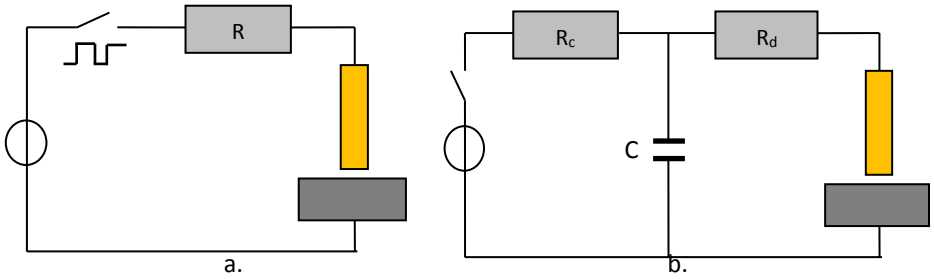

Fig. 2.20: Electrical scheme EDM generators: (a) transistor based generator; (b) relaxation generator.

Due to the often difficult flushing conditions in micro-EDM milling (e.g. small holes with high aspect ratio) dielectric fluids with a low viscosity are required. Both water based fluids and hydrocarbon oils are commonly used. Besides this, the use of air or gasses has been shown to be effective in dry EDM milling. Kunieda et al. [51] showed that dry EDM milling can be beneficial regarding removal rate, tool wear and surface integrity.

Electrical Discharge Grinding (EDG)

The EDM process can also be applied in a configuration similar to the conventional grinding process (see Fig. 2.21). When machining extremely hard materials like polycrystalline diamond (PCD) and polycrystalline boron nitride (PCBN) with conventional grinding it can lead to rapid wheel loading (i.e. clogging of pores in binder material), glazing (i.e. flattening of abrasive grains) and high normal forces which result in inaccuracies. The EDG process reduces the previously mentioned disadvantages of conventional grinding and results in significant reductions in machining time i.e. EDG is 2 to 3 times faster in machining hard materials compared to conventional grinding [52]. Also an increase in MRR compared to conventional EDM is noted due to the rotation of the tool leading to an improved flushing action.
In the EDG process graphite, copper or copper/tungsten electrodes are used in combination with a hydrocarbon oil. However, in practice, graphite is the most suited material from both cost as practical perspective. The EDG

process is applied in the production of PCD and PCBN cutting tools as in the production of razor blades by the use of commercial machine tools for this specific process [53].

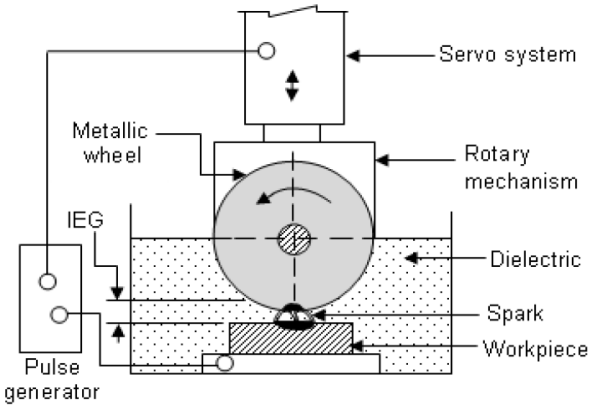

Fig. 2.21: Machine setup of EDG process [51].

As the EDG process is still a pure EDM variant, the surface roughness is relatively high compared to conventional machining processes. To lower the roughness and to improve the machining speed, an abrasive action can be added to the EDG operation by the addition of hard non-conductive grains (e.g. diamond, SiC) to the tool material, the so called **abrasive electrical discharge grinding (AEDG) process**. In this process the simultaneous removal of material by the abrasive action of the non-conductive grains and the erosive action of the metallic bond material (see Fig. 2.22) results in an increased MRR. At the same time the thermal effect of EDM softens the workpiece material and hence reduces the normal forces. As an example, the MRR of the AEDG process when machining an Al-SiC composite is five times higher than for the EDM process and twice that of the EDG process [54].
Besides the erosive impact on the workpiece, also debris particles that accumulate on the metallic bonder are removed. This inherent self-dressing action strongly reduces costly machining time and guarantees a constant MRR during operation. Opposed to conventional grinding, no energy is lost in friction between the wheel bond and the workpiece as there always exists a gap. This can lead to a reduction in energy ranging from 25 to 40% [55]. Also the wear ratio can be strongly reduced, being 5 to 10 times smaller compared to conventional grinding [53].

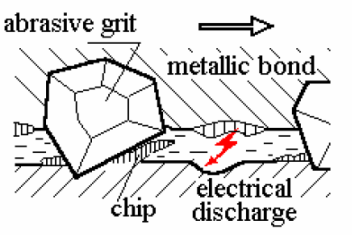

Fig. 2.22: Schematic of AEDG process [53].

Although the surface roughness can be strongly reduced compared to the EDG process, the conventional grinding process results in a roughness of 40% lower compared to AEDG [53]. Therefore, it is beneficial to use the AEDG process for roughing purposes and shift to the conventional grinding process for finishing purposes. This can be done in one machine setup as it is possible to change the dominant process.

Wire Electrical Discharge Grinding (WEDG)

A variant of the EDG process concerning the process goal of shaping or dressing tools is the wire electrical discharge grinding (WEDG) process. However, the machine configuration is completely different compared to a grinding setup. In the WEDG process cylindrical rods are shaped by means of a travelling wire (Fig. 2.23.a.). The workpiece, in most cases the tool electrode for EDM milling, is subjected to a rotational and downward movement resulting in a reduced tool diameter or complex shaped electrode (Fig. 2.23.b-c). By combining the WEDG process with micro-EDM milling in one machine setup, the run-out error, which mostly occurs when clamping the tool electrode, can be reduced to almost zero. By reversing the polarity, the fabricated electrode can be directly used for machining without the need for unclamping the electrode.

Compared to other on-machine tool fabrication methods (e.g. sacrificial block method), the WEDG process leads to higher accuracies and smaller electrode diameters [6]. By reducing the discharge energy, diameters down to 5 µm diameter can be machined [56]. Egashira et al. [57] even report on the fabrication of a tool with a diameter of 1 µm by decreasing the open voltage to 20V. Moreover, these small diameters can be obtained along a significant length of the electrode enabling the machining of large aspect ratio holes.

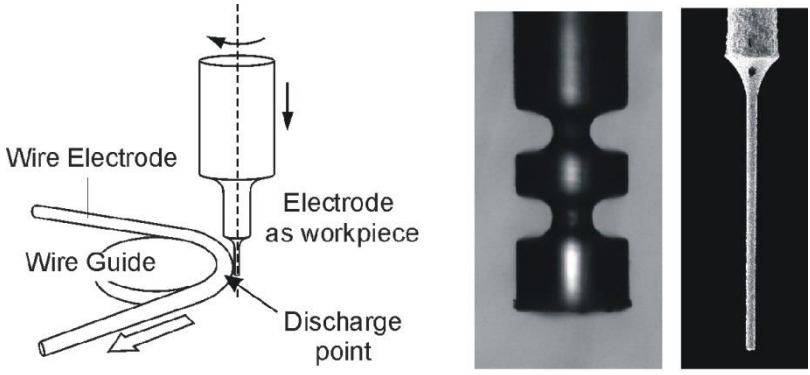

Fig. 2.23: (a) Wire Electrical Discharge Grinding: WEDG concept; (b) complex shaped electrode by WEDG; (c) reduction in tool diameter by WEDG.

Besides the described techniques in this section, a wide variety of other EDM techniques exists. Section 6.3 will highlight some of these techniques, especially those that are being used in a hybrid manner.

2.1.4. Machines used in the research

The research outlined in this work focuses on two variants of the EDM process, each performed on a different machine setup. Because the machine performance has a significant influence on the results, a short description of the used machines is given in this section.

Sinking EDM setup

The research work on sinking EDM was carried out on a sinking EDM machine, type Charmilles Technologies Roboform 350 ɣ (see Fig. 2.24). This is a 4-axis machine with controlled rotational axis for e.g. machining helicoidal features. To cover the entire range from roughing to finishing, the machine is equipped with a static pulse generator and a relaxation generator which allow machining with current values ranging from 1 A to 128 A and pulse durations ranging from 0.8 µs to 3200 µs. The control software (DPControl®) offers different default technologies depending on a broad range of materials used and applications (surface machining, rib machining, punch machining, etc.). As an output the control software gives a proper sequence of regimes (regime = combination of generator and machining settings) to obtain a surface and dimensional quality with minimal tool wear or maximal removal rate. Flushing nozzles are available for cases where the

flushing effect of the electrode is not sufficient. The dielectric used is Total MS 7000 with a flash point of 102 °C and a viscosity of 3.4 mm^2/s (at 20 °C).

Fig. 2.24: Roboform 350γ.

Micro-EDM milling setup

The research on micro-EDM milling was performed on a Sarix SX-HP-100 (Fig. 2.25) which is a 3-axis micro-EDM machine with a working envelope of 250 mm x 150 mm x 150 mm in respectively X, Y and Z direction. This setup is equipped with a spindle which can attain speeds up to 600 rpm. In this setup the worktable moves in X and Y direction while the spindle and electrode move along the Z axis. The setup can be extended with 2 axes to allow 5-axis machining for e.g. drilling of high aspect ratio cooling channels in turbine blades.

Being a micro-machine, the need for precise and repeatable machining is firstly evidenced by the integration of linear motor drives in both X and Y axis. The Z axis, on the contrary, is lead screw driven. Secondly, precise machining requires the generation of low-energy discharges which is achieved with what is believed to be a mixed transistor-RC generator. This generator can generate pulse widths of 40 ns and more with peak currents from 0.05 A to 15 A. Moreover, the machine is equipped with a WEDG-unit to reduce electrode diameter and to shape the electrode (also called dressing). As an example, a tool electrode with a minimum diameter of 8 µm and an aspect ratio of 5 was successfully machined using this WEDG setup [58]. Finally, electrode tool wear is automatically compensated to guarantee flat and smooth surfaces.

Flushing of the working gap occurs by nozzles positioned close to the working spot or by high-pressure flushing through the electrode to enable good machining conditions when e.g. drilling deep holes. The dielectric fluid used is HEDMA 111 with a flash point of 101 °C and a viscosity of 2.4 mm²/s.
Programming of complex milling operations is performed with an add-on to the standard CAM software of Esprit for conventional machining operations. EDM specific issues like compensation for frontal and side gaps and tool wear compensation strategies are taken into account.

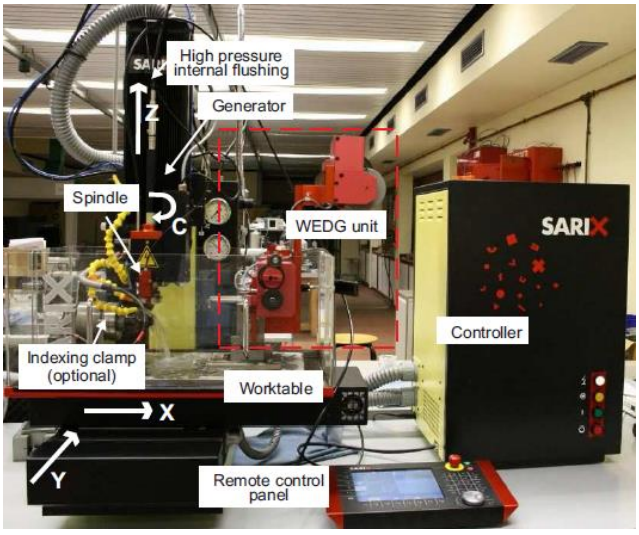

Fig. 2.35: Sarix SX-HP-100.

2.2. Necessity for a proper process planning

2.2.1. Process planning in a manufacturing environment

For every part that needs to be manufactured a process plan needs to be established, either in a basic or detailed manner. The activity of process planning consists of defining which manufacturing processes and machines need to be used and the sequence in which these need to be applied in order to convert a part from its initial to its final form. Activities that play an essential role in process planning are process parameter selection, process time and cost estimation, tool and clamping/fixture definition, NC programming and process and work center selection. The process plan is a direct input for the production planning. Whereas the process plan is established on product level, a production planning is established on a higher level with the purpose of efficiently organizing the use of resources. Typical activities involved in production planning or production control are order and capacity follow-up, monitoring of overall equipment effectiveness (OEE) and management of the supply chain.

The establishment of a process plan comes already into play in an early stage of the product realization process as it serves as the basis for a quotation. To be competitive a fast and accurate process plan definition is essential. The consequences of an improper process plan can be tremendous. For example, financial losses can result from cost overruns as a consequence of underestimation of machining costs or incorrect assessment of machining operations. Likewise, an incorrect assessment of the machining operations can lead to an inferior part quality or passed delivery dates which can result in customer dissatisfaction and eventually in loss of customers.

The establishment of a proper process planning has been the subject of research since several decades. Depending on the application different types of process planning methods can be distinguished.

- ***Variant or retrieval process planning***. In this method the process plan of a new part is derived from existing process plans of similar parts manufactured in the past. This is achieved by classifying the part within a specific part group with similar geometrical features and/or technical specifications. For every part group a standard process plan has been established in which some parameters can be adjusted to suit the specific

case. This method is very useful when manufacturing a lot of similar parts but becomes problematic when a new part does not fit within a group [59]. In that case the classification needs to be updated.

- ***Generative process planning.*** This type of process planning is based on manufacturing knowledge captured in decision trees, manufacturing rules or database structures. Information about the machining case (part geometry, material, tolerances, desired surface integrity etc.) is progressed and evaluated through several technical and logical decisions towards an appropriate process plan [60]. As a consequence, this method is not tied to existing process plans, making it easier for new challenging parts to be evaluated. On the other hand, decision trees or rules are rather static as these respond poorly to new manufacturing situations. Hence an adaptation requires a significant amount of effort to rewrite at least a portion of the logic due to conflicts with existing rules.

- ***Hybrid variant/generative process planning.*** In this type of process planning the part is first classified within a group followed by an evaluation by a corresponding set of rules or decision trees. This method combines the advantages of the previous methods but can become rather complex due to the multitude of rules or decision trees [61].

- ***Learning systems or process planning with neural networks.*** Unlike the previous methods which require the effort of capturing human information in classes or rules and decision trees, neural networks hardly require human involvement making them suitable to adapt to changing conditions and to continuously update information without a tremendous increase in time and cost. Neural networks have been defined for different steps in process planning. For example, in [62] two neural networks have been established for the machining of rotational parts: one for the definition of basic machining operations based on machining features and their attributes and one for the further refinement of operations into roughing, semi-finishing and finishing. In [63] a neural network has been established to cope with the classification problem of tool selection for milling, turning and grinding operations. In addition, in [64] the operation sequencing for turning operations has been optimized by means of neural networks with the goal of minimization of total cost.

All methods rely on information which can be made digitally available (e.g. type of feature, dimensions, tolerances, surface quality requirements, etc.). Ultimately, the process plan is automatically defined based on the parts CAD file. However, this is far from feasible as some kind of manual intervention is always needed. However, the amount of manual intervention should be limited as this is a person dependent action based on gained experience and knowledge, most likely leading to a difference in processes, tools, machines or operation sequence for a specific machining case. This in combination with the larger need for automation, integration of the process planning activity in a computer integrated manufacturing (CIM) environment with a certain level of automation is needed to increase consistency and planning quality. This computer integration, often referred to as **Computer Aided Process Planning (CAPP)**, is a direct link between CAD and CAM and reduces the time spent between part design and actual manufacturing, enabling faster offering.

CAPP systems are often company specific software tools/modules as these need to be adapted to the specific company situation. Large companies have established their own research groups to develop their own CAPP systems as many existing CAPP systems were far from effective. However, for SMEs such an investment cannot be justified. Nowadays machine tool builders also provide process planning software mainly aiming at aligning multiple distinct processes, such as Multi Process Preparation [65]. In the past, SMEs mainly relied on CAPP systems developed by universities or research organizations which are often more general in nature. Examples of such CAPP systems can be found in a wide range of manufacturing applications. Some examples are briefly described in the following. A first example is related to process planning for low to medium volume sheet metal parts. An important aspect in this case is to consider the specific aspects of all used processes. In [66] this has been studied for the combination of laser cutting and air bending. For laser cutting, the main driver is the reduction of material waste by nesting parts whereas for air bending the main driver is the minimization of setups by intelligent tool selection and bend sequencing. However when combining both processes, an optimization performed for one process can counteract the efficiency of the other process. Therefore, an integrated approach has been suggested which aims at optimizing the number of parts per sheet and minimizing the setup time for air bending in order to reduce material waste and throughput time. Another study [67], [68] uses the manufacturing cost as main driver for the process planning of sheet metal parts. Based on the

CAD file technological features are automatically detected and are assigned to possible manufacturing operations. For these operations cost estimations based on neural networks have been established with an accuracy between 5 to 15% enabling an accurate process planning. Also in the highly competitive field of the die and mold making, process planning is a valuable tool. An example of a CAPP system is DieEx [69], developed for 3-axis milling operations. This knowledge based system with expandable database structure defines a process plan (tool type, parts fixturing method, feed direction, machining strategy, depth of cut, etc.) based on input parameters like surface type, workpiece and tool materials and the type of application (roughing/semi-finishing/finishing) with the goal of minimizing the total tool changing time.

2.2.2. Process planning for EDM operations

A noted before, EDM has specific advantages compared to other manufacturing processes which makes it a highly valuable technique in the tool and mould making sector. Driven by an increased competition from the Far East and reduced time-to-market, western tool and mould manufacturers are forced to increase their overall productivity. There are different ways to achieve this, for instance on technological side by further process optimization or an increasing level of automation. But also efforts put in an efficient use of resources by the development of new and further optimization of existing process planning methods can deliver the necessary contributions.
In the past decades research has been conducted to enable further refinement of process planning tools for EDM operations. The following will give a short overview of CAPP tools specific for EDM operations.

Especially in the mould making sector combination of conventional cutting operations (e.g. milling, drilling, grinding) and EDM operations are common in order to meet goals like minimal throughput time or minimal cost. Within this perspective, Lauwers et al. [70] developed a hybrid variant/generative CAPP tool based on process planning features that define the feature in a geometrical and technological manner. For each process planning feature type generic process plans have been developed. Each process plan consists of a set of manufacturing rules and defines all possible operations needed to manufacture the feature. In this work both conventional operations (milling, grinding, drilling) as well as EDM operations (sinking EDM, milling EDM, wire

EDM) were considered. Fig. 2.26 shows an example of a generic process plan for a pocket feature. An evaluation of the process plan results in a set of feasible operations for which the variable cost (machining cost, tool cost, setup cost) is estimated. First operations are grouped per setup based on the existence of similar technological requirements and to prevent geometrical errors. Then the variable cost is minimized by performing a branch-and-bound method on the cost estimates.

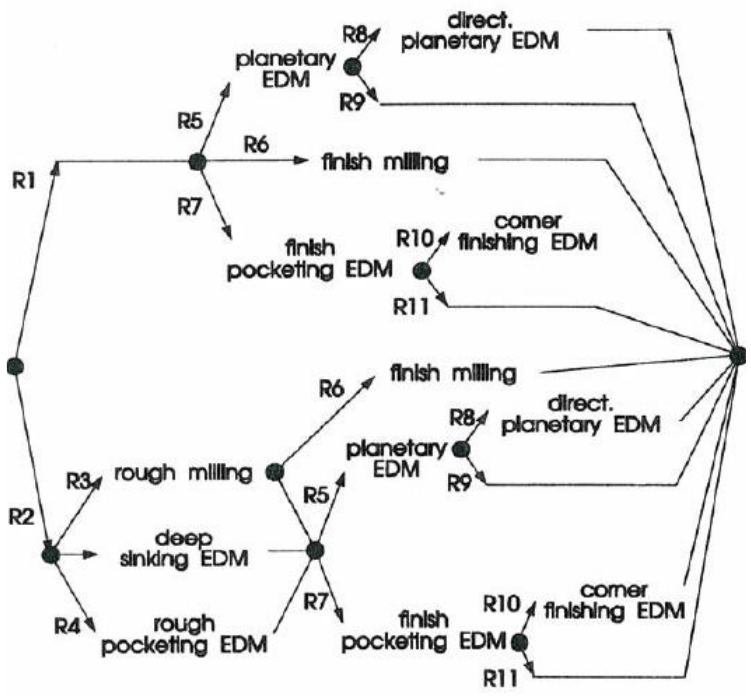

Fig.2.26: Generic process plan for pocket feature [70].

Opposed to the previous study, also process planning tools purely on the EDM level have been developed. In the study of Jain et al. [71] a generative process planning approach for sinking EDM operations has been established. This interactive CAPP tool starts with the selection of a proper machine tool based on workpiece dimensions. In a second step geometrical features are interactively defined and grouped for simultaneous machining when having the same machining direction, similar surface finish and tool material and if the total area is lower or equal to the maximum permissible surface area for simultaneous machining. For each group or operation the process parameters are interactively selected and the removal rate is calculated

based on empirical data. Finally, the operation sequence is defined by taking dimensional, geometrical and technological constraints into account. As the main part of the logic and knowledge is captured within the CAPP tool, the activity of process planning becomes more accessible for a larger audience. This trend of a lower level of process knowledge needed to define process plans is demonstrated by the low entrance level of many EDM machine tool software products. Most of the current EDM machine software tools are based on an interactive definition of the machining case. The user defines the number of cavities, machining direction, required roughness, priorities and machining passes given a set of predefined tool electrodes. With this information the most suitable machining operation, process parameters and the resulting NC code are automatically defined. Fig. 2.27Fig. 2. shows an example of the operation definition in a commercial machine software tool for sinking EDM operations.

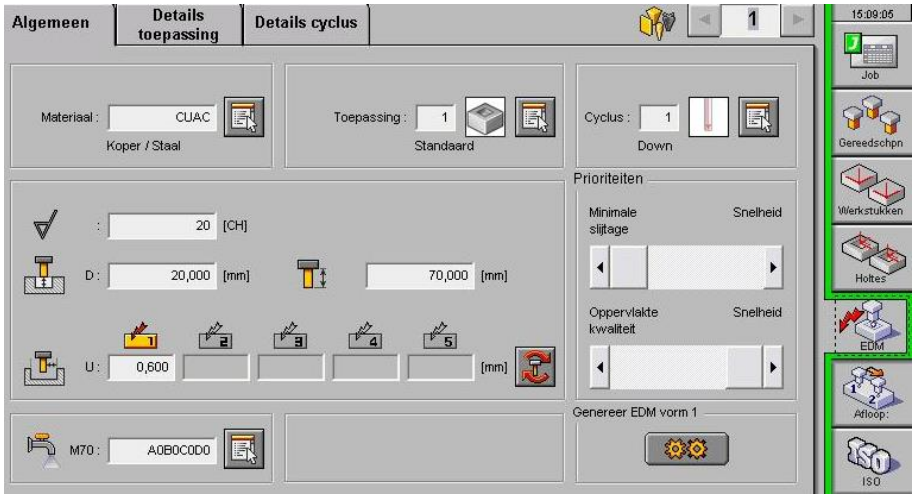

Fig. 2.27: Operation definition in EDM machine tool software.

Also for micro-EDM operations studies have been performed to accommodate reliable process planning. For example, Meeusen et al. [72] developed a CAPP tool based on a library of manufacturing features that are predefined and a set of user-defined manufacturing features. A producibility check is performed on both feature types and is able to handle interfering features. Each predefined feature contains a parametric toolpath that is adjusted according to dimensions and shape. After the generation of the toolpath process parameters are optimized and the tool wear is compensated.

However, in order to achieve a reliable and robust process planning for EDM operations several obstacles still need to be tackled. Examples of improvement areas are the robustness of the EDM process, the reliability of EDM time estimation, the reliability and generality of knowledge based systems, the development of planning systems for hybrid processes and machines and the further integration and elaboration of CAD/CAM and CAPP functionality in a CIM environment.

2.3. Objectives of this research

The previous sections have shown the necessity of process planning for a production environment and highlighted achievements made in process planning for EDM operations. However, there are still some issues that need to be tackled prior to achieving accurate process plans for EDM operations. In this study two topics have been selected for further investigation:

- Indispensable for a reliable process plan is an accurate knowledge of the EDM machining time. Unlike for conventional machining processes, estimating the machining time for EDM operations is a very complex task due to the unpredictable influence of flushing conditions and electrode geometry which can lead to large variations in machining speed as no constant feedrate can be set. The EDM process is adaptively controlled based on the gap conditions which heavily depend on the flushing conditions. This is especially the case in sinking EDM where the evacuation of the generated debris from the sparking gap can be heavily disturbed by the electrode geometry. Lack of knowledge about the machining time can heavily affect the total cost and throughput time, ultimately leading to lost offers, financial losses or customer dissatisfaction. Therefore, this study aims at **improving the accuracy of time estimations for sinking EDM operations** by determining the major influencing factors and modelling their effects. This will be elaborated in Part 1 of this study. A more detailed problem description and state of the art regarding sinking EDM time estimation can be found in Chapter 3. At the end of Chapter 3 the specific objectives regarding this research topic are stated.

- The trend towards hybridization has also emerged in micro-manufacturing both on process level and on machine level. Often micro-EDM techniques are involved due to their contactless nature and the ability to accurately remove tiny pieces of material, even in hard materials. In order to make optimal use of a hybrid machining platform, process planning tools need to be developed which are based on process characteristics of all constituting processes and characteristics of the specific machining platform. In this study an **automated process planning tool for a hybrid micro-EDM machining platform** will be developed. This will be elaborated in Part 2 of this study. A more detailed

problem description and reasoning for the selection of the specific hybrid machining platform will be elaborated in Chapter 6. From this the specific objectives regarding this research topic are stated.

PART I:
Time Estimation for Sinking EDM Operations

Chapter 3 Assessment of current practice and objectives

3.1. Sinking EDM time estimation – State of the art

Knowledge about lead times of manufacturing processes is indispensable for the development of a solid process planning. Strongly over or under estimating processing times can have severe impacts like lost offers, loss in reliability and customer dissatisfaction, cost overruns and capacity problems. As the electrical discharge machining process is often a time intensive step in an entire chain of manufacturing processes, an accurate knowledge about its lead time is essential. It is not unusual that the real EDM time is two to three times the estimated time [73].

In conventional machining processes like milling and turning, an assessment of the lead time is rather straightforward when having proper knowledge about feedrate, depth of cut and the total volume to be removed. These are all parameters which are defined beforehand and are kept constant during one machining pass. As a consequence, accurate processing times can be calculated enabling a reliable process planning. On the contrary, the machining speed in EDM is not a constant value but is strongly dependent on the generator parameters (e.g. pulse current, pulse duration) and more important depends on the conditions in the gap between tool electrode and workpiece. Information about the gap conditions serves as an input for the feedback control of the EDM process. Because the gap conditions change during machining, the assessment of the machining speed becomes a complex matter. Moreover, the gap conditions are strongly dependent on the flushing conditions and the electrode geometry of which the exact influence on the machining speed is not yet fully quantified. This is especially the case in sinking EDM operations where the flushing conditions can have a heavily irregular behavior. This all, makes time estimation for EDM operations a complex and cumbersome task.

In the last couple of years, due to the higher performance of EDM machines and the development of automatic flushing techniques, the repeatability of the EDM process has significantly increased [3]. This should help to foster the development of accurate time estimation methods. Several attempts have been made to develop algorithms and models to achieve accurate EDM time estimations. The next paragraphs give an overview of different modelling techniques applied on the topic of EDM time estimation, all with a different

starting point. From literature two main approaches can be distinguished namely theoretical and empirical.

3.1.1. Theoretical models for time estimation

One way to assess the machining time or removal rate is to find a relation with the physics taking place in the machining gap. Since the early 1970s several researches have been conducted to develop thermal models aiming at finding both qualitative and quantitative relations with performance criteria like removal rate, tool wear and surface quality, which can be eventually used in process planning. In these models, the plasma channel is acting as a heat source locally melting and evaporating minuscule parts of the tool and workpiece material.

Due to the very complex behavior of the phenomena in the sparking gap, several assumptions have been made on different grounds like type of heat source, heat transfer and heat flux, distribution of input energy, radius of the plasma channel. In Snoeys' model [74] the plasma channel is assumed to be a disk heat source in which 50% of the energy is transferred to the cathode (workpiece), seen as a semi-infinite cylinder. The radius of the plasma channel is considered to be constant whereas the removed material is considered to be equal to the molten material. This model results in bowl-shaped, flat bottomed isotherms. Van Dijck [17] adapted Snoeys' model to incorporate the cathode as a finite cylinder resulting in isotherms with a more circular shape and higher affected depth. However, the comparison with empirical results showed a MRR of 4.461 mm^3/min for a voltage of 25 V, a current of 12.8 A and a pulse duration of 42 µs, which is 8.83 times higher than the experimental MRR [75]. To account for the phenomenon of plasma channel growth Jilani [76]–[78] developed a model with the assumption that the temperature in the center of the cathode spot remains constant throughout the pulse duration and equals to the boiling temperature. Opposed to the previously discussed disk heat source models, DiBitonto [79] developed a model where the plasma channel is considered as a point heat source which only distributes 18% of the total input energy to the cathode. Due to the circular heat flux a nearly hemi-spherical shape of the crater is obtained. Moreover, the effective thermo-physical material properties of the material over the entire temperature range were considered leading to more accurate results. Yeo et al. [75] compared the previous models with experimental results and concluded that DiBitonto's model has the strongest agreement to reality when looking at the crater diameter and the removal rate for the energy range of 0.33 to 952 mJ for the

material combination steel-copper. The crater diameter ratio (model diameter/real diameter) ranged between 1 and 1.9 whereas the removal rate ratio (model MRR/real MRR) ranged between 1.2 and 46.1. Although DiBitonto's model shows the closest agreement to reality, the disk heat source models better match the circular paraboloid crater geometry noted in practice (see Fig. 3.1). By incorporating a lower cathode energy fraction and the dependence of the plasma channel radius on the pulse duration, significantly better results were achieved [75].
Further improvements are made by incorporating the relationship between pulse duration and pulse current on the one hand and channel diameter on the other hand. This leads to average deviations of 8.2% on the MRR when machining St-37 with copper electrodes for energies ranging from 0.192 to 36 mJ [80]. A further refinement was made by Joshi et al. [81] by incorporating the latent heat of melting and a Gaussian distribution of the heat flux. Fig. 3.1 shows a comparison between the crater diameter obtained by this model and the experimental determined crater diameter. Finally, an attempt has been made by Yeo et al. [82] to account for the fact that not all of the molten material is expelled from the workpiece but only the superheated material. Results show close agreement with the empirical removed volume, though this has only been investigated for micro-EDM.

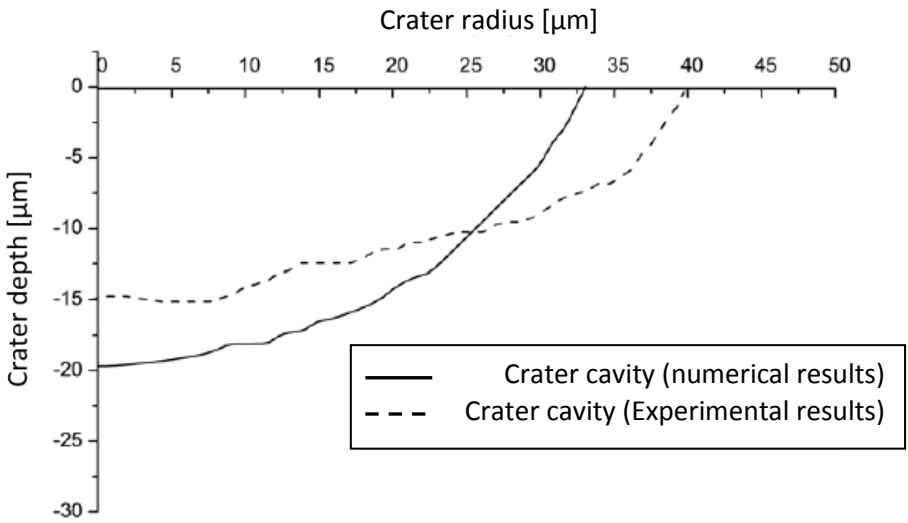

Fig. 3.1: Comparison of crater shape obtained empirically and numerically for the combination steel-copper with u_e 25 V, i_e 12.8 A, t_e 42 µs and t_0 3.2 µs [81].

Considering thermal models as a way to estimate the machining time, one has to take into account that these are all subject to inevitable assumptions and simplifying approaches of the behavior in the machining gap (e.g. neglecting effects of vaporization, neglecting recast layer, not taking into account the random behavior of debris). This will lead to an overestimation of the removal rate for practical machining cases. Although the predicted MRR closely matches the real MRR in most models, there is a strong lack of validation with different material combinations and machining cases in which different flushing conditions can be expected. This severely limits the applicability of these models for a reliable process planning.

3.1.2. Empirical-based time estimation methods

Next to the theoretical models from the previous section, which are mainly based on thermo-physical material properties, other modelling techniques have been used to determine the removal rate by making use of empirical data. In these models mainly tangible process parameters are considered. The following sections discuss several of these empirical-based techniques.

Neural networks

Since the 1990s neural networks are and have been extensively used as a modelling technique. This type of modelling has shown to be highly flexible and capable of learning the mathematical mapping between input variables and output features, especially for non-linear systems. Literature has reported several successful implementations for the modelling of machining processes [83]–[89]. Also in the field of EDM, neural networks have been applied for e.g. the recognition of pulse types for online monitoring purposes [90]. Besides this, neural networks have been developed for predicting the performance of the EDM process in terms of removal rate, tool wear and surface roughness [91]–[93].

Neural networks are characterized by the number of nodes, the number of hidden layers, the type of activation function and the type of learning algorithm used to optimize the weights between nodes in order to minimize the error between measured and predicted value (see Fig. 3.2). Therefore different network structures exist with their own specific performance. Tsai et al. [94] compared 6 different network structures for the purpose of predicting the removal rate in sinking EDM operations. These networks all had 8 input nodes (tool polarity, discharge duration, discharge current, pulse

interval time, open voltage, servo voltage, tool and workpiece material), 1 hidden layer and 1 output node (removal rate). It was found that the adaptive-network-based fuzzy inference system (ANFIS) leads to the best results. A validation with the material combination copper – steel/aluminum showed a mean prediction error of 16% with a maximum error of 35%. Mandal et al. [95] used a back-propagation network with 2 hidden layers and 3 input nodes (discharge current, discharge duration, pulse interval time) resulting in a mean prediction error of 3% and maximum error of 9% for the material combination copper-steel.

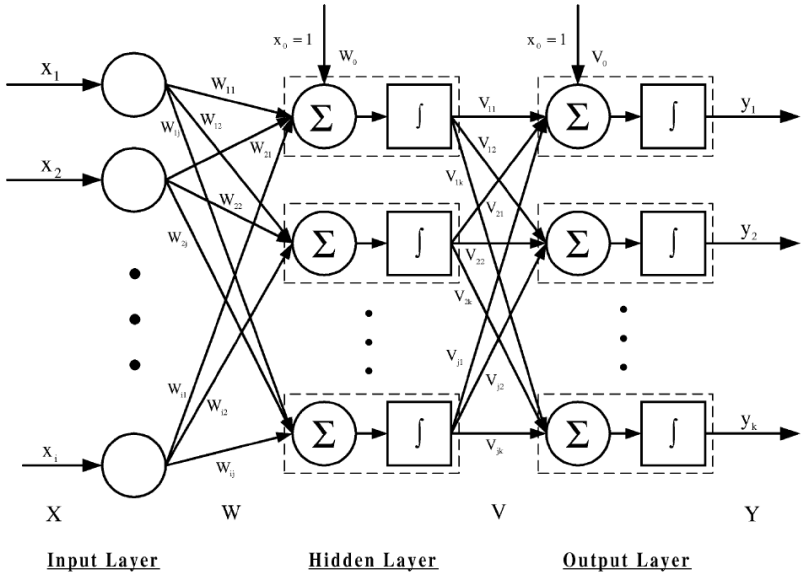

Fig. 3.2: Structure of neural network [94].

Besides the previous mentioned network, literature also reports about the use of hybrid modelling techniques i.e. neural networks combined with genetic algorithms to optimize the weights. Wang et al. [96] report about such a technique, considering a network with 6 input nodes (discharge duration, pulse interval time, discharge current, open voltage and 2 control parameters i.e. compression and gain) and 1 hidden layer. Validated for the material combination copper-nickel alloy an average error of 5.6% was reported. Although this seems quite promising, a check for the underlying relations showed a poor resemblance with reality i.e. a decreasing trend of the removal rate with increasing pulse duration was observed. Su et al. [92] also mention this combined technique for the integrated solution to the problem of modelling and optimization of process parameters during various

stages of machining. Five different neural networks were developed, each valid within a certain surface area range. Unfortunately no report is made about the performance of the model as a prediction tool instead of an optimization tool. In order to avoid the costly and time consuming experimental data collection for the network training Joshi et al. [97] developed a back propagation neural network with 4 input nodes (discharge duration, discharge current, discharge voltage and duty cycle) and 2 hidden layers based on data obtained by thermal simulation results. Low prediction inaccuracy has been proven, ranging from 0.03% to 3.53%, when comparing the network outputs with the thermal simulation results. Though, the results are not that surprising as the thermal models are inherently based on mathematical equations, providing a well-defined base for the neural network development. In this case the accuracy of the thermal model defines the applicability of the neural network in practice.

As a conclusion, neural networks have shown to be a good alternative for estimating the removal rate. However, it remains a black box as the relations between input and output parameters (e.g. removal rate) cannot be easily understood. Unfortunately, the reported validations were performed for a limited set of material combinations and machining cases, so no statement can be made about the generality of these models.

Regression models

As it is as important to know the importance of influencing parameters and their relation with the removal rate as the prediction itself, analytical modelling techniques have been used for this purpose. Chen et al. [98] report about a regression model based on discharge duration, discharge current, open gap voltage and pulse interval time. A factor Fc was introduced representing the proportionality of removal rate to discharge energy. This factor needs to be empirically determined as it is dependent on the tool - workpiece material combination and dielectric fluid. Besides this, other assumptions have been made like spherical shape of craters and identical discharge cycles. Tests with a copper-steel combination showed a good agreement with practice. It should be noted that tests were performed in a relatively small testing window with similar flushing conditions. Another model based on dimensional analysis has been reported by Wang et al. [94]. Besides process parameters as discharge current, discharge duration and polarity, the model is also based on thermal (thermal conductivity, specific

heat, latent heat of fusion and vapour), physical (density) and electrical (electrical conductivity) material properties. The calculations of coefficients and powers of the dimensional equations are based on experiments with pure metals. Verification experiments showed average errors of 32% and 44% for respectively the material combinations copper-aluminum and copper-iron by using specific models for each material combination. Although the model works well for one material combination, it is not adequate for extension to other materials due to differences in microstructure and removal mechanisms. Yahya et al. [99] also elaborated a mathematical model based on dimensional analysis. Besides electrical and material properties, a dimensionless constant was introduced to account for the plasma flushing efficiency and the resolidification effects. The model showed good agreement with experimental results.

Another way to achieve a regression model is by using the design of experiments technique which holds a statistical analysis. Literature extensively reports about the application of this technique for assessment of the EDM performance. One example is the study made by Puertas et al. [100] in which the influence of discharge current, discharge duration and duty cycle on the MRR of 94WC-6Co was investigated. By using a central composite design a second order model was developed with an R^2 value of 0.998. A graphical representation of the model is shown in Fig. 3.3. Unfortunately, no report is made about verification experiments.

In most cases regression models are developed for specific material combinations and specific machining conditions making them lack generality. When new and advanced materials appear, it has not been possible to use existing models. Hence additional experimental investigations are required which are not always economically justified.

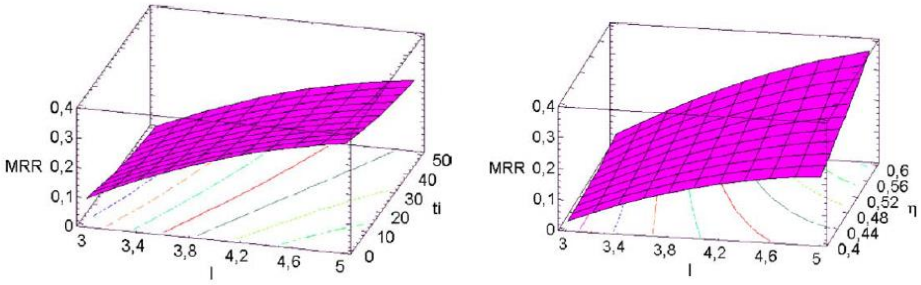

a. b.

Fig. 3.3: Response surface of MRR (a) in function of discharge current I and pulse duration t_i; (b) in function of discharge current I and duty cycle η [100].

3.1.3. Other methods for time estimation

Qualitative methods

Besides the previously discussed modelling techniques which result in a quantitative assessment of the removal rate, literature extensively reports about qualitative assessments of the effect of a large range of factors on the removal rate. Main interest has gone to the influence of process parameters on the removal rate. Khan [101] reported about the machining of mild steel and aluminum with copper and brass electrodes. It was observed that an increase in current resulted in a sharp increase in removal rate. The highest removal rate was noticed for the material combination brass – aluminum. In another study Che Haron et al. [102] observed that the application of low discharge current is more effective for smaller electrodes whereas the application of higher discharge current is more effective for larger electrodes. Lee et al. [103] investigated the effect of various parameters on the removal rate when machining tungsten carbide with a copper tungsten tool. They concluded that, opposed to the machining of conventional steels, a negative tool polarity results in the highest removal rate. In addition, an optimal flushing pressure was found.

Literature also reports on the relative importance of electrode materials for different workpiece materials on the removal rate. Che Haron et al. [104] observed higher removal rates for copper compared to graphite when machining XW42 tool steel. Singh et al. [105] compared 4 electrode materials

for the machining of EN-31 tool steel. It was found that copper results in the highest removal rate at high levels of discharge current. To conclude, Aas [106] compared 2 graphite grades for the machining of a nickel-based alloy. It was observed that the coarser grained graphite significantly outperformed the finer grained variant in terms of removal rate. On the other hand, the finer grained graphite shows a better performance during finishing operations.
Besides the process parameters and the materials used, the effect of flushing conditions on the MRR has also been subject to research. Section 3.2 will elaborate this in more detail.
Although these investigations did not result in quantitative formulations of the removal rate, these can serve as guidelines when being faced with a new product to be EDMed or when process parameters need to be changed. They can also be used as a starting point for subsequent quantitative investigations.

Knowledge based systems

Practical implementations of EDM time estimation into EDM machine software are up till now seldom. There is one reference to a commercial software named EDcam [73], [107] which is developed specifically for sinking EDM machines. Based on position data, machining geometries and number of workpieces this software firstly classifies the machining case into three distinctive groups: deep machining, shallow machining and standard machining (Fig. 3.4). In a following step the machining process and machining efficiency are determined which serve as the final input for the time estimation module. Experimental verification results showed an accuracy of 40%.

Opposed to the models discussed in sections 3.1.1 and 3.1.2, this method uses geometrical and flushing related information. However the entire system acts as a black box as the algorithms and concepts behind it (e.g. meaning and calculation of machining efficiency) are unclear.

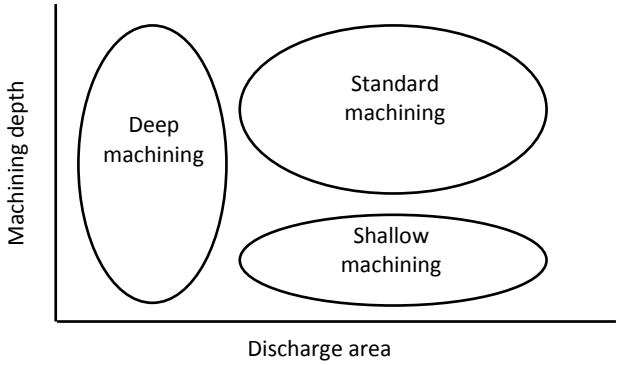

Fig. 3.4: Classification of machining case in EDcam software.

Technology curves

Opposed to the limited development of time estimation functionality, EDM machine tool builders mostly provide machine performance values. These are displayed in a 'technology curve' and represent the removal rate and surface roughness to be obtained per regime (see Appendix A). Here, a regime is defined as a group of generator settings (discharge current, discharge duration, etc.) and process parameters (e.g. parameters related to electrode motion) which define a certain step in the entire operation sequence. As an EDM job is composed of a sequence of regimes, knowledge about the removal rate per regime and the volume to be removed can lead to an estimation of the entire process time. Appendix A shows the technology curve for the material combination copper-steel with normal polarity applicable on the Charmilles Roboform 350ɣ. Besides an indication of the removal rate and the surface roughness, the expected volumetric electrode wear is also displayed.

Each EDM machine tool builder has his own procedure for determining technology curves. The following briefly outlines the procedure used by Charmilles Technologies. For every material combination and every regime a machining test is performed with a cylindrical electrode machining a cavity in the workpiece material. In the center of the cavity, a smaller hole is pre-machined acting as a flushing channel (see Fig. 3.5). During machining the flow through the flushing channel is adapted in such a way to obtain the maximal removal rate for a certain regime. Moreover, the frontal electrode area is chosen in such a way to obtain a current density or loading within the

range 5 to 15 A/cm² for copper electrodes and 5 to 10 A/cm² for graphite electrodes.
Although being a good means to relatively assess the regimes, the resulting time estimation will always lead to an underestimation mainly due to less optimal flushing conditions in practical machining cases being the result of complex electrode geometry or non-existence of flushing holes. Also deviations in current density can lead to inaccuracies.

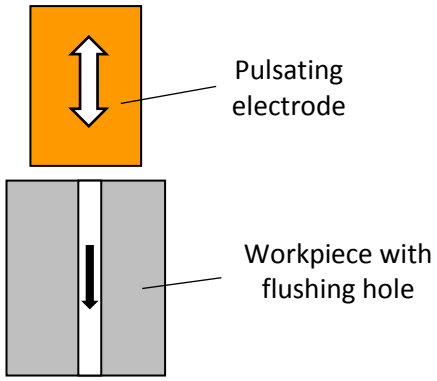

Fig. 3.5: Test setup to determine removal rates listed in technology curves.

Time estimation based on experience

Nowadays time estimation for sinking operations is mainly based on the operator's experience due to the lack of accurate and easy-to-use alternatives. For frequent recurring machining cases this is very straightforward leading to accurate time estimations. Also for machining cases which slightly differ from common cases in terms of slightly different material composition, small difference in dimensions of the features to be machined, etc. time estimations can be performed within acceptable limits. On the other hand, for machining cases which strongly differ from common cases (e.g. different set of geometrical features), for cases with a complex geometry and for cases with a low final roughness the estimation error can run up to 200% or even 300% [73].
This again highlights the need for the development of a time estimation concept which considers all main influencing factors without the burden of excessive testing.

3.2. Flushing

The majority of the previously discussed methods do not account for the influence of flushing properties on the process performance. However, removal of debris from the sparking gap is an important action for a stable and efficient EDM process. In order to understand the influence of flushing on the machining performance, this section gives an overview of literature stating the effect of flushing.

3.2.1. Influence on process performance

The quality of a discharge and hence its efficiency is to a great extent determined by the characteristics of the dielectric fluid, more specifically determined by the dielectric strength. As the machining progresses, debris are released in the working gap reducing the dielectric strength. A certain debris concentration is beneficial as it enhances the initiation of new discharges. Would this not be the case, higher energies per discharge would be needed and would result in a poor surface quality. In addition, a small concentration of debris would lead to a smaller working gap with the risk of introducing short circuits and the consequent unstableness [108]. On the other hand, a local accumulation or general saturation of the working gap with debris has to be avoided as it can lead to short circuits or arcs which strongly reduce the machining efficiency and deteriorate the surface quality of the workpiece and induce a significant amount of tool wear. This leads to the conclusion that an optimal debris density exists [109] resulting in a good process performance in terms of machining speed, tool wear, surface integrity and accuracy.

The ejection of debris from the working gap or flushing is thus an essential part of the EDM process. Ideally, flushing should lead to an optimal debris density which is uniform along the entire working gap. With most of the common flushing techniques it is difficult to obtain a uniform debris distribution. In [110] the flow fields in the frontal gap were modelled and experimentally verified. It was shown that the gap size at the outlet of the working gap is significantly larger compared to the inlet during pressure flushing due to a higher level of debris density. Moreover this study reported that the inclination of the bottom surface depends on the applied pressure which directly relates to the debris density. When simulating an increased and uniform debris density by using powder based dielectrics, it is shown that a widening of the gap occurs increasing the flushing potential of the working

gap [109]. Moreover, the higher concentration of particles shortens the ignition delay time resulting in an increase of the machining speed.
Besides the influence on MRR and accuracy there also exists an effect of the flushing conditions and debris density on the surface integrity. Zones in the working gap with a higher debris density, as a result of a low flushing rate, result in a higher crack density and thicker recast layer [111]. Similar results are noted when applying higher flushing rates that lead to a larger quenching effect of the EDM surface, initiating cracks. This shows that an optimal flow rate exists in terms of surface quality. Also in terms of MRR optimal flow rates have been determined [112].

3.2.2. Types of flushing

From all EDM types, the flushing conditions and hence debris density are the most difficult to control and influence in sinking EDM. Therefore, different flushing techniques have been developed to make the machining more consistent. The flushing techniques can be divided in two groups: direct and indirect flushing.
In direct flushing the removal of debris is performed by applying a forced fluid movement. A first way to perform this is by applying pressured fluid from the bottom of the cavity through a flushing hole (see Fig. 3.6.a). This is the most common approach [113], though it results in tapered cavities and electrode wear due to the higher concentration of debris ('dirty' fluid) at the side walls. In suction flushing the dielectric is drawn from all gaps through a flushing hole at the bottom of the cavity (Fig. 3.6.b) delivering clean fluid to the gap hence avoiding the disadvantages of tapered walls and increased wear. Another way is to locate the flushing hole in the electrode extracting the contaminated fluid (Fig. 3.6.c). All these methods need flushing holes which are mostly not desired. Direct flushing can also be applied by using nozzles that are aimed at the intersection of electrode and workpiece. The placement of the nozzles is essential for the good removal of debris. Some guidelines exist but mostly rely on the experience of the operator as every machining case is different. Fig. 3.7 shows the effect of the nozzle configuration on the flatness of the machined surface and the corresponding debris concentration. In case of opposite placed nozzles a groove in the middle of the surface is noticed as a result of the increased debris concentration in this area (Fig. 3.7.a). When applying the fluid from one side the groove is located to the outlet of the gap, again as a result of the higher debris concentration in that zone (Fig. 3.7.b). The flushing can be improved by applying a sweeping movement to nozzles located at both sides of the

sparking gap [108]. This results in a more uniform debris concentration and increased flatness (Fig. 3.7.c).

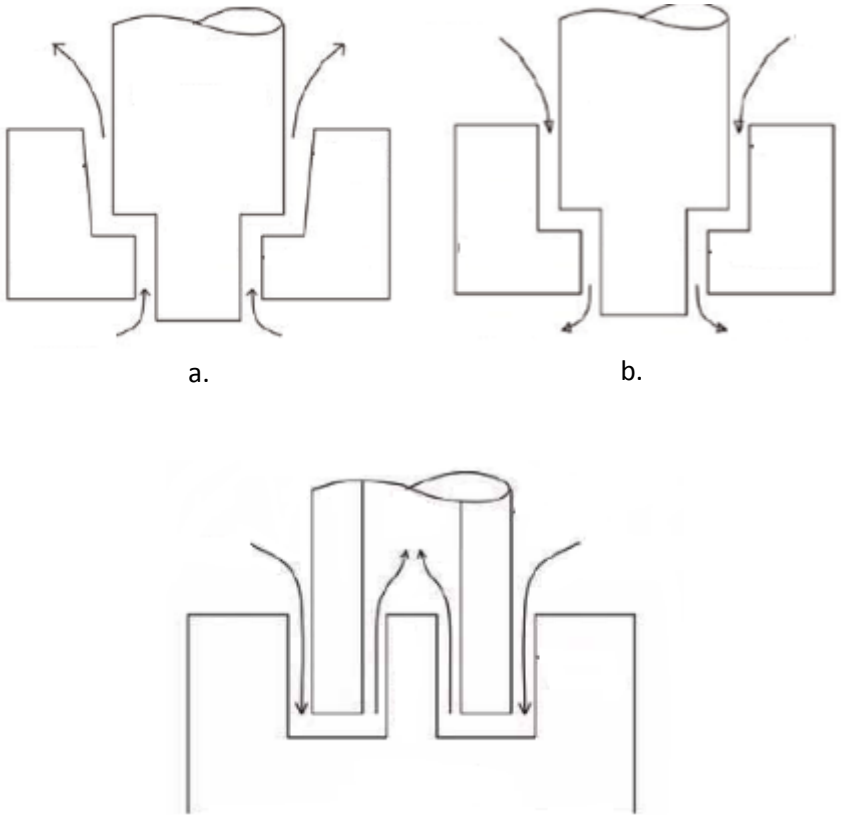

Fig. 3.6: Direct flushing methods: (a) Pressure flush from bottom; (b) suction flush from bottom; (c) flushing holes in electrode [113].

In indirect flushing techniques the fluid is moved by applying a movement to the tool or workpiece. The commonly used technique nowadays is the periodically lifting of the electrode that induces a pumping action on the fluid in the working gap. This is often the most effective method in case direct flushing cannot be applied. However, it should be considered that a major part of the machining time is lost to the pulsation movement. Moreover inaccuracies due to deflection of thin electrodes can occur and the technique

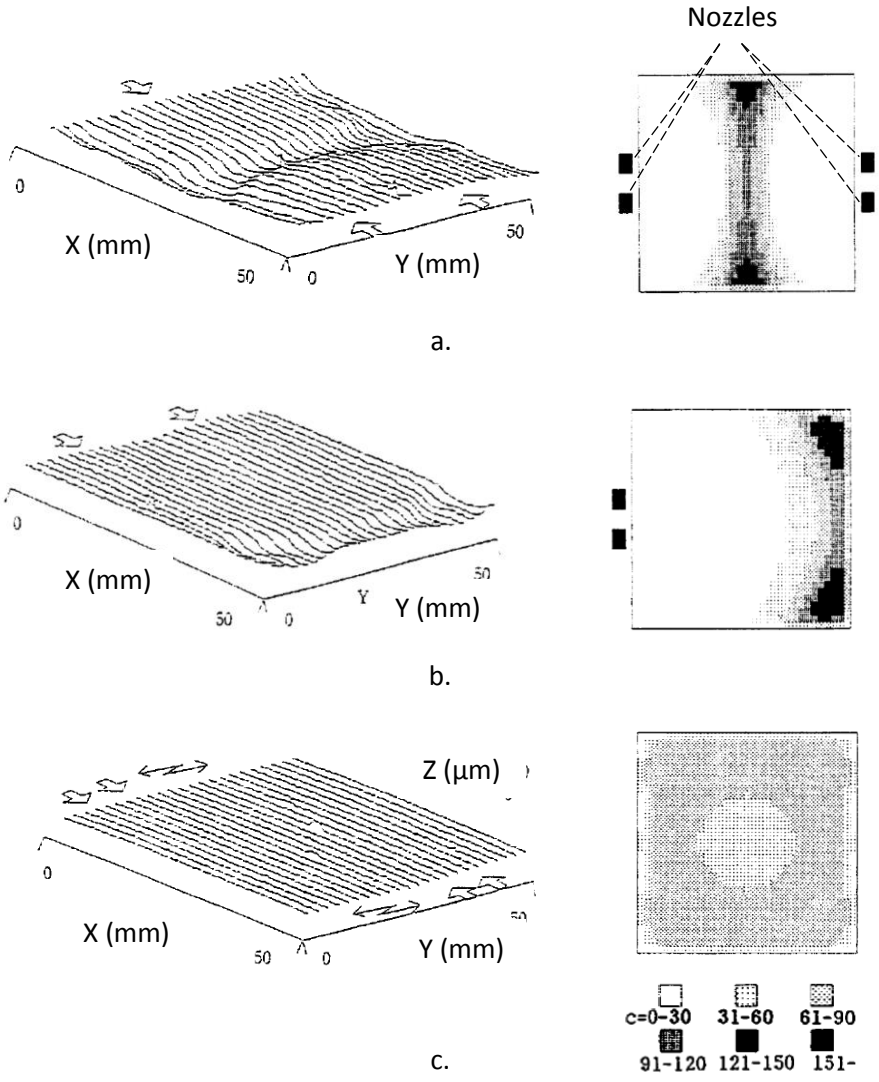

Fig. 3.7: Relation between flow fields and debris concentration for different flushing con: (a) nozzles at opposite sides; (b) nozzles at the same side; (c) flushing with sweeping method [108].

has the tendency to form dead points (i.e. locations where no flow exists) [108]. Recently this pulsation movement has been improved by applying linear motor systems instead of rotary motor systems with ball screws. With these linear motor systems shorter response times to changes in the gap are possible and problems with twist and backlash are avoided resulting in more accurate machining [114]. Another advantage compared to ball screw type

machines are the larger jump speeds (36 m/min and even higher) that can be obtained meaning that larger jump heights are possible. This increase in jump height has several positive effects on the EDM performance. The larger the jump height, the more effective debris is removed from the working gap as a larger volume of clean dielectric is introduced in the working gap [115], [116]. Fig. 3.8 shows the simulated movement of debris in the working gap during a pulsation movement with small jump height (Fig. 3.8.a) and large jump height (Fig. 3.8.b). These figures show that small jump heights only remove a fraction of the initial amount of debris, whereas large jump heights remove the majority of the initial amount of debris. As more debris is removed from both bottom and side gaps, the occurrence of secondary discharges is lower resulting in a reduced concavity of the side walls [117]. In addition, the lower debris density results in a smaller gap improving the accuracy of the operation. With these kind of linear motor systems it even becomes possible to obtain an effective machining operation for deep and narrow grooves (ribs) without the need for other flushing methods.

Opposed to the common pulsation movement, higher frequency pulsations have been tested for their effectiveness. By applying pulsation movements with ultrasonic frequencies and amplitudes in the order of magnitude of several microns an increase in MRR was noted, especially in finishing operations where small gaps apply [118]. A further increase in MRR is possible when combining the ultrasonic movement with a rotation of the electrode.

Besides pulsation movements the electrode can also be moved in a plane perpendicular to the sinking direction. This planetary movement is often applied in finishing operations to improve the difficult flushing conditions as a result of the narrow gaps during finishing. In [119] a combination of a pulsation downward movement and planetary movement, by adding a small movement in the horizontal plane to the pulsation, proved to result in an increased MRR. The larger the X-movement, the larger the effect on the MRR.

Other methods to improve the evacuation of debris from the working gap have been tested. In [120] the application of magnetic fields to transport the debris has shown to improve the removal efficiency. In [121] the application of a horizontal EDM setup shows to improve the machining speed on condition that an electrode rotation is applied.

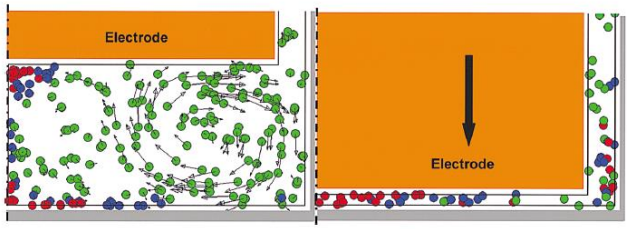

a.

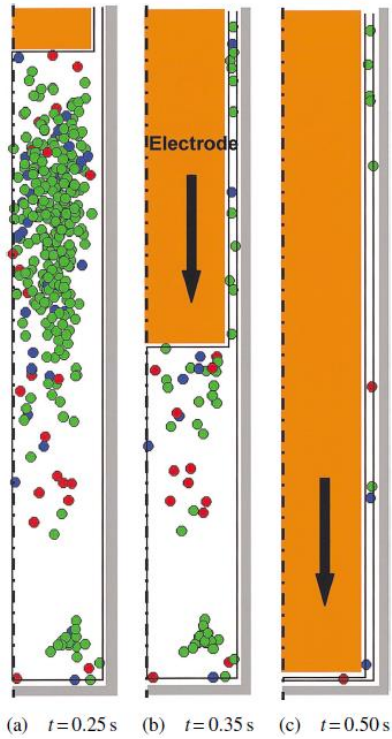

b.

Fig. 3.8: Simulation of debris movements during pulsation with linear motor system for (a) jump height of 2.4mm and (b) jump height of 38mm [117].

3.3. Research objectives for sinking EDM time estimations

As the EDM process is a time intensive process with large variations in machining time depending on the machining case, it is crucial to have this knowledge prior to machining in order to be able to establish a solid process planning. Especially for sinking EDM operations accurate knowledge of the machining time is needed as the flushing conditions have a large impact on the machining speed.

Since the introduction of the EDM process many attempts have been made to estimate the machining time. In the previous sections two approaches for EDM time estimation were discussed: theoretical and empirical modelling. On the one hand the theoretical models rely on assumptions, simplifications of reality and do not consider the effect of the flushing conditions. This results in underestimations of the actual machining time and, due to the specific nature of each model, lacks evidence for a broad range of applications. On the other hand empirical models, which are most often based on a limited set of (mostly electrical) parameters and are developed for a specific material combination, lack generality. In practice, most often time estimations are based on user experience or on technology tables provided by the machine tool builder. Although, being accurate for common cases, estimation errors can run up to 300% for complex or new cases.

Therefore, this study aims at establishing and elaborating a solid concept for time estimation of sinking EDM operations with the following approach and corresponding objectives.

- **Determination and quantification of the most important influencing factors** on sinking EDM time to provide an understanding of the numerous phenomena that have an effect on the machining speed. The focus in this study will be on machining cases with prismatic cavities as an inquiry among various European mould makers has shown that the main part of EDMed cavities have a prismatic shape. Opposed to previous attempts in EDM time estimation, special attention will be given to flushing related parameters.

- **Development of a mathematical model** based on an understanding of the underlying effects evidenced through machining experiments. The developed model will allow accurate time estimations with an estimation error lower than current methods. Assessments of the developed model will be based on the technology tables provided by the machine tool builders. The purpose of this model is to be applicable for a broad range of applications without the burden of performing excessive testing.

- **Implementation in a software tool** of the developed model to allow automated time calculations starting from user specifications and the CAD file of the cavity to be machined.

Chapter 4 Development of concept of time estimation for sinking EDM operations

4.1. Concept of time estimation

The concept of time estimation for sinking EDM operations that will be elaborated in this study consists of correcting reference values for material removal rate (MRR) or machining times, which are determined according to a predefined procedure. The corrections are based on deviations from the reference situation. The following paragraphs describe in more detail the elaboration of the proposed concept.

4.1.1. Reference values

Every EDM machine tool builder provides technology tables with material removal rates for every regime (i.e. combination of generator settings). An example of such technology table with the generator settings per regime can be found in Appendix A. Using these material removal rates as reference rates seems attractive, but the conditions under which these tests have been performed are mostly not known. Therefore, it was decided to develop an own calibration procedure. By performing a limited number of tests, the machine is characterized under known conditions (e.g. dielectric, etc.). The reference rates are determined empirically for every regime or generator setting hence including the effect of electrical parameters like discharge current, discharge duration, pulse interval time, servo etc. Moreover each regime has specific settings regarding electrode motion (maximum speed, time in between two motions etc.) which are then also taken into account in the reference. Although this looks similar to the procedure outlined in Section 3.1.3, the reference values in this concept are determined under machining conditions which resemble more to the daily practical use of EDM. Here, no additional flushing action, like the suction of debris as mentioned in Section 3.1.3, is applied resulting in more realistic values.
A more detailed description of the calibration procedure will be given in Sections 4.2.1 and 4.3.1.

4.1.2. Correction factors

A time estimation solely based on reference values will not give accurate results. Initial experiments showed that deviations from the reference values occur when comparing different machining cases although machining took place with identical generator settings on the same EDM machine. These deviations are the result of a difference in debris density in the sparking gap as already discussed in Section 3.2.1 The debris density is mainly influenced by two groups of parameters: flushing related parameters (e.g. electrode geometry, machining depth) and efficiency related parameters (e.g. i_e, t_e, t_0, current density). In the concept of this study deviations are taken into account by correcting the reference values. This correction is dependent on the machining case and machining conditions and is therefore function of factors causing a deviation in debris density. Mostly, an EDM program consists of a sequence of several regimes, each regime is characterized by a specific combination of generator settings often applied with a decreasing level of discharge energy. The total EDM time is then given by a summation of all corrected reference values over all applied regimes (Eq. 4.1).

$$\text{EDM Time} = \sum_{i=1}^{n} C_x \cdot \text{time}_{\text{ref, i}} \qquad \text{(Eq. 4.1)}$$

With: n number of regimes;
C_x correction on the reference time;
$\text{time}_{\text{ref,i}}$ reference time determined during calibration for regime i.

4.1.3. Distinction between roughing and finishing operations

In standard EDM operations two kinds of operations can be distinguished namely roughing and finishing operations. Roughing operations refer to the part of an EDM operation in which high energetic generator settings are used in combination with a sinking electrode movement (Fig. 4.1.a). These operations remove the bulk of the material in a relatively fast way and can be seen as volume removal operations. On the other hand finishing operations refer to the part of an EDM operation in which low energetic generator settings are used in combination with either a sinking or a planetary electrode movement (see Fig. 4.1.b) resulting in a much lower machining speed. The purpose of these operations is to obtain the desired end

roughness and geometrical accuracy making it rather a surface finishing operation than a volume removal operation. Moreover, the flushing conditions during finishing are different from those during roughing operations due to the significant smaller gap and the additional orbital electrode movement. In addition, another set of parameters will have an influence on the machining time in both types of operation meaning that other corrections need to be applied. Therefore, different analytical models have been developed for roughing and finishing operations based on the general concept given in Equation 4.1. The total EDM time is then estimated as the summation of the estimated roughing and finishing time (Eq. 4.2).

$$\text{EDM Time} = \sum_{i=1}^{n} C_{\text{roughing}} \cdot \text{time}_{\text{ref,i}} + \sum_{j=1}^{m} C_{\text{finishing}} \cdot \text{time}_{\text{ref, j}} \quad \text{(Eq. 4.2)}$$

With:
- n — number of regimes during the roughing operation;
- $C_{roughing}$ — correction on the $time_{ref,i}$ time for roughing operations;
- $time_{ref,i}$ — reference time determined during calibration for regime i.
- m — number of regimes during the finishing operation;
- $C_{finishing}$ — correction on $time_{ref,j}$ for finishing operations;
- $time_{ref,j}$ — reference time determined during calibration for regime j.

The modelling of the machining time for roughing and finishing operations will be discussed in the following paragraphs.

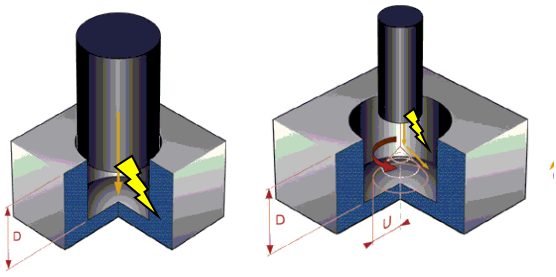

a. b.

Fig. 4.1: Distinction between a roughing operation (a) and finishing operation (b).

4.2. Time estimation for roughing operations

Roughing operations are defined as that part of the EDM operation removing the main part of the cavity volume. As the volume is the main driver for a roughing operation, the material removal rate (MRR) is a more suitable parameter to base the formulation on. With proper knowledge of the machining volume the roughing time can be calculated. The formulation given in Eq. 4.2 can be rewritten as follows:

$$\text{EDM Time}_{\text{roughing}} = \sum_{i=1}^{n} \frac{Vol_i}{C_R \cdot MRR_{ref,i}} \quad \text{(Eq. 4.3)}$$

With: n number of roughing regimes;
Vol_i volume to be removed during regime i;
C_R correction on $MRR_{ref,i}$ for roughing operations;
$MRR_{ref,i}$ reference value in terms of removal rate for regime i.

4.2.1. Calibration procedure for roughing operations

The procedure for determining the reference values for roughing operations consists of machining a cylindrical cavity by applying a downward electrode movement without electrode rotation, with electrode pulsation and without external flushing. The size of the cavity and the frontal electrode area are chosen in such a way to obtain a current density of 9 A/cm², as this is a commonly applied current density. As the MRR varies heavily along the machining depth, the obtained values for the MRR (MRRref) are determined per machining step of 1 mm. This is performed until a total machining depth of 20 mm is reached as it is seldom that larger machining depths need to be attained in practice.
The MRRref values need to be determined for every roughing regime, workpiece-electrode material combination and for every EDM machine. In this way the developed models and procedures can be applied for different machines. This procedure can be seen as a cumbersome task, but it can be done fairly simple in an automated manner with a relatively small set of simple electrodes. A repetition of the calibration procedure can also be seen as a way to assess the machine performance.

Fig. 4.2 shows an example of MRRref for regime E394 (see Appendix A for generator settings) for the combination copper-steel. It can be seen that the MRRef values are a function of the machining depth. Replications of the calibration procedure show that the variation on the reference values is small (see Fig. 4.2).

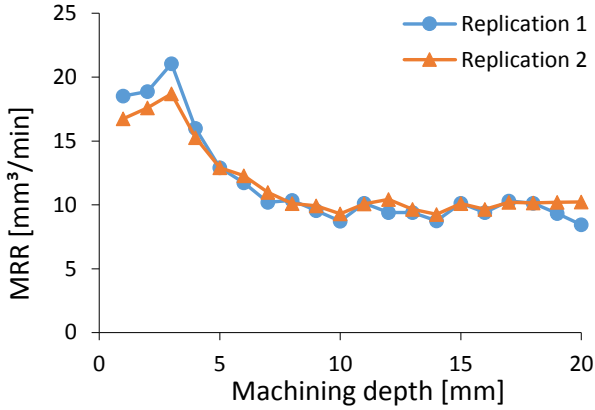

Fig. 4.2: Calibration values for regime E394 (cylindrical electrode – frontal area 1 cm²).

It is important to note that when small updates to the control strategy (including changes to pulsating electrode movement) of the machine are performed, this can influence the reference values as it directly affects the gap conditions. Fig. 4.3 shows the comparison of reference values for regime E434 between 2 software versions on the same EDM machine.

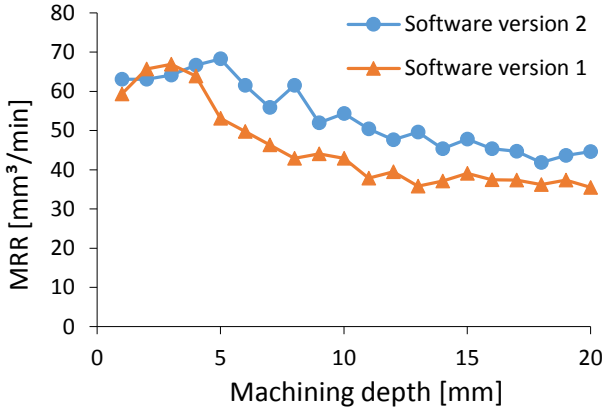

Fig. 4.3: Comparison of reference values for regime E434 for different versions of EDM software.

4.2.2. Determination of influencing factors

The correction on the reference values consists of all influences that lead to a deviation from the reference values. Based on an initial set of machining experiments and following the results of an enquiry performed within the frame of the EU-FP6 KnowEDM project (COLL-CT-2006-030238) [122], the effects of the following factors have been investigated and will be discussed in the next paragraphs:

- machining depth;
- frontal surface area;
- current density;
- electrode geometry;
- heat removal capacity;
- electrode material.

The effect of these parameters on the material removal rate (MRR), in terms of the deviation from the reference conditions, has been investigated. Observed trends and phenomena are further investigated by examining the influence of a factor on the debris density. As will be discussed further in this text, pulse classifications are used to correlate the machining conditions to the debris density hence the MRR.

All experiments are performed on a copper-steel (AISI D2) material combination, unless specified otherwise. In addition, all experiments are conducted with electrode pulsation and without external flushing.

Machining depth

The machining depth of an EDM operation is defined as the depth during machining with respect to a specific reference plane. This reference plane corresponds to the top plane of the cavity and does not necessarily coincides with the starting depth of the EDM operation (e.g. in the case of a pre-milled cavity). With this definition the depth is closely related to the flushing conditions, namely the machining depth relates to the distance debris need to travel to escape from the cavity. Literature has shown that this largely influences the machining performance [116]. As the operation progresses the flushing conditions change, influencing the debris density. As there exists an optimal debris density [109] flushing conditions which are highly effective result in a low debris density leading to a lower machining speed or removal rate. On the other hand, poor flushing conditions can

result in the accumulation of debris at the bottom of the cavity also reducing the machining speed.

The importance of flushing and its relation to the machining depth is shown in Fig. 4.4. Here the machining of a cavity is compared to the case in which a free surface without surrounding walls (see Fig. 4.5) is machined with the same machining parameters. In the case of the free surface no significant change in MRR was noted in relation to the machining depth due to constant flushing conditions i.e. debris can easily escape from the sparking gap resulting in a stable debris density and machining speed. Hence machining was only performed for the first millimeter of machining depth. On the other hand, flushing conditions change during the machining of a cavity resulting in fluctuations in MRR.
In this study only the machining of cavities will be considered. Nonetheless, these models can be applied for open machining cases by considering machining at small machining depth.

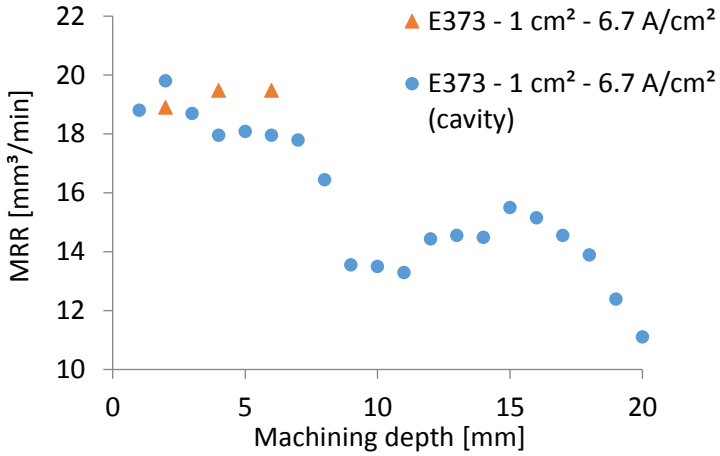

Fig. 4.4: Comparison of MRR in function of machining depth for the machining of a free surface and cavity under the same conditions.

As the machining depth has a large influence on the MRR during roughing operations, the calibration procedure is performed by logging the machining time every millimeter for a total depth of 20 mm (e.g. see Fig. 4.2). In this way the effect of the machining depth is already included. However, in practice deviations are noticed which are dependent on the machining depth. Fig. 4.6 shows an example

with a machining case in which the frontal surface area is twice as big as during calibration. The figure shows that the deviation from the reference values (given by the correction i.e. the ratio of the measured MRR to the reference MRR) is dependent on the machining depth.

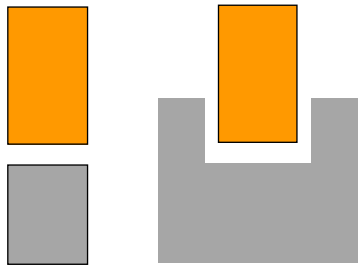

Fig. 4.5: Schematic representation of (a) free surface machining and (b) enclosed cavity machining.

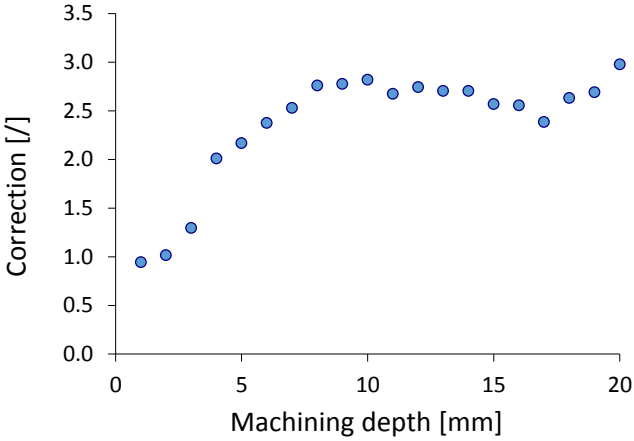

Fig. 4.6: Correction on reference MRR in function of machining depth for the machining of a rectangular cavity with frontal area 2 cm², current density of 4.5 A/cm² and regime E394.

As will be discussed in the following paragraphs, interactions between the machining depth and other parameters exist, meaning that the influence of the machining depth can vary with the machining conditions. In Section 3.2.2 it is already described that the influence of the machining depth is closely related to the flushing conditions.

Determination of the relation between external parameters and the machining behavior can be performed by monitoring and analyzing the pulses. Therefore, a pulse monitoring software has been developed to assess the type of pulses that occur at a certain moment during machining. In this study, three types of pulses are considered namely short circuits, arcs and normal pulses. A detailed explanation about the pulse analysis and classification can be found in Appendix B.

Fig. 4.7 shows a visual representation of the pulse analysis in function of the machining depth for the machining of a square cavity with a surface area of 50 mm², machined with regime E394 (current density 17.9 A/cm²). As can be seen from the figure, the pulse type distribution changes during machining. It can be seen that a large number of normal pulses is present in the beginning of the operation but decreases and stabilizes at a machining depth of 5 mm. On the other hand, the number of arcs and short circuits increases the first millimeters and stabilizes at larger machining depths. This points to the fact that as the machining progresses more debris gets accumulated in the machining gap leading to a higher debris density. As a consequence, the operation needs more time to remove the excess of debris hence resulting in a decrease of MRR. Due to the online adaptation of parameters like pulse interval time, duration of pulse train and duration of electrode pulsation the removal of debris stabilizes and leads to a constant MRR.

Frontal surface area

Besides the machining depth other parameters which influence the flushing conditions are likely to affect the MRR. One of these parameters is the frontal surface area of the electrode. This is the projection of the total active surface area of the electrode along the feed direction. Fig. 4.8 shows the frontal surface area A_1 at machining depth D_1. As for the elaboration of the model only prismatic electrodes will be considered, the frontal surface area is constant throughout the entire machining operation.

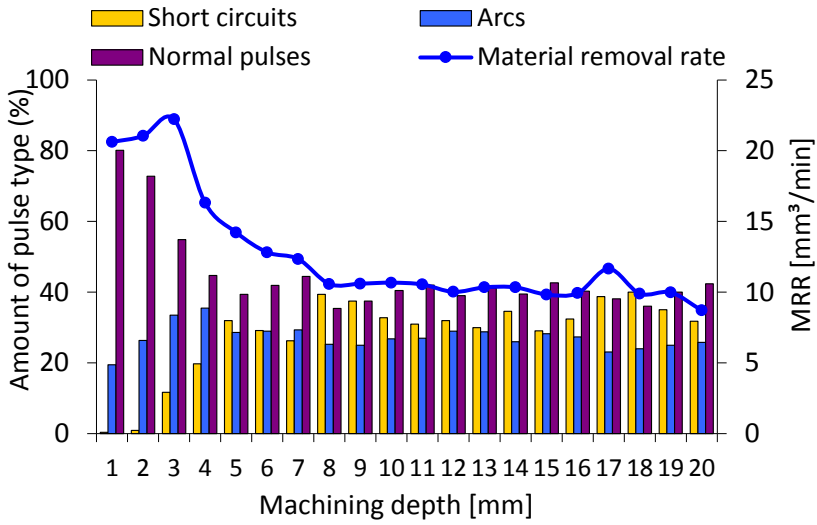

Fig. 4.7: Pulse distribution and MRR in function of machining depth for the machining of a rectangular cavity with frontal area 0.5 cm², current density 17.9 A/cm² and regime E394.

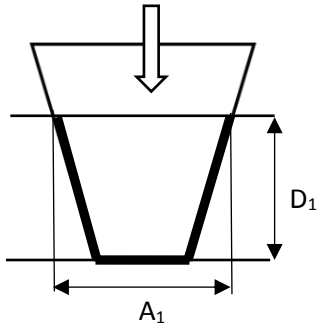

Fig. 4.8: Frontal surface area is projection of total active surface area along the feed direction.

The influence of the frontal surface area on the MRR has been shown by comparing the machining speed of electrodes with a different number of rectangular protrusions. In order to solely identify the effect of the frontal surface area, the current density is kept constant by using the same total frontal surface area for each electrode. All protrusions per electrode are identical and are situated far enough from each other in order to not disturb the outflow of debris from each sparking gap. In this way the frontal surface area per protrusions is the differentiating factor between the tested cases. Therefore, in the

remainder of this paragraph only the frontal area per protrusion will be mentioned. Machining experiments have been performed with electrodes with a total frontal surface area of 300 mm² and with four different frontal surface areas per protrusion ranging from 50 mm² (6 protrusions with frontal areas of 50 mm²) to 300 mm² (1 protrusion with a frontal area of 300 mm²). Table 4.1 lists the test setup.

Table 4.1: Test setup for determining the influence of the frontal area on MRR.

Frontal surface area/protrusion [mm²]	# Protrusions	Total frontal surface area [mm²]	Current density [A/cm²]
50	6	300	10.67
100	3	300	10.67
150	2	300	10.67
300	1	300	10.67

The effect of the considered frontal surface areas on the MRR in relation to the machining depth is shown in Fig. 4.9. This figure shows that the largest removal rates are obtained for frontal areas between 100 mm² and 150 mm². For smaller and larger frontal areas, respectively 50 mm² and 300 mm² significant ($\alpha = 0.05$) smaller MRR values were obtained. Similar results were obtained in the recent work of Kirchmann et al. [123] where frontal areas per protrusion ranging from 30 mm² to 140 mm² were studied. In this study, an increasing trend of the MRR in function of the frontal area was noticed.
For all tested frontal areas a decreasing trend of the MRR in function of the machining depth can be noticed. As the machining progresses deeper into the cavity the removal of debris from the sparking gap gets more difficult leading to an accumulation of debris which results in a higher number of arcs and short circuits. This is evidenced in Fig. 4.10 which shows a clear relation between the MRR and the number of normal pulses. The increasing number of arcs and short circuits denotes that the accumulation of debris in the sparking gap is due to poor flushing conditions. The fact that the largest MRR is noticed at frontal areas of 100 mm² and 150 mm² reflects better flushing conditions compared to the flushing conditions at 50 mm² and 300 mm². On the other hand, the MRR is the lowest at 300 mm² reflecting

flushing conditions which are less able to remove the accumulation of debris.

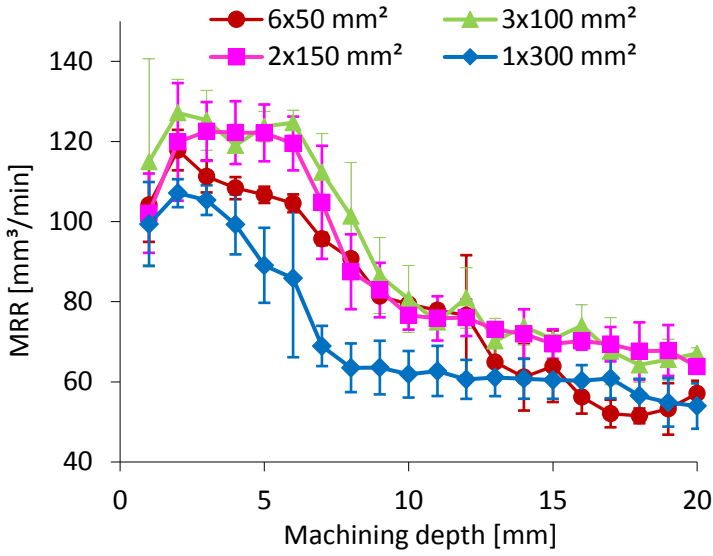

Fig. 4.9: MRR in function of the machining depth for different frontal areas and current density of 10.67 A/cm².

When comparing the influence of the frontal area on the MRR at different depths, it can be seen that a small interaction effect exists with the machining depth. Fig. 4.11 to Fig. 4.13 show that throughout the entire operation an optimal MRR is obtained for frontal areas between 100 mm² and 150 mm². Although in all figures the MRR is optimal at 100 mm² to 150 mm², this is not always reflected by the number of normal discharges. When making a distinction between normal discharges with a long t_d and a short t_d (see Appendix B for procedure of determining long and short t_d values), it can be shown that even if the total number of normal discharges decreases the number of normal discharges with a short t_d can increase (see Fig. 4.13). An increase in the number of normal pulses with a short t_d at the expense of normal pulses with a long t_d means that more pulses can occur during a certain time period when using a static pulse generator, resulting in a higher machining efficiency hence increase in machining speed. From the figures below it can be seen that the MRR follows a similar trend as the number of normal pulses with a short t_d in function of the frontal area. The increasing number of pulses with short delay

times point out that a higher debris density is present in the sparking gap which is mostly linked to the presence of more arcs (see Fig. 4.13).

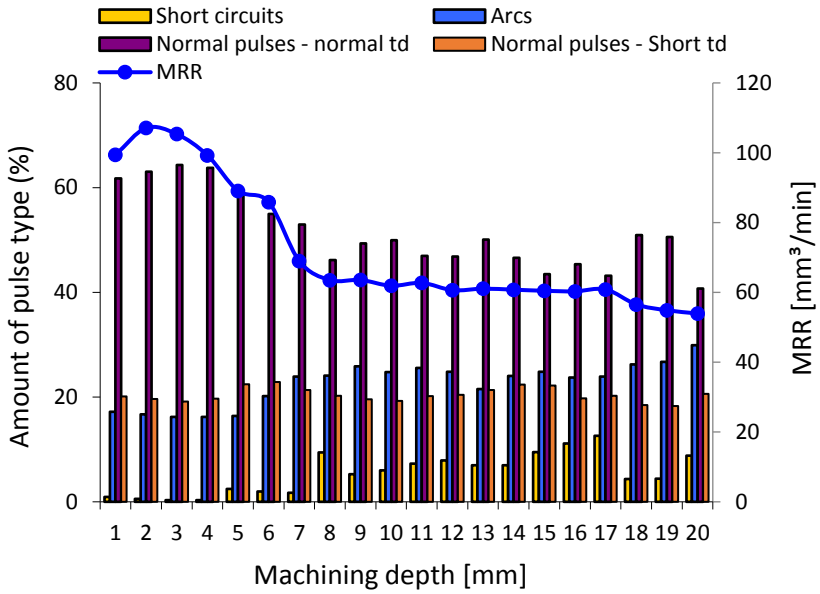

Fig. 4.10: Comparison of MRR and number of pulse types in function of the machining depth at a current density of 10.67 A/cm² and for a frontal area/protrusion of 300 mm².

Further experimentation showed that the optimal frontal area is dependent on the applied current density. Fig. 4.14 shows the results of similar machining experiments as those displayed in Table 4.1 but with a current density of 4.5 A/cm² by applying a lower energetic regime. This figure shows that for this current density the larger the frontal area the higher the MRR for machining depths until 15 mm. Despite the large spread on the results, the differences in MRR are significant ($\alpha = 0.05$), except for the difference in MRR between 100 mm² and 150 mm². The MRR is relatively constant throughout the operation, except for the first millimeters of depth, due to the stable gap conditions at this level of current density. Fig. 4.15 shows the pulse analysis in function of the machining depth for the case of 1 protrusion of 300 mm². Compared to Fig. 4.10 the number of arcs and short circuits is significantly lower in this case pointing to a lower debris density. At some points during the machining operation this even leads to a higher MRR than when applying the higher energetic regime like shown in Fig. 4.9.

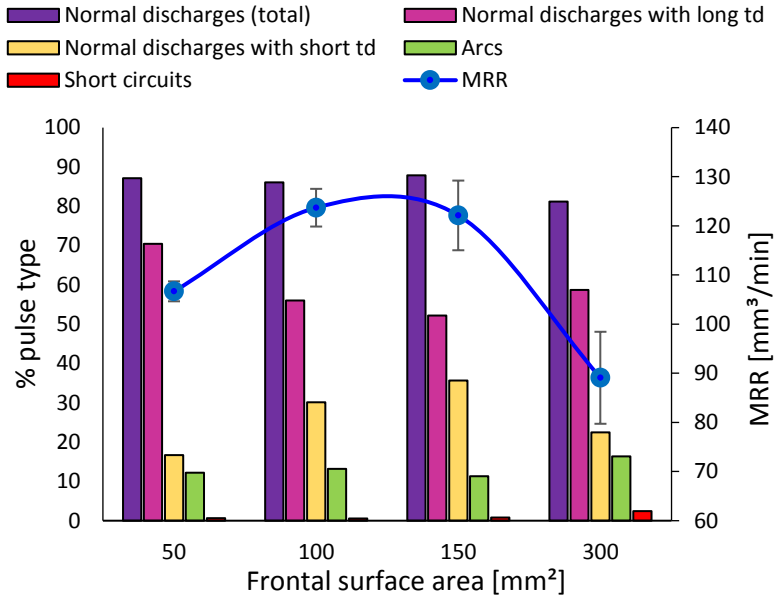

Fig. 4.11: MRR and number of pulse types in relation to the frontal surface area for a machining depth of 5 mm.

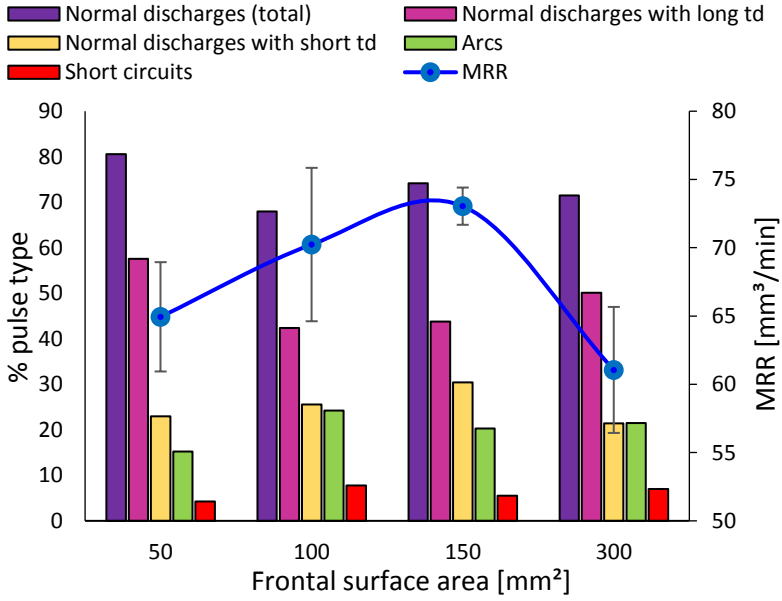

Fig. 4.12: MRR and number of pulse types in relation to the frontal surface area for a machining depth of 13 mm.

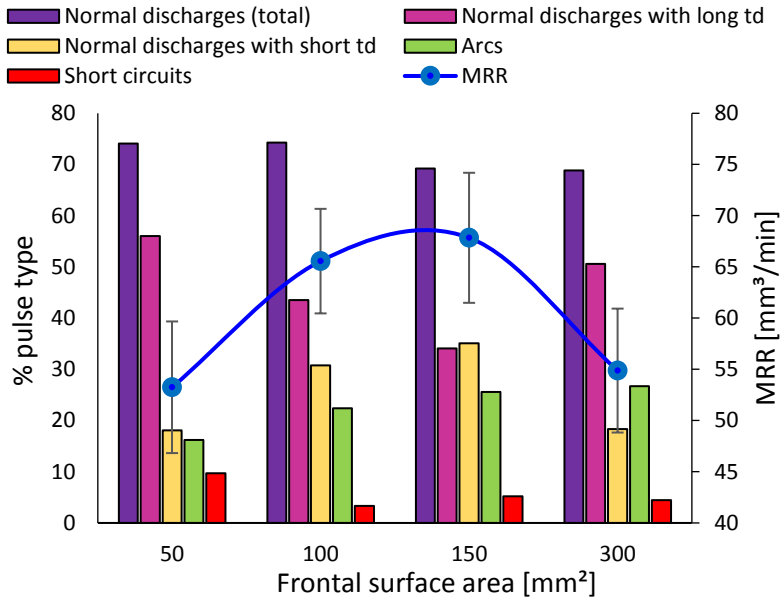

Fig. 4.13: MRR and number of pulse types in relation to the frontal surface area for a machining depth of 19 mm.

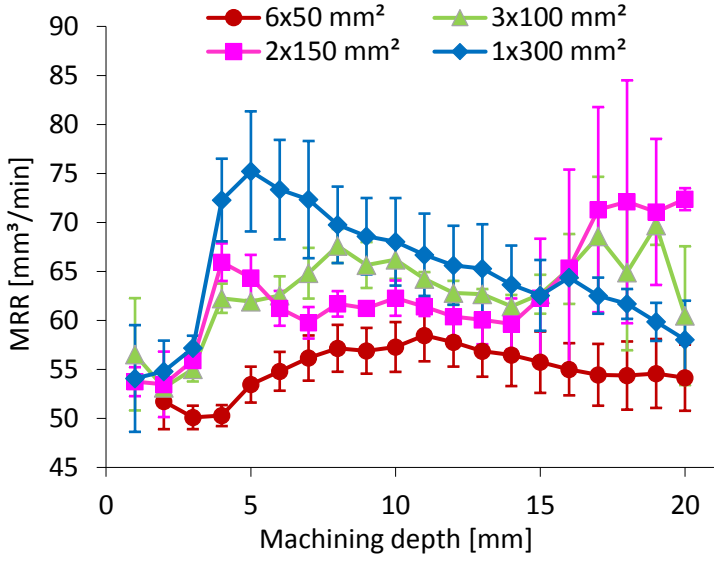

Fig. 4.14: MRR in function of the machining depth for different frontal areas and current density of 4.5 A/cm².

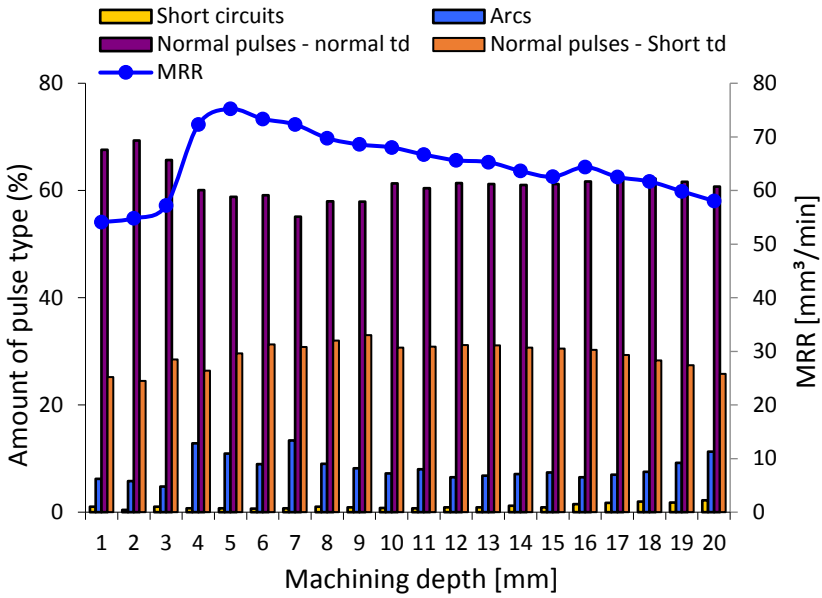

Fig. 4.15: Comparison of MRR and number of pulse types in function of the machining depth at a current density of 4.5 A/cm² and a frontal area/protrusion of 300 mm².

Whereas the interaction between the frontal surface area and the machining depth was small at the higher level of current density (see Fig. 4.9), an interaction effect exists for the lower level of current density. This is shown in Fig. 4.16 where the MRR is plotted in function of the frontal area for different machining depths. The increasing trend of the MRR in function of the frontal area at small machining depths changes to an optimal MRR at frontal areas between 100 mm² to 150 mm² at larger machining depths. This can be explained by the lower debris density occurring at the lower level of current density (4.5 A/cm²). Initially the debris density is suboptimal and increases faster for the cases with less protrusions as more debris are present in the same sparking gap i.e. MRR(1 x 300 mm²) is higher than MRR(3 x 100 mm²). As the machining progresses, the debris density increases due to more difficult flushing conditions and eventually can evolve to a situation comparable to the case of machining at the higher current density (10.67 A/cm²). This interaction effect is in agreement with a study of Lonardo et al. [124] where the combination of good flushing conditions and large sized electrodes lead to higher MRR.

It can be concluded that the influence of the frontal surface area on the MRR is affected by both the machining depth and the applied current density. The lower number of short circuits and arcs at 100 mm² and 150 mm² at the higher energy level, due to more stable flushing conditions, results in a higher MRR.

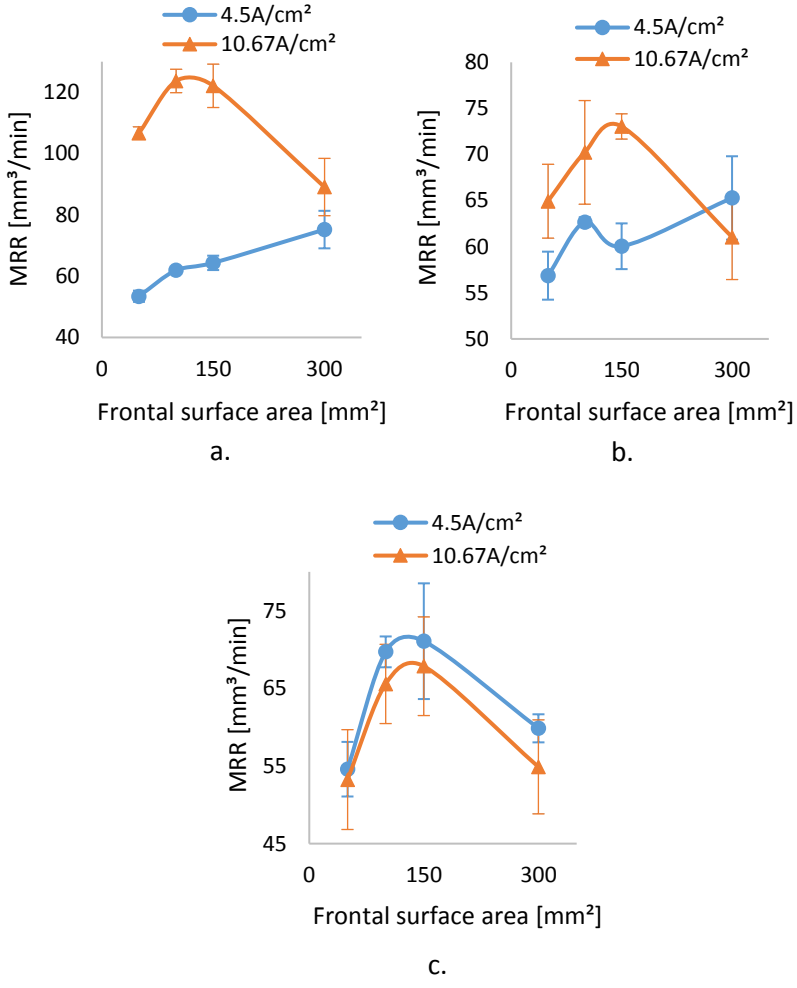

Fig. 4.16: MRR in function of the frontal surface area for 2 levels of current density at different machining depths: (a) 5 mm; (b) 13 mm; (c) 19 mm.

Loading/current intensity

As was shown in the previous paragraphs, the flushing conditions and the flushing behavior have a strong influence on the MRR due to their effect on the debris density. Besides the flushing conditions, also the applied energy, determined by the generator settings, has a significant influence on the debris density hence MRR. However, even for machining cases with identical flushing conditions and applied energy a difference in machining speed can be noticed. An example of this is the difference between machining with an electrode with one protrusion and machining with an electrode with multiple identical protrusions (see Fig. 4.17) with the same generator settings. In the case of machining with one protrusion all debris is concentrated in one sparking gap, whereas in the case of multiple identical protrusions the generated particles are spread over multiple sparking gaps, making it easier to be removed from the sparking gap. As this difference is related to the concentration of discharges per unit of active electrode area, the current density or loading [A/cm²] is a good measure to characterize this. The current density is defined as the ratio of the mean current flowing through the sparking gap during machining and the active frontal area. As for now, only prismatic geometries are considered and the loading during one generator regime is constant.

As was shown before, the effect of flushing related parameters is closely linked to the applied current density. Given that an optimal debris density exists (see Section 3.2.1), good flushing conditions in combination with a low current density, for a specific level of applied energy, will lead to a low debris density and hence a low machining speed. Moreover, the combination of poor flushing conditions and a high current density, for a specific level of applied energy, will lead to a high debris density (i.e. accumulation of debris) and hence a low machining speed. Combinations like high current density and good flushing conditions or a low current density and poor flushing conditions are more likely to result in a high machining speed. Although, in the latter case an accumulation of debris in the sparking gap is likely to occur as the machining progresses.

It should be noted that the current density should be limited to avoid local overheating of the electrode materials and arcing. Guidelines for

the maximal permissible current density for copper and graphite are respectively 15 A/cm² and 10 A/cm² [125].

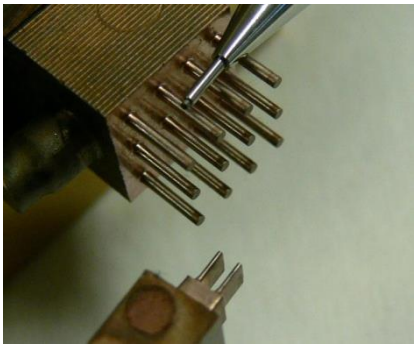

Fig. 4.17: Electrodes with multiple identical protrusions.

A change in current density can be caused by the following parameters:

- active frontal surface area;
- number of protrusions, which implies a change in the total active frontal surface area;
- generator regime.

As it is difficult in practical machining cases to decouple the influence of flushing related parameters and current density, an experiment with a setup shown in Fig. 4.18 has been conducted to investigate the influence of the current density independently of the flushing conditions. The setup consists of the machining of a cylindrical workpiece with a cylindrical electrode of the same diameter. By varying the frontal area of the electrode at constant discharge energy, the current density changes but the flushing conditions are assumed to stay constant due to the open machining case. Fig. 4.19 shows the results in terms of MRR and pulse type distribution of tests performed with this setup. It shows that the MRR decreases as the current density increases. This is caused by a change in pulse type distribution i.e. as the current density increases, the number of normal pulses decreases and the number of arcs and short circuits increases. This means that the downward trend of the MRR can be attributed to a higher debris density when increasing the current density. In addition, the overheating of the electrode as a consequence of a large current

density (e.g. in case of 34.46 A/cm² in Fig. 4.19) also induces arcs resulting in a lower MRR.

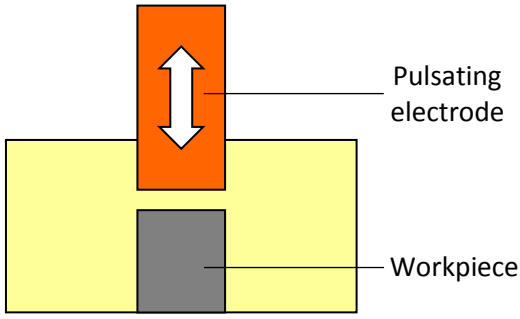

Fig. 4.18: Test setup for investigating the effect of the current density with constant flushing conditions.

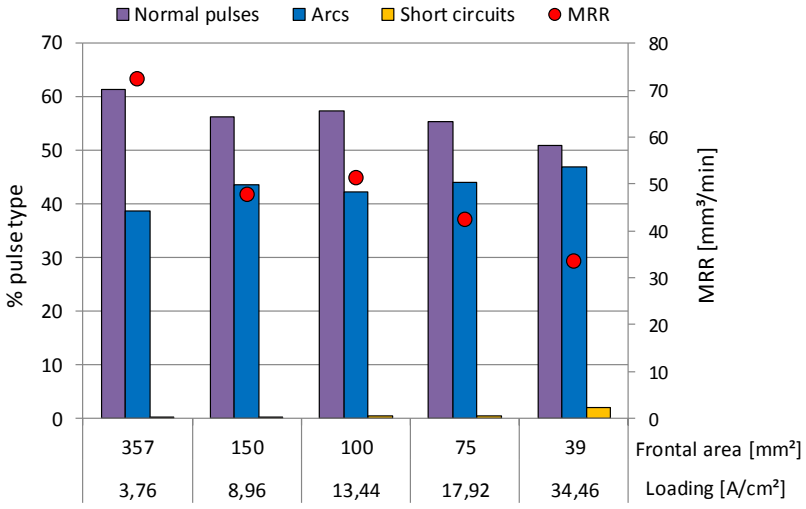

Fig. 4.19: Comparison of pulse types and MRR in function of the current density when machining with constant flushing conditions with regime E402.

This decreasing trend of the MRR in function of the current density can also be noticed when machining a cavity (see Fig. 4.4). Moreover, an interaction effect with the machining depth exists. This has been investigated by comparing the MRR of cases with a different number

of identical protrusions. In this way flushing conditions are kept constant by excluding the effect of the frontal electrode area. Table 4.2 shows the cases that were tested. From Fig. 4.20 different trends can be distinguished depending on the level of the current density:

- **Current density ≤ 4.5 A/cm²**: the MRR increases as the machining progresses down into the cavity. As the debris are divided over several 'working volumes', the debris density in the beginning of the operation is relatively low. As the machining progresses, the removal of debris will get less effective resulting in an increase of the debris density. Based on the increasing MRR it can be assumed that the density rises towards the optimal debris density.
- **Current density ≥ 6 A/cm²**: the MRR decreases as the machining progresses down into the cavity. The higher the current density, the larger the effect of the machining depth on the MRR. In this case the debris are located in a smaller 'working volume'. When the machining progresses and the flushing becomes less effective an accumulation of debris is likely to occur leading to a higher debris density. Due to the negative effect on the MRR it can be concluded that in these cases the debris density is higher than the optimal debris density.

For cases between 4.5 A/cm² and 6 A/cm² the MRR follows a similar trend for the first millimeters of machining depth as cases with a current density below 4.5 A/cm². However, for larger machining depths a trend similar to the one noticed for current densities above 6 A/cm² can be seen (see Fig. 4.20).

Table 4.2: Testing plan for determining the influence of the current density.

Frontal surface area/protrusion [mm²]	# Protrusions	Total frontal surface area [mm²]	Current density [A/cm²]
100	3	300	4.5
100	2	200	6.72
100	1	100	13.44

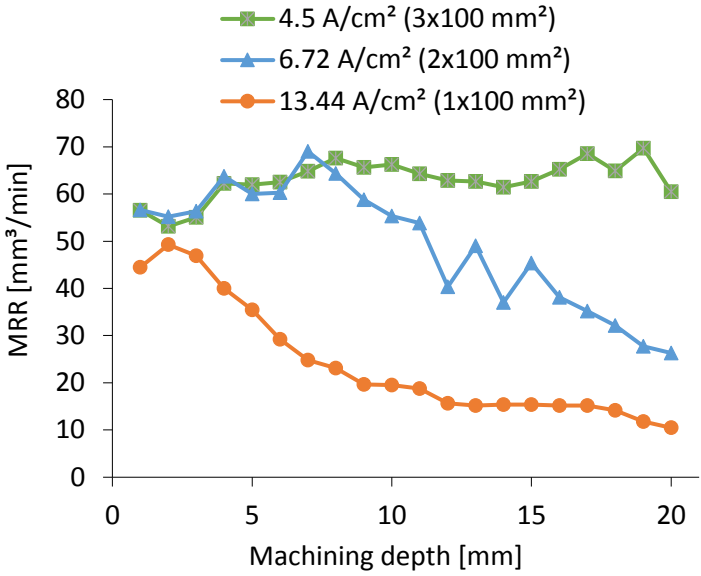

Fig. 4.20: Evolution of the MRR in function of the machining depth for different current densities when machining with regime E414.

Evidence for these trends can be found by performing a pulse analysis. Fig. 4.21 shows the evolution of the pulse type distribution and MRR along the machining depth for machining cases with different current density but with similar flushing conditions (frontal area: 6 x 50 mm²). As these cases cover different generator regimes, only qualitative comparisons can be made. For low current densities (4.5 A/cm², see Fig. 4.21) very low numbers of arcs and short circuits are noted. However, the increase in the number of normal pulses with short t_d points on an increase in debris density. As these pulse types also contribute to the removal of material, the MRR increases likewise. The difference in trend can be seen by comparing the case of 4.5 A/cm² with machining cases with higher current densities. For higher current densities a higher number of arcs and short circuits occurs (see Fig. 4.2 to Fig. 4.24) due to the existence of a higher debris density. Due to the higher current density a higher number of debris is located in similar working gaps. Moreover, the higher the current density the higher the number of short circuits. Also along the machining depth changes in pulse type distribution can be deducted from these figures. In the beginning of the operation the number of arcs and short circuits is relatively low resulting in an initially high MRR. When the machining progresses deeper into the cavity, the number of arcs and/or short

circuits increases hence lowering the machining speed. From Fig. 4.22 to Fig. 4.24 it can be seen that the higher the current density, the faster this decrease occurs.

It must be noted that the machine reacts to an increase in arcs and short circuits by adapting parameters like pulse interval time, pulse train time and parameters related to the vertical electrode movement. In cases where a high debris density occurs, more time is needed to evacuate the excess of debris from the sparking gap hence reducing the machining speed. In the continuous process of adaptation the machine controller tries to reduce the number of arcs and short circuits. Depending on the situation, the machining speed stabilizes or slightly decreases. An example of this is shown in Fig. 4.4 where the MRR drops at 3 mm depth due to an increase in the number of short circuits. Around 7 mm in depth, the machine controller can stabilize the increase of short circuits which stabilizes the MRR. Still a small decrease in MRR is noted for larger machining depths due to the less effective flushing.

These results confirm why electrodes with multiple protrusions are widely used in industry. When applying the same generator settings, it is more beneficial in terms of MRR to machine several cavities simultaneously with an electrode with multiple protrusions instead of machining every cavity with an electrode with a single protrusion. This conclusion is strengthened by the recent work of Kirchmann et al. [123] that also found that using electrodes with an increasing number protrusions is more beneficial in terms of MRR. However, this does not say anything about which generator setting to use. When aiming at a certain current density, it is possible to achieve this with a low energetic regime with a low number of protrusions or with a high energetic regime with a high number of protrusions. Fig. 4.25 shows different machining cases with similar current density but different regimes and different number of identical protrusions resulting in comparable flushing conditions. By comparing the cases in pairs of similar current density it can be concluded that the high energetic regimes (denoted by a higher E-number) combined with a high number of protrusions are beneficial with respect to the MRR (e.g. 21 A/cm² - E463 results in significantly higher MRR compared to

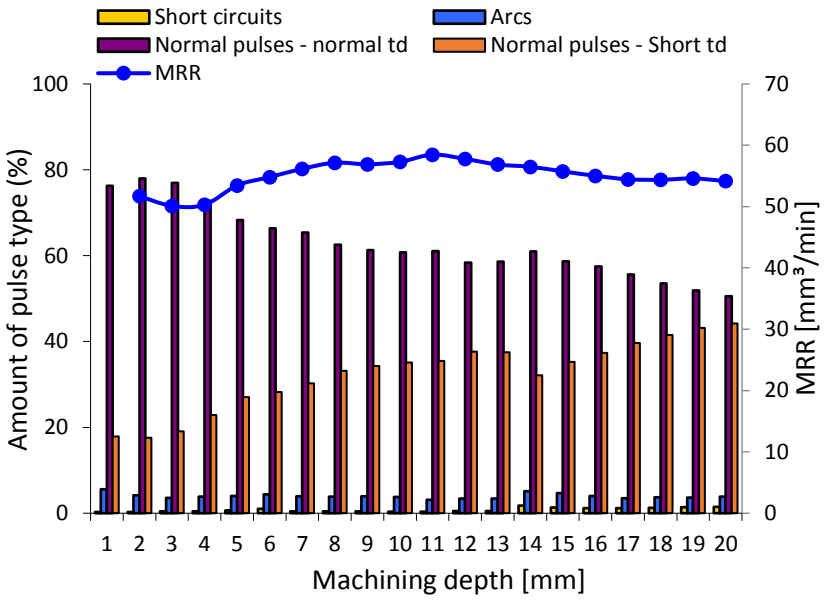

Fig. 4.21: Pulse type distribution and MRR in function of machining depth at 4.5 A/cm² (E414 – 6x50 mm² electrode protrusions).

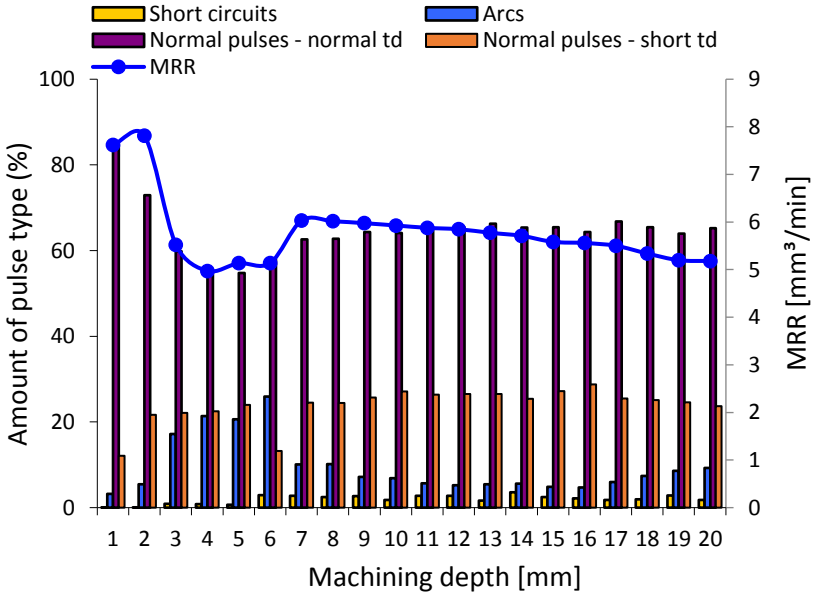

Fig. 4.22: Pulse type distribution and MRR in function of machining depth at 6.9 A/cm² (E323 –1x50 mm² electrode protrusion).

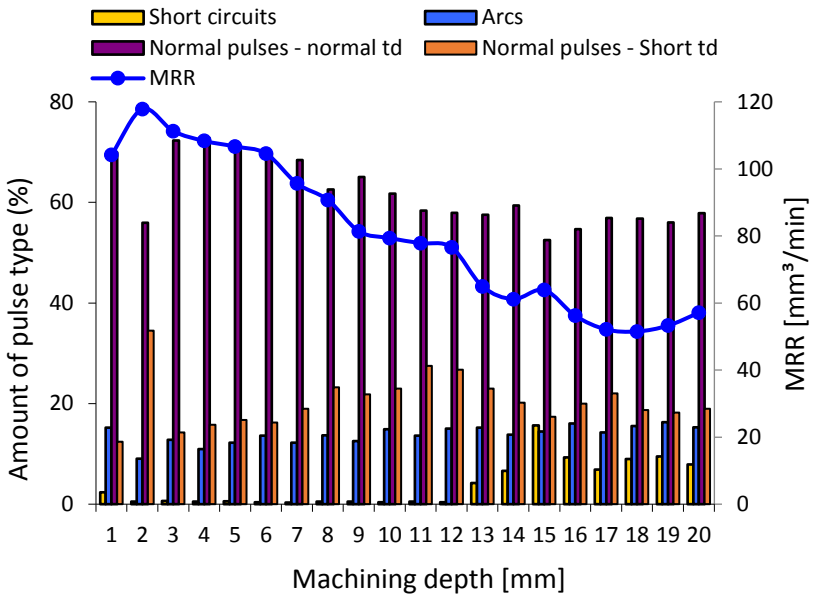

Fig. 4.23: Pulse type distribution and MRR in function of machining depth at 11 A/cm² (E453 –6x50 mm² electrode protrusion).

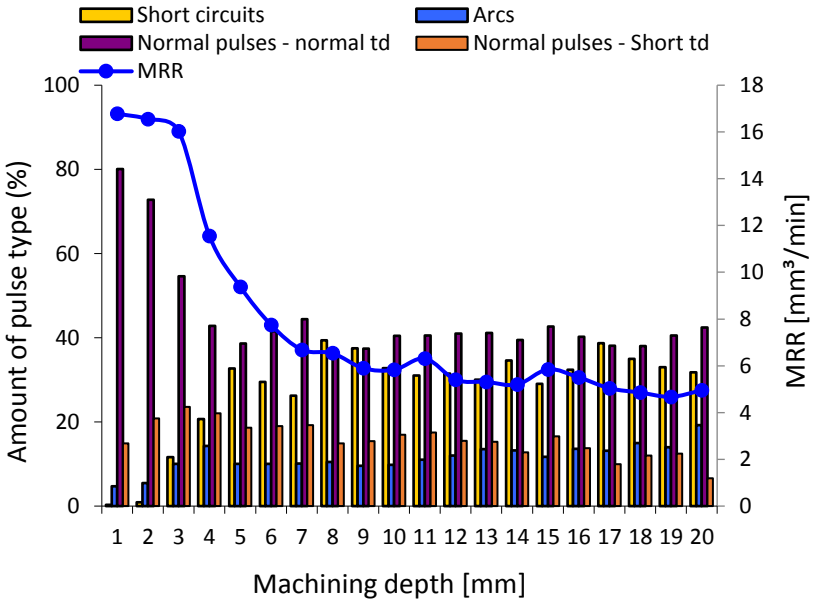

Fig. 4.24: Pulse type distribution and MRR in function of machining depth at 17.9 A/cm² (E394 –1x50 mm² electrode protrusion).

20 A/cm² - E434). This is due to the fact that for the same current density, the debris are divided in several sparking gaps which results in a more effective flushing of the sparking gap.

As a conclusion for practical machining cases, the previous has shown that a low current density achieved by a high energetic regime in combination with an electrode with multiple protrusions leads to the highest MRR.

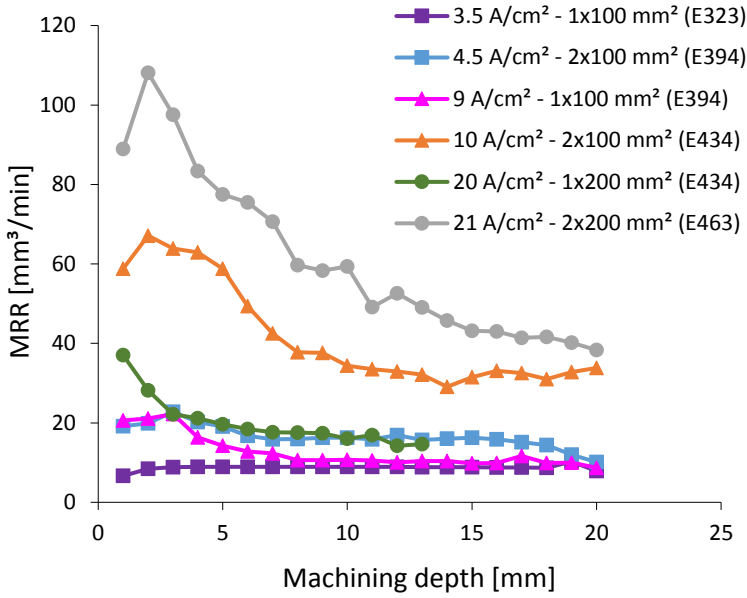

Fig. 4.25: Comparison of MRR in function of machining depth in pairs of similar current density between machining cases with identical frontal surface area per protrusion but different energy settings.

Electrode geometry

Besides the machining depth and the frontal surface area of the electrode also the electrode geometry is influencing the flushing conditions in the sparking gap and hence influencing the machining speed. A questionnaire distributed among European tool and mould makers within the frame of the EU-FP6 KnowEDM project showed that

the most common sinking EDM features are prismatic. Therefore, in this research initial experiments were conducted with rectangular, cylindrical and triangular shaped electrodes. In order to be able to exclusively investigate the influence of the electrode geometry, other parameters like frontal surface area and generator settings were kept constant. Fig. 4.26.a shows a comparison of the MRR for the considered geometries with a frontal area of 3 cm^2 and by applying generator regime E373 resulting in a current density of 2.25 A/cm^2. This figure shows that a similar trend exists for all geometries but that a significantly higher MRR is obtained for a cylindrical electrode. The MRR for triangular and rectangular electrodes is similar. On the contrary, when performing the same machining experiments by applying a higher current density (6.7 A/cm^2; regime E434) similar MRR values are obtained for cylindrical and triangular electrodes which are significantly higher compared to rectangular electrodes (see Fig. 4.26.b). The results at the higher current density level suggest that cylindrical and triangular geometries can more effectively remove debris from the sparking gap as the debris density tends to be higher at this current density level. However, within the scope of this study no clear explanation for these observations could be made. Nonetheless, these observations show that there is an interaction effect between the electrode geometry and the current density. When comparing the deviations in MRR with reference to the rectangular case (see Fig. 4.27) it can be noted that for low current densities a model based on rectangular geometries would lead to acceptable deviations in the order of ±20% whereas for higher current densities such a model would lead to large overestimations of the MRR. This shows that a model purely based on rectangular cavities has the risk of a certain level of estimation inaccuracy.

Within the group of rectangular electrodes a further distinction can be made based on the ratio length to width (L/W). Shapes with a large L/W ratio are so-called rib-like shapes. These shapes are widely machined by sinking EDM as these are not easy to machine by using a conventional machining process. Due to the large L/W ratio it can be expected that the flushing behavior will deviate from a simple pocket (rectangular cavity with small L/W ratio). Therefore, most machine tool builders define different technologies for pockets (standard application) and ribs (ribs application). The major difference is that

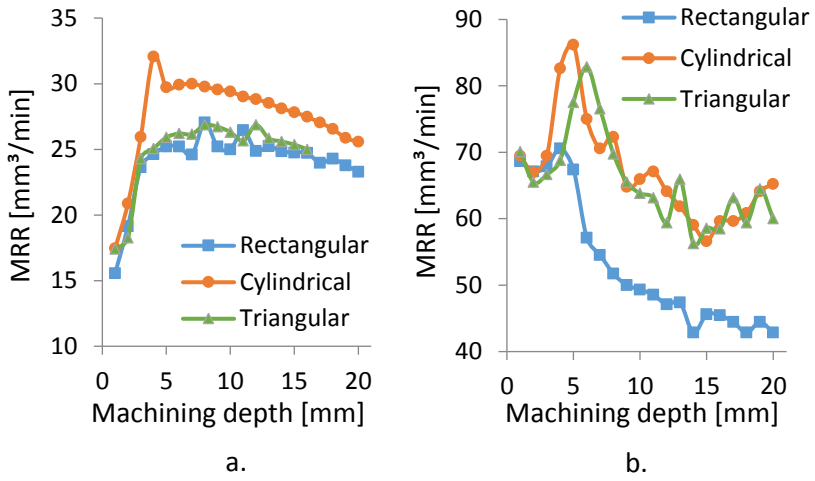

Fig. 4.26: MRR in function of machining depth for different electrode geometries and different current densities: (a) 2.25 A/cm²; (b) 6.7 A/cm².

when applying the rib application the maximal velocity, acceleration and jerk during the vertical electrode movement are significantly higher compared to the standard application. A comparison of the MRR between pockets on the one hand and rib-like features machined with both standard and rib application (see Fig. 4.28) shows that a significant difference in trend can be noted between pockets and ribs when using the standard application. This shows that the flushing behavior is different. From Fig. 4.29, which displays the results of numerous experiments with different conditions, it can be concluded that deviations in MRR can run up to 80% or more.

On the other hand, when applying the rib application for machining rib-like features a similar trend as when machining a pocket with the standard application can be noted. Due to the different flushing related parameters the flushing behavior seems to be comparable. Here the deviations in MRR are much smaller i.e. 80% of the tested cases show deviations within 25% of the MRR for a comparable pocket. This shows that for most of the machining cases where rib-like features are present a time estimation based on pockets can be used.

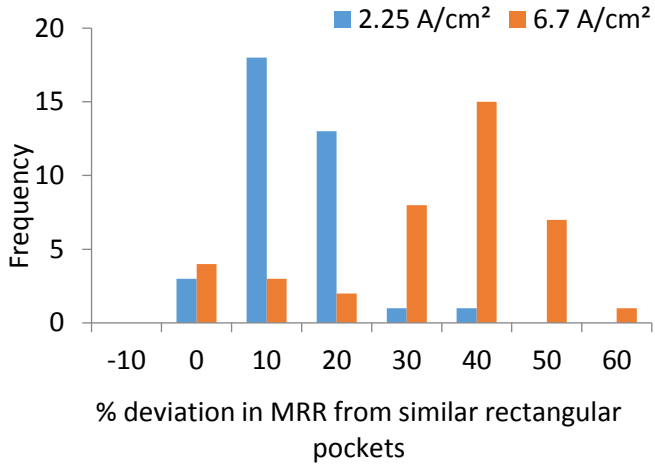

Fig. 4.27: Histogram of % deviation in MRR between rectangular and non-rectangular electrode geometries for current densities of 2.25 A/cm² and 6.7 A/cm².

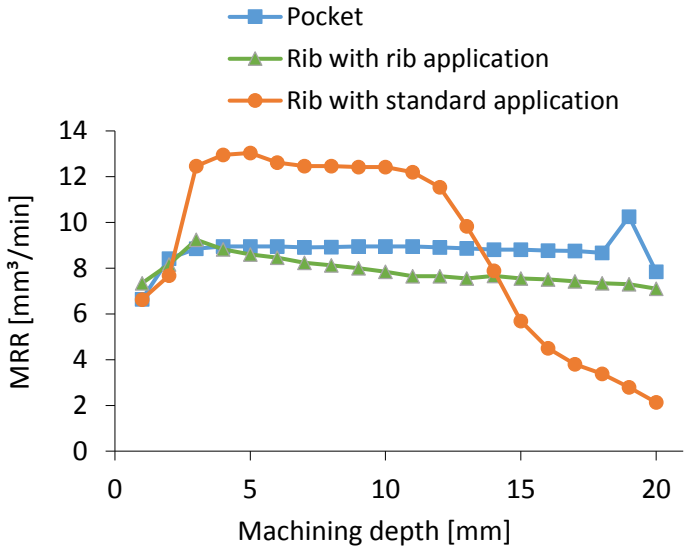

Fig. 4.28: Comparison of MRR for machining pockets and rib-like features with different technologies (standard and rib application) with regime E323, frontal area of 1 cm² and current density of 3.5 A/cm².

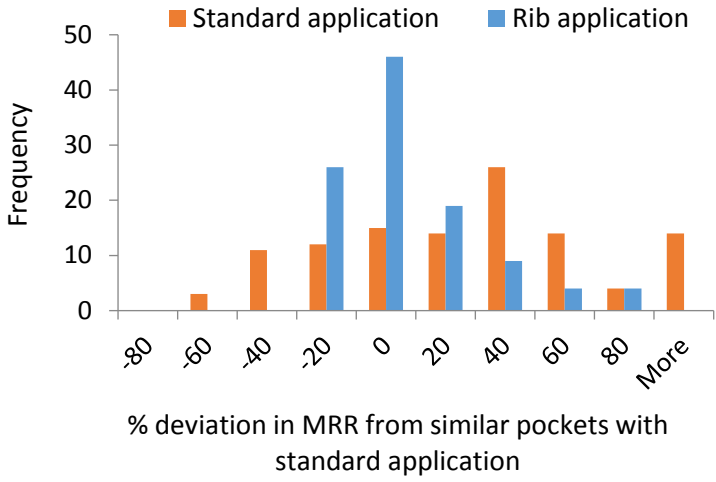

Fig. 4.29: Histogram of deviations in MRR for machining rib-like features with standard and rib application compared to machining pockets with the same frontal area by using the standard application.

Capacity to remove heat

The previous paragraphs discussed parameters that were considered due to their effect on the flushing conditions and debris density. As EDM is an electro-thermal process, parameters that influence the thermal behavior are also likely to have an impact on the MRR. In his work, Van Dijck states that up to 90% of the electrical input energy is dissipated through the solid volume of the electrodes [17]. Hence, parameters that influence the heat dissipation are likely to influence the MRR. Natsu et al. [126] measured the difference in plasma temperature between electrodes with a difference in diameter by using the same generator settings. It was shown that in cases with a higher thermal resistance, a higher temperature in the plasma and at both cathode and anode side was measured. In addition, the effect of the electrodes temperature on the MRR was shown by Essiptchouk et al. in the application of electric-arc gas heaters [127]. The higher the cathode temperature, the higher the MRR. In line with these findings, experiments were conducted to investigate the influence of the electrode (anode) shape on the MRR with cases in the application range of this study. The parameter that is considered is the ratio of the

total electrode surface area and the electrode volume (A_{tot}/Vol) as it reflects the possibility to evacuate the heat from the electrode to the dielectric by convection. The purpose of this parameter is to examine the effect on the MRR of the electrode geometry which is not actively taking part in the machining operation. A testing plan with electrode properties as displayed in Table 4.3 was performed by using a high energy setting (E463 – i_e: 64 A). Two levels of current density were applied by varying the frontal electrode area. Fig. 4.30 shows the electrodes of cases 3 and 4 with a clear difference in heat dissipation potential to the dielectric. During the experiments the temperature was measured with a thermocouple at a distance of 1 cm from the active electrode area (bottom surface of electrode) to monitor the temperature evolution during machining.

Table 4.3: Overview of electrode properties for testing plan regarding the influence of the electrode shape on the MRR.

#	Area (A_{tot}) [mm²]	Volume (Vol) [mm³]	Area/volume (A_{tot}/Vol) [mm^{-1}]	Frontal area [mm²]	Current density [A/cm²]
1	7600	32000	0,23	200	22,7
2	21011	32090	0,65	200	22,7
3	8823	39233	0,22	500	9,1
4	27151	39295	0,69	500	9,1

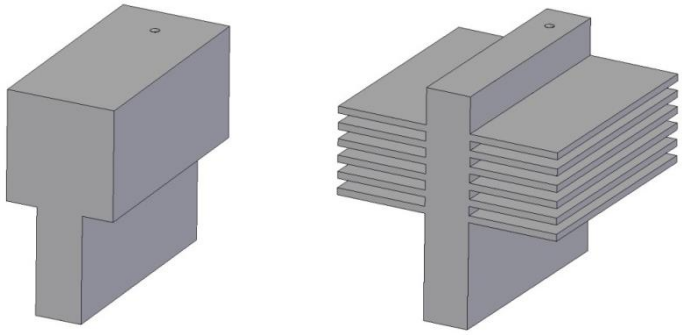

Fig. 4.30: Electrodes with different A_{tot}/Vol ratio (left: A_{tot}/Vol = 0.22; right: A_{tot}/Vol = 0.69) but identical frontal surface area (500 mm²).

Fig. 4.31 shows the results of the temperature measurements in the electrodes. It can be seen that for both levels of current density, the

cases where A_{tot}/Vol is high result in the lowest temperature due to a good heat dissipation to the surroundings. In the case of 22.7 A/cm² the electrode immediately heats up to its maximal temperature and keeps a stable temperature throughout the operation. On the contrary, in the cases of 9.1 A/cm² or frontal area of 500 mm² the electrodes temperature keeps increasing during the operation due to the lower thermal resistance in the vicinity of the sparking area (2.5 times lower as a result of the larger frontal area) in the area where the measurement was performed. The effect of the different temperature profiles on the MRR is shown in Fig. 4.32. It would be expected that a lower A_{tot}/Vol ratio results in a higher MRR, though the results do not show a significant difference (α=0.05) between the considered A_{tot}/Vol levels. A significant difference in MRR between the levels of current density can be noticed. However, this cannot be attributed to a difference in heat dissipation. As these experiments concern the machining of cavities, the flushing conditions as a result of a difference in frontal area and current density cannot be neglected.

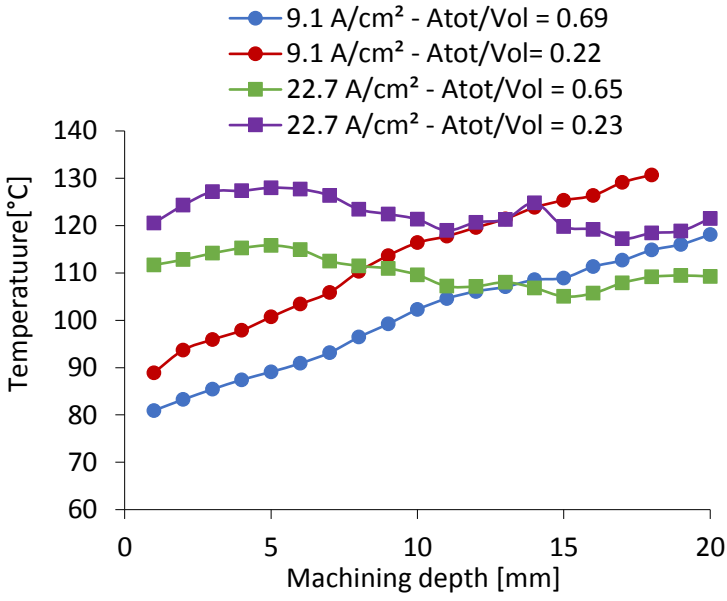

Fig. 4.31: Evolution of temperature measured at 1cm from the active electrode area for different current densities and A_{tot}/Vol ratio.

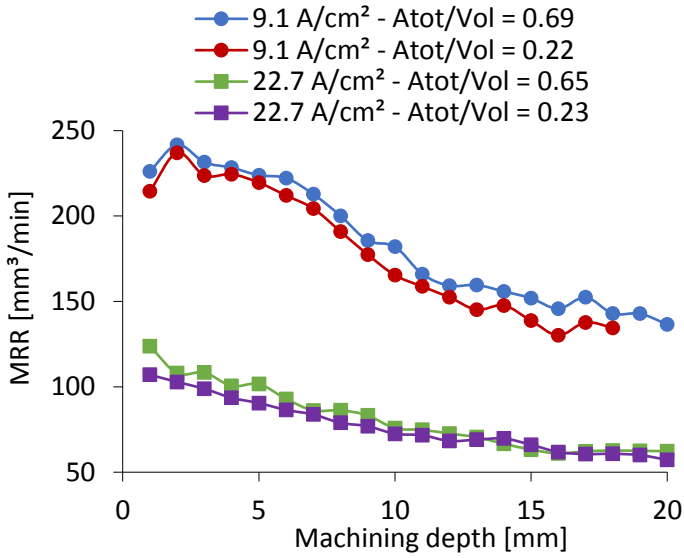

Fig. 4.32: Evolution of MRR for different current densities and A_{tot}/Vol ratio.

It can be concluded that the way the electrodes volume above the active area is designed has an influence on how the heat is dissipated to the surroundings but has no significant effect on the MRR.

Electrode material

As explained in Section 4.2.1, the reference values are determined for each material combination (workpiece – electrode). The following paragraph discusses why this needs to be done and what the effects are on the time estimation model.

In literature the performance in terms of MRR, tool wear and surface finish for a broad range of electrode materials has been investigated. The results of these studies have to be considered apart from each other as the workpiece-electrode material combination determines the performance. For example Che Haron et al. [104] showed that copper outperforms graphite regarding MRR when machining XW42 tool steel, whereas in the study of Amorim et al. [128] the application of graphite as electrode material with negative polarity results in a higher MRR when machining AISI P20 tool steel.

In this study machining cases with copper electrodes have been compared to identical machining cases with graphite electrodes (material: POCO – EDM3 with particle size < 5 µm). Comparisons have been made with identical generator settings in order to exclude their effect. When performing the calibration procedure for both electrode materials with generator settings displayed in Table 4.4 with a frontal electrode area of 1 cm² (hence current density of 8.96 A/cm²) different trends can be noticed (see Fig. 4.33.a), especially in the beginning of the operation. The difference in trend is confirmed by comparing MRRref values for both materials with other generator settings. From this it can be concluded that the calibration procedure has to be performed for every electrode material.

Table 4.4: Generator settings used for comparing the copper and graphite technology.

Discharge current i_e [A]	Pulse duration t_e [µs]	Pulse interval time t_0 [µs]	Servo(*) [%]
16	400	100	30

(*) Servo acts as a target value for the discharge delay time t_d

More important is to investigate how the MRR deviates from these reference values. Fig. 4.33.b shows an example of such a comparison by using the settings from Table 4.4 for machining a rectangular cavity with an electrode with a frontal area of 0.5 cm², hence a current density of 17.9 A/cm². Here also, the evolution of the MRR along the machining depth is different for both materials. But when looking at the deviation from the reference values a similar trend can be noticed (see Fig. 4.34). As this study focuses on the deviation from the MRRref, no clear explanation for the difference in MRR has been shown. However, it can be assumed that this is possibly due to different control parameters for both materials. On average the difference in deviation from MRRref is around 13% with a maximum of 27% (based on 4 comparison cases). As the example in Fig. 4.33.b deviates both in frontal area as in current density from the reference case, it shows that the combined effect of both parameters is similar for both electrode materials. From this it can be assumed that the time estimation model based on experiments with copper can be used for estimating EDM

times for cases where graphite electrodes are used on condition that the MRRref values from the corresponding material are used.

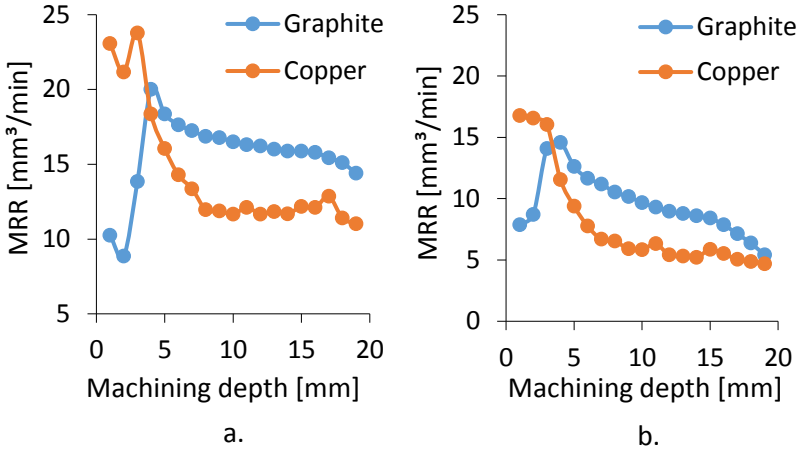

Fig. 4.33: Comparison of MRR for machining with copper and graphite electrode with identical machining conditions (a) 8.96 A/cm²; (b) 17.9 A/cm².

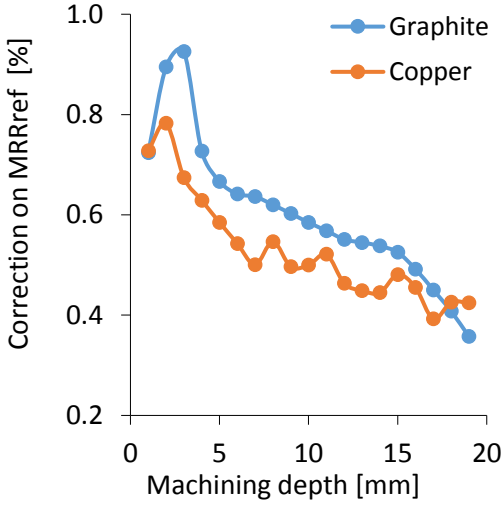

Fig. 4.34: Comparison of deviation from MRRref for machining with copper and graphite electrode with identical machining conditions at a current density of 17.9 A/cm².

4.2.3. Modelling of EDM roughing time

From the previous paragraphs it can be concluded that there are 3 main parameters which need to be taken into account for estimating the machining times of prismatic cavities, namely machining depth, frontal surface area and current density. Hence the correction C_R (see Eq. 4.3) on MRR_{ref} will be a function of these parameters. As there are 2 sets of influencing parameters the correction C_R will be split up into two correction factors: a flushing factor $C_{flushing}$ and an efficiency factor $C_{efficiency}$. $C_{flushing}$ corrects MRR_{ref} for the effect of flushing related parameters (e.g. frontal electrode area, machining depth) on the EDM roughing time. On the other hand $C_{efficiency}$ corrects MRR_{ref} for the effect of efficiency related parameters, e.g. effect of multiple protrusions or current density when flushing conditions are similar. Applied to the common case of an electrode with multiple identical protrusions $C_{flushing}$ takes the effect of the flushing conditions of one protrusion into account. Due to a difference in current density $C_{efficiency}$ takes the additional effect of having more than one of these protrusions into account. The MRR at a certain depth can then be calculated based on Eq. 4.4. Eq. 4.5 shows the redefinition of the formulation for estimation the EDM roughing time by introducing the correction factors.

$$MRR(depth) = C_{efficiency} \cdot C_{flushing} \cdot MRR_{ref}(depth) \qquad \text{(Eq. 4.4)}$$

$$EDM\ Time_{roughing} = \sum_{i=1}^{n} \frac{Volume_i}{C_{efficiency,i} \cdot C_{flushing,i} \cdot MRR_{ref,i}} \qquad \text{(Eq. 4.5)}$$

With:
- n — number of roughing regimes;
- $C_{efficiency,i}$ — efficiency correction factor for regime i;
- $C_{flushing,I}$ — flushing correction factor for regime i;
- $MRR_{ref,I}$ — reference value for regime i.

The following paragraphs will discuss the elaboration of both correction factors.

4.2.4. Modelling of $C_{efficiency}$

The efficiency correction factor corrects MRR_{ref} for deviations originating from machining cases under identical flushing conditions with different current densities. In the previous section it was already shown that a difference in current density can lead to significant differences in MRR under identical flushing conditions.
The relation with current density was quantified by a set of machining experiments performed with a test setup as shown in Fig. 4.35. Here a cylindrical workpiece is machined with a cylindrical electrode of the same diameter so that the top of the workpiece is removed layer-by-layer, guaranteeing constant flushing conditions throughout the operation. Different electrode diameters (see Table 4.5) in combination with different roughing regimes were applied in order to cover the common working range of 2 A/cm² to 40 A/cm².

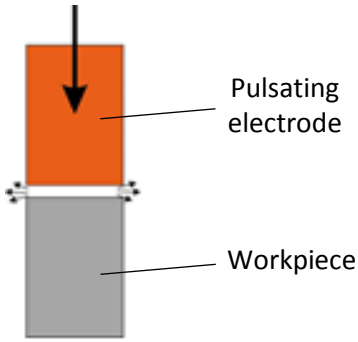

Fig. 4.35: Test setup for determining $C_{efficiency}$.

Table 4.5: Electrodes used for quantifying $C_{efficiency}$ and the corresponding flushing factor.

Electrode diameter [mm]	Frontal area [mm²]	$C_{flushing}$
7	39	1.26
9,8	75	1.46
11,3	100	1.68
13,8	150	1.21
21,4	360	1.14

Each experiment consisted of determining the MRR when machining the top of the cylindrical workpiece until a depth of 1 mm was reached. Three replications were performed. The MRR was compared to MRR_{ref} determined during the first millimeter of the calibration giving the total correction C_r. As flushing conditions are different from the calibration procedure and do also vary within the experiments, $C_{flushing}$ needs to be quantified for each electrode diameter. This is done by choosing a regime which results in a current density of 9 A/cm², which equals the situation of the calibration. As $C_{efficiency}$ is function of the current density this factor equals 1 at 9 A/cm². Hence the total correction equals $C_{flushing}$ at 9 A/cm². The resulting flushing factors for each electrode diameter are given in Table 4.5. Note that the flushing factors are only valid for the test setup in Fig. 4.35. With the knowledge of these flushing factors $C_{efficiency}$ can be determined for each machining experiment. The results, shown in Fig. 4.36, show a clear decreasing trend of $C_{efficiency}$ in function of the current density meaning that current densities lower than 9 A/cm² result in higher MRR compared to MRR_{ref}, whereas current densities larger than 9 A/cm² result in a lower MRR compared to MRR_{ref}. The trend was quantified by two types of approximations: linear and exponential. Table 4.6 shows that the exponential approximation results in the best fit with the results with an R^2 of 0.88. As practical roughing applications are limited to current densities between 2 A/cm² and 40 A/cm², the relation that will be used for calculating the EDM roughing time is shown by the curve in Fig. 4.37. As no experimental data is present outside this current density interval, $C_{efficiency}$ outside the interval is chosen equal to the interval boundary values.

Table 4.6: Comparison of approximations for the relation between $C_{efficiency}$ and current density (x).

	Linear	Exponential
Equation	1,28 - 0,0204*x	$1,35*e^{(-0,026*x)}$
R^2	0,78	0,88

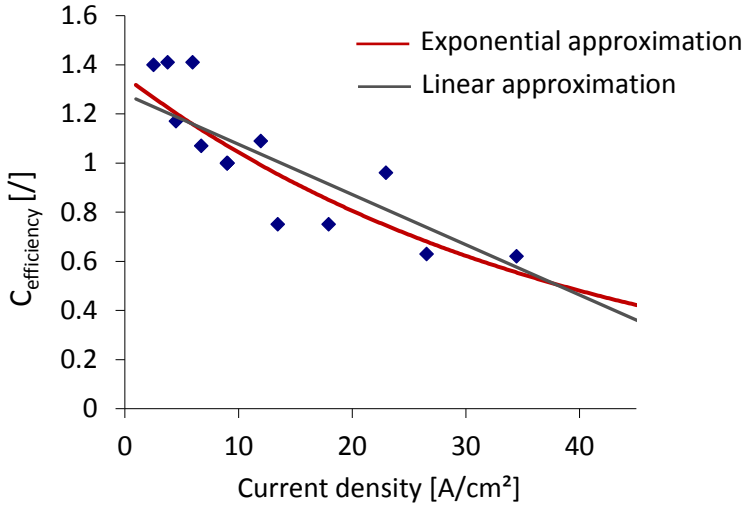

Fig. 4.36: $C_{efficiency}$ in function of current density.

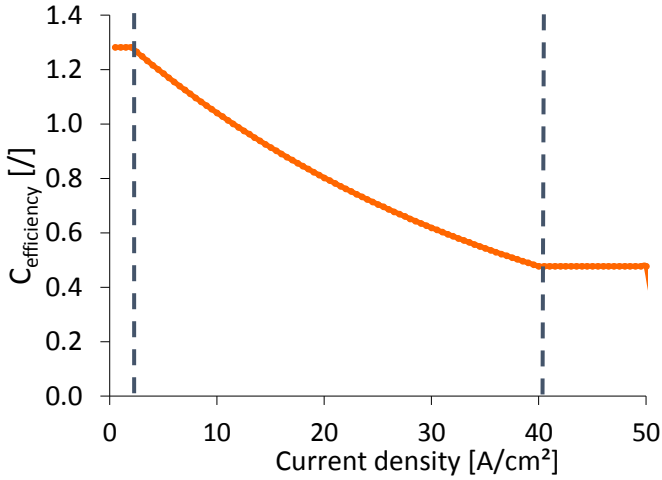

Fig. 4.37: Revised relation between $C_{efficiency}$ and current density.

4.2.5. Modelling of $C_{flushing}$

The flushing factor refers to the part of the deviation from MRR_{ref} caused by the flushing conditions. This factor was determined by correlating flushing related parameters to it. In this study initially only the machining depth and the frontal surface area were considered as influencing parameters. The quantification of $C_{flushing}$ was done by machining rectangular cavities with varying machining depths and frontal surface areas within the ranges shown in Table 4.7. Each experiment was performed 3 times and as a result the MRR was determined. With the knowledge of MRR_{ref} and $C_{efficiency}$ (determined by the trend from Fig. 4.37), $C_{flushing}$ can be quantified according to Eq. 4.4.

Table 4.7: Parameter ranges for quantifying $C_{flushing}$.

Parameter	Range
Machining depth [mm]	1 - 20
Frontal area [mm²]	25 - 400
Current density [A/cm²]	3.5 - 32

The influence of machining depth is already partially included in MRR_{ref} by performing the calibration in function of the machining depth. However, it was shown in Fig. 4.6 that the influence of the machining depth is case dependent and needs to be taken into account. This is shown in Fig. 4.38 where the correction $C_{flushing}$ is clearly a function of the machining depth. This figure also shows that during this machining operation a higher MRR is obtained compared to the calibration case.

Due to the strong dependency of $C_{flushing}$ with the machining depth, the time estimation is split up into small calculation steps corresponding to small machining steps along the machining depth. Each machining step or machining volume then has a specific value for $C_{flushing}$ (see Fig. 4.39). The formulation for estimating the EDM roughing time can then be redefined to Eq. 4.6.

$$\text{EDM Time}_{\text{roughing}} = \sum_{i=1}^{n}\sum_{j=1}^{m} \frac{\text{Vol}_j}{C_{\text{efficiency},i} \cdot C_{\text{flushing},j} \cdot \text{MRR}_{\text{ref},i,j}} \qquad \text{(Eq. 4.6)}$$

With:

m	the total number of calculation steps;
j	j^{th} calculation step;
Vol_j	the volume to be removed during the j^{th} step;
$C_{efficiency,i}$	the efficiency factor corresponding to regime i;
$C_{flushing,j}$	the flushing factor corresponding to the j^{th} calculation step;
$MRR_{ref,i,j}$	the reference value corresponding to regime i and a machining depth corresponding to the j^{th} calculation step.

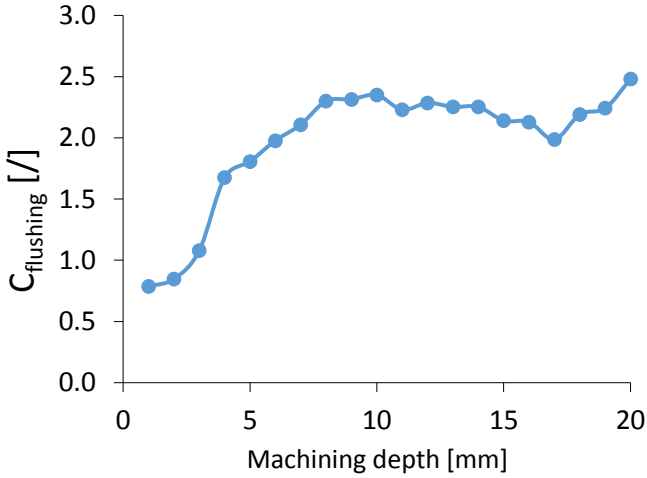

Fig. 4.38: $C_{flushing}$ in function of machining depth (rectangular electrode with frontal area of 2 cm² and current density of 4.5 A/cm²).

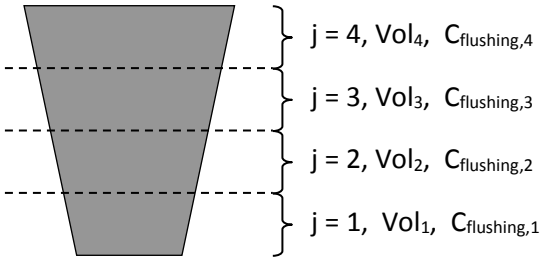

Fig. 4.39: Stepwise calculation of the EDM roughing time.

4.2.6. Evaluation of correction factors

The purpose of using two correction factors is to make a clear distinction between the types of effect that occur on the debris density, hence MRR. Therefore $C_{flushing}$ takes the effect of flushing related parameters like the machining depth and the frontal surface area into account. In addition, $C_{efficiency}$ takes the effect of the current density into account.

When calculating $C_{flushing}$ in function of the machining depth for cases with the same frontal surface area but with different current densities, due to a different number of protrusions, no clear relation can be found (see Fig. 4.40).

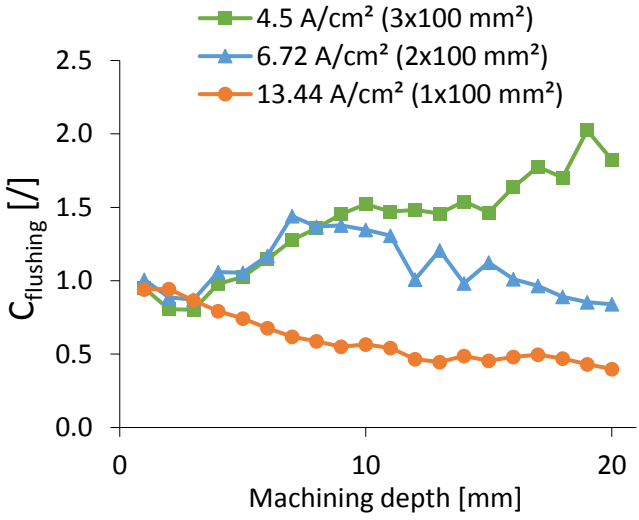

Fig. 4.40: Interaction effect on $C_{flushing}$ between machining depth and current density (rectangular electrode with frontal area 1 cm²).

Furthermore, when displaying the relation between $C_{flushing}$ and frontal surface area for different current densities also no clear trend can be found. As was already mentioned in Section 4.2.2, a strong interaction effect exists between machining depth and frontal surface area on the one hand and the current density on the other hand. Meaning that the effect of the flushing conditions in terms of debris density, determined by geometrical parameters like machining depth and frontal area, is strongly dependent on the applied current density. Therefore, this interaction effect is included in the modelling of $C_{flushing}$. By including current density in the modelling of $C_{flushing}$, $C_{efficiency}$ partially loses its initial meaning of incorporating deviations due to differences in

current density. However, $C_{efficiency}$ can still be used to explain differences in MRR at good flushing conditions (e.g. at small machining depths) when comparing different levels of current density. It can also act as a first assessment of the effect of the current density in case of bad flushing conditions. However, in those cases also the interactions with the flushing related parameters need to be taken into account.

The modelling of $C_{flushing}$ is based on a least squares approximation with machining depth, frontal surface area and current density as variables. The model has been split up into two models depending on the level of current density. As shown in Fig. 4.41 different trends occur for low and high levels of current density with a transition around 9 A/cm².

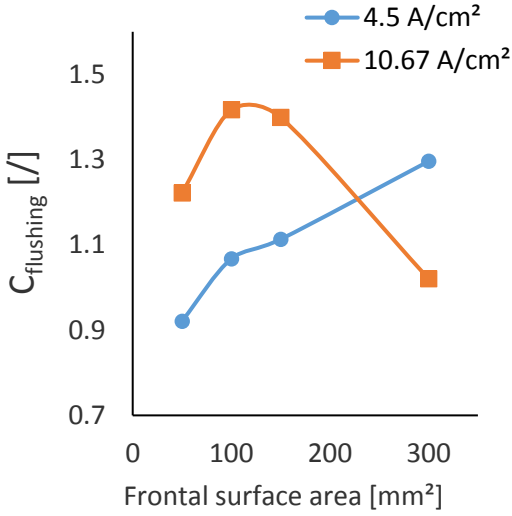

Fig. 4.41: Interaction effect on $C_{flushing}$ between frontal surface area and current density at a machining depth of 5 mm.

For the model for higher current densities a second order polynomial based model is sufficient to include the trends observed during previous testing. On the other hand, the model for lower current density levels is based on a third order polynomial as more curvature is present in the observed trends. In both models the current density is present only in the form of interaction effects as the main effects are already represented in the modelling of $C_{efficiency}$. Table 4.8 gives an overview of the coefficients of the model with the corresponding effect.

Surface plots of the low level model of $C_{flushing}$ are shown in Fig. 4.42 to Fig. 4.44. In Fig. 4.42 the increasing trend of $C_{flushing}$ in function of the machining depth for low current densities can be noticed which becomes less pronounced when the current density increases. Opposed to this, the model for higher current densities shows a clear decreasing trend of $C_{flushing}$ in function of the machining depth (see Fig. 4.45). $C_{flushing}$ decreases when the current density increases, clearly incorporating the results presented in Section 4.2.2. For current densities larger than 35 A/cm² and large machining depths $C_{flushing}$ even drops below 0, possibly resulting in unstable time estimations. However, this will not have practical implications as this combination of parameter levels is unlikely to occur in practice. The same conclusion can be drawn for the combination of high current densities with large surface areas (see Fig. 4.46). Finally, the interaction effect determined in Section 4.2.2 between machining depth and frontal area can be seen in Fig. 4.47.

Table 4.8: Coefficients of least squares models for $C_{flushing}$.

	Low loading levels	High loading levels
constant	0,7814	0,9
D	0,1845	-0,0423
A	0,0175	0,0072
D^2	-0,0151	0,0021
A^2	-2,42E-05	-1,60E-05
DA	0,0007	-1,55E-05
DB	0,0025	-0,0014
AB	-0,0059	-0,0001
DAB	-0,0001	
D^3	0,0003	
A^3	1,00E-08	
DA^2	-4,30E-07	
D^2A	4,60E-07	
A^2B	3,90E-06	
AB^2	0,0005	
DB^2	-0,0009	
D^2B	0,0003	

A: frontal area; B: current density; D: machining depth

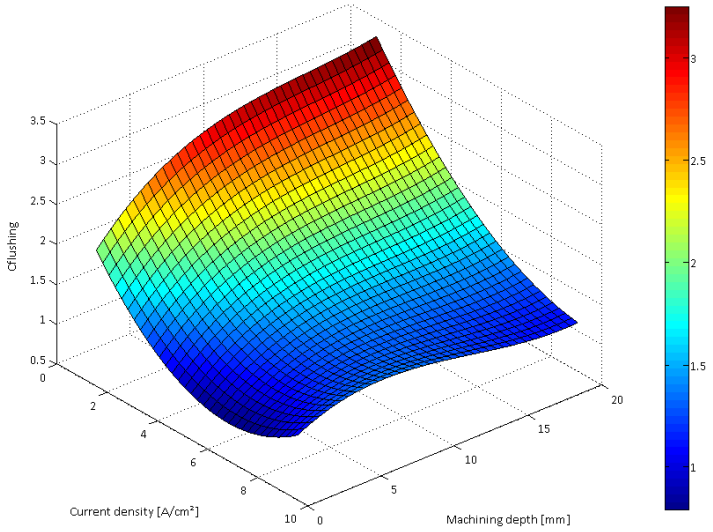

Fig. 4.42: Surface plot of model for $C_{flushing}$ for low current densities in function of machining depth and current density for a frontal surface area of 100 mm.

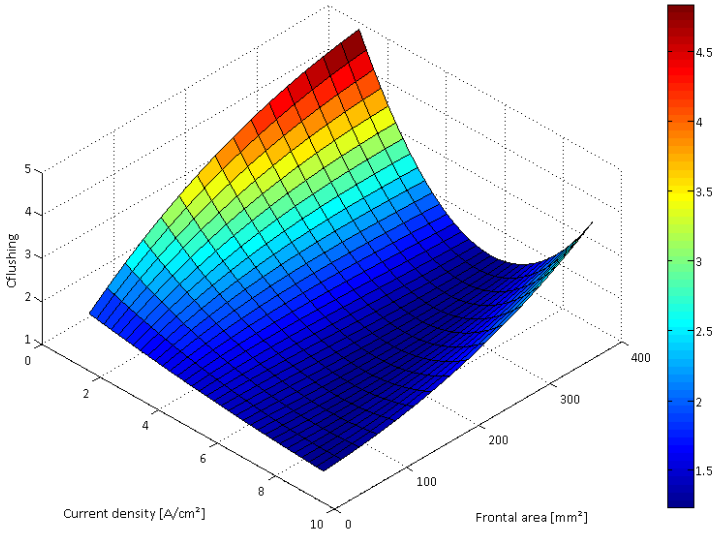

Fig. 4.43: Surface plot of model for $C_{flushing}$ for low current densities in function of frontal surface area and current density for a machining depth of 7 mm.

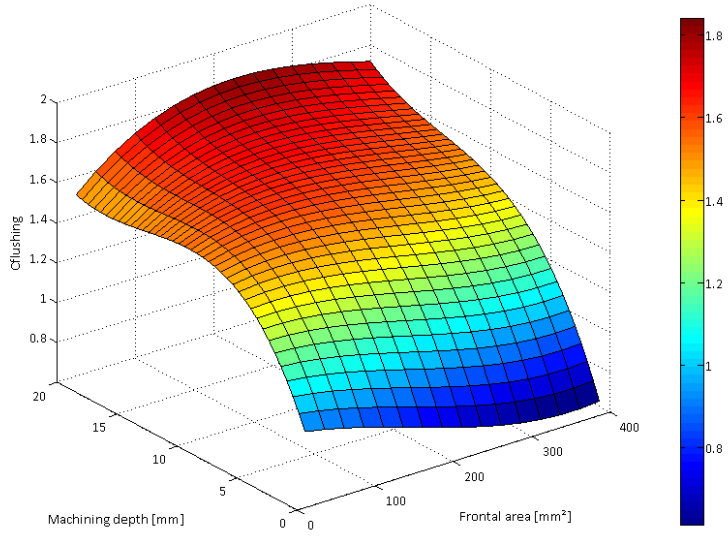

Fig. 4.44: Surface plot of model for $C_{flushing}$ for low current densities in function of machining depth and frontal surface area for a current density of 5 A/cm².

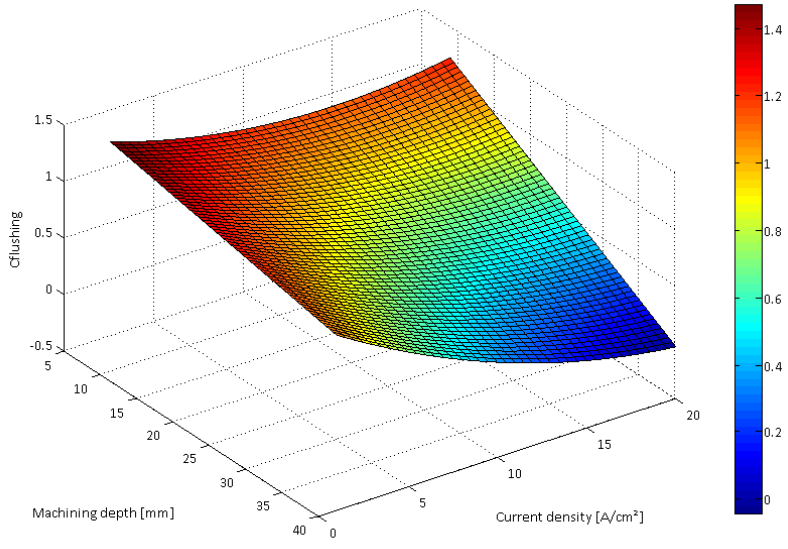

Fig. 4.45: Surface plot of model for $C_{flushing}$ for high current densities in function of machining depth and current density for a frontal surface area of 150 mm.

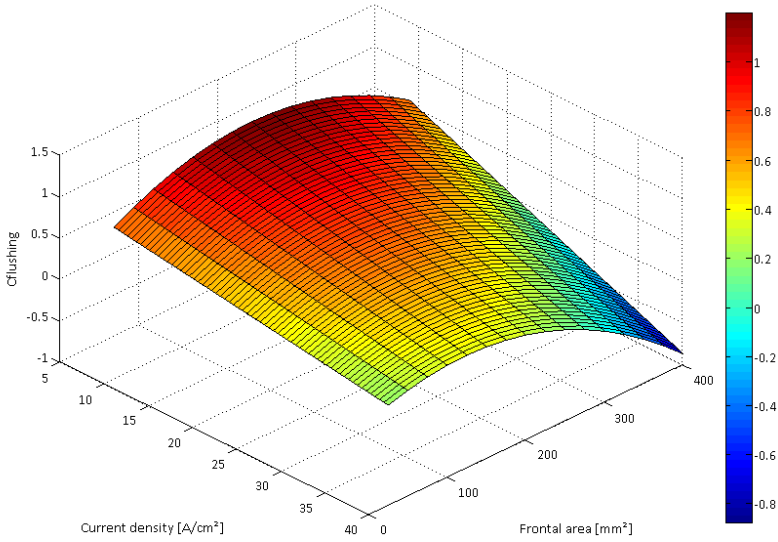

Fig. 4.46: Surface plot of model for $C_{flushing}$ for high current densities in function of frontal surface area and current density for a machining depth of 10 mm.

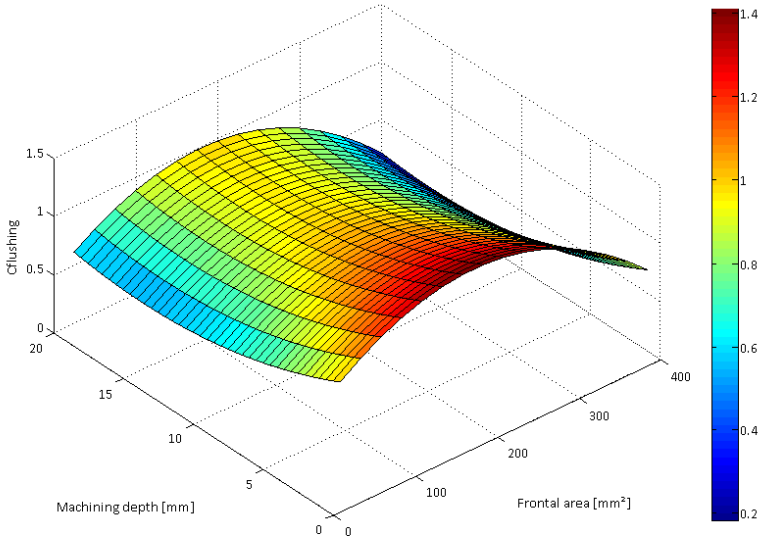

Fig. 4.47: Surface plot of model for $C_{flushing}$ for high current densities in function of machining depth and frontal surface area for a current density of 15 A/cm².

4.2.7. Validation of developed model

The performance of the developed model has been evaluated by applying different sets of empirical data. This data has been obtained by logging the machining time during the machining of a set of prismatic cavities performed on the RoboForm 350Y. Estimation of the EDM roughing time based on the developed models for these data points has been performed within Matlab®. The first set consists of 640 data points (see Appendix C) used for developing the model for $C_{flushing}$ (base set) and acts as a check for the goodness of fit. This set is split up into a set to validate the model for low levels of current density (300 data points), by considering only those data points that were obtained at current densities below 9 A/cm², and a set for high levels of current density (340 data points), by considering only those data points that were obtained at current densities above 9 A/cm². Fig. 4.48 shows an example of a machining case within the base set with 20 data points in terms of MRR along the machining depth with the corresponding estimated values and percentual errors. This example shows there is a good correspondence between the actual and estimated trend for this case. Moreover, the percentual error is within an error band of [-30%, +30%]. Table 4.9 shows the performance of the developed model for all validation sets in terms of the error on the EDM roughing time per millimeter. This table shows that an average absolute percentual error of 15.3% and 25.1% is obtained for machining cases of the base set with respectively low and high levels of current density. 90% of the cases with a current density below 9 A/cm² are within an error range of [-30%, +30%], whereas for current densities higher than 9 A/cm² 70% of the cases result in an error within this range. The histograms in Fig. 4.49.a and Fig. 4.49.b show that the error distribution is centralized around 0 with a larger spread for cases with a higher current density. The majority of these deviations can be explained by deviating trends for MRR and inaccuracies related to the MRR level. As an example, Fig. 4.50 shows a machining case where the estimated trend has a sharper decrease in MRR compared to the actual MRR. This results in large estimation errors as the machining depth increases. Although different linear regression models have been tested and the model that showed the overall best fit has been selected (see Table 4.8), the selected model fails to cover all trends. Besides this, this validation has shown that the majority of large deviations (in terms of percentual errors) is related to machining cases with relative low levels of MRR. Fig. 4.51 shows that even if time estimation by means of the developed models results in a similar trend, and similar values for the MRR,

large percentual errors can occur due to the low level of MRR. This can result in large absolute deviations in machining time. In fact, more importance should be given to data points with a lower level of MRR as these are more likely to have a significant impact on the machining time compared to high levels of MRR. As for current densities above 6 A/cm the MRR tends to decrease in function of the machining depth, more importance in modelling should be given to larger machining depths.

The actual validation set consists of 140 data points (see Appendix C) within the boundaries of the model (see Table 4.7), but different from the base set, obtained by performing machining experiments on the same EDM machine that was used for developing the model. In addition 100 data points outside the model boundaries have also been evaluated, which are also obtained by performing machining experiments on the same machine. Fig. 4.52 shows an example of a machining case within the boundaries of the model with the corresponding estimated values and percentual errors. For these data points a good correspondence in trend and absolute value of the MRR is seen, resulting in acceptable (percentual) errors. The entire set with cases within the boundaries of the model shows an average percentual error of 27.5% with 55% of the cases within the range of [-30%, +30%] (see Table 4.9). Fig. 4.53 shows an example of a machining case within the validation set for which poor correspondence is seen between the evolution of the MRR in function of the machining depth for the actual and estimated data points, resulting in large percentual errors.
For cases outside the model boundaries the model performance is lower (see Table 4.9). This is mainly due to different trends that appear when going beyond the model boundaries.

Table 4.9 shows a comparison of the performance of the developed model with time estimations based on the technology tables. In general it can be stated that better results are obtained with the developed model when looking at the average percentual error and the number of cases with an error outside the range of [-30%, +30%]. However, the error distribution has a larger spread for the developed model but is centralized around 0 (see Fig. 4.49.a-d). Time estimations based on technology tables result mainly in underestimations, reflected by positive errors, (see Fig. 4.49.e-f) whereas the developed model results in a more uniform amount of under as overestimations of the roughing time (see Fig. 4.49.c-d).

The observed deviations can be largely attributed to the inability of the developed linear regression models in modelling the occurring complex interaction effects and non-linear effects. In addition, the use of weighting factors based on the level of MRR can deliver a significant improvement to the developed models (e.g. by using a weighted least squares regression). These drawbacks can be overcome by applying other modelling techniques. In this respect, neural networks can be a useful technique as these are able to model non-linear trends and have the capability of giving more importance to certain levels of the output variable (MRR or EDM time). In addition, neural networks do not require all knowledge of the existing non-linearities and can be continuously supplied with new machining data. Therefore, neural networks can improve the estimation accuracy.

Table 4.9: Comparison of performance of developed model and time estimations obtained from technology tables.

	Developed model				Technology tables			
	Base set		Validation set		Base set		Validation set	
	Low current density	High current density	Inside model boundaries	Outside model boundaries	Low current density	High current density	Inside model boundaries	Outside model boundaries
Avg. % error	15,3	25,1	27,5	41,5	51,6	78	62,9	42,6
Max. % error	47,3	56,6	56,1	89,7	80	95,6	84,6	81,6
Min. % error*	-52,6	-136,87	-91,3	-110,18	27,8	53,5	-31,7	-12,1
# errors < 30%	90	69,7	55	38,6	0,3	0	12,8	13,4

** negative values reflect overestimation of the machining time.*

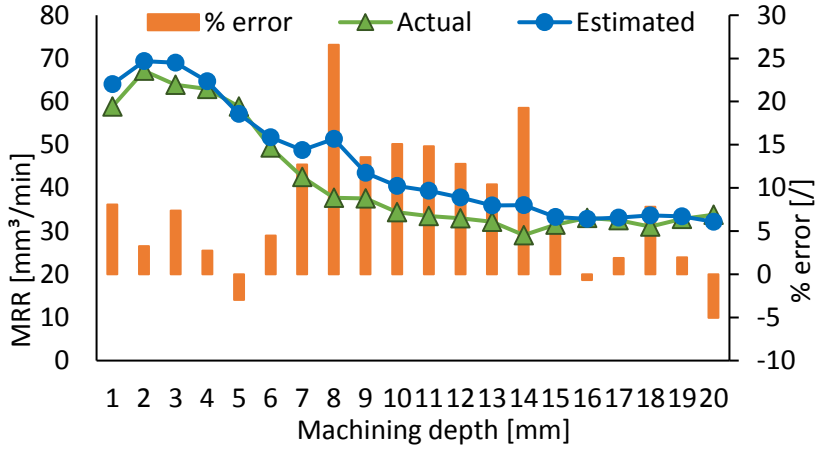

Fig. 4.48: Comparison of actual and estimated MRR and corresponding % error (E434 – 2x100 mm² - 10 A/cm²).

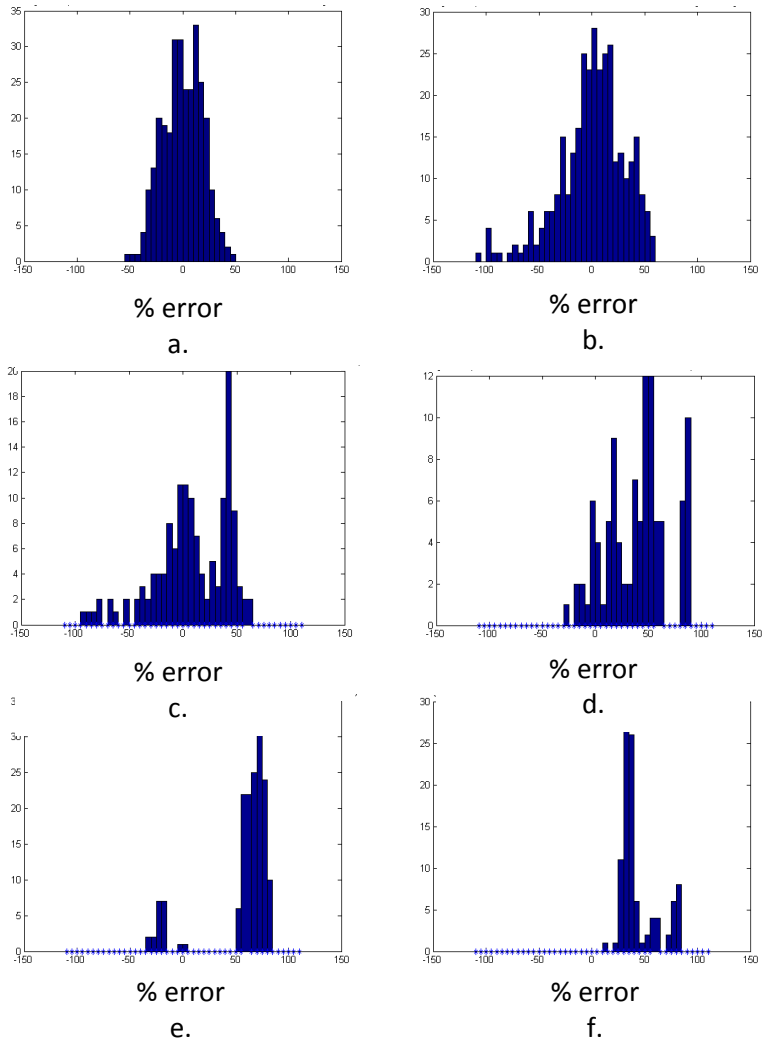

Fig. 4.49: Histogram of % errors on EDM roughing time per millimeter for: (a) base set with current densities < 9 A/cm²; (b) base set with current densities > 9 A/cm²; (c) validation set within model boundaries; (d) validation set outside model boundaries; (e) validation set within model boundaries based on technology tables; (f) validation set outside model boundaries based on technology tables.

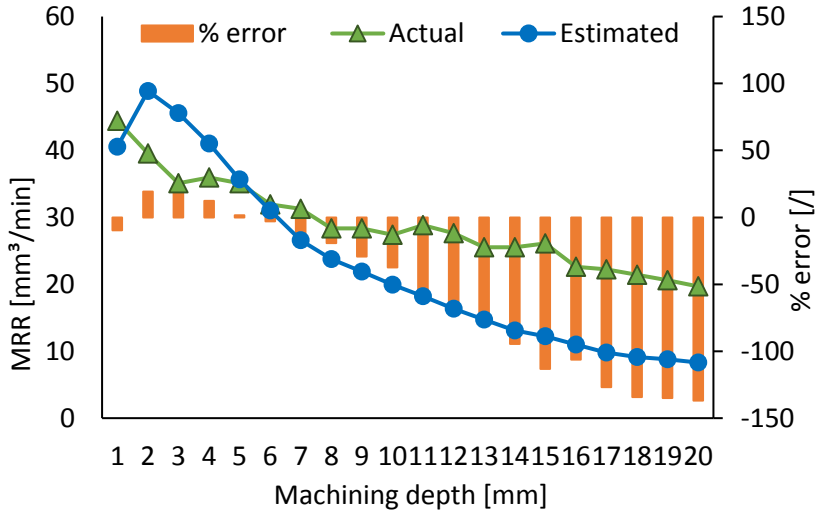

Fig. 4.50: Comparison of actual and estimated MRR and corresponding % error (E453 – 1x100 mm² - 32 A/cm²).

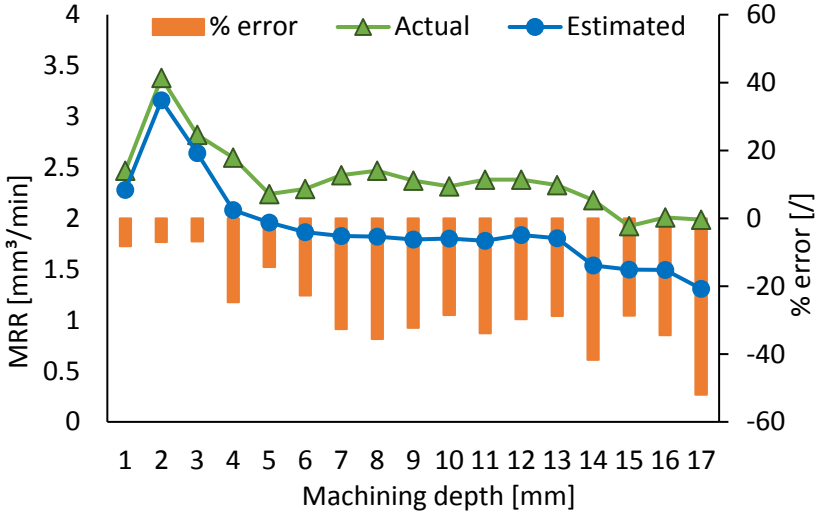

Fig. 4.51: Comparison of actual and estimated MRR and corresponding % error (E303 – 1x25 mm² - 10 A/cm²).

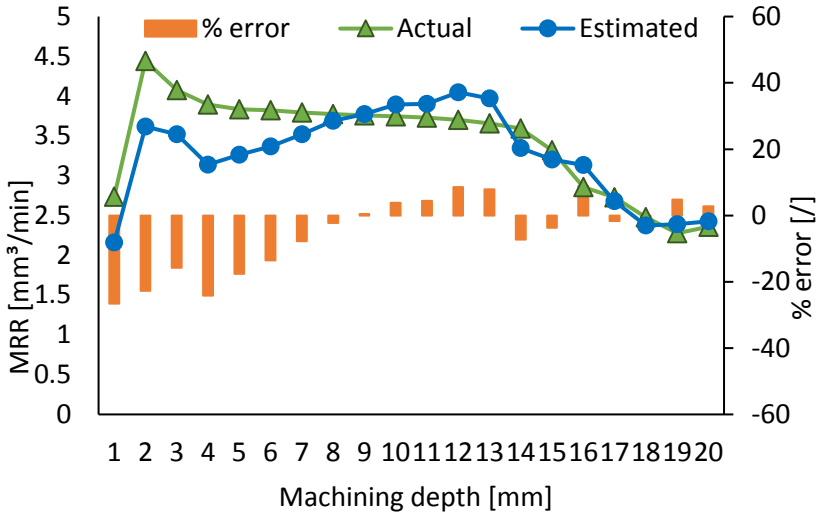

Fig. 4.52: Comparison of actual and estimated MRR and corresponding % error (E303 – 1x37 mm² - 6.6 A/cm²).

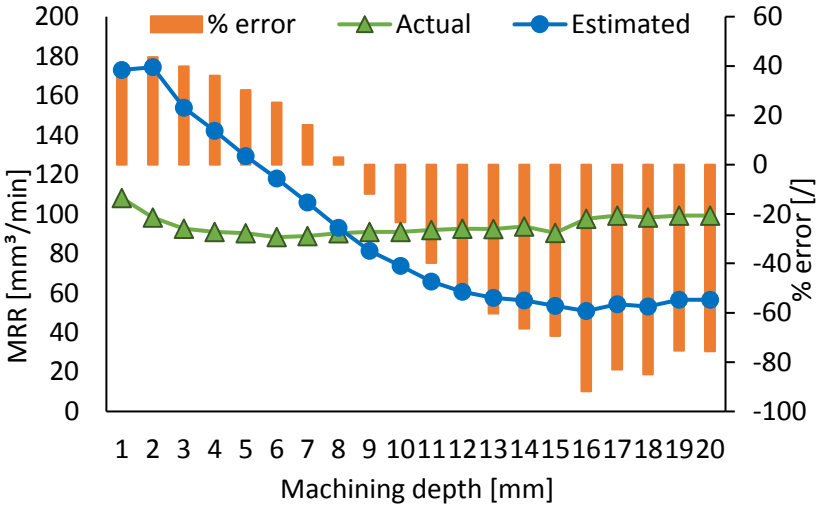

Fig. 4.53: Comparison of actual and estimated MRR and corresponding % error (E463 – 1x400 mm² - 11.4 A/cm²).

4.3. Time estimation for finishing operations

Opposed to EDM roughing operations that act as volume removal operations, EDM finishing operations act as surface enhancement operations where only very small volumes are removed in order to obtain the required surface roughness and to comply with geometrical tolerances. Due to the large uncertainty about the volume to be removed during finishing operations a formulation as in Eq. 4.6 can lead to large estimation errors. Instead of using the MRR, the finishing time will be used as reference.
A finishing operation usually consists of several regimes, each of them reducing the surface roughness. The total EDM finishing time is then the sum of the machining times of all generator settings applied during a finishing operation (Eq. 4.7).

$$EDM\,Time_{finishing} = \sum_{j=1}^{m} C_{finishing_j} \cdot time_{ref_j} \qquad \text{(Eq. 4.7)}$$

With: j the j^{th} finishing regime;
m the total number of regimes;
$C_{finishing,j}$ the correction for the j^{th} regime.

4.3.1. Calibration procedure for finishing operations

Reference finishing times ($time_{ref}$) are determined for every generator setting and material combination by finishing a pre-machined cylindrical cavity with predefined dimensions. Prior to the actual calibration, a fixed starting roughness is applied by using an orbital machining cycle (see Fig. 4.54) finishing operation with a fixed regime (regime X in Fig. 4.55). From this state another orbital machining cycle is applied over a predefined machining length with the regime (regime Y in Fig. 4.55) to be calibrated. The resulting machining time acts as the reference.
On these reference times a correction is applied which takes deviations from $time_{ref}$ into account.

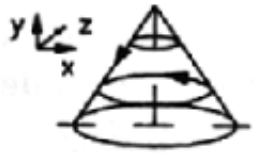

Fig. 4.54: Orbital finishing operation.

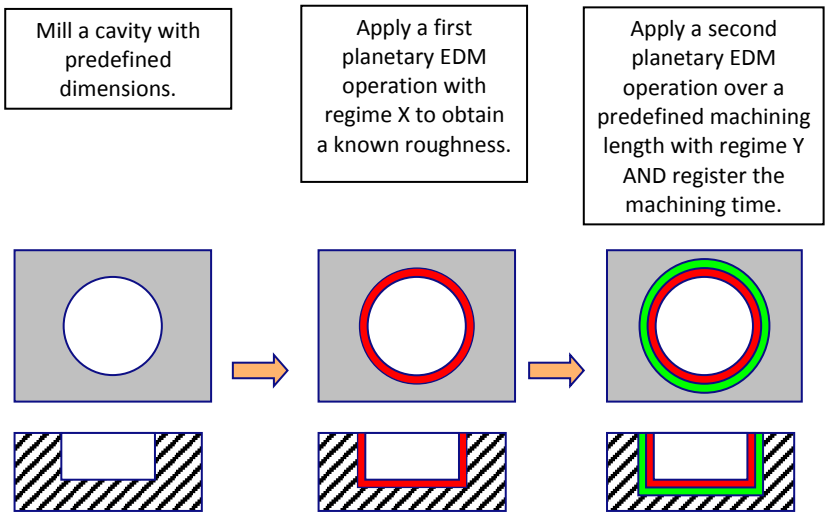

Fig. 4.55: Schematic overview of calibration procedure for finishing operations for regime Y.

4.3.2. Determination of influencing factors

The correction on the reference values consists of all influences that lead to a deviation from the reference values. Based on an initial set of machining experiments and following the results of an enquiry performed within the frame of the EU-FP6 KnowEDM project (COLL-CT-2006-030238) [122] the effects of the following factors have been investigated and will be discussed in the next paragraphs:

- machining length;
- surface area (lateral + frontal);
- starting roughness;
- electrode geometry.

The effect of these parameters on the EDM finishing time, in terms of the deviation from the reference conditions, has been investigated.
All experiments are performed on a copper-steel (AISI D2) material combination, unless specified otherwise. No external flushing is applied.

Machining length

The machining length is defined as the machining distance in lateral and frontal direction during orbital machining cycles. As this parameter directly influences the volume to be removed, it can be expected that a positive trend

exists with the finishing time. Fig. 4.56 shows this trend obtained from experiments in which identical pre-machined cylindrical cavities were finished with different machining lengths and different finishing regimes. From this figure it is clear that an increase in machining length leads to a proportional increase in finishing time, hence proportional increase in $C_{finishing}$.

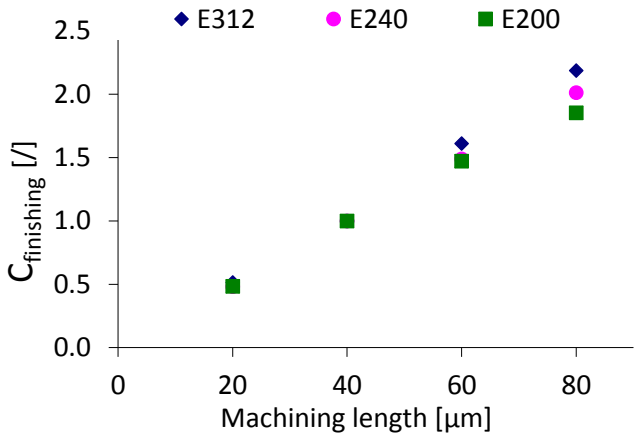

Fig. 4.56: $C_{finishing}$ in function of machining length for different finishing regimes with a reference machining length of 40 µm for cylindrical cavities.

Due to the wide range of finishing regimes, it is useful to use matching machining lengths during calibration i.e. for low energetic finishing regimes it is more time efficient to use small machining lengths. As a consequence, it is more useful to state the relative machining length (ratio of actual machining length and machining length during calibration) as variable. Fig. 4.57 shows that there exists a linear relation between $C_{finishing}$ and the relative machining length.

Surface area (lateral + frontal)

Next to the machining length also the area to be finished determines the volume to be removed in EDM finishing operations. As the considered finishing operations are performed with an orbital movement, the area to be considered is the summation of the frontal and lateral area. Fig. 4.58 shows the relation between $C_{finishing}$ and the total area as a result of machining experiments consisting of finishing pre-machined cylindrical cavities with a predefined machining length with varying surface areas and different

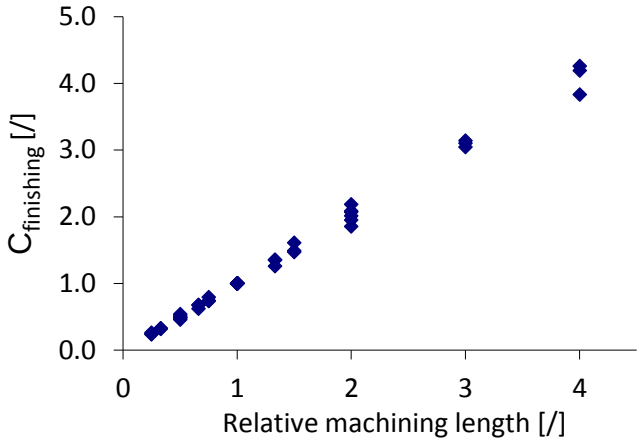

Fig. 4.57: $C_{finishing}$ in function of relative machining length for different finishing regimes for cylindrical cavities

finishing regimes. This figure shows that a doubling of the total area leads to less than a doubling in finishing time. Similar to the machining length, the relative total area can be defined as the actual total area divided by the total area during calibration.

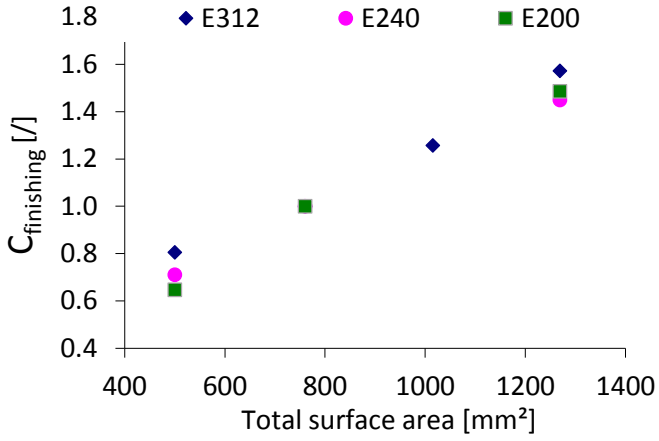

Fig. 4.58: $C_{finishing}$ in function of total area for different finishing regimes with a reference area of 760 mm² for cylindrical cavities.

Starting roughness

An EDM finishing operation mostly consists of a sequence of several finishing regimes with decreasing energy. It has been shown that the starting roughness of the finishing operation can be heavily affected by the machining case as a result of the influence of the frontal area and the electrode geometry on the end roughness of the roughing operation [129]. This means that there is an uncertainty on the roughness values defined by the machine tool builder when applying a sinking electrode movement. Fig. 4.59 shows the influence of a difference in starting roughness on the total finishing time (= summation of machining times for all finishing regimes) when wanting to reach a final roughness of 1 µm Ra (= 20 CH). From this figure it is clear that the higher the starting roughness, the lower the total finishing time will be. An explanation for this can be given based on Fig. 4.60.a and Fig. 4.60.b. It should be noted that for the purpose of clarity these figures show exaggerated conditions. When applying the same machining strategy (i.e. with the same machining length L_m) more volume needs to be removed when starting from a roughness profile with a small value (Fig. 4.60.a) compared to a larger starting roughness value (Fig. 4.60.b) resulting in larger machining time. The case shown in Fig. 4.60a corresponds to the common practice by removing the initial roughness profile and including an allowance for the thermal influenced zone and the variation in sparking gap, based on the work of Staelens et al. [130], [131]. The case in Fig.4.60.b will seldom occur in practice as the machining step should remove the entire roughness profile. The influence of a deviating starting roughness is mainly visible in the first finishing regime. After a certain machining length the influence of the starting roughness disappears resulting in similar machining times for the subsequent finishing regimes. Hence the trend shown in Fig. 4.59 becomes less pronounced for smaller values of the end roughness as the reduction in machining time for the first finishing regimes cannot outweigh significant larger machining times for the final regimes.

Fig. 4.61 shows the influence of the starting roughness on $C_{finishing}$ for one finishing regime (E240). A significant smaller finishing time can be noted in case of a significantly higher starting roughness as a result of the roughing operation.

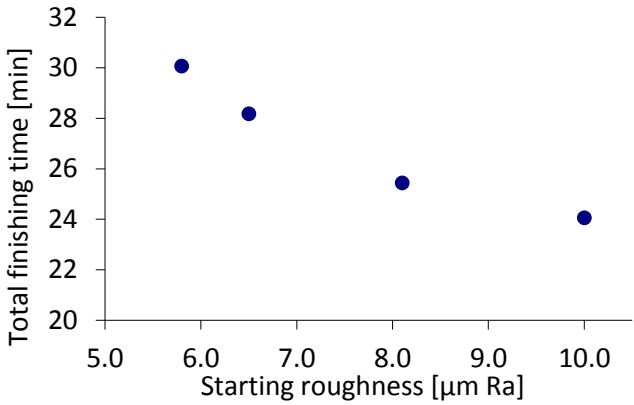

Fig. 4.59: Total finishing time in function of starting surface roughness for a finishing operation of a 17 mm x 17 mm x 7 mm (LxWxD) square cavity with a desired end roughness of 1 µm Ra (20 CH).

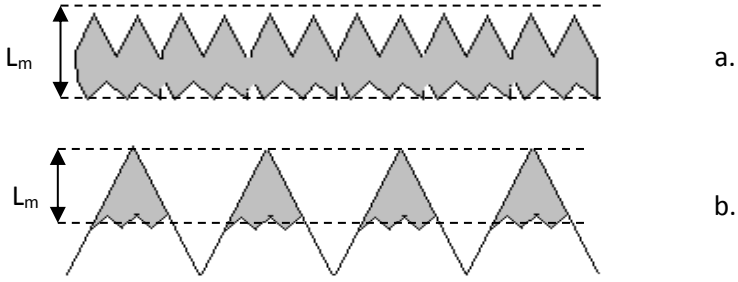

Fig. 4.60: Volume to be removed for different starting roughness with the same machining length: (a) low starting roughness; (b) high starting roughness.

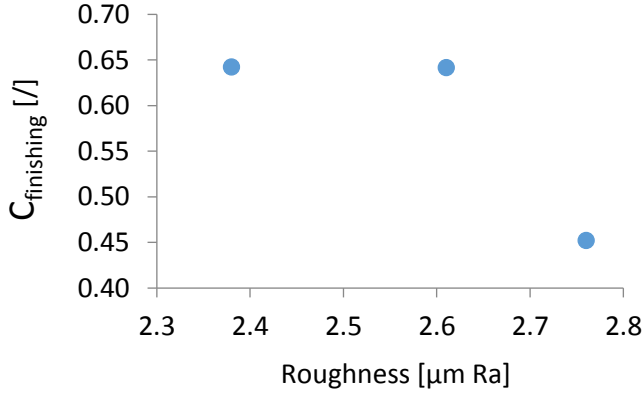

Fig. 4.61: $C_{finishing}$ in function of starting surface roughness for a finishing operation with regime E240, machining length 20 µm, total area 1360 mm².

Geometry

The previous discussed influencing parameters exert an influence on the volume to be removed, hence influencing the finishing time. Under conditions of equal theoretical machining volume, the geometry of the cavity can exert a significant influence on the finishing time. Fig. 4.62 shows a comparison of the finishing time, in terms of $C_{finishing}$, of three geometrical shapes for two different machining cases where theoretically the same volume needs to be removed. It appears that the machining of cylindrical cavities is significantly more time efficient compared to rib-like and square cavities. The reason for this can be found in the variation of the momentary active lateral electrode area. For cylindrical cavities the active lateral electrode area is constant during one rotation. On the other hand, for cavities with corners the active lateral electrode area varies with the angle of rotation i.e. large when being aligned with the cavity walls (for a rectangle at an angle of 0°, 90°, 180° and 270°) and small when passing by the corners or 'dead zones' of the cavity. As a consequence, more rotations are needed to remove the same volume at the cavity walls given a constant rotational speed. This then results in a larger finishing time.

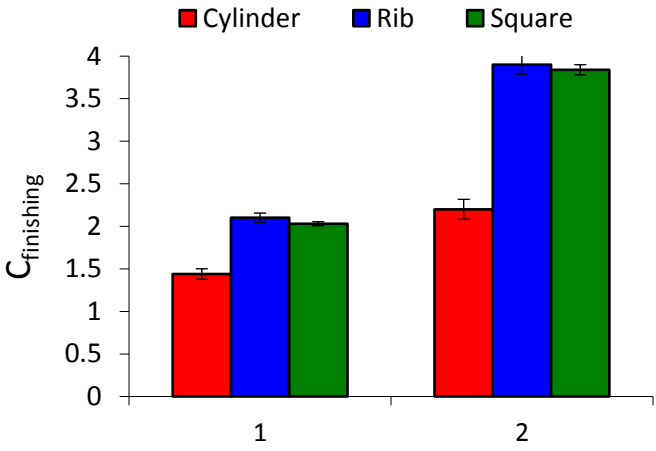

Fig. 4.62: $C_{finishing}$ for three geometries for two machining cases by applying an orbital finishing cycle with regime E240. (1) Machining length: 60 µm; total surface area: 750 mm²; (2) Machining length: 60 µm; total surface area: 1300mm².

4.3.3. Modelling of EDM finishing time

The previous paragraphs discussed the main influencing parameters on the EDM finishing time. Influences due to deviating values for these parameters from a reference situation (calibration) are taken into account by applying a correction factor $C_{finishing}$ on reference finishing times ($time_{ref}$), given by Eq. 4.7. The following will discuss the modelling of $C_{finishing}$ in function of the previously discussed parameters.

The modelling of $C_{finishing}$ is based on a mixed full factorial design of experiments (DoE) with parameters and their respective levels given in Table 4.10. For both machining length and total surface area 2 levels are defined due to the previously determined linear relation with $C_{finishing}$ (see Fig. 4.56 and Fig. 4.58). On the other hand 3 levels for the starting roughness are defined due to the previously determined non-linear relation with $C_{finishing}$ (see Fig. 4.61). In addition 3 types of geometries are investigated namely cylindrical, rib-like and square cavities. Each experiment has been replicated 3 times resulting in a total set of 108 experiments. Each experiment consisted of finishing a pre-machined cavity with predefined dimensions (listed in Table 4.11) with finishing regime E240.

Table 4.10: Levels of selected parameters for DoE for determining $C_{finishing}$.

DOE level	Machining length [µm]	Total area [mm²]	Geometry	Roughness [µm]
Low	20	750	cylinder	2,38
Intermediate	-	-	square	2,61
High	60	1400	rib	2,78

Table 4.11: Dimensions of pre-machined cavities.

	Cylinder	Rib	Square
Depth [mm]	11,17/22,8*	3,84/8,54*	10,13/21,17*
Dimensions [mm]	Ø16	3,72 x 63,2	13,84 x 13,84

* Each depth corresponds to a level for the total area.

An ANOVA analysis of the resulting machining times with a significance level of 0.05 results in P-values listed in Table 4.12. The column denoted as 'Initial' shows the P-values when taking all main effects and interactions of all considered parameters into account. It shows that all main effects are significant, confirming what was stated in the previous paragraphs. In addition the analysis shows that the geometry has a significant influence on the effect of both machining length and surface area (interaction AB and AC). From Fig. 4.63.a and Fig. 4.63.b it is clear that the effect of machining length and surface area is less pronounced in case of cylindrical cavities. In general, finishing times of cylindrical cavities are lower than for the other considered geometries.
This geometrical dependency of the finishing time can be incorporated in the modelling by introducing a geometry related parameter. However, no clear parameter was found which can be related to the determined effects. An alternative approach would be to develop separate models for round geometries and geometries with corners. However, in practice combinations of both types of geometries will occur excluding this option.

As the trends of the significant effects among the different type of geometries are similar, a regression model for the finishing time has been developed based on the previous test results, but by neglecting the geometry as an influencing parameter. Table 4.12 lists the P-values for all relevant effects in the column 'without geometry'. By neglecting the geometry the analysis shows that the starting roughness has no significant effect anymore. This can be attributed to larger variations due to neglecting the effect of the geometry. The only significant interaction exists between the machining length and the surface area, namely the effect of the machining length on the finishing time, is higher in case of larger surface areas (see Fig. 4.64). However, a doubling in machining length translates into a doubling of the finishing time, this for both levels of surface area.

As a conclusion, the regression model for $C_{finishing}$ will be function of machining length (B), surface area (C) and the interaction between both (B*C). Eq. 4.8 shows $C_{finishing}$ in function of the influencing parameter set.

$$C_{finishing} = c_0 + c_1*B + c_2*C + c_3*B*C \qquad \text{(Eq. 4.8)}$$

Table 4.13 lists the coefficients of the model which result in a R^2 value of 85.8%.

Table 4.12: P-values for main effects and interactions in the modelling of $C_{finishing}$.

Effect	Initial	Without geometry
Geometry (A)	< 0,01	
Machining length (B)	< 0,01	< 0,01
Surface area (C)	< 0,01	< 0,01
Starting roughness (D)	< 0,01	0,668
AB	< 0,01	
AC	< 0,01	
AD	0,045	
BC	< 0,01	< 0,01
BD	< 0,01	0,76
CD	0,761	0,996
ABC	< 0,01	
ABD	0,584	
ADC	0,327	
BCD	0,09	0,899
ABCD	0,648	

Table 4.13: Coefficients for all significant effects in coded terms in modelling $C_{finishing}$.

	Value
Constant	1,6209
B	0,9725
C	0,4574
CD	0,2809

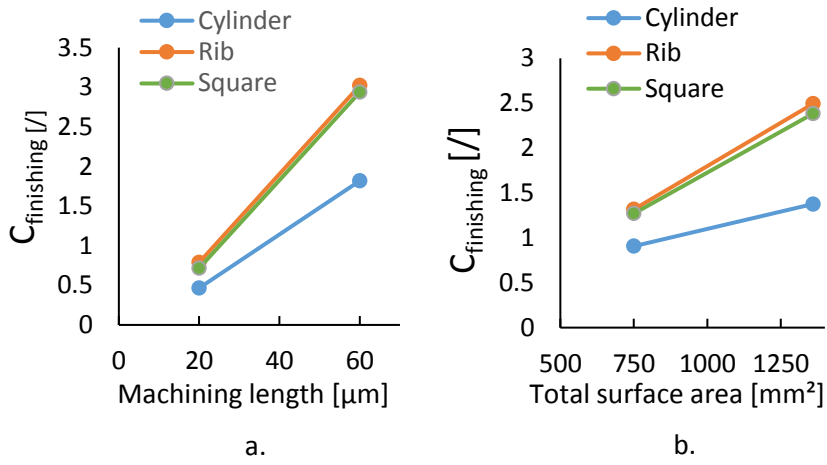

Fig. 4.63: Interaction effects for $C_{finishing}$ between geometry on the one hand and (a) machining length and (b) surface area.

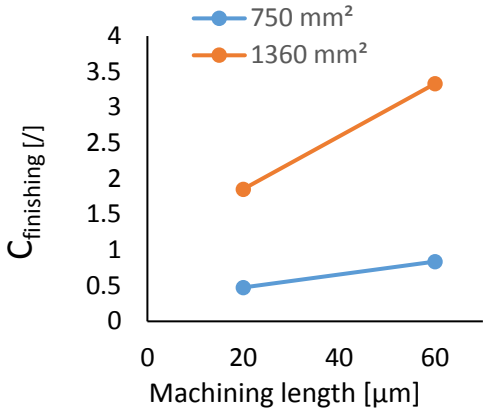

Fig. 4.64: Interaction effects for $C_{finishing}$ between machining length and surface area.

4.3.4. Validation of developed model

The performance of the developed model has been evaluated by applying a set of 72 machining cases (see Appendix C). This set consists of cases with cylindrical, rib-like and square geometries, different finishing regimes, machining lengths and surface area. The entire set of cases has been machined on the RoboForm 350Y. Estimation of the EDM finishing time

based on the developed model for these cases has been performed within Matlab®. Table 4.14 shows the performance of the model with an average absolute percentual error of 18.4% and with almost 85% of the tested cases within an error range of [-30%, +30%]. The histogram in Fig. 4.65.a shows that the error distribution is centralized around 0 with larger errors located on the negative side. These overestimations can be attributed to cases with cylindrical cavities as for these cavities it was previously shown (see Fig. 4.62) that significantly smaller finishing times are noticed which results in large overestimations. This suggests that incorporating the geometry effect in the modelling by means of a geometry dependent correction factor or by means of the addition of a geometrical parameter in the regression model could result in an improved estimation accuracy.
When comparing the actual finishing times with times based on a rough estimation of the volume to be removed and the values for removal rate from the technology tables a higher average percentual error was noticed (see See Table 4.14 and Fig. 4.65.b). Although all errors are relative large, the variation on the errors is significantly lower compared to the variation on the errors resulting from the developed model.

Table 4.14: Comparison of time estimations for finishing operations between the developed model and times resulting from technology tables.

	Developed model	Technology tables
Avg. % error	18,4	81,5
Max. % error	23,8	87,8
Min. % error	-57,4	68,1
# errors < 30%	84,72	0

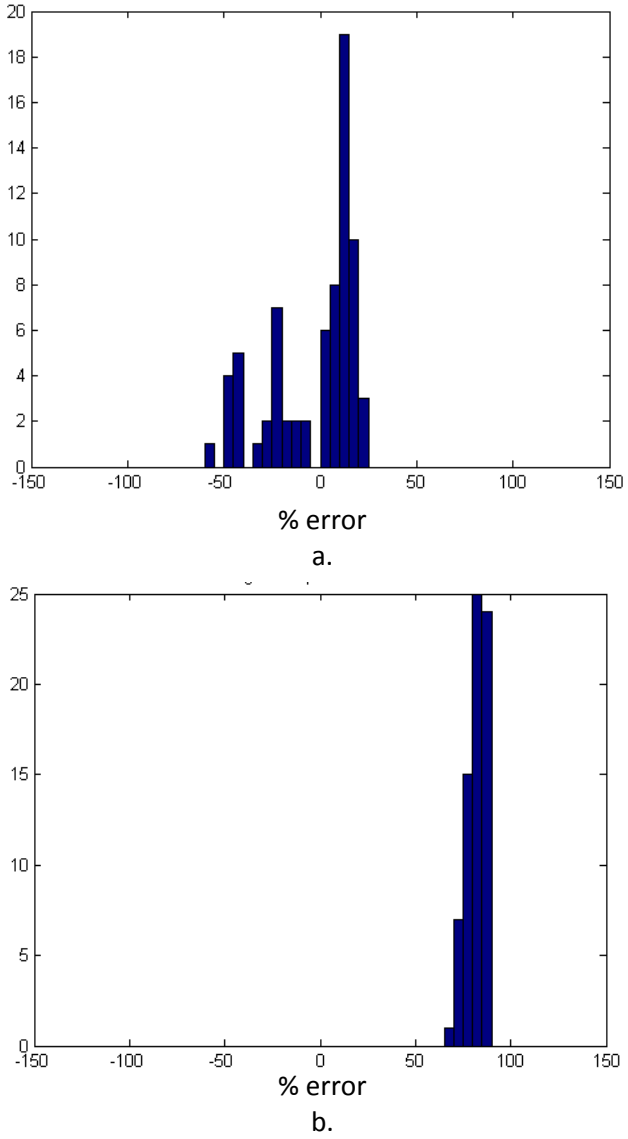

Fig. 4.65: Histogram of % errors for EDM finishing time (a) based on developed model, (b) based on technology tables.

4.4. Summary

The proposed concept for EDM time estimation is based on machine dependent 'reference' values which reflect the effect of the electrical generator parameters and the machine behavior during machining. The reference values are determined by a fixed procedure (calibration) that needs to be performed for every machine type. As deviations from these reference values are likely to occur in practice, machine independent corrections are applied which reflect the influence of the specific machining case. In this way the concept can be seen as a 'plug and play' time estimation as for every machine only the calibration has to be performed. Within the concept a distinction has been made between high energetic roughing operations and low energetic finishing operations due to a different set of influencing factors and machining conditions. In addition different calibration procedures and time estimation algorithms apply for both types of operation.

For roughing operations the main influencing factors are machining depth, frontal electrode area and current density. An important interaction between the machining depth and current density exists with a transition around 9 A/cm². Below this level the machining speed increases for higher machining depths as a result of an increasing debris density that steadily approaches the optimal debris density. On the opposite, for current densities higher than 9 A/cm² the machining speed strongly decreases for higher machining depths due to a saturation of the sparking gap with debris. The modelling of the roughing time has been performed by defining two correction factors. An efficiency factor accounts for the effect of current density whereas a flushing factor accounts for the effect of machining depth, frontal area and interactions between both and the current density. As the trends for current densities below and above 9 A/cm² are very different two models have been defined based on machining experiments with prismatic electrodes. A validation of these models for the machining of prismatic cavities results in an average percentual error of 27.5% with 55% of the tested cases within an error range of [-30%, +30%].

A study of the effects on the finishing time showed four influencing factors when finishing prismatic cavities: the machining length, total surface area (lateral + frontal), starting roughness and the cavity geometry. An empirical model was developed without considering the cavity geometry for the sake

of simplicity. The model shows an average percentual error of 18.4% with 85% of the tested cases within an error range of [-30%, +30%] when considering finishing operations on prismatic cavities.

Both models show a significant improvement for the machining of prismatic cavities in comparison to existing estimation techniques (e.g. based on technology tables). However, higher estimation errors can be expected when dealing with complex shaped cavities due to different flushing conditions. In addition, only orbital movements are investigated to be used during the finishing operation resulting in less accurate results when applying other electrode movements during finishing.

Chapter 5 Automation of sinking EDM time estimations

Within the process of elaborating a proper process planning, time estimations of machining operations are an essential part to be time and cost effective. In order to be fully effective, adequate input from previous operational processes is indispensable. A determination of the machining processes to be performed forms the starting point for a proper time estimation. As this often can be a cumbersome and time intensive task, automation of these operational processes is needed. Therefore, this chapter will describe how the developed estimation algorithms are incorporated into an automated operations evaluation system, with the focus of use in mould manufacturing.

5.1. Architecture of operations evaluation system

Fig. 5.1 shows the general concept of the developed operations evaluation system. The input for the system is a part geometry (e.g. mould) represented as a faceted model (STL-file). Regions to be EDMed are automatically detected, followed by the interactive definition of electrode geometries. One electrode geometry is seen here as a set of part triangles which contains the geometrical part information for one sinking EDM operation. Together with user entered parameters such as required roughness, tolerances and machining preferences, a list of EDM operations is generated. For each operation (e.g. EDM of a cavity with a given electrode shape), the EDM strategy definition module proposes a machining strategy. This strategy describes a sequence of sub-operations (roughing, finishing_1, finishing_2,…, finishing_n) with an associated sequence of generator regimes to machine a certain region. Most commercial EDM machines have software functionality to generate these strategies. Therefore, it was decided to integrate the strategy definition module CT-expert from AgieCharmilles (as the RoboForm 350ɣ is used within this research). But in case of other machine types, it should be replaced by another machine dependent strategy module. The decision to opt for a machine specific strategy module is also supported by the fact that optimal EDM strategies are very often machine dependent. For each machining step, associated by a machine specific regime, reference

material removal rates are available from the calibration procedures (see Section 4.2.1 and Section 4.3.1). EDM machining time is then calculated based on the available reference rates and the developed models.

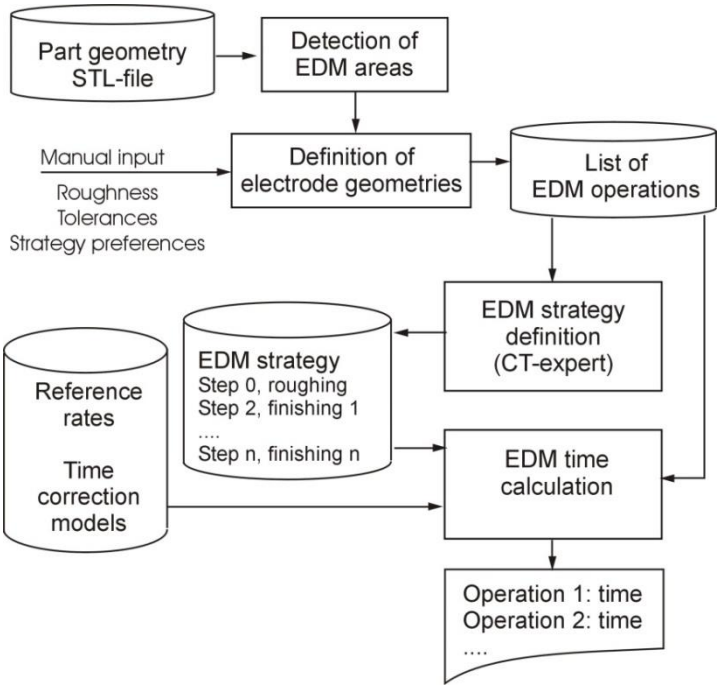

Fig. 5.1: Architecture of the developed operations evaluation system.

5.2. Detection of EDM areas and electrode geometries

A commonly applied rule in mould manufacturing is to remove most of the material by milling operations. Based on the part geometry, represented by an STL-file, regions that can be milled by a given set of milling tools are automatically identified by a 3-axis millability check algorithm. In the developed system, the millability check (3-axis milling) is performed by slicing the mould with parallel planes perpendicular to the top surface of the mould resulting in a set of contours. In each point of the contour it is checked whether the milling tool can access the point without gauging. Locations

where gauging occurs are locations where an EDM operation needs to be performed. A simplifying rule is used to determine the volume to be EDMed: an area determined as non-millable will be completely machined by EDM. Fig. 5.2 shows the result of the millability check performed on a sample mould. Other milling region detection algorithms will result in other EDM areas. For example, a 5-axis millability check algorithm will identify all regions that can be machined by a 5-axis milling operation. Compared to 3-axis machining, a 5-axis milling operation will remove more material, hence leaving smaller areas to be EDMed. Instead of having an automatic detection of milling regions, the user can also indicate milling and EDM areas in an interactive way. Detected EDM areas, represented as a collection of triangles in XTL (Extended STL language [132]) format can be combined to create electrode geometries. As an example, Fig. 5.3 shows an electrode geometry defined by two EDM areas. Electrode geometries are defined as shapes which can be machined in one operation (e.g. roughing by sinking and finishing by an orbital movement) by combining the geometries on one electrode. By slicing the electrode geometry by planes perpendicular to the EDM sinking direction, a number of contours can be generated as a function of the depth (Fig. 5.3), resulting in valuable information for the actual time estimation. By not closing the contours on places where no sparking occurs the EDM time estimation algorithms can take the effect of the improved flushing in this kind of situations into account. Based on the number of contours (polylines) in each slice, the number of protrusions can be derived. These kind of simple shaped electrodes occur very often in daily practice. The evolution of the contours as a function of depth also gives valuable information. Contours can be closed at start (deeper in the cavity) and become open for smaller depths (less deep). At certain depths, contours can merge together, which means that the electrode will go deeper than the height of some protrusions. In addition, the contours can also be used to calculate volumes and the active areas (frontal area) as a function of the depth.

5.3. Definition of EDM operations

In order to have the EDM operations or strategies generated automatically, the EDM machine software has been incorporated into the time estimation module of the operations evaluation system. In this work a specific EDM software (CT-expert) has been chosen. In the future the time estimation module can easily be adapted to other EDM machine software systems by redefining the communication of the module with the machine software.

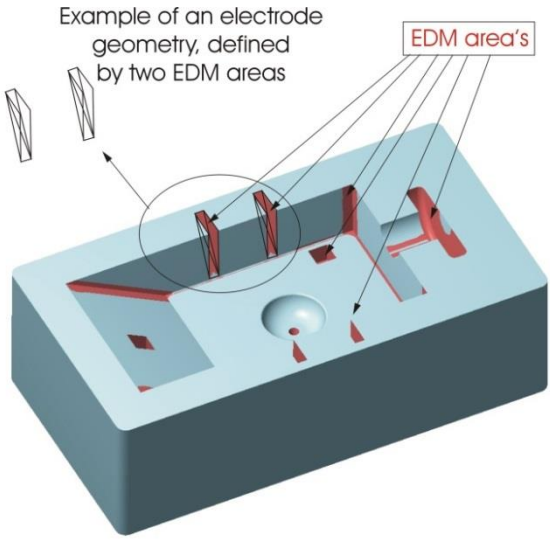

Fig. 5.2: Detection of EDM areas and determination of electrode geometries.

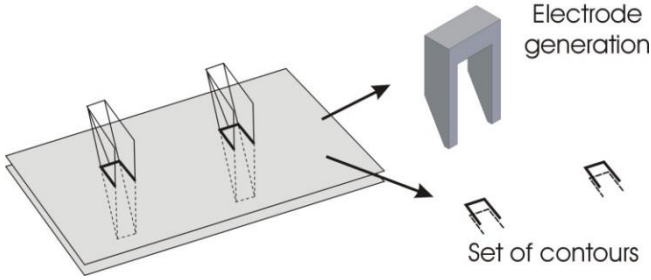

Fig. 5.3: Contours resulting from the slicing of electrode geometries.

The machine software generates the EDM sequence based on a limited number of inputs. Two types of inputs can be defined. The first type of inputs directly comes from the user: the desired end roughness, the electrode undersize (opposed to earlier methods, the undersize acts as an input parameter for the EDM machine software), electrode material, the electrode movement and priorities to speed, tool wear or surface quality. The second set of input is related to the shape to be machined and is extracted from the XTL representation of the EDM areas. This involves parameters like the maximal frontal surface area of the electrode, total depth of machining and the type of feature of the cavity (standard, rib, surface). Based on these

inputs the EDM software generates for each electrode geometry a sequence of generator regimes by the depth of machining and the electrode movement (see Fig. 5.4). The output of the machine software is the EDM sequence which is stored in an XMLJ (Extensible Markup Journal Language) file.

#			Lchg [mm]		[mn]		Flush (M70)	[rpm]	P [A]	A [µs]	B [µs]	S [%
1	**298**	**1**	**0.300**	**B**	**0**	**ON**	**A0B0C0D0**	**0**	**64.0**	**6.4**	**100.0**	
2	288	2	0.105	B	0	ON	A0B0C0D0	0	64.0	6.4	100.0	
3	278	2	0.092	B	0	ON	A0B0C0D0	0	64.0	3.2	100.0	
4	268	2	0.082	B	0	ON	A0B0C0D0	0	64.0	3.2	100.0	
5	258	2	0.069	B	0	ON	A0B0C0D0	0	48.0	3.2	100.0	
6	230	2	0.053	B	0	ON	A0B0C0D0	0	6.0	6.4	6.4	
7	210	2	0.033	B	0	ON	A0B0C0D0	0	2.0	6.4	3.2	
8	190	2	0.019	B	0	ON	A0B0C0D0	0	1.5	3.2	1.6	
9	170	2	0.010	B	0	ON	A0B0C0D0	0	1.0	3.2	1.6	
10	150	2	0.005	B	0	ON	A0B0C0D0	0	0.5	1.6	1.6	

Fig. 5.4: EDM strategy definition.

5.4. EDM time estimation

As described before, the calculation of the EDM machining time is based on reference removal rates (or reference machining times), which are corrected to take deviations from the reference conditions into account. Deviations from the reference might change during one EDM operation. Therefore, time estimation calculations are performed for small machining steps and machining conditions are assumed to be constant during one step. The summation of the machining times of all machining steps then represents the total EDM time (see Eq. 4.1). For both the determination of $time_{ref}$ and the modelling of the correction factor, distinction is made between roughing and finishing operations. In this study, roughing operations, removing larger volumes, are done by a simple sinking EDM movement with high energy settings, while finishing is performed by an orbital movement with low energy settings. For roughing operations the time estimation is performed by splitting up the total volume of the roughing operation in discrete prismatic volumes along the sinking direction (Fig. 5.5). This is done by slicing the XTL representation of the electrode geometry with planes perpendicular to the machining direction (see Fig. 5.5). As a result contours are defined which are protruded along the machining direction for half of the distance between 2 consecutive slices up and downwards. For each of these generated volumes, a correction factor $C_{R,i}$ will be applied to $MRR_{ref,i}$

corresponding to the generator regime active during the machining step. For small machining steps, the value of C_R can be considered to be constant.

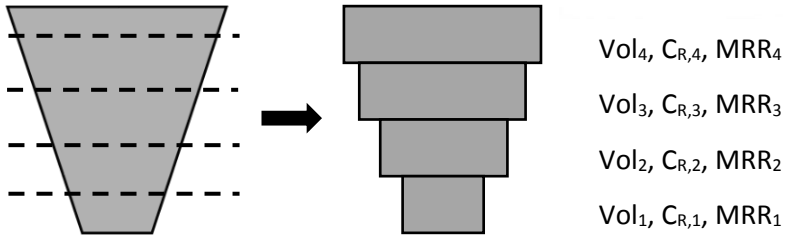

Fig. 5.5: Discretization of machining volume for roughing operations based on slicing along the machining direction with corresponding C_R and MRRref.

Opposed to roughing operations, each calculation step in finishing operations corresponds to an orbital electrode movement step, each associated by a different finishing regime and an eccentricity or machining length value. For each regime a correction factor is applied to the reference time obtained from the calibration. An important geometrical parameter is the total active area which can be extracted from the detected EDM areas. Besides the EDM strategy defined by the EDM machine software, the EDM time estimation algorithms require the following geometrical inputs:

- number of protrusions on the electrode;
- evolution of the frontal area in function of the machining depth for each protrusion;
- starting and ending depth for each protrusion;
- lateral surface area for each protrusion;
- closed/partially open machining;
- depth at which protrusions merge. This is important because at that depth the flushing conditions can change heavily due to the bad removal of debris.

5.5. Graphical user interface and software functionality

The purpose of the operations evaluation system is to give the user an easy-to-use tool for quickly determining EDM areas and calculating corresponding EDM times. In this way, different machining strategies can be compared and the optimal strategy can be chosen.
Fig. 5.6 shows a screenshot of the developed software which acts as a standalone tool. The user interface is divided in different sections which provide the following functionalities.

Graphical section
Displays the mould geometry and highlights the EDM areas.

'Model' section
Loading of STL file of mould or electrode. When selecting a mould a millability check can be performed resulting in different electrode geometries for which EDM times can be calculated. It is also possible to calculate EDM times starting from an electrode geometry and by defining the machining depth.
Indication of *machining direction* of milling tool and electrodes.

'Mill settings' section
Definition of milling tool diameter and tip radius. Ideally, the smallest milling tool is defined here to maximize the number of cavities that can be machined by milling.

'Time settings' section
This section defines parameters related to the EDM time estimation. These settings can be altered for every electrode geometry:

- *Step size*: distance between 2 slices when establishing volumes for calculation of EDM roughing time.
- *Materials*: selection of electrode material.
- *Undersize*: defines the undersize per electrode.
- *End roughness*: defines the desired roughness after each operation.
- *Machining cycle*: defines the electrode movement.
- *Cavity type*: defines the type of cavity (standard, rib, surface).

'Electrodes' section

Lists all electrode shapes resulting from the millability check. Several electrode shapes can be combined to one electrode geometry.

Result section

When selecting an electrode geometry and clicking the 'EDM Time' button the graphical section will show the electrode geometry with highlighted active area with the corresponding slices generated for estimating the roughing time (see Fig. 5.7). The upper slice corresponds to the first volume to be machined during the roughing operation. The total EDM time is given on the lower right side of the screen. In the result section below the EDM time, corresponding depth, number of protrusions, frontal area and active generator regime are displayed for every slice.

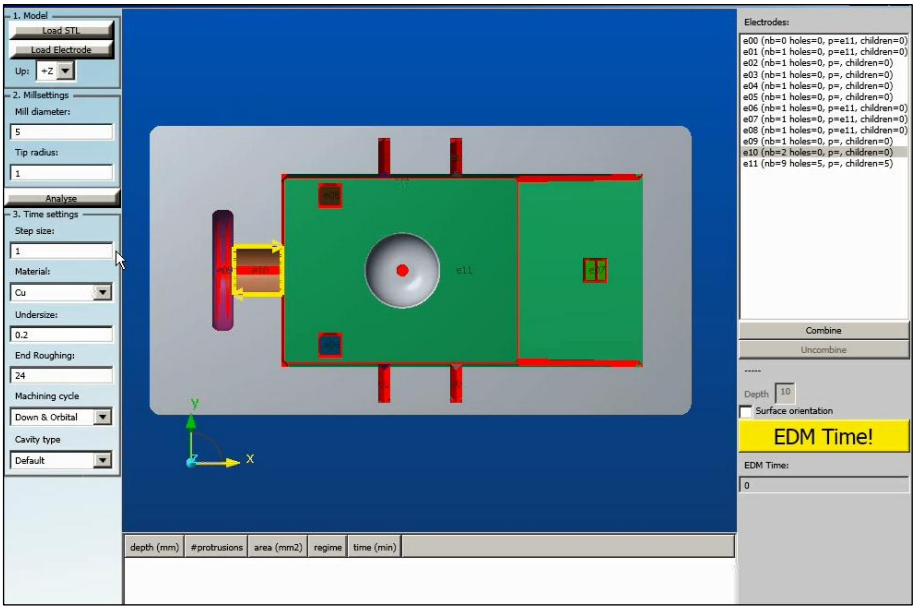

Fig. 5.6: Screenshot of operations evaluation software.

5.6. Validation with practical cases

In addition to the validation tests performed in Chapter 4 which focus on prismatic cavities, the developed models have been validated with a limited set of more complex industrial cases by means of the developed software tool. Opposed to the previously describes validation which consisted of machining prismatic shapes, the software tool gives the opportunity to perform time calculation for more complex machining cases. Fig. 5.8.a shows an example of a complex validation case submitted to the developed software. Two EDM areas/cavities are identified which are machined by two independent EDM operations (see Fig. 5.8.b-c for the corresponding electrodes). Real and estimated machining times for the two cavities are given in Table 5.1. For comparison, the estimated machining times based on reference rates given in the technology tables are also given. Also for this case, the developed models outperform other existing time estimation methods.

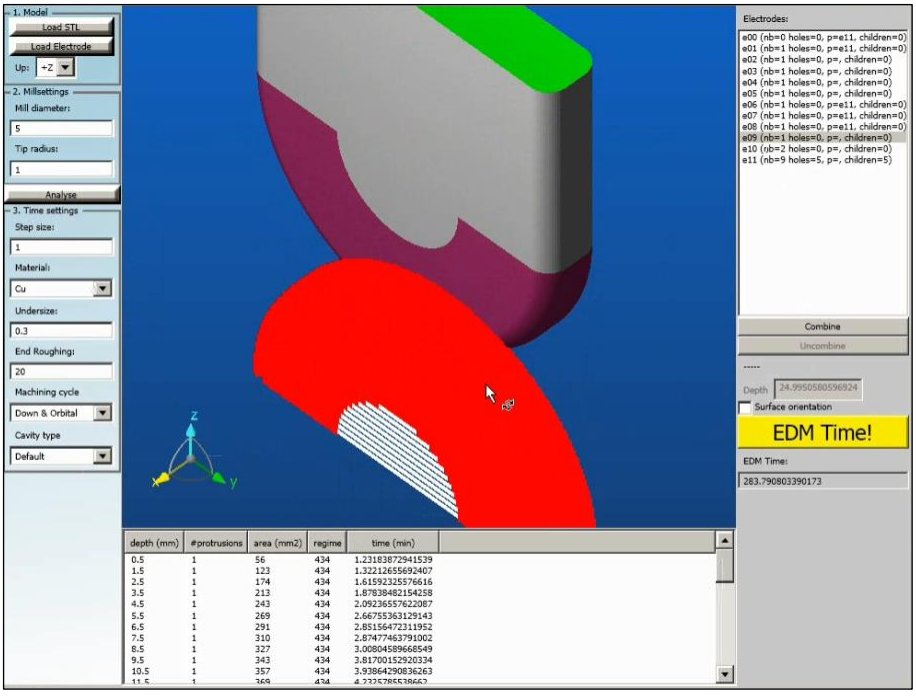

Fig. 5.7: Screenshot of result of time estimation software.

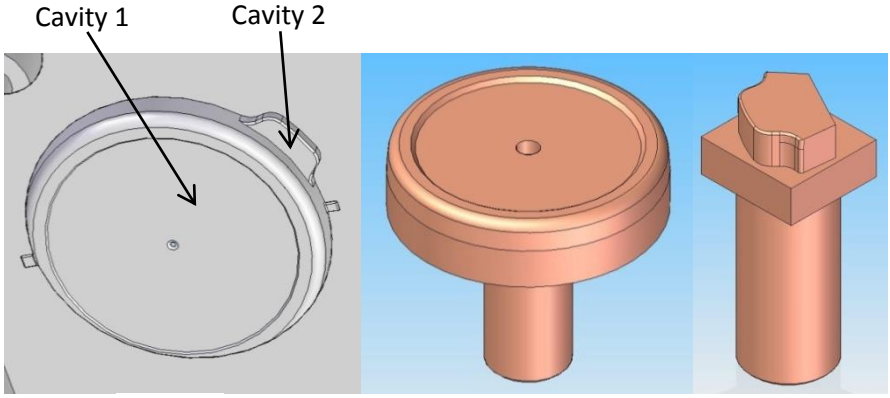

a. b. c.

Fig. 5.8: Validation case: (a) mould geometry; (b,c) electrodes.

Table 5.1: Validation results of machining case presented in Fig. 5.8.

	Roughing		Finishing	
	Cavity 1	Cavity 2	Cavity 1	Cavity 2
Real time [min]	44	4	111	6,3
Estimated time based on developed models [min]	43,6	3,8	81,2	8,4
% error	1	5	26,8	-34,5
Estimated time based on machine reference [min]	47	2,6	61,4	2,3
% error	-6,8	35,2	44,7	64,3

5.7. Summary

In order to be able to estimate the machining time for complex machining cases, the developed models have been incorporated into an operations evaluation system which automatically calculates all necessary inputs and results in an estimate of the machining time for each applicable EDM operation. This is achieved by extracting all areas to be machined by EDM from the parts file by performing a millabilty analysis. If needed, areas can be combined in one EDM operation by defining a proper electrode geometry. For each electrode geometry an EDM strategy is defined by interacting with the EDM machine software. Based on this EDM strategy and the electrode geometry the total EDM time is calculated in an automated way. This software tool allows the user to iteratively assess and compare different machining strategies by altering the electrode geometry to come to an optimal machining strategy in terms of machining time. When an effective strategy is found one can start with the actual milling of the electrodes. Accurate knowledge of the EDM machining time ultimately increases the reliability and robustness of the process planning.

PART II:
Process Planning for a Combined Micro-EDM and Micro-milling Machining Platform

Chapter 6 Push towards hybrid micro-manufacturing

Besides the need for advanced process planning tools on the level of macro machining (see Part I), there is also a need for proper planning tools suited for machining operations on micro scale. In order to situate the second part of this study, this chapter will first discuss the state of the art in micro-manufacturing and the current trend towards hybridization. As many hybrid processes and machines for micro-applications are micro-EDM related, an overview of micro-EDM related hybrid processes with their benefits and limitations will be given. Among this large set of hybrid processes, it has been chosen to focus on a combined electro-erosive and abrasive machining action by integrating the micro-EDM and micro-milling process onto one machining platform. In a next section, the platform characteristics and its peculiarities will be discussed. Based on this, the specific objectives of this part of this study will be discussed in more detail.

6.1. State of the art in micro-manufacturing

Many industries have been making parts with micron dimensions for some time, but in the last decade the market for miniaturization has expanded. The demand is not only for small parts, but also for small complex features on larger parts [133]. The medical and electronic industries are the most active in this area. In both cases the incentives are the same: making smaller parts with more capabilities at lower cost. For example, cell phones have significantly diminished in size whereas the functionality and performance has increased tremendously. Also the aerospace and automotive sector demand very small components like small actuators and miniaturized spray holes in fuel injection systems reducing the fuel consumption. Other examples of micro-parts are miniaturized implants to restore lost body functions or micro-reactors to ensure that chemical reactions require smaller amounts of reagents and can take place in a safer and more controlled process. Another important market for micro-components is microfluidics for assay testing, drug discovery and environmental testing in research laboratories and pharmaceutical and biomedical applications [50].

Micro-manufacturing techniques can be classified in two groups: MEMS-based techniques, which are often derived from the semiconductor industry, and non-MEMS-based techniques [50].
The MEMS-based techniques are well understood and are suited for large series production. One of the key processes in MEMS-based manufacturing are lithography-based processes in which a 2.5D structure is build up on a substrate. A common variant is the LIGA process in which a metallic pattern is electroplated on a substrate with the aid of photoresistant material subjected to X-ray beams. The end product can be used as a stamping tool, mould or as a final part. Advantages of this process are the high attainable aspect ratios (up to 100), straight walls and smooth surface finish (see Fig. 6.1.a). However, LIGA is not able to produce complex geometries and is restricted to a small set of materials [134]. This, in combination with the huge capital investment, restricts its application mainly to mass production in the semiconductor industry.
Another common MEMS-based manufacturing technique is chemical etching. Although the mask used in the etching process can specify a pattern with a good precision, the obtained accuracy and the attainable aspect ratio are rather poor due to the isotropic behavior of the process. On the other hand, the obtained surface is smooth (see Fig. 6.1.b) free from damage, residual stresses and heat effects [134].

Non-MEMS-based manufacturing techniques mainly refer to macro-manufacturing technologies that have been downscaled to suit demands for micro-manufacturing like a proper equipment precision, three dimensional flexibility and cost effectiveness.
A commonly applied subgroup of non-MEMS-based manufacturing techniques covers processes that rely on the principle of plastic deformation and solidification. Examples of this are respectively hot embossing and injection moulding. Both types of processes rely on pre-shaped dies or moulds and are ideally suited for mass production, unlike other non-MEMS-based processes. In addition, small complex features can be manufactured in a wide range of materials. For example, wall thicknesses of 20 µm with details in the range of 0.2 µm and aspect ratios up to 30 can be obtained for polymer injection moulding [135] (see Fig. 6.2.a). However, these techniques suffer from loss of accuracy due to post-process deformations (see Fig. 6.1.c).

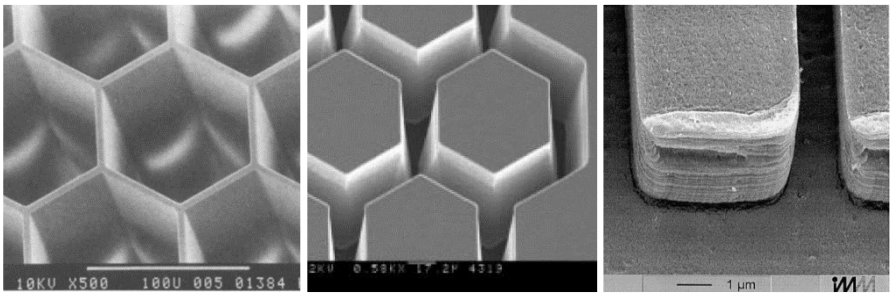

a. b. c.

Fig. 6.1: Typical geometries fabricated with (a) LIGA [136]*; (b) chemical etching* [137]*; (c) hot embossing* [138]*.*

Another subgroup of non-MEMS-based processes refers to micro-mechanical processes like micro-milling, micro-turning and micro-grinding. These processes have the advantage of a good geometrical correlation between the tool path and the machined surface due to the constant contact of the tool with the workpiece. However, the corresponding process forces are significant hence reducing the accuracy, attainable aspect ratio and limiting the machinable size due to elastic deformation of the tool [134]. Although the application of these processes on a micro-scale incorporates similar characteristics as on the macro-scale, factors that can be ignored with conventional machining need to be considered in micro-manufacturing e.g. vibration, tool offset, material homogeneity, temperature, rigidity of the tools and the machine structure and chip removal. In order to remove small units of volume, micro-milling tools need to be produced with an edge radius around 1 µm. Fig. 6.2.b shows an example of a complex 3D micro-geometry machined with micro-milling. For micro-grinding, it is either required to provide a small feeding resolution or to produce grinding tools with ultrafine abrasive grains. In [139], a surface roughness of 1.14 nm Ra and 0.79 nm Ra for the machining of respectively Al_2O_3-TiC and SiC is reported by using a grinding tool with diamond particles embedded in a soft tin plate.

Another popular group of techniques for micro-manufacturing refers to electro-thermal and electrochemical processes like micro-EDM and micro-ECM. Unlike mechanical processes, materials irrespective of their hardness can be machined. In addition, very small and thin features can be machined as process forces are very low. However, there are limitations on the attainable accuracy as micro-EDM suffers from severe tool wear and in micro-ECM the control of the gap is crucial. Micro-ECM differentiates itself

from micro-EDM by its non-thermal behavior. As a result, no thermal stresses, heat affected zones or thermal damages occur on the surfaces of machined parts. In addition, a better surface finish can be obtained (down to 0.13 µm Ra [50]) making micro-ECM a preferable technique in biomedical, electronic and MEMS applications and for deburring operations.
A final commonly applied non-MEMS-based process is laser ablation. Here very tiny pieces of material are removed in a controlled manner making it a precise though rather slow process. Due to the application of excimer and femtosecond lasers, a wide range of materials can be processed with few surface defects, high dimensional accuracy (see Fig. 6.2.e) and feature size down to 0.1 µm [50].

In Table 6.1 a comparison of all previously discussed processes is made. In section 6.3 the characteristics of these processes are discussed in more detail.

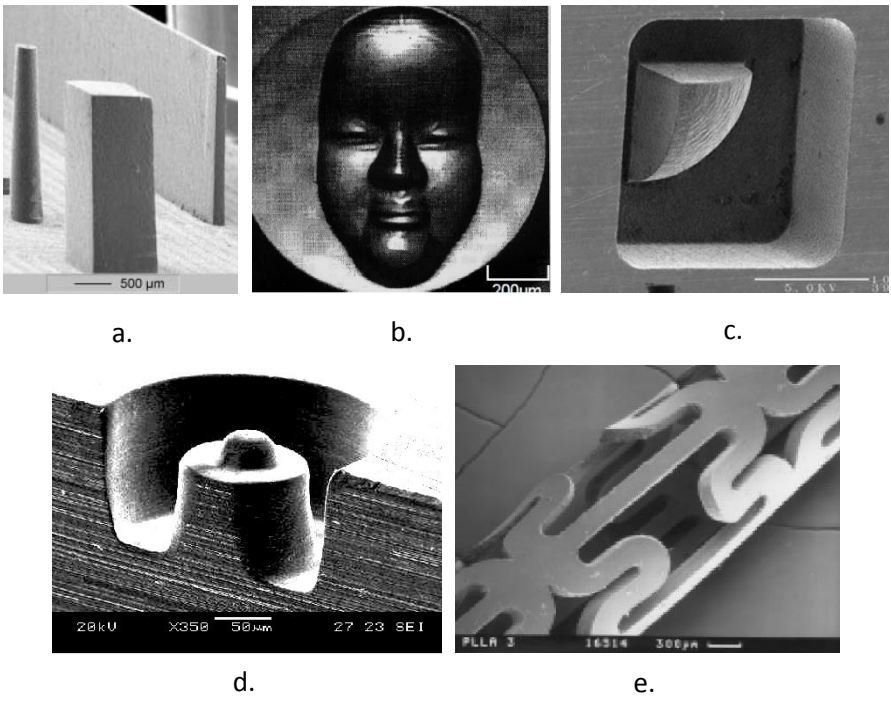

Fig. 6.2: Geometries fabricated with (a) micro injection moulding [135]*; (b) micro-milling* [134]*; (c) micro-EDM* [50]*; (d) micro-EDM* [50]*; (e) laser ablation* [134] *.*

Table 6.1: Comparison of common micro-manufacturing techniques, as an extension of [50], [134].

Process \ Criterion	Machining speed	Range of materials	Surface integrity	Geometrical complexity	Mass production	Investment effort
LIGA	-	-	+	-	+	-
Chemical etching	o	o	+	-	+	o
Hot embossing	+	o	o	o	+	+
Injection moulding	+	+	+	+	+	+
Micro-mechanical processes	+	o	+	+	o	+
Micro-EDM	o	o	-	+	-	+
Micro-ECM	o	o	+	+	-	+
Laser ablation	-	+	o	-	-	o

+ Good o Fair - Poor

6.2. Hybridization in micro-manufacturing

As many micro-components need to be produced in large lot sizes in an even faster and cost effective manner with increasing demands on accuracy, micro-manufacturing technologies are pushed towards their limits. In some cases this even means the transition to another suboptimal process or to a sequence of different processes on different machines, ultimately increasing throughput time and loss of accuracy. To comply with the increasingly stringent demands, there is a trend towards hybridization in micro-manufacturing.

Often the term hybrid is used for different types of combined process technologies. However, the International Academy for Production Engineering (CIRP) narrows the definition of hybrid processes down to: “processes based on the simultaneous and controlled interaction of process mechanisms and/or energy sources/tools having a significant effect on the process performance” [140]. According to this definition, machines that integrate different sequential processes are excluded. However, these can be denoted as hybrid machines. According to Lauwers [140], hybrid processes can be classified in two groups. The first group consists of

processes where two or more energy sources/tools are combined and have a synergetic effect in the machining zone. A further classification can be made in assisted hybrid processes where the primary process sets the material removal mechanism and is assisted by other processes (e.g. laser assisted milling). On the contrary mixed hybrid processes denote those processes where different removal mechanisms are present (e.g. electrochemical discharge machining). The second group of hybrid processes consists of those processes where a controlled combination of effects is present that are conventionally caused by separated processes.
Hybridization is a more general term covering both hybrid machines and hybrid processes. Hybridization is not new, lathes are already many years equipped with milling spindles and vertical milling machines are equipped with a rotating horizontal table for turning operations. Also the machining of PCD cutting tools with a hybrid process consisting of grinding and EDM is available since early 1990s.

The ultimate goal of hybrid manufacturing is to enhance the advantages and to eliminate the potential disadvantages of the separate processes. The productivity of hybrid processes or hybrid machines is usually much higher than the summed up results of the individual processes due to synergetic effects. Similar results have been achieved with respect to energy consumption and surface finish [54]. In addition technological process limits (e.g. material restriction, geometrical features) can be strongly extended. Hybrid machines show the potential to reduce capital outlay by purchasing only one machine tool rather than several machine tools, each having its own controller, tooling systems, etc. Moreover, the setting time is reduced and the transfer time between machining operations is eliminated resulting in an increased accuracy and repeatability.

6.3. Micro-EDM related hybrid machining

The EDM process has a large application range, covering several materials, especially those materials which are difficult-to-cut by conventional machining processes. Moreover, high accuracy can be obtained which makes it suitable for the manufacturing of precision components. On the other hand, the thermal nature of the EDM process often causes a deterioration of the machined surface, such as micro-cracks, a recast layer and heat affected zone with residual stresses and a rough machined surface. In addition, the removal rate is relatively low compared to other machining processes.

Currently, EDM generator technology and flushing systems are already at a mature level, requiring more efforts for further improvement. To facilitate further improvements several assisted and combined machining processes have been developed. Fig. 6.3 gives an overview of hybrid and sequential machining processes which combine the removal mechanisms of EDM and an abrasive, electrochemical, laser assisted or ultrasonic assisted machining process. The following sections will describe in more detail a selection of existing processes and their specific benefits and applications.

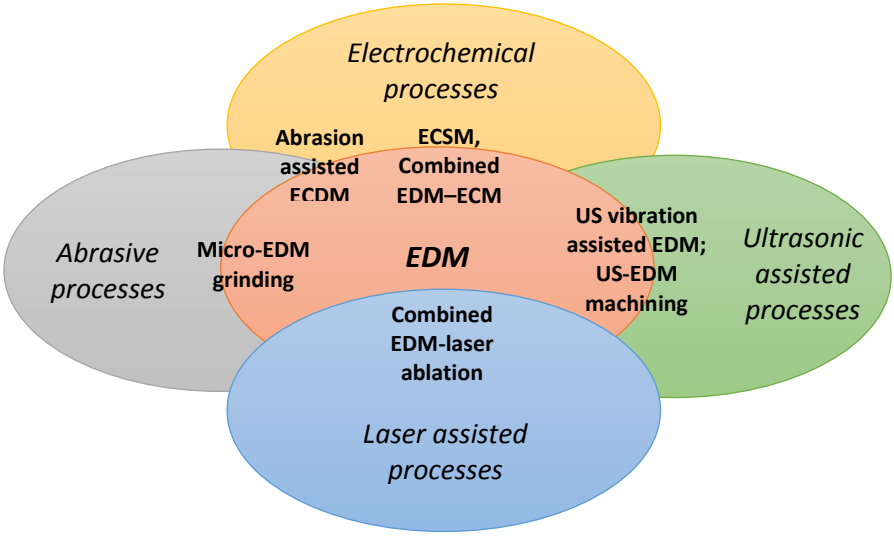

Fig. 6.2: Overview of EDM related hybrid and sequential processes.

6.3.1. Abrasion based machining

Several hybrid processes consist of an abrasive mechanism, mainly to increase the machining speed. For example, in electrochemical grinding the abrasive action continually removes the passivation layer in-process, enhancing the electrochemical removal action [141]. Also in laser milling/grooving it has been shown that an air jet mixed with abrasive particles directed at the melt pool increases the machining speed and lowers the heat affected zone [142]. Also in combination with EDM, hybrid processes exists with an abrasive action. For example, in section 2.1.3 two hybrid processes with an abrasive action have been described namely abrasion assisted wire EDM and abrasive electrical discharge grinding. These suggest the feasibility to implement this combination on micro scale.

The combination of an abrasive and an electro-erosive removal mechanism on micro scale can be achieved by electrodepositing a composite coating, consisting of a metallic layer containing a dispersion of non-conductive second-phase particles like diamond, SiC and Al_2O_3, onto an EDM electrode. A micro tool like the one displayed in Fig. 6.4.a can be obtained. As the operation mostly happens on a micro-EDM platform, the electrode is pre-shaped by the WEDG-unit and coated in an electroplating bath. During operation, there is a synchronous action of the EDM process in which the metallic layer acts as the electrode and the grinding process in which the hard non-conductive grit material removes the recast layer induced by the EDM process (see Fig. 6.4.b). This so called micro-EDM grinding process shows to result in synergetic effects as the heat generated by the EDM process lowers the energy needed to cut away the recast layer. Hence a higher removal rate and lower process forces can be obtained when comparing with the individual processes. In addition, the helical tool shape (see Fig. 6.4.a) assists in removing the generated debris from the sparking gap. Important for this hybrid process to be successful is the tuning of the generator settings in order to regulate the sparking gap to be lower than the exposed height of the grit material. With this hybrid process surface roughness values down to 0.107 µm Ra with tool diameters below 0.3mm for a machining depth of 300 µm can be obtained [143].

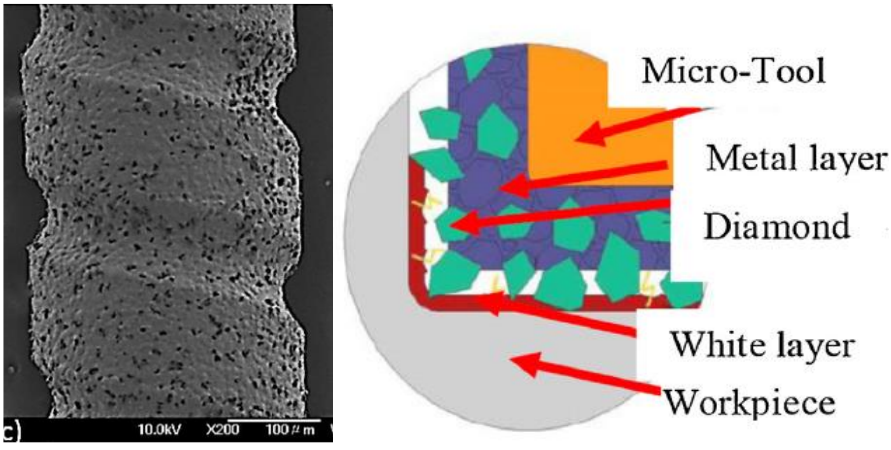

a. b.

Fig. 6.3: (a) Tungsten carbide electrode with Ni-Co/diamond deposition; (b) removal principle of micro-EDM grinding [143].

The fabrication of such coated tools on a micro-EDM machining platform eliminates the difficulty of the highly repetitive precise positioning of grinding tools. In addition, the WEDG-unit offers the possibility to create complex tool electrodes by shaping these directly onto the machining platform followed by an electroplating treatment on the same platform. Fig. 6.5.a shows an example of a spherical tool fabricated on such a hybrid machining platform. With this tool a cavity like shown in Fig. 6.5.b with a roughness down to 0.353 µm Rz can be obtained [144], which is much lower than the roughness after a micro-EDM operation with a similar tool.

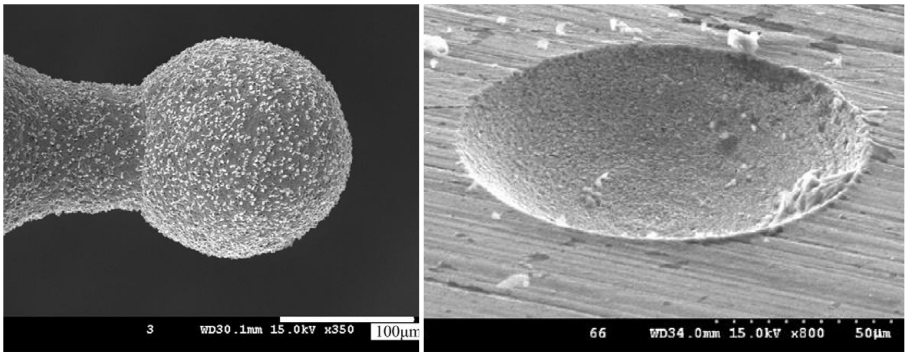

a. b.

Fig. 6.4: (a) Spherical grinding tool fabricated on micro-EDM platform; (b) cavity with depth of 25 µm and diameter of 100 µm machined with spherical tool [144].

6.3.2. Electrochemical based machining

Similar to the EDM process, 2 electrodes placed within a fluid at a certain distance from each other are used in electrochemical machining. Though, the differences are the opposite polarity compared to EDM and an electrolyte as process fluid. As a consequence, electrochemical reactions occur, removing material at the anode (workpiece). As ECM is a contactless and non-thermal process, no stresses are induced in the machined surface. In addition, low roughness values can be obtained without significant tool wear. These complementary benefits make ECM an ideal process to be used in combination with EDM.

Sequential EDM – ECM

In the sequential EDM-ECM machining process, EDM acts as a roughing process whereas ECM is used to enhance the surface quality of the EDMed surfaces. In this process the same tool is used for both operations and machining can be performed in the same process fluid, e.g. distilled water [145]. It has been shown that the surface roughness can be improved significantly by adding an ECM-finishing operation in either sinking, milling, drilling or wire cutting operations [145]–[148]. This can be clearly seen in Fig. 6.5 showing the surface quality of a cavity machined with micro-EDM milling (Fig. 6.6.a) and finished with micro-ECM milling (Fig. 6.6.b). In this example both surface roughness and thickness of the recast layer have been reduced.

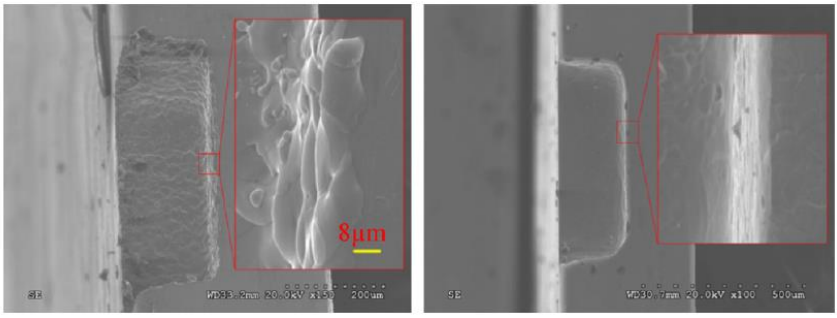

a. b.

Fig. 6.5: Example of micro-cavity machined by combined micro-EDM/ECM with Ø0.1 mm tungsten electrode, 304 stainless steel workpiece in $NaClO_3$ solution: (a) after EDM operation; (b) after ECM-finishing operation [147].

Although the surface quality can be improved by introducing the ECM process, it remains difficult to produce mirror-like surfaces with this combined process. To counteract this, ceramic abrasives (e.g. Al_2O_3) are added to the fluid during the ECM operation to enable a kind of lapping action. The abrasives remove the oxidized layer during ECM and deliver a significantly reduction in roughness. Roughness values down to 0.07 µm Ra have been obtained [149]. Fig. 6.7 shows a comparison of surfaces machined by micro-EDM (Fig. 6.7.a), micro-ECM (Fig. 6.7.b) and micro-ECM-lapping (Fig. 6.7.c) respectively. Although some reports have been made about the use of the combined process in macro applications, most of the research in this area has been conducted for the machining of micro parts.

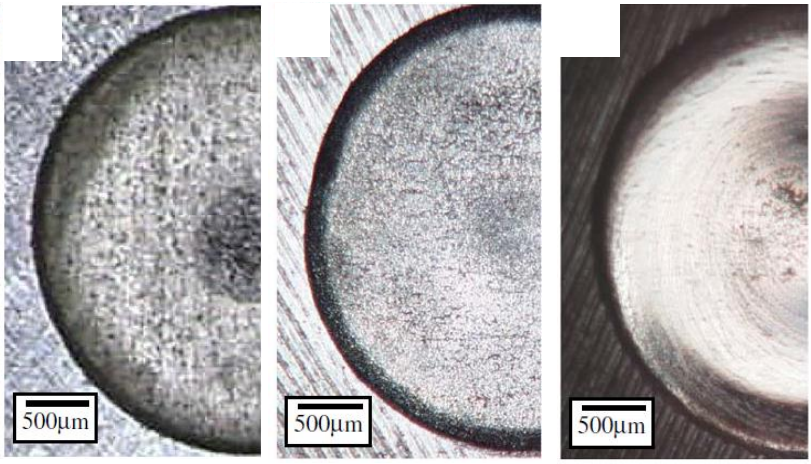

a. b. c.

Fig. 6.6: Surfaces machined with (a) micro-EDM; (b) micro-ECM; (c) micro-ECM lapping [149].

Electrochemical spark machining (ECSM)

The ECSM process combines the features of electrochemical machining (ECM) and electrical discharge machining (EDM). Generally, the process consists of a cathode (tool electrode) and an anode which is either the workpiece or an auxiliary electrode. Depending on the nature of the material to be machined different names are used for this hybrid process. Machining conductive materials is denoted as Electro-Chemical Arc Machining (ECAM) following from the fact that relatively long pulses occur, classifying them as arcs [150]. On the other hand, the machining of non-conductive materials is denoted as Electro-Chemical Discharge Machining (ECDM) or Spark Assisted Chemical Engraving (SACE) as shorter pulses occur [151]. In both ECAM and ECDM tool electrode (mostly highly corrosion resistant metal like stainless steel, copper, tungsten, nickel, etc.) and workpiece are submerged in an electrolyte. Common electrolytes used in ECSM are NaOH, KOH, $NaNO_3$ and NaF [152]. A constant DC or pulsed DC voltage is applied to the tool electrode and workpiece in case of ECAM, which makes the setup similar to an ECM setup. When machining non-conductive materials an auxiliary non-dissolving electrode, placed several centimeters from the tool, serves as anode (see Fig. 6.8).

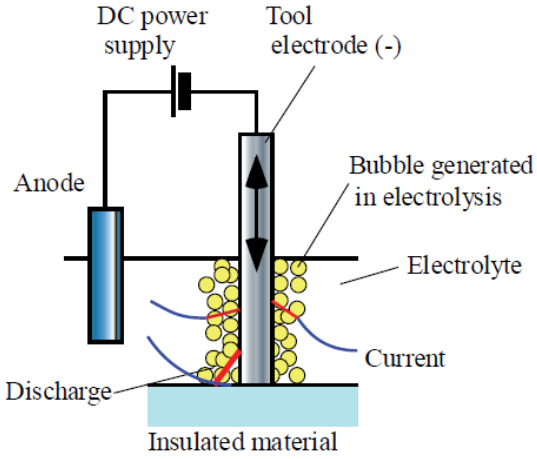

Fig. 6.7: Working principle of ECSM [153].

The removal action of the ECSM process consists of two phases. In the first phase, material is electro-chemically dissolved. In addition, the applied voltage leads to the generation of hydrogen bubbles at the tool side. Increasing the voltage will lead to more bubbles that, when nearly reaching the breakdown voltage, will coalesce to form a gas film around the tool electrode. In the second phase, the rapid decrease of the current and the induced e.m.f. generates a spark. In case of ECAM, where the workpiece is positively charged, the spark will occur between the tool and the nearby placed workpiece. In case of ECDM, the workpiece is not charged meaning that the spark occurs between the tool and the electrolyte. By submerging the tool electrode only a few millimeters in the electrolyte and putting the workpiece in the close vicinity of the tool (sometimes even in direct contact), the heat of the spark is most likely used for melting and evaporation of the workpiece material. However, until now the exact material removal mechanism is not yet fully understood.

In **Electro-Chemical Arc Machining** the obtained MRR can be as much as 5 and 40 times higher than those obtained in ECM and EDM respectively [154]. This is mainly due to the combined action of electrochemical dissolution at the beginning of the voltage pulse and the electro-erosive material removal at the end of the voltage pulse. Besides this, the gap size is larger compared to EDM leading to more stable conditions, hence raising the machining efficiency [155]. The ECAM process can be used as a drilling operation, a 3D structuring operation, a wire cutting operation and also as a trueing and

dressing operation of metal bonded CBN grinding wheels [156]. An example showing the potential of ECAM is the wire-ECDM of Al_2O_3 particle reinforced aluminum alloy 6061 where machining speeds ranging from 40 to 80 mm^2/min can be obtained [157].

Opposed to ECAM, **Electro-Chemical Discharge Machining** lacks high removal rates. As a result, the ECDM process is mainly used for machining micro-parts. The most common materials to be machined are glass, quartz, Al_2O_3 and composite materials (e.g. glass-epoxy, kevlar-epoxy) [158]. A remarkable fact is that although EDM and ECM cannot be used to machine these materials, the hybrid ECDM process is able to perform the job. Compared to other micro-machining processes like laser beam machining, ultrasonic machining and chemical etching, ECDM results in less thermal damage and leaves less surface cracks behind. Moreover, ECDM can be used for machining any non-conductive material irrespective of its mechanical, physical or metallurgical properties. The material removal can be mainly attributed to the erosive impact of the generated sparks assisted by chemical dissolution which is accelerated by the elevated temperatures due to the sparks [159]. The ECDM process can be used in different configurations: as a micro-drilling operation, a 3D micro-structuring operation or as a wire cutting operation. Fig. 6.9 shows some examples of micro-structures machined with ECDM. Important in all configurations is that the tool electrode is submerged only a few millimeters in the electrolyte in order to allow the generation of a gas film around the entire electrode surface. This limits the total depth of cut and the workpiece thickness, e.g. plates with a thickness up to 10 mm can be efficiently cut by wire-ECDM [152]. Nevertheless, aspect ratios up to 11 have been achieved for drilling in glass by intensified process enhancements [159]. Typical removal rates obtained for wire-ECDM of glass, quartz and Al_2O_3 are respectively 0.9 mm^3/min, 0.6 mm^3/min and 0.06 mm^3/min [160].

An improvement in the removal rate of ECDM can be achieved by adding an abrasive action to the process, denoting the entire process as **abrasion-assisted ECDM.** In wire-ECDM abrasives can be added to the electrolyte resulting in an increase of 33% in MRR when machining Pyrex glass [161]. Moreover, the addition of abrasives reduces the surface roughness due to the lapping action, e.g. 0.8 µm Ra for Pyrex glass [161], and reduces the kerf loss. Besides this, the use of a wire coated with abrasive particles in wire-

ECDM can lead to an increase in MRR of 350% compared to normal wire-ECDM [153].
Also the removal rate in drilling-ECDM is limited due to a limited availability of gas bubbles at the bottom of the electrode as the tool electrode is often pressed against the workpiece. Impregnating the tool with abrasive particles results on the one hand in a constant and small gap between tool and workpiece, facilitating the generation of bubbles in that area. On the other hand, the abrasive particles assist in the removal of softened material. These two effects lead to a significant increase in removal rate [162].

Although the potential and the application range of the ECSM process is large, the process has not yet been introduced in industry since its inception 40 years ago. Though, it can be expected that especially wire-EDM machines will be equipped to facilitate the ECAM process to obtain higher MRR.

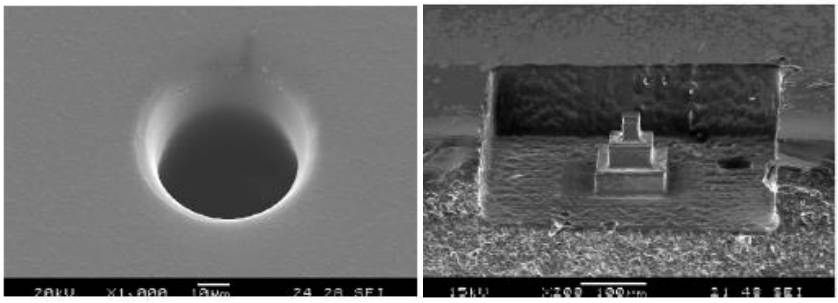

a. b.

Fig.6.8: Microstructures machined with ECDM: (a) micro hole Ø 65 µm hole entrance, Ø 55 µm hole exit, 150 µm thick soda lime glass plate; (b) 3D micro-structure on Pyrex glass with Ø 30 µm electrode [189].

6.3.3. Laser based machining

Although EDM as a micro-manufacturing technique has a large miniaturization potential, the feature size is limited to the smallest available tool diameter. Commercial tools have diameter down to 50 µm whereas with the application of a WEDG operation tool diameters down to 10 µm can be obtained. These small diameters are mostly subjected to significant wear. As an alternative a laser beam can deliver focal spots down to 3 µm [163] without any tool wear and regardless of the materials electrical conductivity. Though a laser ablation process is relatively slow and lacks the machining of

high aspect ratio features. Hence, combining both processes on one machining platform would widen up the application range. Several studies have been performed on the integration of both processes in one machine setup [163]–[165]. Mostly the EDM process serves as a roughing operation, removing the bulk of the material followed by a laser ablation operation for the machining of fine details or structures. Fig. 6.10 shows two applications of such a sequential machining operation. In both examples a significant reduction in machining time and increase in accuracy was obtained when compared to the standalone processes.

A major issue in this sequential operation is the sensitivity of the laser ablation process to variations in the working plane in intersection areas of both processes as a result of tool wear during the EDM operation or as a result of differences in absorption properties during laser ablation. This can be tackled by measuring the depth and flatness optically or acoustically after each process or machining layer. The incorporation of these measurements results in a maximal deviation of 2 µm on the required depth and 1 µm on the flatness [163].

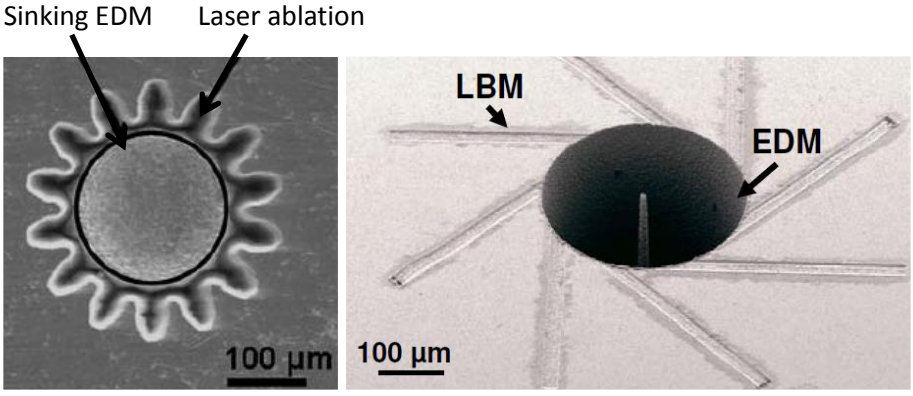

a. b.

Fig. 6.9: (a) Gear wheel structure machined with sinking EDM and laser ablation [164]*; (b) structure machined with EDM-milling and laser ablation* [163].

In other setups the laser ablation process is used as a pre-machining operation for EDM-drilling and EDM-milling resulting in significant reduction of machining time [166]. A specific application for this sequential process is the machining of injection nozzles as the demand for higher energy efficiency and less pollutant emissions to the environment requires hole sizes in diesel

fuel injection nozzles to less than 145 µm in diameter. In this setup the laser ablation process serves as pre-drilling step resulting in a pilot hole for EDM-drilling (see Fig. 6.11.a). The EDM-drilling step then removes the heat affected zone of the ablation process and provides the required dimensional accuracy (see Fig. 6.11.b). With this combined operation a reduction of 70% in machining time [167] (compared to only EDM-drilling) was obtained due to the fast removal of material by the ablation process and the improved flushing conditions during EDM as a result of the pilot hole. Additionally, the improved flushing results in an improved parallelism of the hole walls.

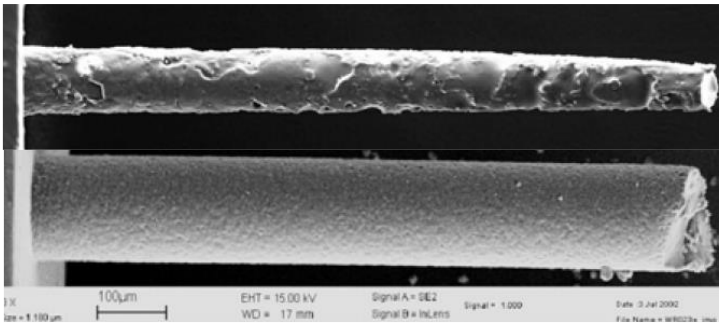

Fig. 6.10: SEM image of plastic impressions of (a) laser drilled pre-hole with diameter 80 µm; (b) laser-EDM hole with a diameter of 140 µm [167].

6.3.4. Ultrasonic based machining

Although having a wide application range, the major drawback of the EDM process is the relatively low machining speed. As was mentioned in Chapter 3 the flushing conditions are the main determining factor for the machining speed. Therefore the flushing behavior during process has strongly evolved in the past decades by adding for example planetary movements and periodical lifting of the electrode. To further increase the machining speed, combined processing techniques with ultrasonic vibration have been developed.

Ultrasonic vibration assisted EDM

In this technique the EDM machine is equipped with an ultrasonic transducer enabling an ultrasonic movement of the electrode. Frequencies range from 20 to 40 kHz with amplitudes of several microns. There are several phenomena occurring during the ultrasonic vibration that improve the

process efficiency. In [168], [169] it is stated that during the downward electrode movement the MRR decreases as a result of the pressure rise whereas during the upward movement the MRR increases due to the pressure drop. The total increase in MRR is explained by the gain due to pressure drop is higher than the less due to pressure rise. Besides this effect on the hydrostatic pressure, the ultrasonic vibration also results in a significant amount of bubbles that coalesce forming large bubbles with an increased velocity [170]. In their way up, the bubbles entrain the generated debris hence enhancing the removal of debris from the sparking gap. As flushing conditions are worst in either finishing operations or micro-EDM operations, the largest benefits were observed there. For finishing operations gains up to 400% [168] were noted whereas for micro-EDM operations gains up to 6000% [171] were noted. A further improvement of the flushing conditions and increase in MRR in combination with the ultrasonic vibrations is possible by the use of rotating single notch electrodes [172] and the addition of a planetary electrode movement [173].

The enhanced flushing due to the ultrasonic vibration makes it also possible to machine holes with a higher aspect ratio. As an example, Fig. 6.12.a shows an 80 µm hole with aspect ratio of 12. By adding a planetary movement to the electrode the aspect ratio could even be increased to 29 [173]. Moreover the ultrasonic vibrations reduce the heat affected zone and the size and number of micro-cracks compared to a conventional EDM operation. Hence, the fatigue resistance can be increased. In most cases, tool wear and surface roughness are comparable to conventional EDM.

The effect of ultrasonic vibrations has also been investigated in combination with the wire EDM process. In [174] it was shown that the cutting rate can be increased with 30% when the vibration is in line with the cutting direction. In addition, the surface quality can be improved and residual stresses can be diminished. No additional improvement on accuracy was noted.

The combined ultrasonic and EDM action has been successfully integrated into a machining platform by Posalux (see Fig. 6.12.b) for the machining of diesel injection nozzles. Also modern die sinking EDM machines are equipped with functionality to provide additional high frequency vibration for better material removal.

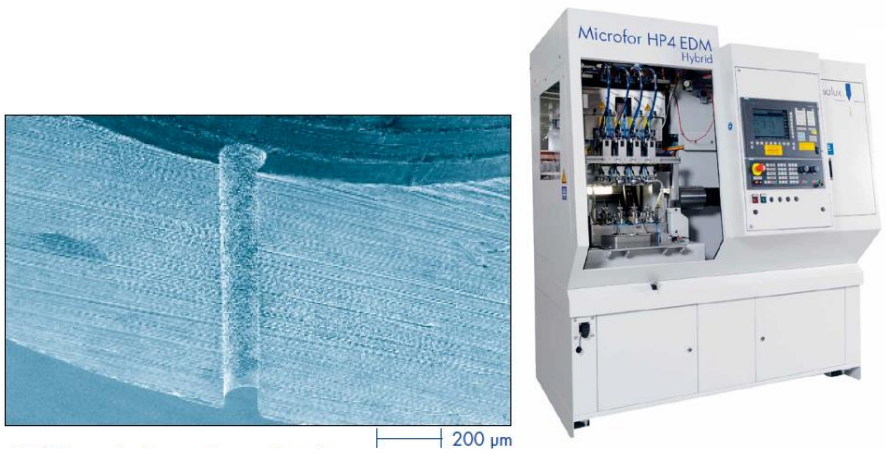

a. b.

Fig. 6.11: (a) 80 µm hole machined with ultrasonic assisted micro-EDM; (b) Commercial ultrasonic assisted EDM machine tool for the machining of fuel injection nozzles [175].

Ultrasonic-EDM machining

The machining of ceramics is often performed with an ultrasonic machining operation in which an abrasive slurry is moved along the working gap with an ultrasonic vibrated tool. This results in a good surface integrity but has the drawback of a low machining speed. As EDM can deliver higher machining speeds for some technical ceramics, a combination of both processes seems to be beneficial. Experiments have been performed with an Al_2O_3 based ceramic with B_4C abrasive particles dispersed in deionized water [176]. Instead of a pulsed power supply, a DC power supply is used leading to one discharge per vibration cycle (see Fig. 6.13). Due to the high frequency pumping action of the tool which promotes the evacuation of debris a MRR higher than the sum of the MRR of a solely EDM and the MRR of a solely ultrasonic machining operation can be obtained. In addition, the obtained surface roughness is higher than a solely ultrasonic machining operation but is lower than a solely EDM operation. Moreover, the motion of the tool lets less liquid material recast on the machined surface.

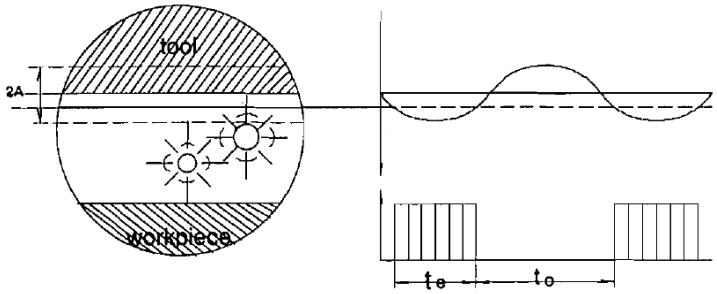

Fig. 6.12: Spark erosion performed by vibrating tool [176].

6.4. Sequential micro-EDM and micro-milling machining platform in this study

The previous section has shown that many hybrid micro-machining solutions involving micro-EDM exist. As the micro-EDM process is a relatively slow process generating heat effects which can reduce the parts quality (e.g. micro-cracks in the recast layer), the combination with a process with a high machining speed and able to obtain a good surface integrity is to be preferred. Therefore, in this study an abrasive process, more specifically micro-milling, has been chosen to be integrated with the micro-EDM process. As micro-EDM is able to machine hard materials and geometrical features sensitive for deformation (e.g. thin ribs), a lot of complementarities become apparent and result in the extension of the material palette, increase of surface integrity and geometrical accuracy. In addition, the combination of micro-EDM and a micro-mechanical cutting process is already a part of the logical process chain, though applied on separate machining platforms. For example, in molding and manufacturing applications micro-EDM is generally followed by a grinding process to remove the recast layer. Also when reflecting to the macro scale, the manufacturing of moulds includes the sequential use of milling and EDM.

Despite the large potential of a sequential use of EDM and milling, literature reports only few studies. Aspinwall et al. investigated the sequential combination of milling and EDM for macro applications by the integration of an EDM servo system onto a high speed milling machine tool [177]. In this setup the milling operation was used for bulk material removal whereas the EDM operation was used for texturing 2D and 3D surfaces. In another work, the combination was also integrated on a machining platform which

performs electrode milling, sinking EDM and ECM finishing with separate process fluids and power supplies for EDM and ECM [178]. With this hybrid machining platform the heat affected layer could be completely removed and mirror-like surfaces could be obtained. In the work of Asad et al. a hybrid machining platform able to perform micro-EDM, micro-milling, micro-turning, micro-WEDG and micro-ECM operations has been developed by the integration of high, middle and low speed spindles [179]. This hybrid machining platform allows to fabricate very fine electrodes used to reproduce high aspect ratio structures.

The machining platform of this study is a Sarix SX-200 micro-EDM machine (see Fig. 6.14) with a working envelope of 320 mm x 200 mm x 200 mm in respectively X, Y and Z direction. The platform is equipped with linear motor drives in both X and Y axis giving a positioning resolution of 0.1 µm and a positioning uncertainty of 2 µm. In [180] the positioning uncertainty in the XY plane of an identical Sarix SX-200 machine was confirmed to be less than 1 µm. The eroding spindle can deliver rotational speeds up to 800 rpm with a runout precision of less than 1 µm and an indexing precision of less than 0.05°.

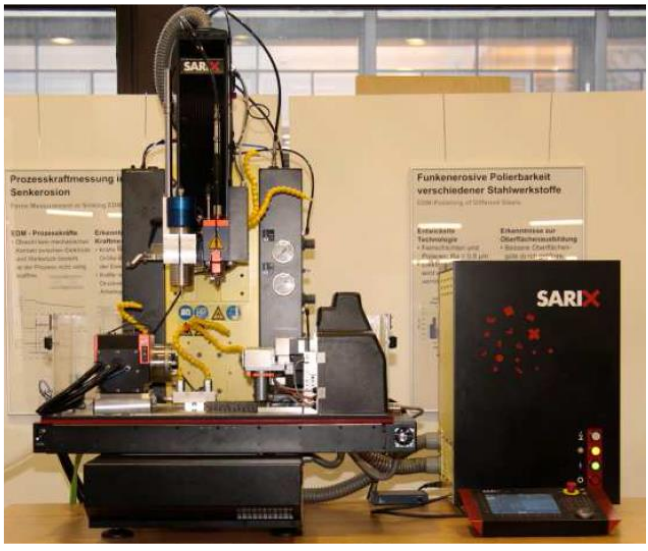

Fig. 6.13: Integrated micro-EDM and micro-milling machining platform.

The Z-axis of the machining platform is equipped with an adapter plate to fit both the EDM spindle and a micro-milling spindle. The latter is a Westwind D1722 high speed ultraprecise air bearing spindle with rotational speeds in

the range from 20.000 to 160.000 rpm with a dynamic run-out lower than 10 µm at 160.000 rpm. The high speed spindle is integrated on the Z-axis with an electrical contact device with sliding graphite contact brush (see Fig. 6.15) for measuring the zero-datum of cutting tools by using the existing electrical touching functionality of the micro-EDM machining platform. This allows depth measurement with rotating tool (see Fig. 6.16). The rotational speed of the high speed spindle is directly controlled by the EDM machine controller through communication with a frequency converter.

Besides the use of milling and drilling tools, grinding tools can also be mounted on the high speed spindle hence enlarging the application range of the machining platform. A possible application could be the machining of materials with a non-conductive ceramic coating where the non-conductive coating can be locally removed with a grinding operation followed by either a micro-milling or micro-EDM operation, e.g. micro-hole drilling in coated turbine blades.

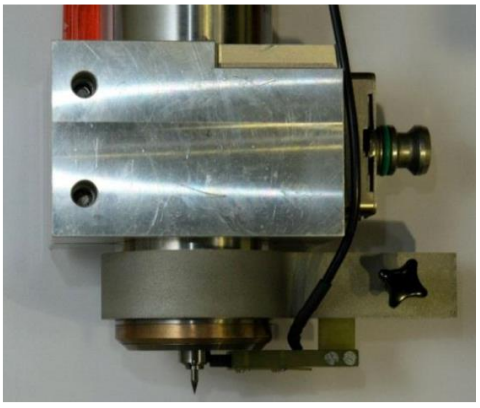

Fig. 6.14: Electrical contact device for air bearing spindle.

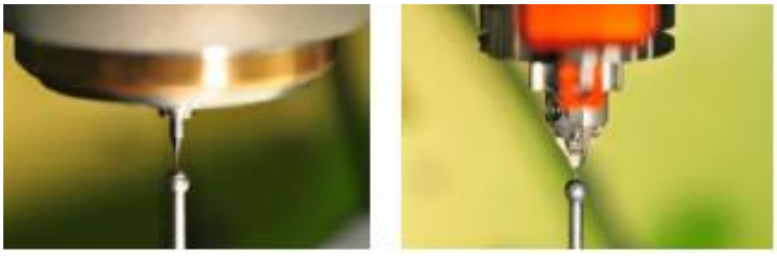

a. b.

Fig. 6.15: Zero-datum reference for (a) micro-milling; (b) micro-EDM.

The introduction of two different manufacturing processes in the same work environment leads to a problem of compatibility of all the materials involved: tools, consumables, machine parts and material removed. In the particular case of hybridization of micro-EDM and micro-milling the main compatibility issue seems to be related to the mixture of process fluids: dielectric for EDM and cutting lubricant for micro-milling. Both for micro-EDM and for micro-milling specific process fluids exist, each delivering optimal performance for the corresponding process. Mixing of both fluids should be avoided because it would result in chemical waste and would negatively influence the performance of both processes. Due to the stringent demands put onto EDM dielectrics, it has been chosen to use a dielectric with properties that allow a good cutting operation. The selected process fluid, namely IonoGrind 63 (see Table 6.2), was initially developed for use in abrasive electrical discharge grinding (see section 2.1.3). The suitability of this process fluid was confirmed by micro-milling performance tests by measuring tool wear, process forces and the resulting surface roughness. These tests showed that the IonoGrind 63 fluid outperforms the initial EDM dielectric and results in performance characteristics similar to specific cutting fluids.

Table 6.2: Properties of process fluid.

	IonoGrind 63
Flash point	63 °C
Viscosity (20 °C)	2 cSt
Density (15 °C)	0,78 kg/l
Color	Fluorescent green

As the flash point of the process fluid is relatively low (see Table 6.2) and the performance of a micro-milling operation is affected by the fluid temperature, an additional process fluid cooling system has been installed which guarantees a constant fluid flow within 0.1 °C. In addition, an extra filtration step is integrated to filter out the larger chips generated by the milling operation before reaching the EDM filter.

The major part of the machining experiments that will be discussed in the next chapters is performed on the Sarix SX-200 machining platform. In addition, micro-EDM experiments are also performed on the Sarix SX-100 machine (see section 2.1.4) with similar characteristics as the integrated platform.

6.5. Research objectives for planning of sequential micro-EDM and micro-milling operations

The trend of continuing miniaturization in a cost effective manner of micro-products from different sectors with increasing functionality pushes micro-fabrication techniques to their limits and opens up the way for hybridization. Although many of the previously presented hybrid processes are not yet fully mature for industrial introduction, they show to have a large potential in meeting the ever growing demands on lead-time, cost, accuracy and ecology related performance measures. Among micro-processes, micro-EDM and micro-milling have a widespread application and offer a wide range of complementarities to extend the application range and to increase surface integrity and accuracy. In order to comply with an increased performance, it has been proposed to integrate both processes onto one machining platform.

In order to fully deploy the capabilities of a sequential micro-EDM and micro-milling machining platform, this study will first **evaluate the technological boundaries and assess the performance of both processes** in terms of dimensional and geometrical accuracy, cost and time effectiveness, energy consumption and surface integrity. This knowledge will support the development of an **automated process planning tool** for the integrated platform which serves the goal of choosing the most optimal process or sequence of processes for a given geometrical feature with the corresponding tool(s). In addition, the process planning tool will define the optimal sequence of operations for micro-parts with multiple geometrical features. As this is an initial study for such integrated platform, the focus will be on the machining of common prismatic micro-features.

Chapter 7 Comparison of micro-milling and micro-EDM operations

7.1. State of the art

When dealing with a combined machining platform one wants to make optimal use of each machining process. In order to do this (and to make a proper process planning) it is essential to know the specific advantages and disadvantages and the technological boundaries of each process.
It is generally known that micro-EDM is a relative slow machining process but due to its contactless nature it is often used to machine very hard materials. Micro-EDM is also suitable to machine high aspect ratios up to 18 [181]. On the contrary, micro-milling is a fast machining process able to machine complex shapes with a good surface quality. However the attainable aspect ratio is limited [182]. Fig. 7.1 shows combinations of milling tool diameter (Dc) with their maximum penetration depth for commercially available milling tools. For tools with Dc between 0.5 mm and 2 mm aspect ratios up to 10 are feasible. For tools with Dc lower than 0.5 mm aspect ratios up to 5 are feasible.

Until now literature only reported on the performance of both processes for high aspect ratio holes and ribs [183]. For other types of geometry the outcomes of these studies only serve as a rough guideline. Additionally it is important to examine, next to aspect ratio and accuracy, other relevant performance criteria in order to make a proper decision about which (combination of) processes to use. Therefore both processes were compared on the ground of several performance criteria like dimensional and geometrical accuracy, surface quality, machining time, energy consumption and machining cost. For this a large set of experiments were conducted with a special focus on rectangular geometries, as these are common geometries in micro-moulding following an enquiry performed within the European FP7 Integ-µ project. The results of these tests are discussed in the following sections. The test results and extracted trends will form the basis for the automated process planning that will be elaborated in Chapter 8.

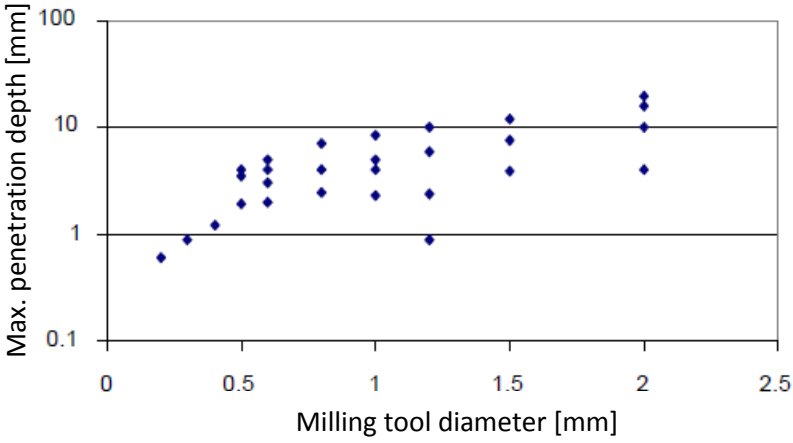

Fig. 7.1: Commercially available milling tool diameter - penetration depth combinations [184].

7.2. Experimental assessment of the performance of micro-EDM and micro-milling

7.2.1. Experimental setup

The performance of both processes has been investigated by machining several geometrical features covering the meso to micro range. The main geometries of focus of this study were circular and rectangular geometries, namely shallow cavities and deep slots with aspect ratios up to more than 7. The machining was split up into a roughing step, wall finishing step and a floor finishing step.
For both processes similar toolpaths were generated and the same tool diameters were used for both processes in order to obtain good comparison cases. However, some parameters needed to be optimized according to the machining process (e.g. cutting depth a_p, feedrate v_f,etc.).

The machining experiments were performed on two workpiece materials, namely hardened steel 1.2343 (DIN X38CrMoV5-1) with a hardness of 57 HRC and brass 2.0371 (DIN CuZn38Pb1.5). As a process fluid for this machining platform IonoGrind63 was used as it shows to be suited for both types of operation (see section 6.4).

Micro-EDM operations were performed with tungsten carbide electrodes. Depending on the machining case side flushing and/or flushing through the electrode was used. Tools for roughing operations were not dressed to counteract runout of the spindle. On the contrary, electrodes for the wall and floor finishing operations were dressed to their respective diameter.
Micro-milling operations were performed with coated solid carbide milling tools. Different tools were used depending on the workpiece material. All milling tools were shortened in length to provide more stability and hence less vibrations.

7.2.2. Quality control of machined parts

In this research several measurement techniques were used to assess the quality and accuracy of a machined part. The measurement of flatness, surface roughness and depth accuracy was performed with a profile meter (Taylor Hobson Form Talysurf 120L). Because of the tactile measurement principle results obtained with this technique can be seen as reliable. On the other hand, measurements of 2D dimensional accuracy (length, width and diameter) and 2D geometrical accuracy (straightness, roundness, parallelism and perpendicularity) in the XY plane were performed with a digital microscope (Leica VMM 200 + QuadraCheck 200). By comparing results it was noticed that the results obtained by this technique need to be handled with care. The reason for this is the rather subjective nature of the measurement. More specific, the results are based on points and lines drawn by the user on the digital image. A slight deviation from the real boundary can cause a significant deviation in the result. This is shown in Table 7.1 where the measurement results of 2 users are listed for the measurement of the depth accuracy (measurement performed after cutting the cavity into 2 halves). Deviations between the 2 persons under equal settings vary between 1 to 31 µm for which the difference for cavity 1 shows to be significant ($\alpha = 0.05$). Also between microscopes significant differences were noticed. When comparing 2 digital microscopes (type Keyence VHX-100 and Leica VMM 200) deviations from 15 up to 39 µm were noticed by the same user. Moreover, the magnification level of the microscope can cause deviations up to 22 µm. This knowledge makes the results of this measurement technique very unreliable. For the same cases the depth was also measured tactile (see Table 7.1). A comparison with the digital microscopes shows that microscope 2 approximates the tactile measurement the best. The deviations from the tactile measurements run

up to only 2 to 4 µm on average. So by using this microscope the measurement of the dimensional and geometrical accuracy becomes more reliable. However, one should take a possible error of 2 to 4 µm into account when analyzing the results.

Table 7.1: Comparison of microscopic measurements (unit: millimeter).

Device	Microscope 1						Microscope 2		Tactile	
Magn.	50X				100X		10X			
Person	1		2		2		2		1	
Cavity	1	2	1	2	1	2	1	2	1	2
# 1	2,526	2,501	2,514	2,502	2,528	2,515	2,490	2,479	2,496	2,479
# 2	2,523	2,503	2,513	2,494	2,527	2,515	2,492	2,481	2,497	2,482
# 3	2,529	2,501	2,513	2,503	2,529	2,516	2,491	2,480	2,493	2,479
# 4	2,530	2,503	2,508	2,509	2,526	2,507	2,493	2,478	2,496	2,483
# 5	2,539	2,510	2,514	2,494	2,523	2,516	2,489	2,477	2,491	2,481
Avg.	2,529	2,504	2,512	2,500	2,527	2,514	2,491	2,479	2,495	2,481
Stdev.	0,006	0,004	0,003	0,006	0,002	0,004	0,002	0,002	0,002	0,002

7.2.3. Dimensional accuracy

When considering prismatic cavities like rectangular and circular cavities the dimensional accuracy consists of the accuracy in the horizontal plane (cavity length, width or diameter) and the accuracy in the vertical direction (depth). Depending on the dimensional direction different results were obtained.

When comparing the accuracy in the horizontal plane distinction should be made based on the cavity size. The applied process parameters within this test setup are shown in Table 7.2. When looking at cavities in the meso-range (10 mm x 10 mm) both processes lead to the same accuracy (see Fig. 7.2). On the contrary, for smaller cavities different results were obtained. Micro-EDM results more often in undersized cavities whereas micro-milling results in general in oversized cavities. When looking at the absolute values of the deviations for cavities with a size in the range of 1 mm x 1 mm no significant difference in accuracy can be noticed. On the contrary, for the smallest considered cavities (0.3 mm x 0.3 mm) a significant difference was noted between both processes. On average larger deviations were noted for micro-milling. This can be due to higher rotational speeds that are used for these cavities namely 144 kRPM for 1 mm x 1 mm and 160 kRPM for 0.3 mm x 0.3 mm in order to attain a good cutting speed. These higher rotational speeds increase the runout of the milling tool. This is evidenced in Fig. 7.3 which shows the results from a referencing action of the top plane of the workpiece

by means of a touching action with the milling tool. When comparing to the reference case (touching without rotation) larger deviations were noticed as the RPM increases. These results are in close agreement with the runout characteristics defined by the spindle supplier [185]. The effects of runout are not appearing during micro-EDM operations as rotational speeds are several orders of magnitude lower than those in micro-milling and as the finishing electrodes are dressed prior to machining hence canceling out the possible runout.
Installation of a proper measurement system for tool diameter and runout (e.g. laser measurement) can help in improving the accuracy.

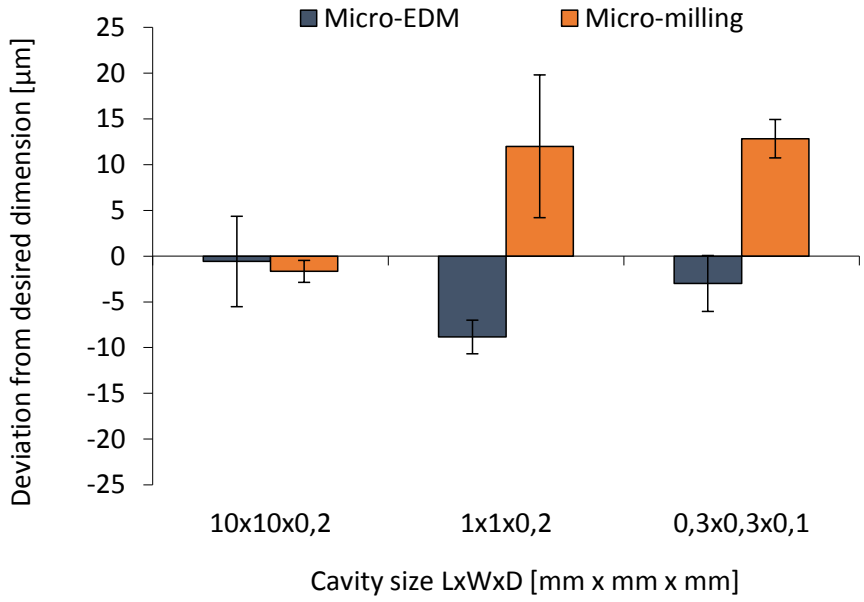

Fig. 7.2: Errors for accuracy in the horizontal plane for different cavity sizes.

When looking at the accuracy in the vertical plane or depth accuracy experiments showed that no significant differences could be noticed between both processes when machining shallow cavities of different sizes (see Fig. 7.4) with process parameters as shown in Table 7.2. As the combined machining platform has evolved in time the same experiments were conducted with a separate coolant conditioning system. The large heat dissipated by the pump of this system could not be evacuated effectively resulting in high coolant temperatures. As in micro-machining only 10% of

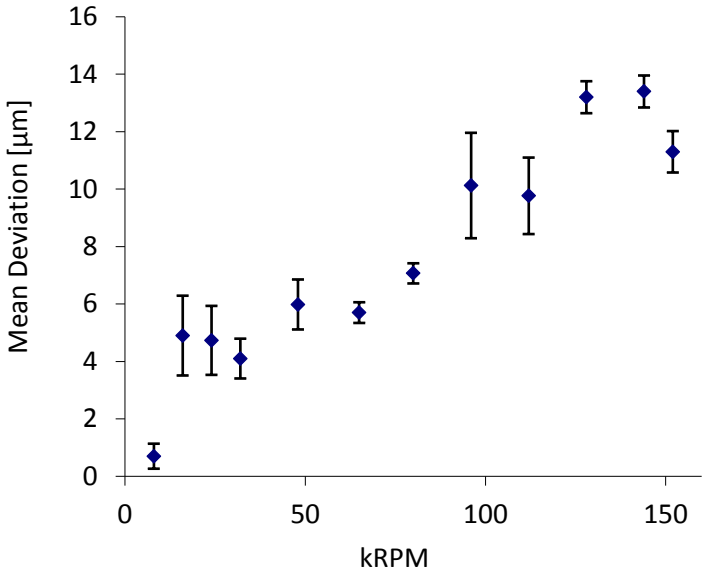

Fig. 7.3: Deviation from zero plane in function of rotational speed during touching action.

the heat generated is dissipated by chips [167] a good coolant system is indispensable for an effective removal of excess of heat. This is evidenced in Fig. 7.4 where significant overcuts in depth are shown as a consequence of thermal expansion of workpiece and tool.

When looking at the depth accuracy in function of the cavity depth distinction can be made between both processes. When applying the process parameters listed in Table 7.3 the depth accuracy resulting from micro-milling operations shows to be stable in function of the cavity depth (see Fig. 7.5). On the contrary, for micro-EDM operations larger deviations from the desired depth are noted as the cavity depth increases (e.g. difference 0.2 mm – 4 mm). This can be explained by the fact that the depth accuracy of micro-EDM operations is highly dependent on the accuracy of the wear compensation strategy. The tool wear is compensated by a linear compensation strategy with intermediate measurements of the tool length.

Table 7.2: Process parameters during tests on dimensional accuracy.

Cavity dimensions LxWxD [mmxmmxmm]	Roughing					Finishing				
	Ø Tool [mm]	Micro-milling			Micro-EDM	Ø Tool [mm]	Micro-milling			Micro-EDM
		kRPM	f_z [mm/rev]	a_p [mm]	a_p [mm]		kRPM	f_z [mm/rev]	a_p [mm]	a_p [mm]
10x10x0,2	1	32	0,01	0,025	0.0085	0,5	56	0,015	0,015	0.0009
1x1x0,2	0,3	96	0,005	0,0025	0.0015	0,2	144	0,005	0,01	0.0015
0,3x0,3x0,1	0,1	160	0,0012	0,01	0.0005	0,1	160	0,0018	0,03	0.0005

Table 7.3: Process parameters during tests on depth accuracy.

Cavity dimensions LxWxD [mmxmmxmm]	Ø Tool [mm]	Micro-milling			Micro-EDM
		kRPM	f_z [mm/rev]	a_p [mm]	a_p [mm]
10x10x0,2	1	32	0,01	0,025	0.0085
2.5x0.55x2.5	0.5	56	0.005	0.06	0.0035
2.5x0.55x4	0.5	56	0,005	0.06	0.0035

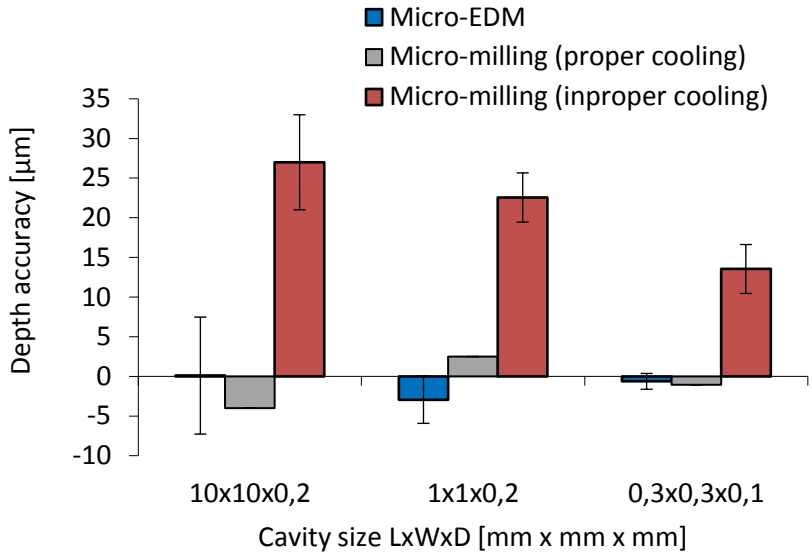

Fig. 7.4: Comparison of depth accuracy for different cavity sizes.

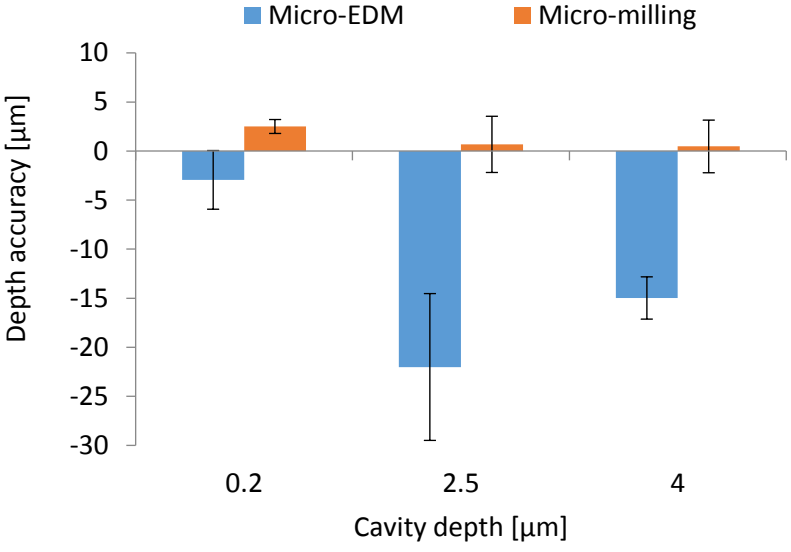

Fig. 7.5: Comparison of depth accuracy in relation to cavity depth.

7.2.4. Geometrical accuracy

For the prismatic geometries considered in this study a limited set of geometrical parameters has been evaluated for both processes. This set of parameters was based on an inquiry performed within the scope of the Integ-Micro project (FP7 NMP-2007-3.5-2).

Flatness

The flatness was evaluated with a profile meter (Taylor Hobson Form Talysurf 120L) for both the flatness of the bottom surface and the flatness of the side surfaces of prismatic cavities. Fig. 7.6 shows the flatness of the bottom surface for both processes and two machining strategies. A significant difference ($\alpha = 0.01$) between both processes can be stated. In addition the machining strategy is clearly reflected in the measured profile e.g. the larger deviations on the diagonals for micro-milling with the concentric-out movement reflecting points on the tool path where the milling tool spends more time due to decelerating and accelerating. In case of micro-EDM operations the obtained surface profile is strongly influenced by the wear compensation strategy. Fig. 7.6 shows that in case of concentric-out movements the bottom surface has a pyramidal shape. The wear compensation strategy does not compensate enough (increase of depth from center to boundaries) for the higher than expected wear. In case of a zig-zag movement for micro-EDM operations, a better flatness is obtained because the electrode is moving constantly from one side of the cavity to the other side. In case of a suboptimal wear compensation strategy the result will be an inclined bottom surface but the deviations from this inclined surface will be smaller than those obtained with a concentric-out movement.

Also the evaluation of the flatness of the cavity walls shows a significant difference between micro-milling and micro-EDM. For micro-milling a wave-shaped pattern can be noticed as a consequence of the tool rotation (see Fig. 7.7.a), whereas for micro-EDM a rough and spiky surface can be noticed (see Fig. 7.7.b). On average flatness values of 6 µm and 25 µm can be obtained for respectively micro-milling and micro-EDM operations of deep cavities.

	Concentric-out	Zig-zag
Micro-milling	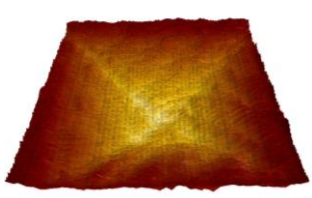 Flatness = 0,0025mm	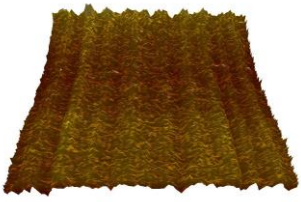 Flatness = 0,0026mm
Micro-EDM	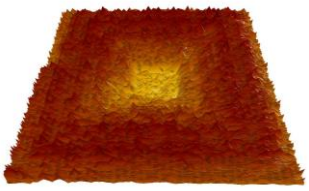 Flatness = 0,018mm	 Flatness = 0,011mm

Fig. 7.6: Comparison of the flatness of the bottom surface for different machining strategies for micro-milling and micro-EDM.

Straightness and conicity

Similar to previous performance criteria the straightness is evaluated in the horizontal and vertical plane. Evaluation of the straightness in the horizontal plane showed for micro-milling operations small distortions in the vicinity of the cavity corner. So called 'overshoots' can be seen on Fig. 7.8.a which only appear at high feedrate. When lowering the feedrate similar straightness values as for micro-EDM are measured (3 to 5 µm). The reason for this phenomenon at high feedrate (20 mm/s) is that the controller of the Sarix platform is not equipped to handle high decelerations and accelerations in the vicinity of corners. This could be proved by a lowering of the feedrate which clearly reduces this phenomenon (see Fig. 7.8.b), though at the expense of the machining time. Therefore, when applying a micro-milling operation on the combined platform a lower feedrate should only be applied during the finishing operation.

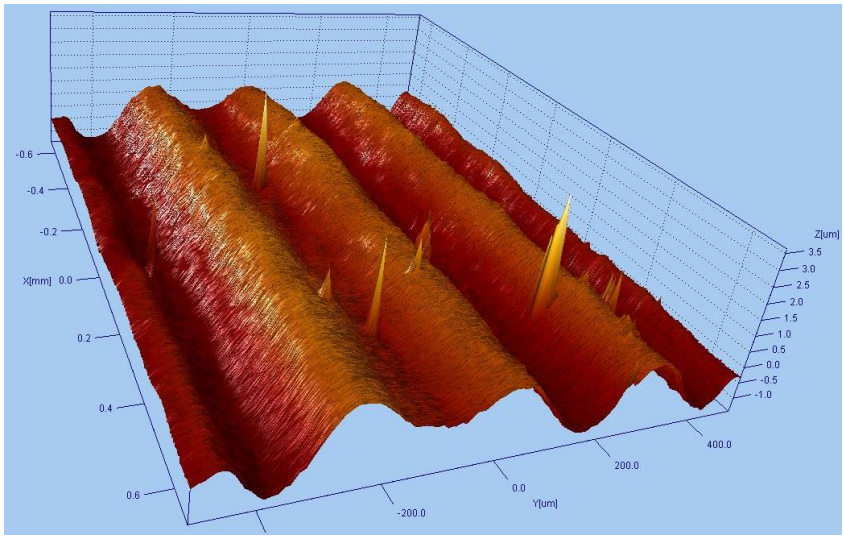

a.

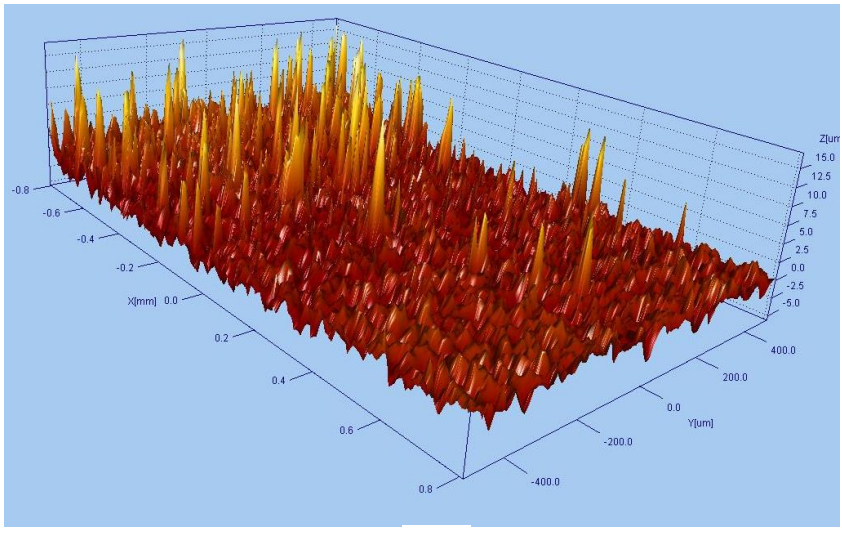

b.

Fig. 7.7: Comparison of surface profiles of side surfaces (1.6 x 1 mm²) machined with (a) micro-milling and (b) micro-EDM.

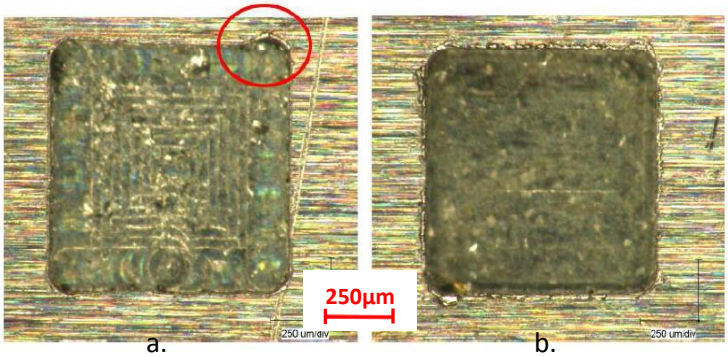

Fig. 7.8: Comparison of geometrical accuracy in corners in hardened steel (a: 20 mm/s; b: 2 mm/s) cavity 1x1x0.2 mm³.

The straightness in the vertical plane is an important performance parameter for the machining of slot type cavities. Micro-EDM showed to result in similar straightness values as those obtained for the straightness in the horizontal plane. However, micro-milling shows to result in deviations from a straight line like the measured profile shown in Fig. 7.9 for a cavity with a depth of 4 mm.

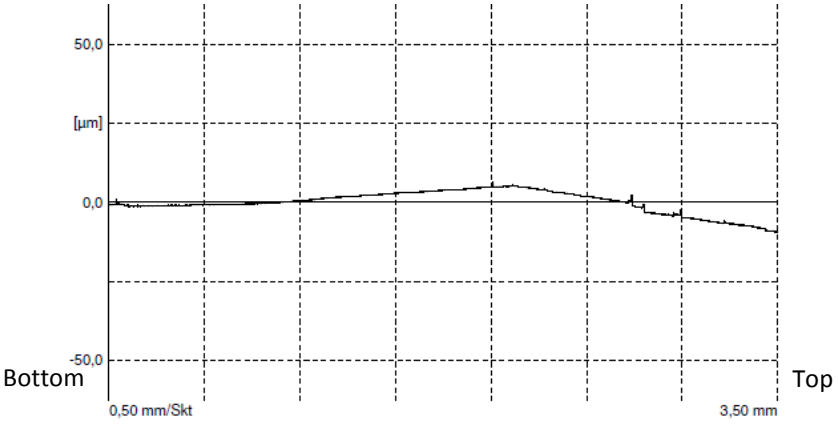

Fig. 7.9: Measured profile of vertical wall machined by micro-milling.

Besides the straightness an important parameter for the machining of slot type cavities is the parallelism of the side walls or the conicity represented by the inclination angle. Optical measurements showed that both for micro-milling and for micro-EDM the inclination angle approximates 90° (see Fig. 7.10) for different cavity depths. Only deviations up to 1° were measured.

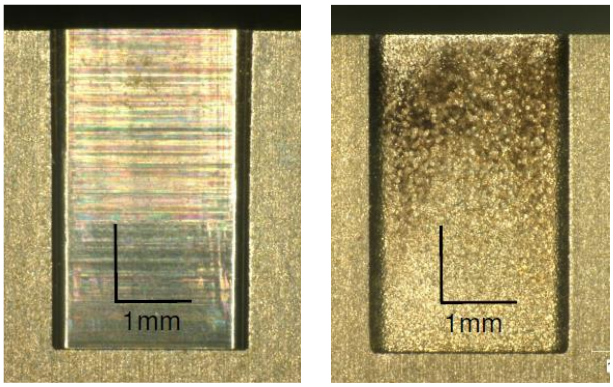

a. b.

Fig. 7.10: Section view of side wall of slots machined with (a) micro-milling and (b) micro-EDM.

7.2.5. Surface quality

The surface quality of prismatic cavities was assessed by evaluating the surface roughness of bottom and side surfaces. From literature it is known that micro-milling operations most often result in lower roughness values compared to micro-EDM [182], [183]. Though for a given process, variations in surface roughness can occur due to the influence of a wide range of parameters like tool and workpiece material, cutting or generator parameters, machining strategy, etc. Although it is not the purpose of this study to quantify all these influences, Fig. 7.11 displays the effect of rotational speed and machining strategy on the roughness of a 10x10 mm² cavities bottom surface machined with micro-milling with the parameters listed in Table 7.2. Higher feedrates, reflected by higher rpms for constant feed/tooth, result in higher roughness values. On the other hand, the zig-zag strategy results in lower roughness values.

Evaluation of machining experiments on deep cavities showed that for both processes the roughness varies along the depth of the cavity wall. More specifically, the top zone of the cavities wall shows to have higher roughness values compared to the bottom zone of the wall. This means that the machining of shallow cavities results in smaller roughness values of the walls compared to the machining of deep cavities. This is evidenced in Table 7.4

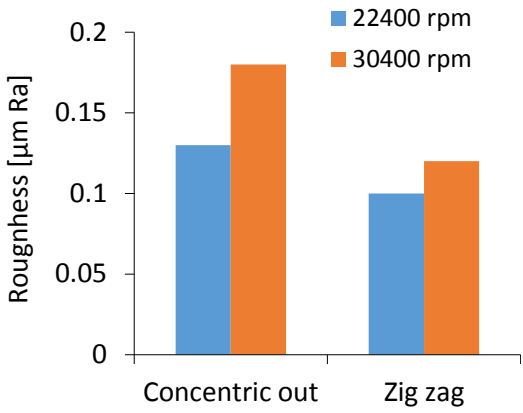

Fig. 7.11: Influence of rotational speed and machining strategy on the surface roughness of a 10x10 mm² cavity for micro-milling operations on hardened steel.

which compares the roughness values of the bottom zone of the side wall with the roughness measured along the entire depth for both operations. Though, different phenomena cause this variation for both processes. During micro-EDM secondary sparks occur along the electrodes lateral surface. As the top zone of the side wall is longer subjected to secondary sparks, higher roughness values are noted (see Fig. 7.10.b). This is also evidenced in Fig. 7.12 showing the tool wear on an EDM electrode gradually decreasing from bottom to top. Also during micro-milling a difference in roughness is present. As shown in Fig. 7.9 distortions on the vertical profile are present near the top of the cavity as a result of contact with the tool shaft. This rubbing action then results in higher roughness values near the top of the cavity or in higher roughness values along the entire depth compared to shallow cavities.

It should be noted that the values given in this section are only exemplary for their respective operations. Deviations can occur depending on the applied process parameters. In addition, for both processes lower surface roughness values can be obtained with specific tooling and optimized process parameters.

Table 7.4: Surface roughness of side walls for micro-EDM and micro-milling.

	Micro-EDM		Micro-milling	
	Ra [µm]	Rz [µm]	Ra [µm]	Rz [µm]
Entire depth	0,87	5,71	0,26	4,32
Bottom zone	0,42	2,40	0,02	0,12

Fig. 7.12: Tool wear on EDM electrode due to secondary discharges.

Another important criterion in assessing the surface quality is the occurrence of burrs. Due to the mechanical nature of the process burrs only occur in case of micro-milling operations. It is crucial to avoid burrs in micro-applications due to their detrimental effect on the accuracy during assembly. Burr formation is a very complex problem which is caused by the interaction of several factors (sharpness of cutting tool, feedrate, cutting depth, cutting speed, hardness of workpiece material, etc.). It was shown that too conservative values for feedrate and cutting depth increase the chance of having burrs. This is caused by the fact that in this case the tool rubs over the surface and pushes the material away instead of cutting. In addition, experiments pointed out that burrs are more likely to occur when the cavity dimensions and/or tools become smaller and when the aspect ratio increases. Nonetheless no hard conclusions can be drawn. This means that if it is important to avoid burr formation micro-milling should be avoided. If this is not possible there is still the possibility to apply micro-EDM as a deburring operation [186].

7.2.6. Machining time

It is common knowledge that micro-milling outperforms micro-EDM regarding machining time as a result of the higher feedrates that can be applied during micro-milling. Often the difference between both operations is one order of magnitude or more. As the cavity gets smaller, smaller tools are required which limit the machining conditions (e.g. cutting depth and feedrate for micro-milling and peak current for micro-EDM). As a consequence, smaller values of MRR are noted as the cavity or feature size decreases. In addition, the performance of micro-milling is also affected by the hardness of the workpiece material: the harder the workpiece material, the more stringent the limitations on the machining conditions. The foregoing results in a decrease of the relative difference in machining time between both operations as the cavity gets smaller. This is shown in Fig. 7.13 by displaying the ratio of micro-EDM time and micro-milling time for 2 materials: hardened steel and brass. For hardened steel the difference even lowers to a factor of 2.5 for the smaller cavities. The ratios for brass are higher due to a larger increase in MRR for micro-milling compared to micro-EDM. It should be noted that the dressing time for EDM electrodes is not taken into account in Fig. 7.13.

Mostly a micro-milling and a micro-EDM operation consists of several machining steps. Firstly a roughing operation is performed to remove the bulk of the material with a relative high speed followed by one or more finishing operations to reach a certain quality of the surface. In most cases the finishing operation consists of an operation to finish the side walls of the cavity (wall finishing) and an operation to finish the bottom of the cavity (floor finishing). Fig. 7.14 shows the machining time of the different machining steps for micro-milling (Fig. 7.14.a) and micro-EDM (Fig. 7.14.b). It should be noted that the decreasing trend of the machining time in function of the cavity size purely depends on the selected cases. The smaller the cavity, the smaller the tool, the more conservative the process parameters will be (see Table 7.2) hence the lower the MRR. Though in these cases a relatively larger volume had to be removed for the larger cavities resulting in larger machining times. In addition, it can be noticed that in all cases the finishing operation (wall + floor finishing) accounts for the largest part of the total machining time. The percentage of roughing time is relatively constant for different cavity dimensions. For micro-EDM operations the electrode dressing time also needs to be taken into account. The percentage of the dressing time largely depends on the difference in stock electrode diameter

and actual machining electrode diameter. For the smallest cavities electrodes with a stock diameter of 0.3 mm were dressed to electrodes of 0.1 mm diameter (both for roughing and finishing). This explains the high percentage of the dressing time for these cavities.

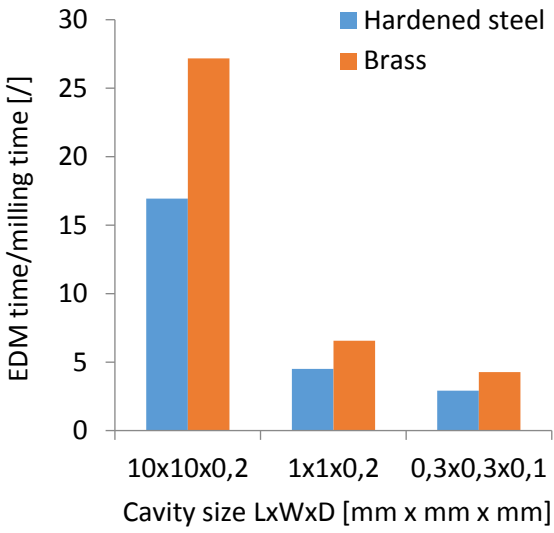

Fig. 7.13: Ratio of EDM time and milling time in function of cavity dimension and workpiece material.

In addition, differences regarding machining time between machining strategies have been noticed for micro-milling. For this process the zig-zag strategy shows to be faster than the concentric-out strategy due to fewer points on the toolpath where accelerations are needed. Due to the limited acceleration of the platform the tool can operate at a higher average feedrate during zig zag. For micro-EDM no difference in machining time for these strategies was noted due to the lower applicable feedrates.

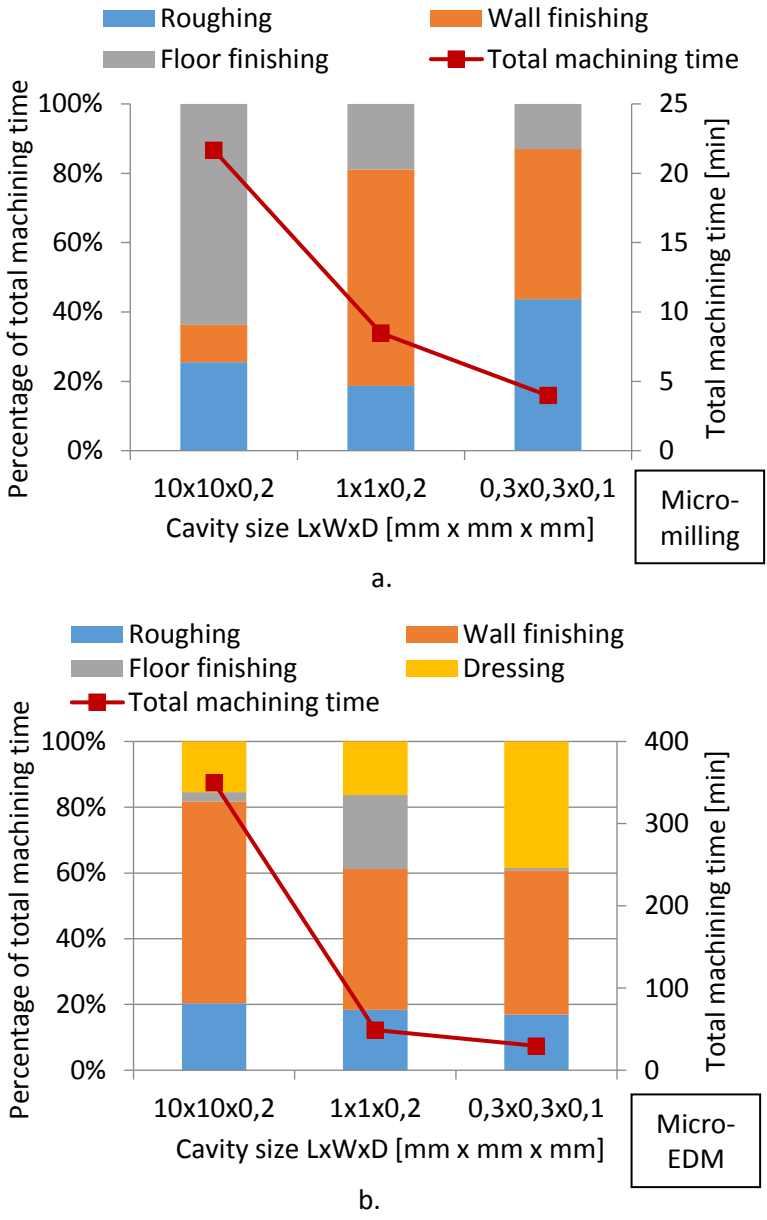

Fig. 7.14: Distribution of total machining times in function of cavity size for (a) micro-milling; (b) micro-EDM.

7.2.7. Energy consumption

Besides the pure technical criteria assessed in the previous sections also other criteria which refer to economical and ecological needs were assessed. As a first criterion the energy consumption of both processes was quantified and compared. Fig. 7.15 shows the instantaneous power during a micro-EDM operation on the Sarix SX200 machining platform. This figure shows that the main energy consumer of the platform is the dielectric system (75% of total) due to its configuration of pumps. Only 25% of the total instantaneous power is used for the machining process itself (e.g. axes movement, spark generation). When looking at the different steps of the machining operation it can be noted that there is no significant difference in instantaneous power between roughing and finishing operations. It can be stated that the micro-EDM process itself requires 60 W to 70 W, depending on the applied energy level.

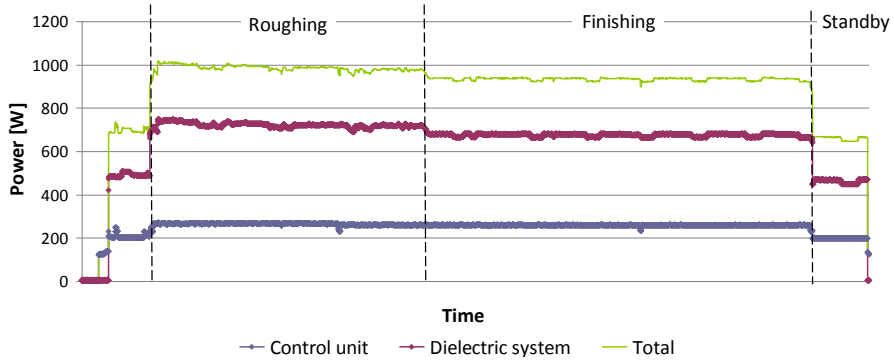

Fig. 7.15: Instantaneous power used during different modes of operation of machining platform Sarix SX200.

When performing a micro-milling operation on the machining platform, the milling spindle becomes a significant energy consumer. Fig. 7.16 shows the average power of the milling spindle in function of the rotational speed in unloaded state. This shows that the average power rapidly increases when higher rpms are needed (e.g. when using small milling tools). Besides the rotational speed also the cutting depth a_p and the cutting width a_e influence the average power. This is shown in Fig. 7.17 for different a_p and a_e values at a rotational speed of 48000 rpm. However, the deviations from the unloaded state are rather small (up to max. 5%) so that for further assessments and calculations only the dependency on the rotational speed will be considered.

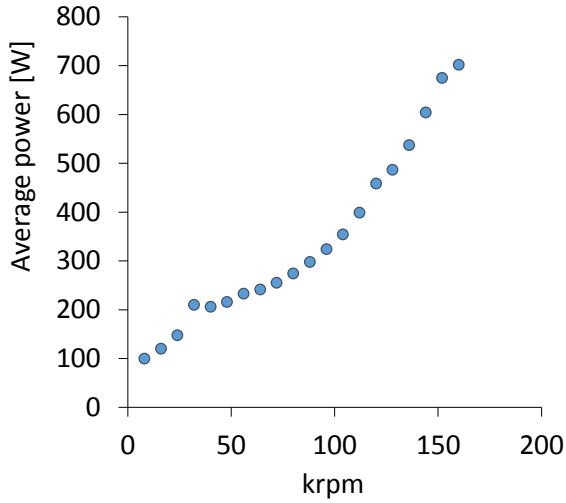

Fig. 7.16: Average power of milling spindle in function of rpm.

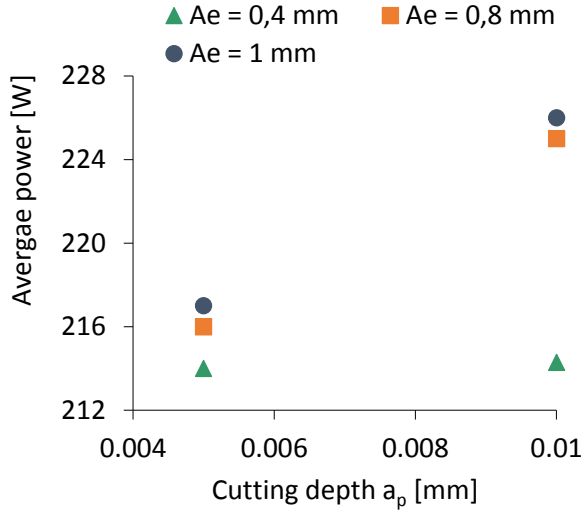

Fig. 7.17: Average power of milling spindle during machining in function of a_p and a_e at 48000 rpm.

From the foregoing it can be concluded that the average power for a micro-EDM operation is lower than that for a micro-milling operation on the considered platform. However, as micro-milling is significantly faster than micro-EDM the total energy consumption will be lower. This is especially true for large cavities or features. The smaller the machining feature, the smaller

the required tool hence the higher the required rpm to obtain the desired cutting speed. At certain rpms micro-EDM can become competitive to micro-milling regarding energy consumption. For example, from Fig. 7.18 it is apparent that for rotational speeds of 150 krpm and more the average power is almost the double of a comparable micro-EDM operation. If the machining time for the micro-EDM operation is less than the double of the machining time of the micro-milling operation, the energy consumption can be lower for micro-EDM. This is especially true for smaller machining features as was already shown in Fig. 7.13.
However, in general it can be stated that micro-milling outperforms micro-EDM regarding energy consumption. Compared to a solely micro-EDM operation, a combined milling-EDM operation will be more energy efficient.

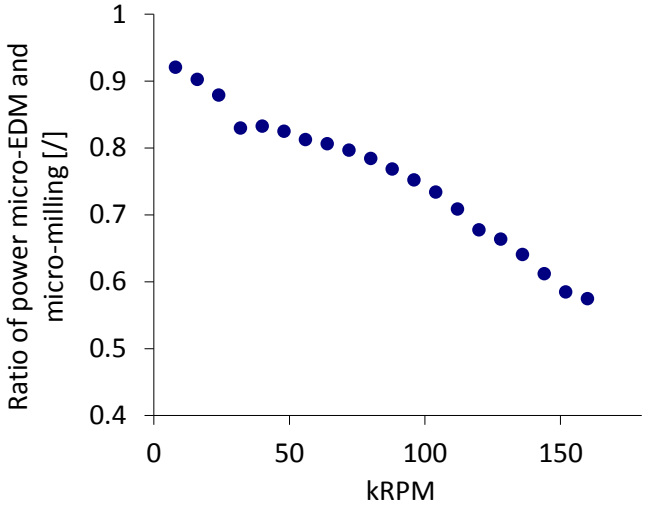

Fig. 7.18: Ratio of power used for micro-EDM and micro-milling in function of rotational speed of milling spindle.

Similar conclusions can be drawn for the specific energy consumption. Table 7.5 displays specific energy results obtained by machining cavities with different dimensions for two different workpiece materials. These results clearly show that for a specific machining case the specific energy for a micro-milling operation is lower for micro-milling. As the cavity size decreases, the specific energy increases significantly. For micro-milling, this can be attributed to the fact that smaller cavities require smaller tools, hence higher rpms are needed which require a higher power level. In addition, section 7.2.6 has shown that the MRR decreases for smaller cavities. For micro-EDM, the decrease in specific energy for smaller cavities can be explained by the

usage of lower energy levels resulting in a smaller MRR. Similar effects can be noted when comparing the machining of brass and steel. The specific energy when machining brass is significantly lower than when machining steel as less conservative process parameters need to be used resulting in higher MRRs.

Table 7.5: Comparison of specific energy results for micro-milling and micro-EDM operations for different cavity sizes and workpiece materials.

Workpiece material	Cavity size LxWxD [mm x mm x mm]	Specific energy micro-EDM [Wh/mm³]	Specific energy micro-milling [Wh/mm³]
Brass	10x10x0,2	84	4
	1x1x0,2	1275	335
	0,3x0,3x0,1	16889	1556
Steel	10x10x0,2	205	16
	1x1x0,2	3150	1075
	0,3x0,3x0,1	23333	15000

7.2.8. Machining cost

Next to meeting technical demands, the cost effectiveness is also a determining factor in choosing a proper process. The total cost that can be attributed to a machining case consists of:

- the machine cost;
- the tooling cost;
- the energy cost;
- and the operator cost.

Firstly, the machine cost of the machining platform is related to the hourly cost of the machine. Taking into account that the machine is depreciated over a period of 4 years and is used during working days for 8 hours per day, an hourly cost of 25 euros can be claimed. As micro-milling operations are mainly faster than micro-EDM operations, lower machine costs apply.

The tooling cost for a specific operation is depending on the purchasing cost and the tool life or wear rate. Micro-EDM electrodes are relatively inexpensive but are subject to a relatively high wear rate which is dependent on the generator setting. Wear mainly occurs at the bottom of the electrode resulting in a shortening of the electrode. Micro-EDM strategies have built-in compensation methods for this type of wear. Besides this, corner wear reduces the ability to produce cavities with small corner radii. This is counteracted by a cutting operation with the WEDG-unit which reduces the electrodes length. Also lateral wear occurs (see Fig. 7.12) but this is less relevant as the machining occurs with the bottom of the electrode. Opposed to EDM electrodes, micro-milling tools are relatively expensive. Tool life is dependent on the applied cutting conditions. Opposed to macro-milling where tool life can be determined with Taylors equation, the situation is more complex for micro-milling as not all factors within the equation are known. Nonetheless, rough estimations of tool life data is supplied by the tool manufacturers. A comparison of the tooling cost for both operations shows that in general micro-EDM is less expensive.

The operator cost is attributed to the time that the operator is actively involved in the machining operation. This consists of time for tool and workpiece changes and alignment operations. In general it can be stated that this time it equal for both operations. From experience, on average 15 minutes of operator time is needed per workpiece.

Finally, the energy cost can be calculated based on the results of section 7.2.7. Although the energy consumed per unit of time is significantly lower for micro-EDM, the energy cost is higher due to longer machining times.
When comparing the total cost for both operations, different distributions can be noticed. For micro-EDM, the machine cost is the determining cost factor (see Fig. 7.19.a) whereas for micro-milling the operator cost is the determining cost factor (see Fig. 7.19.b). For both operations the energy cost is to be neglected. Taking into account that the operator cost for both operations is similar, it can be concluded that micro-milling is more cost effective compared to micro-EDM.

When comparing the total cost for different cavity sizes, an increase in total cost per unit of volume (specific total cost) can be noticed for both processes.

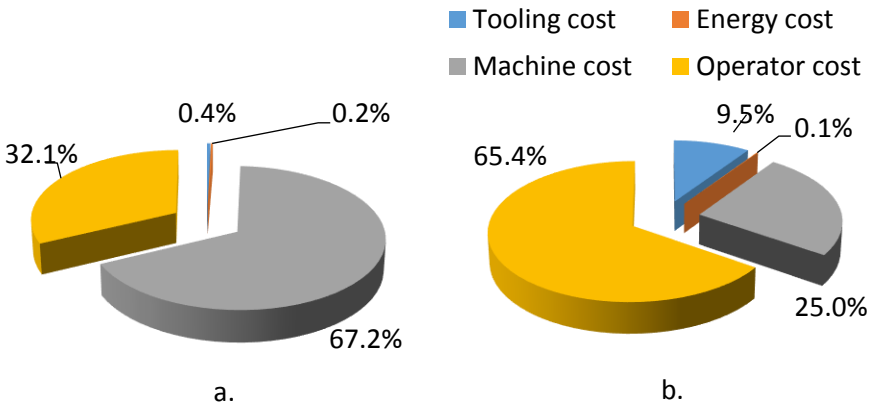

Fig. 7.19: Cost distribution for (a) micro-EDM and (b) micro-milling for a cavity of 1 mm x 1 mm x 0.2 mm.

For example, Table 7.6 shows the specific total cost for cavities with dimensions of different magnitudes. It should be noted that abstraction has been made of the operator cost as this cost does not increase as the volume increases. All other cost factors increase with the volume as these are dependent on the machining time. This table points again on the fact that micro-milling is the preferable technique from cost perspective. Important to note is that the specific total cost sharply increases as the cavity dimension decreases. As for the given cavity sizes corresponding tool diameters and process conditions are used, the figures from this table confirm that it is necessary to use larger tools as much as possible throughout the entire machining operation as these reduce the specific cost.

Table 7.6: Specific total cost for different cavity sizes.

Total cost/volume [euro/mm³]	Cavity dimension [mm x mm]		
	10x10	1x1	0,3x0,3
Micro-EDM	7,8	116	1.284
Micro-milling	0,6	29	434

7.3. Combined machining

The previous sections showed that micro-EDM and micro-milling are both complementary as competitive machining processes. On the one hand, a limitation of one process can often be counteracted by the other process which widens the application range of the considered machining platform. On the other hand, when both processes are feasible the most optimal process can be chosen which meets certain performance criteria. Often a combination of both processes leads to the best results.

An example of a machining feature which requires a combined machining operation is shown in Fig. 7.20.a. The feature is a deep through slot (LxWxD: 7 mm x 1.8 mm x 5 mm) with at the bottom a thin lip of 80 µm thickness. As the cavities depth is too large for commercial milling tools, a micro-EDM operation is indispensable. In addition, the chance of breaking the thin lip at the bottom of the cavity is higher in case of micro-milling. This again urges the need for a micro-EDM operation. However, in order to reduce machining time, part of the operation can be performed with micro-milling. Table 7.7 shows that the bulk of the material has been machined with micro-milling until the maximal cutting depth of the milling tool. The further processing has been performed with micro-EDM. Fig. 7.20.b shows the resulting cavity. When comparing the machining time with a solely micro-EDM operation a reduction of 9 hours was noted (solely micro-EDM: 13.5 h; combined machining: 4.5 h).

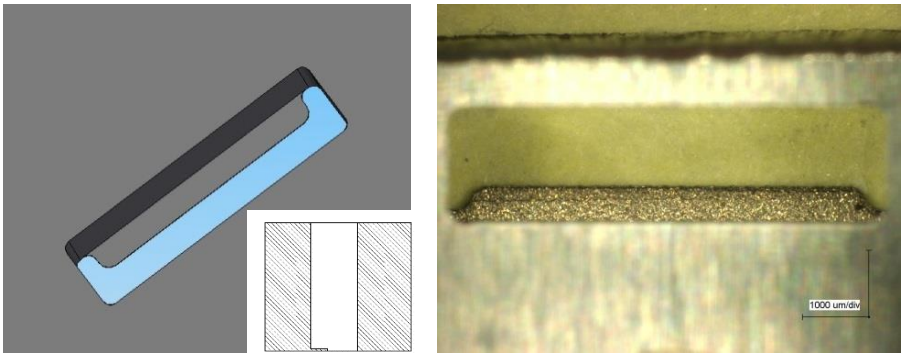

a. b.

Fig. 7.20: (a) 3D representation of thin lip feature with cross section; (b) result with combined machining.

Table 7.7: Machining steps for deep slot feature with thin bottom lip.

Machining step	Process	Final depth	Tool
#1	Micro-milling	3,9 mm	Ø 0,5 mm solid carbide corner radius endmill
#2	Micro-EDM	4,92 mm	Ø 0,5 mm solid carbide electrode
#3	Micro-EDM	5 mm	

7.4. Summary

In order to make optimal use of a combined micro-EDM and micro-milling machining platform it is essential to have knowledge about the capabilities and limitations of each process and the performance regarding several relevant criteria used in process planning. Starting from what can be found in literature, machining experiments were conducted with the focus on prismatic machining features with dimensions within the meso to micro range. These experiments showed that micro-EDM is the preferable technique regarding dimensional accuracy in the horizontal plane, straightness of the cavities edges and for the machining of deep cavities. On the other hand, micro-milling is to be preferred when looking at the depth accuracy, flatness, surface roughness, machining time or MRR, energy consumption and machining cost. However, for the latter three criteria micro-EDM becomes more competitive as the dimensions of the cavity decrease.
By incorporating the micro-milling process onto a micro-EDM machining platform the strengths of both processes can be combined into one machining operation which can lead to even better results compared to a solely micro-EDM operation. From this perspective a preferable strategy would be to remove the bulk of the material with micro-milling, if material properties and dimensions are suitable, and to finish the cavity with micro-EDM.

It should be noted that the characterization of the micro-milling process in this study cannot be transferred to a commercial micro-milling machine as the machining platform in this study puts restrictions on the milling process. For example, the relatively small accelerations and the limited feedrate restrict the performance of the milling process regarding MRR and machining cost. In addition the used air bearing spindle puts restrictions on the attainable dimensional and geometrical accuracy of the milling process.

Often process selection is based on multiple criteria. In those cases, it is not always straightforward to choose one process which best meets all the demands. Therefore, in the next chapter a process selection or planning tool will be elaborated that will define the most optimal process or combination of processes based on the results obtained in this chapter.

Chapter 8 Automated process planning for a multi-process machining platform

8.1. Introduction

The knowledge gained in the previous chapter enables to choose the optimal process for a given machining feature regarding a specific performance criterion to be machined on the machining platform of this study. However, in practice often more than one performance criterion plays a role in process selection. Moreover, the previous chapter showed that a combination of processes can be more beneficial than the separate processes. In addition, performance criteria can be conflicting making process planning a cumbersome task. Therefore an automated process planning tool or CAPP (Computer Aided Process Planning) tool has been developed within this study. The goal of this tool is twofold. First the CAPP tool should make a decision about which process or which combination of processes, available on the current machining platform, is the most suitable to machining a given micro-feature according to the user needs. Secondly the CAPP tool should determine the appropriate tool for each operation and should generate a proper operation planning in order to minimize for example the total machining time.

Process planning tools for parts to be machined by micro milling as well as micro EDM are not commercially available. On macro-level few software tools are available, mostly prototype software developed within a research context. For example, in the first part of this study a standalone software tool has been developed that assists in making a proper choice between high speed milling and die sinking EDM. However, the applicability of this software tool is limited to the macro level. However, some of the resulting ideas and methods can also be applied on the micro-level.
For the separate processes some CAPP functionality already exists, although only on research level. Dhanorker et al. [187] and Li [188] developed functionality which mainly covers the selection of optimal cutting conditions for micro-milling. Whereas for micro-EDM generally the issue of tool wear compensation is covered. As an example, Meeusen [72] developed a prototype system within a commercial CAD/CAM software for feature based design of MEMS to be manufactured by micro-EDM. The system has

functionality to design MEMS structures as well as the electrodes and related toolpaths for the micro-EDM operation (see Fig. 8.1).

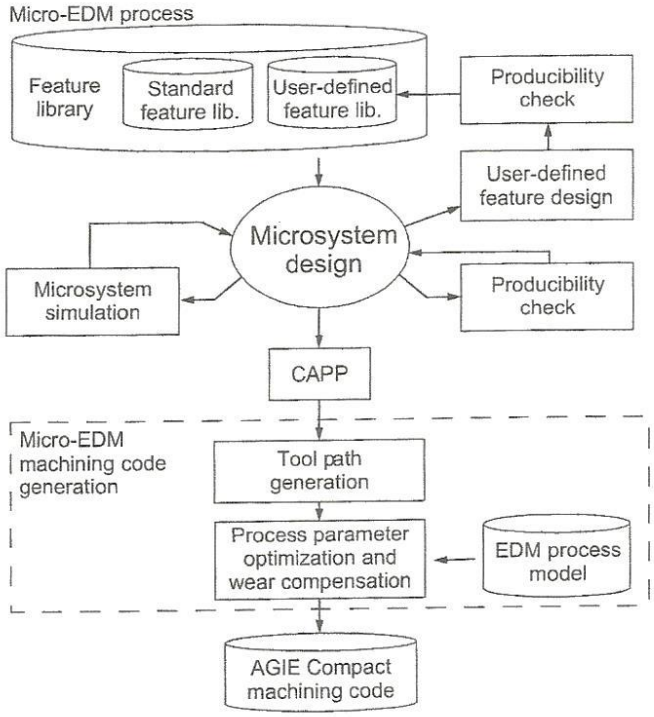

Fig. 8.1: Layout of prototype micro-EDM software [72].

8.2. Structure of CAPP tool

In order to achieve a proper process selection for the machining of several features on a micro-part in the most optimal sequence, the CAPP tool needs to run through several steps. Fig. 8.2 gives an overview of the structure of the developed CAPP tool and the result of every step. Because the process selection needs to be performed for every machining feature, first all features of the micro-part are identified. Secondly, the most suitable process for every feature is selected. In this step first the feasibility of all processes (process is here defined as the combination of a machining process with specified machining strategies for roughing, wall and floor finishing) to machine a given feature will be checked. For example, if the aspect ratio is too high a complete micro-milling operation is not feasible. Other constraints

like material and tool properties are also taken into account. This will result in a set of feasible processes for each feature. From this set of feasible processes the most suitable process or process combination for each feature will be chosen (optimization step, see Fig. 8.2). With 'most suitable' it is meant this process (or process combination) which best suits the user needs. For this all feasible processes are evaluated against five relevant performance criteria: machining cost, machining time, energy consumption, accuracy and surface quality. Each criterion has its own importance level set by the user. The process which scores best to these criteria is selected as the most suitable process. Depending on the requirements set by the user the most suitable process can vary from feature to feature. Based on the selected processes per feature the CAPP tool generates in a following step an operation planning for machining the entire micro-part. In this step the goal is to minimize the total machining time. With the results of the previous steps tool paths per feature can be generated. This is not elaborated in this study. A detailed discussion of the elaboration of the process selection and the implementation in a software tool will be given in the next sections.

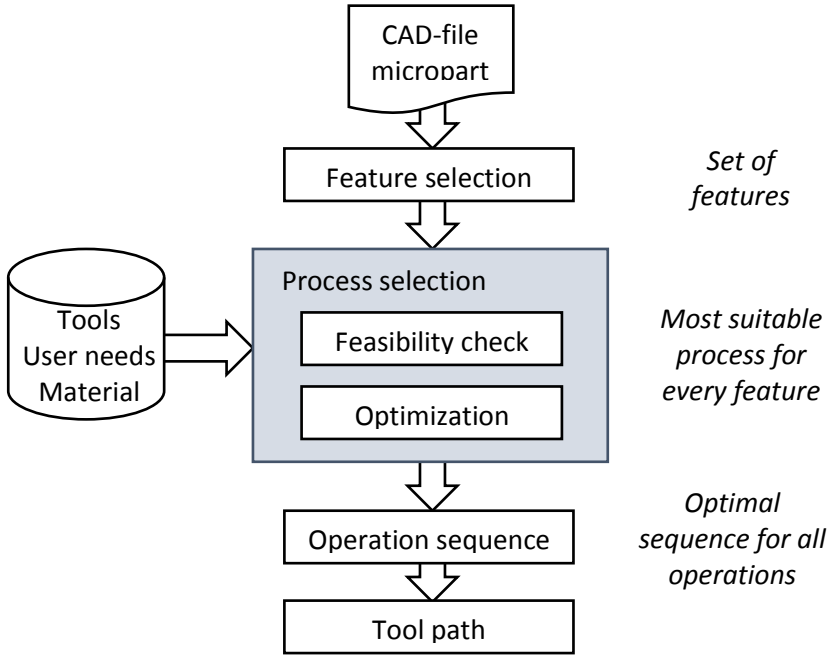

Fig. 8.2: Structure of CAPP tool with the result of every step.

8.3. Process selection

The heart of the CAPP tool is the selection of the most suitable process per machining feature. As often multiple performance criteria are important a systematic approach is needed to solve this optimization problem with multiple objectives.
First a list of processes or combination of processes has been defined based on the results from section 7.2. For this, the entire machining operation has been divided in three suboperations: roughing, wall finishing and floor finishing. For every suboperation a process has been attributed. Table 8.1 lists all possible processes (= combination of suboperations) on the current machining platform with the exclusion of non-realistic processes, for example roughing with micro-EDM and finishing with micro-milling. Note that only the zig-zag strategy is defined due to its better performance in terms of machining time and flatness.

Table 8.1: Processes applicable on the machining platform.

Process no.	Roughing	Wall finishing	Floor finishing
1	micro-milling - zig-zag	micro-milling	micro-milling
2	micro-milling - zig-zag	micro-milling + micro-EDM deburring	micro-milling
3	micro-milling - zig-zag	micro-milling	micro-EDM - zig-zag
4	micro-milling - zig-zag	micro-milling + micro-EDM deburring	micro-EDM - zig-zag
5	micro-EDM - zig-zag	micro-EDM	micro-EDM - zig-zag
6	micro-milling - zig-zag	micro-EDM	micro-milling
7	micro-milling - zig-zag	micro-EDM	micro-EDM - zig-zag
8	micro-milling + micro-EDM - zig-zag	micro-EDM	micro-EDM - zig-zag

The selection of the most suitable process to machine a given feature is performed in two steps. In a first step the feasibility of every process from Table 8.1 to machine a given feature is evaluated on a high level. Decision

criteria at this point are material properties like hardness and electrical conductivity, the aspect ratio, the smallest corner radius and smallest dimension of the given feature. This feasibility check can be summarized with the help of the decision tree displayed in Fig. 8.3. This figure shows that dependent on the decision criteria a set of feasible processes remains.

In a second step the most suitable process among the set of feasible processes will be chosen for machining (= optimization step). This is the process which best suits the user needs. The user needs are reflected by the importance given to performance criteria like machining cost, machining time, energy consumption, accuracy and surface quality. The importance of each criterion is reflected by a weighting factor w which is attributed by the user. This weighting factor will be multiplied with the score for that criterion for the considered process resulting in a 'weighted score' for that criterion. The summation of all weighted scores gives the overall score for a process (see Eq. 8.1). The process with the highest overall score will be selected for machining.

$$Score_a = \sum_{i=1}^{n} w_i \cdot \frac{\min(x_i)}{x_{i,a}} \qquad \text{(Eq. 8.1)}$$

With: $Score_a$ overall score of process a for a given machining feature;
w_i weighting factor for performance criterion i;
x_i value of performance criterion I for process a;
$\min(x_i)$ minimum of all values for the considered processes for criterion i.

The scoring for each criterion is performed in a quantitative way. This means that for each criterion the real value x is calculated based on the test results and trends discussed in section 7.2 (e.g. for the ecological criterion the energy consumption will be estimated). In order to obtain a uniform scoring among all criteria, every criterion score is calculated as the ratio of the minimal value of all feasible processes for that criterion for the given machining feature divided by the real or estimated value for that process (see Eq. 8.1). Here the minimum value is chosen as the optimum lies in a minimization of all parameters.

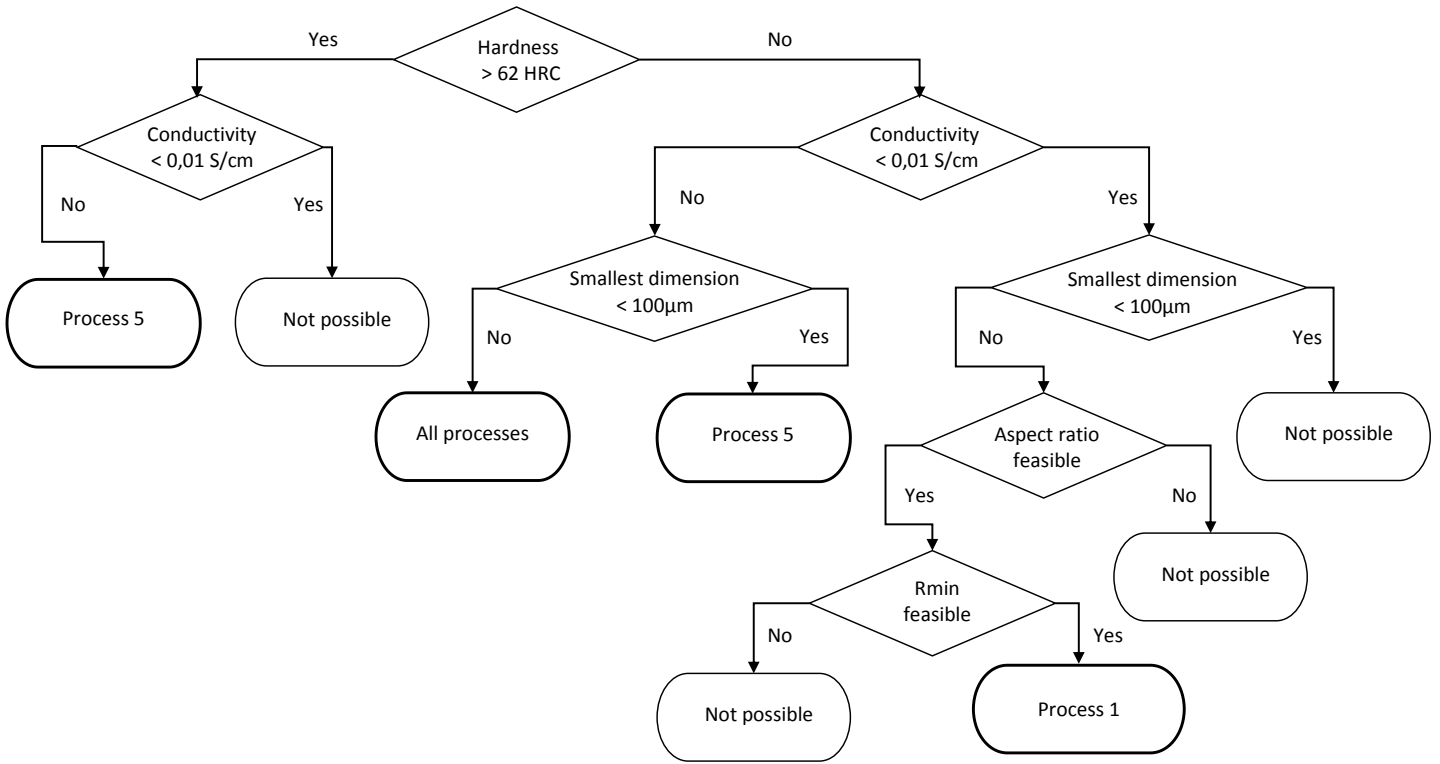

Fig. 8.3: Feasibility check - decision tree.

The criterion score obtained in that way can maximally be 1. However, it is not always necessary to obtain the minimal value. Often obtaining a predefined value is more relevant (e.g. when dimensional tolerance is defined). In that case some processes can perform better than the specification resulting in a value higher than 1. In order to not influence the scores of other criteria, the criterion score will be limited to 1 in such cases.
An example of such a calculation is given in Table 8.2 in which process 1 and 5 (see Table 8.1) are considered for machining, given a specific feature. The calculation of the criterion scores are given in the upper tables. For the machining time values of 15 min and 35 min are estimated resulting in a criterion score of respectively 1 and 0,43. It should be noted at this point that the knowledge of machining times is essential in calculating scores for cost, machining time and energy consumption. The criterion score for accuracy and surface quality consists of several so called subscores. For instance, in the example in Table 8.2 the considered performance criteria for the accuracy are flatness and depth accuracy. The individual scores for each process are determined based on the results of section 7.2. This leads to a score of 0,6 and 0,62 for respectively process 1 and process 5. Note that each performance criterion (flatness and depth accuracy) is given equal importance (weighting factor of 0,5).
When all criterion scores are calculated the overall score for each process is calculated based on Eq. 8.1 (see Table 8.2). In this example process 1 results in the highest overall score.
This methodology is performed for all machining features resulting in a list of processes to be applied. From this list the operation sequence will be defined (see section 8.4.4).

Table 8.2: Example of calculation of weighted score for process 1 and 5.

Machining time	Real	Rel.
Process 1	15min	1
Process 5	35min	0,43

Accuracy	Flatness		Dimensional		Criterion score
	Real	Rel.	Real	Rel.	
Process 1	2,6µm	1	13µm	0,19	0,60
Process 5	11µm	0,24	2,5µm	1	0,62

Weighted score	Cost		Machining time		Energy		Accuracy		Surface quality		Overall score
	High	0,8	Low	0,2	Low	0,2	High	0,8	Mid	0,5	
Process 1	1		1		0,2		0,60		1		**2,02**
Process 5	0,55		0,43		1		0,62		0,8		1,62

8.4. Implementation

As shown in Fig. 8.2 the CAPP tools runs through several steps from feature selection to definition of the operation sequence. For some steps a certain amount of interactivity with the user is required. To provide this functionality the CAPP tool is developed as an add-on to a commercial CAD/CAM system namely NX6 with the aid of the API (Application Programming Interface). The tool is setup in such way that the user needs to run through several dialogs which correspond to the steps in the selection process. The implementation of all steps will be discussed in the following paragraphs.

8.4.1. Feature identification

As the selection of the most suitable process is performed per feature, in a first step all features that need to be machined must be identified. This is done in a semi-automatic way by selecting edges and faces, depending on the type of feature (see Fig. 8.4). Five feature types are defined namely hole, counterbore hole, pocket, surface and 3D geometry each with their specific selection method and geometrical parameters. The selection process generates a solid body that corresponds to the volume to be machined. Note that all features that have been defined are represented with the corresponding solid body which gives the user a good overview. All geometrical information that can be used in the process selection step (e.g. cavity dimensions, volume, smallest corner radius) is automatically calculated from the generated solid bodies and is displayed in the dialog. Besides this the user can set the desired roughness values for each face of a feature. For example, for a pocket roughness values of the side and bottom faces can be defined (see Fig. 8.4). Moreover tolerances can be set for every feature. The type of tolerances depends on the selected feature type. The defined roughness values and tolerances will set restrictions on the process selection step.

8.4.2. Operation setup

Besides the geometrical input generated during feature identification, the process selection also requires input concerning the user needs. This is translated in priorities attributed to each performance criterion (see

Fig. 8.5.a). A selection can be made between low, middle and high priority each corresponding to a specific weighting factor. In the same dialog, the workpiece material and cost factors like hourly cost, operator cost and energy cost can be defined. Another important input for the process selection is knowledge about the available tools. Either a tool list can be loaded or can be defined. The definition of a micro-milling tool consists of parameters like tool diameter, flute length, cutting edge radius, number of flutes, cutting depth and feedrate per tooth. On the other hand, the definition of a micro-EDM electrode consists of parameters like inner and outer tool diameter and the material used.

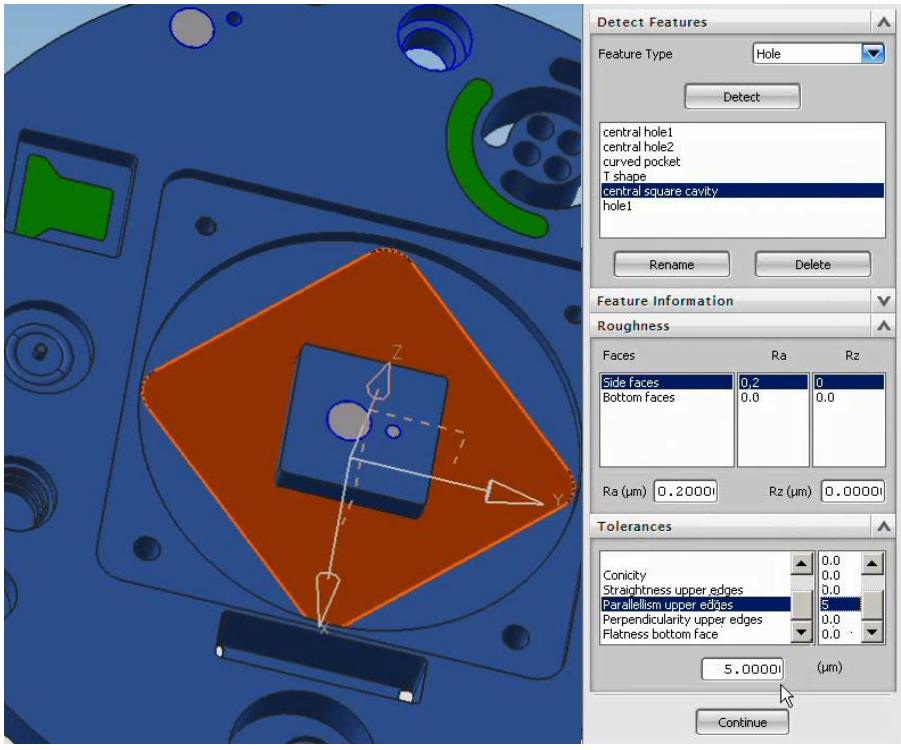

Fig. 8.4: Feature identification dialog.

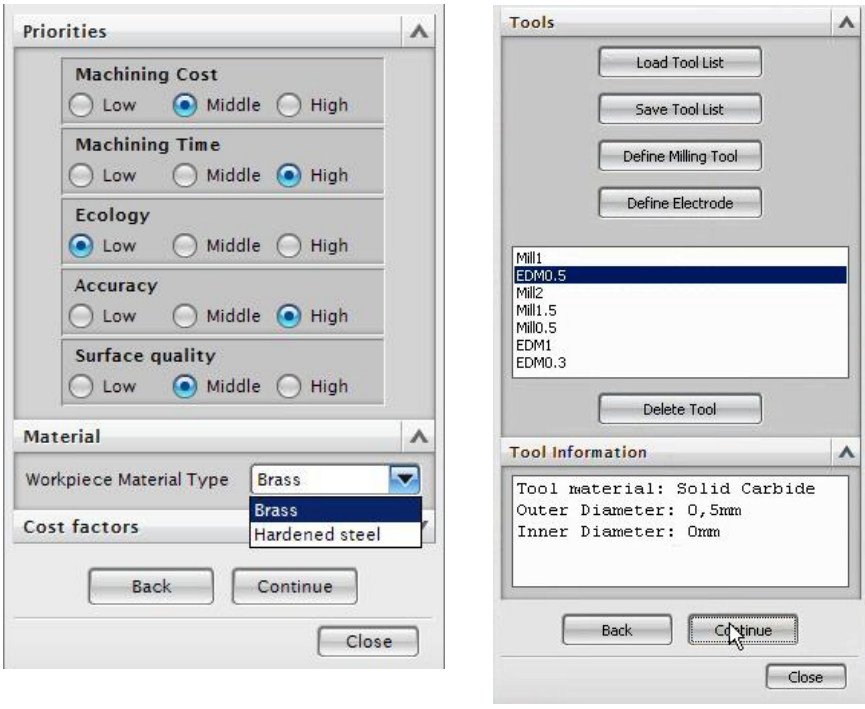

a. b.

Fig. 8.5: (a) User requirements dialog and (b) tool definition dialog.

8.4.3. Process selection

The selection of the most suitable process consists of two consecutive steps. First the feasibility of each process from Table 8.1 is assessed based on the decision tree in Fig. 8.3. In the next step, from this set of feasible processes the process which best suits the user needs is chosen. Within this step tools need to be selected for each feasible process within the boundaries set by the given machining feature in order to be able to assess the performance criteria. When selecting proper tools the smallest corner radius of the machining feature defines the finishing tool. The roughing tool is selected in such a way that machining time is minimized and that the operation will not lead to un-machined zones. In case of micro-EDM an optimal ratio (Eq. 8.2) between roughing tool radius R and finishing tool radius r exists. An important restriction in this matter is that the wall allowance should be at least equal to the finishing tool radius to avoid a non-uniform tool wear.

$$\left(\frac{R}{r}\right)_{opt} = \frac{\sqrt{2}}{\sqrt{2}-1} \qquad \text{(Eq. 8.2)}$$

With: R radius of roughing electrode;
r radius of finishing electrode.

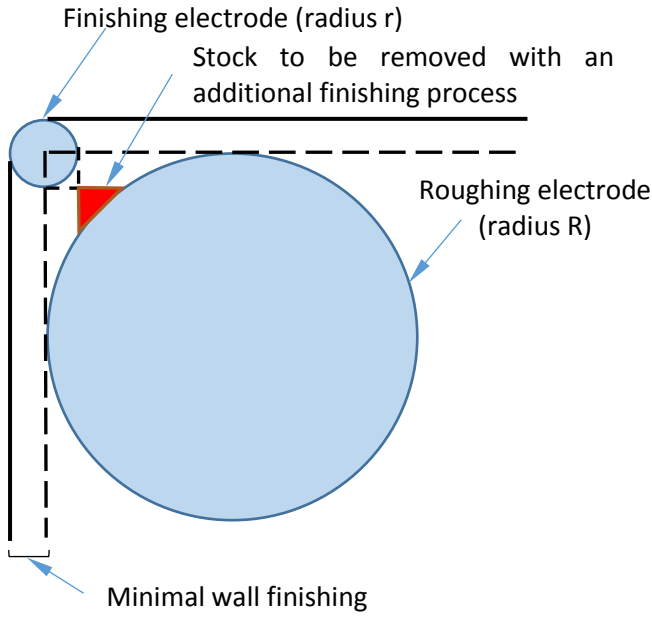

Fig. 8.6: Restriction on roughing electrode diameter.

If the optimal ratio is exceeded, some material is left un-machined and will have to be removed by an additional finishing process (see Fig. 8.6) costing valuable programming and machining time.

The actual process selection is performed by using Eq. 8.1 on all feasible processes for the given feature. For performance criteria like machining time, energy consumption and machining cost estimations are performed which all rely partially on the machining time. For micro-milling the machining time is calculated based on the feedrate, cutting depth, cutting width and the volume to be removed. This approximation corresponds well with the actual machining time. For micro-EDM the calculation is based on values of the

removal rate and the volume to be removed. This approximation is less accurate compared to the approximation for micro-milling but corresponds well enough to the real values. On the other hand, the assessment of performance criteria like accuracy and surface quality is based on empirical values which are stored in a database for each process. Comparison of the scores for all feasible processes leads to the process which best suits the user needs, namely the process with the highest score.
This methodology is performed for all machining features resulting in a list of processes to be applied. Fig. 8.7 shows the dialog displaying the processes and tools defined per machining feature. From this list the operation sequence will be defined (see section 8.4.4).

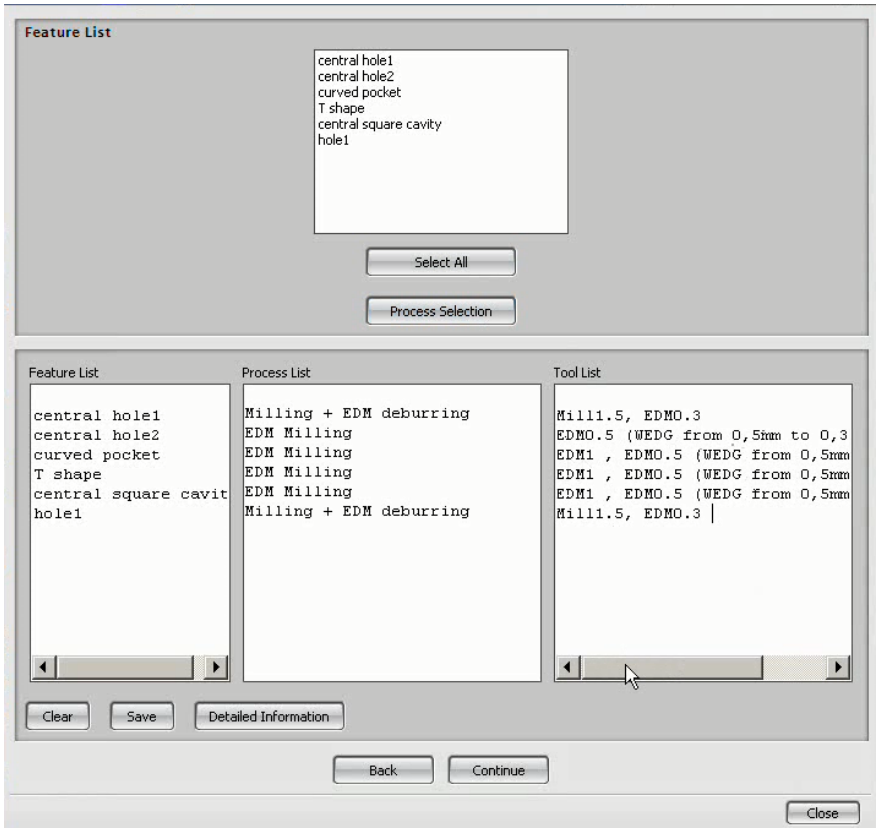

Fig. 8.7: Output of process selection.

8.4.4. Operation sequence

When for every feature a process has been selected, the last step in the CAPP tool is to define the sequence in which these processes or operations need to be performed. The overall goal of this step is to minimize the total machining time. The general rule is to perform first all micro-milling operations followed by the micro-EDM operations as this applies to the most common processes. When defining a sequence within a set of micro-milling operations or within a set of micro-EDM operations, the operation with the largest tool is put first and operations with the same tool are grouped. In case of micro-milling this saves a considerable amount of setup time whereas for micro-EDM the time needed for dressing the electrodes is reduced. In some cases deviations from these rules will occur. For instance, when having a pocket within a pocket and the lower pockets needs to be machined with a larger tool than the upper pocket. In this case first the smaller tool needs to be applied. Fig. 8.8 shows the dialog displaying the result of the operation sequence step. This figure shows that all processes are split up into their suboperations. In this dialog the user still has the possibility to alter the proposed sequence. Based on the generated sequence, toolpaths can be defined within the Sarix module of the Esprit CAM system.

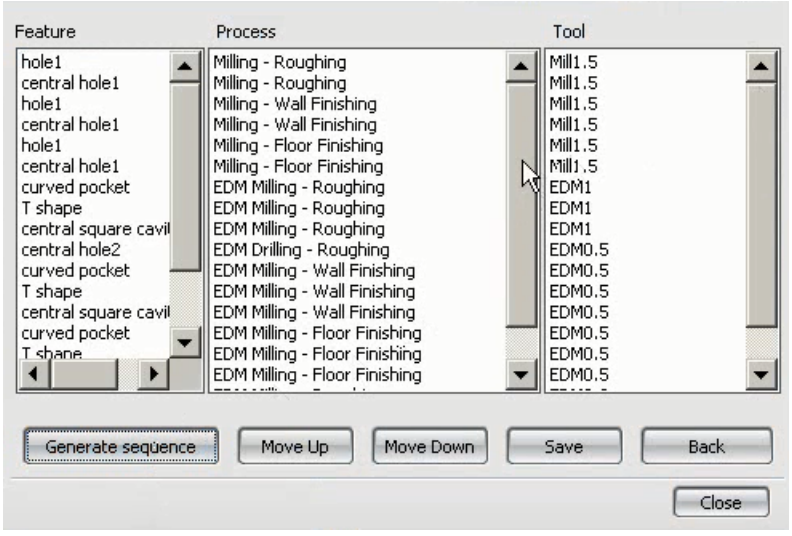

Fig. 8.8: Dialog displaying the operation sequence.

8.5. Summary

Based on Chapter 7, decisions on which process to apply regarding one specific performance criteria can be made. However, in practice a proper process planning requires to consider multiple performance criteria that can be conflicting. In addition, a combined operation of micro-EDM and micro-milling showed to be beneficial in certain machining cases. In order to address the question of finding the most suitable process, given a specific machining feature and given the user requirements, a semi-automated planning tool (CAPP) has been developed. The goal of this CAPP tool is twofold. First for every machining feature the process which best meets the user requirements needs to be defined. This is done based on the assessment of five performance criteria (accuracy, surface quality, machining time, energy consumption and machining cost) which reflect the user requirements by attributing weighting factors. All available processes on the machining platform are first checked whether these are feasible. All feasible processes are scored against all performance criteria either by performing estimations or by comparison with empirical data. The process that has the best score will be chosen for machining.

The second purpose of the CAPP tool is to define an optimal sequence of all determined suboperations. This is mainly based on minimizing the total machining time and the rule that first all micro-milling operations should be performed. The result of the CAPP tool is a sequence that lists all suboperations with their respective tools. This data can then be used for programming the machining operations.

Chapter 9 Conclusions and future work

Driven by reduced time-to-market and further cost effectiveness, the manufacturing industry is forced to increase its overall productivity. Gains in productivity can be made on technological side by for example process optimization and a higher level of automation. But also efforts put in an efficient use of resources by the development of improved process planning methods can deliver the necessary contributions. Sectors using the EDM technology struggle already for decades in defining a reliable process plan. Therefore this study aimed at the development of tools to increase the reliability and robustness of process planning for EDM.

9.1. Conclusions of this study

Indispensable for a reliable process plan is an accurate knowledge of the EDM machining time. Especially for sinking EDM operations accurate knowledge of the machining time is needed as the flushing conditions can have a large impact on the machining speed. In past studies the effect of flushing was often neglected resulting in time estimation methods with a limited application range. However in this study, besides the already known influencing factors, the effect of the flushing conditions and related parameters were taken into account. This is achieved by adjusting reference values, which are determined under predefined conditions, with correction factors to account for deviating process conditions. Reference values are determined for every generator setting, material combination and machine. In this way the effects of generator and machine related parameters are already taken into account. As the correction factors are independent of the machine, the proposed concept of time estimation can be seen as a plug-and-play concept as for every machine only the calibration has to be performed. Due to different process conditions, separate time estimation models for roughing and finishing operations were developed.

For roughing operations the main influencing factors are machining depth, frontal electrode area and current density. Empirical data has shown that strong interactions exist between these parameters as these all influence the debris density hence affecting the machining speed. For example, it has been shown that an important interaction exists between the machining depth

and current density with a transition around 6 A/cm². Below 6 A/cm² the machining speed increases for higher machining depths as a result of an increasing debris density that steadily approaches the optimal debris density. On the opposite, for current densities higher than 6 A/cm² the machining speed strongly decreases for higher machining depths due to a saturation of the sparking gap with debris. The modeling of the correction has been split up into two correction factors. On the one hand the flushing factor accounts for the portion of the deviation from the reference values caused by the flushing conditions hence reflecting the influence of machining depth and frontal area. On the other hand the efficiency factor accounts for the other part of the deviation under constant flushing conditions reflecting the influence of the current density. However, it has been shown that the effect of flushing related parameters cannot be separated from the effect of the current density, diminishing the meaning of the flushing factor as a purely flushing related correction factor.
A validation of the developed model based on machining cases within the boundaries of the model results in an average absolute error of 27.5% with 55% of the cases within an error range of [-30%, +30%]. This is a strong improvement in estimation accuracy compared to time estimations based on technology tables. However, given that not all trends seem to be equally covered in the developed model, other modelling techniques like neural networks should be considered when further improving the estimation accuracy.

Unlike the developed model for roughing operations which is based on reference values for MRR, the model for finishing operations is based on reference values for EDM time. Experiments have shown that factors like machining length, total surface area (lateral + frontal), the starting roughness of the finishing operation and the electrode geometry mainly account for the deviations that occur from the reference values. However, for prismatic geometries, only the machining length and the total surface area were considered in the modeling. A validation of the developed model based on machining cases within the boundaries of the model results in an average absolute error of 18.4% with 85% of the cases within an error range of [-30%, +30%]. Compared to time estimations based on technology tables a significant improvement in estimation accuracy has been achieved. Further improvement in estimation accuracy can be achieved by incorporating the geometry in the modelling.

The developed time estimation models have been incorporated into an automated operations evaluations system to allow an automated time estimation for complex machining cases. Based on inputs from the CAD-file, user requirements and EDM machine software this software tool calculates the EDM time per regime for all electrodes needed to machine a given machining case. This software tool allows the user to iteratively assess and compare different machining strategies by altering the electrode geometry and the process parameters to come to an optimal machining strategy in terms of machining time.
The need for effective process planning tools also in the manufacturing of micro-components is apparent due to increasing demands on throughput time, cost effectiveness, component functionality and accuracy. This pushes existing processes to their limits and acts as a strong incentive for the development of hybrid processes and machines. As both micro-EDM and micro-milling are commonly used in the manufacturing of micro-components, the effective exploitation of a combined micro-EDM and micro-milling machining platform has been studied.

In order to make optimal use of this hybrid machining platform, in a first step the technological boundaries and performance of both processes were assessed in terms of determining criteria in the act of process planning, like dimensional and geometrical accuracy, cost and time effectiveness, energy consumption and surface integrity. For this a large set of machining experiments were performed on the machining platform for different materials, machining strategies and process parameters. These experiments showed that micro-EDM is the preferable technique regarding dimensional accuracy in the horizontal plane, straightness of the cavities edges and for the machining of deep cavities. On the other hand, micro-milling is to be preferred when looking at the depth accuracy, flatness, surface roughness, machining time or MRR, energy consumption and machining cost. However, it should be noted that the performance of the micro-milling process cannot be compared one on one with micro-milling on a commercial micro-milling machine as the studied hybrid platform restricts the process performance.

In practice a proper process planning requires the consideration of multiple performance criteria that, in some cases, can be conflicting. In addition, it has been shown that a combined operation of micro-EDM and micro-milling can be more beneficial than the separate processes. In order to propose the most suitable process plan amongst many feasible process plans, a computer

aided process planning (CAPP) tool has been developed. In this software tool the user first selects all machining features and defines the technological specifications. In a second step, for every machining feature all feasible processes are defined by progressing through a decision tree. Among the set of feasible processes the most suitable process, i.e. the process that best suits the set of user requirements and their corresponding priorities, is chosen based on the evaluation of all relevant performance criteria. In a final step, the overall machining sequence is defined covering all machining features by minimizing the total machining time.

9.2. Further research

Further enhancements of the covered research topics should focus on:

- **Extension of application range of EDM time estimation models.** The models have been developed for prismatic features but have shown to give satisfactory results for more complex machining cases. However, it can be expected that for cases with a significant difference in flushing behavior larger deviations will occur (e.g. difference between machining an enclosed cavity and a half open cavity). To assess the flushing conditions, CFD simulations can be performed backboned with empirical flushing tests.

- **Further improvement of estimation accuracy by using other modelling techniques.** For example, neural networks are an effective manner to model the complex effects and interactions. As within this study the most important influencing factors were determined, these can act as the input nodes. Moreover, neural networks can be continuously supplied with new machining data hence improving the estimation accuracy.

- **Extension of the application range of CAPP tool.** In this study only prismatic micro-features have been studied, although in practice also complex 3D-shapes need to be machined. This will require to evaluate the existing set of performance criteria again as well as to evaluate other geometrical criteria. Besides this, also the material palette can be extended as this study only focused on hardened tool steel and brass applications. As the process-material interaction will be different for other materials, a deviating performance can be expected.

- **Further exploitation and verification of combined micro-EDM and micro-milling strategies.** In this study, the combined approach has been applied on a limited set of machining cases. However as the complexity increases, the process parameters of both operations need to be adapted to each other to allow an efficient transition between both operations. In addition, the high speed spindle integrated on the machining platform also allows to apply grinding operations. This additional process can also extend the application range.

Bibliography

[1] *VM120: Vonkerosie theorie en praktijk*. Zoetermeer: Vereniging FME, 2008.

[2] A. Anders, "Tracking down the origin of arc plasma science I. Early pulsed and oscillating discharges," *IEEE Trans. Plasma Sci.*, vol. 31, no. 5, pp. 1052–1059, 2003.

[3] K.H. Ho and S.T. Newman, "State of the art electrical discharge machining (EDM)," *Int. J. Mach. Tools Manuf.*, vol. 43, no. 13, pp. 1287–1300, Oct. 2003.

[4] A. Descoeudres, "Characterization of electrical discharge machining plasmas," Ecole polytechnique fédérale de Lausanne, 2006.

[5] R.C. Crosson and H. J. Abrahams, "Colloidal metals in nonaqueous solvents by Bredig method," *J. Chem. Educ.*, vol. 23, no. 6, p. 289, 1946.

[6] M. Kunieda, B. Lauwers, K. Rajurkar, and B. Schumacher, "Advancing EDM through Fundamental Insight into the Process," *CIRP Ann. Manuf. Technol.*, vol. 54, no. 2, pp. 64–87, 2005.

[7] J. A. McGeough, *Advanced methods of machining*. Springer Science & Business Media, 1988.

[8] B. R. Lazarenko, "Inversion of the erosion of metals and measures against contact devastation," Moscow University, 1943.

[9] B.R. Lazarenko, *Electrospark machining of metals (Vol. 2)*. 1964.

[10] B. M. Schumacher, R. Krampitz, and J.-P. Kruth, "Historical Phases of EDM Development Driven by the Dual Influence of 'Market Pull' and 'Science Push,'" *ISEM*, vol. 6, pp. 5–12, 2013.

[11] D.F. Dauw and B. Van Coppenolle, "On the evolution of EDM research. Part 2: From fundamental research to applied research," in *International symposium for electromachining*, 1995, pp. 133–142.

[12] "Advances in EDM for aerospace." [Online]. Available: http://www.radical-departures.net/articles/advances-in-edm-for-aerospace. [Accessed: 27-Jun-2012].

[13] Norliana Mohd Abbas, Darius G. Solomon, and Md. Fuad Bahari, “A review on current research trends in electrical discharge machining (EDM),” *Int. J. Mach. Tools Manuf.*, vol. 47, no. 7–8, pp. 1214–1228, Jun. 2007.

[14] “No Title.” [Online]. Available: http://www.charmilles.com. [Accessed: 28-May-2007].

[15] K. Liu, D. Reynaerts, and B. Lauwers, “Influence of the pulse shape on the EDM performance of Si3N4–TiN ceramic composite,” *CIRP Ann. - Manuf. Technol.*, vol. 58, no. 1, pp. 217–220, Jan. 2009.

[16] K. Liu, J. Peirs, E. Ferraris, B. Lauwers, and D. Reynaerts, “Micro Electrical Discharge Machining of Si 3 N 4 -based Ceramic Composites.”

[17] F. Van Dijck, “Physico-mathematical analysis of the Electro-Discharge Machining Process,” PhD thesis, Katholieke Universiteit Leuven, 1983.

[18] K. Brans, P. Bleys, J.-P. Kruth, and B. Lauwers, “Selective Surface Enhancement by Milling EDM with Ti and WC-Co Electrodes,” in *Proceedings of th e15th International Symposium on Electromachining*, 2007, p. 45.

[19] M. Kunieda, M. Yoshida, and N. Taniguchi, “Electrical Discharge Machining in Gas,” *CIRP Ann. - Manuf. Technol.*, vol. 46, no. 1, pp. 143–146, 1997.

[20] B. H. Kim, J. G. Ok, Y. H. Kim, and C. N. Chu, “Electrical Discharge Machining of Carbon Nanofiber for Uniform Field Emission,” *CIRP Ann. - Manuf. Technol.*, vol. 56, no. 1, pp. 233–236, Jan. 2007.

[21] J.P. Kruth, *Niet-conventionele bewerkingsmethoden*. Leuven, 2002.

[22] A. Khanra, L. Pathak, and M. Godkhindi, “Application of new tool material for electrical discharge machining (EDM),” *Bull. Mater. Sci.*, vol. 32, no. 4, pp. 401–405, 2009.

[23] W. König, D.F. Dauw, G. Levy, and U. Panten, “EDM-Future Steps towards the Machining of Ceramics,” *CIRP Ann. - Manuf. Technol.*, vol. 37, no. 2, pp. 623–631, 1988.

[24] B. Lauwers, J. P. Kruth, W. Liu, W. Eeraerts, B. Schacht, and P. Bleys, “Investigation of material removal mechanisms in EDM of composite ceramic materials,” *J. Mater. Process. Technol.*, vol. 149, no. 1–3, pp. 347–352, Jun. 2004.

[25] M. L. Jeswani, “Electricial Discharge Machining in Distilled Water,” *Wear*, vol. 72, pp. 81–88, 1981.

[26] P. Peças and E. Henriques, “Influence of silicon powder-mixed dielectric on conventional electrical discharge machining,” *Int. J. Mach. Tools Manuf.*, vol. 43, no. 14, pp. 1465–1471, Nov. 2003.

[27] J. Mercer, “Copper-Graphite Electrodes Give Companies Doing EDM Machining of Exotic Metals the Boost They Need,” *EDM Europe Buyer’s Guide 2008*, pp. 7–9, 2007.

[28] E. B. Guitrau, “EDM Graphite - selection and fabrication,” *EDM Today*, 2011.

[29] A. Klink, “Aktuelle Forschungstrends im Bereich der Senkerosion - Einsatz von Kupfer and Graphit,” 2015.

[30] R. Kern, “Sinker electrode material selection,” *EDM Today*, 2008.

[31] “Unique 7-Axis EDM System Controls a Twisted Electrode to Allow Creation of CLosed-Channel Helix Geometries,” *EDM Europe Buyer’s Guide 2010*, 2009.

[32] “Ona EDM - Wire EDM.” [Online]. Available: http://www.ona-electroerosion.com/index.php?option=com_content&view=category&layout=blog&id=43&Itemid=112&lang=en. [Accessed: 07-Feb-2014].

[33] M. Kunieda and C. Furudate, “High Precision Finish Cutting by Dry WEDM,” *CIRP Ann. - Manuf. Technol.*, vol. 50, no. 1, pp. 121–124, 2001.

[34] S. Carbon, “Fachtagung Funkenerosion,” in *Fachtagung Funkenerosion*, 2011.

[35] J. Prohaszka, A. . Mamalis, and N. . Vaxevanidis, “The effect of electrode material on machinability in wire electro-discharge machining,” *J. Mater. Process. Technol.*, vol. 69, no. 1–3, pp. 233–237, Sep. 1997.

[36] Y. S. Liao and J. . Woo, “The effects of machining settings on the behavior of pulse trains in the WEDM process,” *J. Mater. Process. Technol.*, vol. 71, pp. 433–439, 1997.

[37] “Cut 1000 OilTech.” [Online]. Available: http://www.gfac.com/content/dam/gfac/PDF-Documents/Brochure-Wire-Cut-EDM/cut-1000/cut1000_en.pdf. [Accessed: 07-Feb-2014].

[38] K. H. Ho, S. T. Newman, S. Rahimifard, and R. D. Allen, “State of the art in wire electrical discharge machining (WEDM),” *Int. J. Mach. Tools Manuf.*, vol. 44, no. 12–13, pp. 1247–1259, Oct. 2004.

[39] I. Menzies and P. Koshy, “Assessment of abrasion-assisted material removal in wire EDM,” *CIRP Ann. - Manuf. Technol.*, vol. 57, no. 1, pp. 195–198, Jan. 2008.

[40] P. Bleys, J.-P. Kruth, B. Lauwers, a. Zryd, R. Delpretti, and C. Tricarico, “Real-time Tool Wear Compensation in Milling EDM,” *CIRP Ann. - Manuf. Technol.*, vol. 51, no. 1, pp. 157–160, Jan. 2002.

[41] E. Aligiri, S. H. Yeo, and P. C. Tan, “A new tool wear compensation method based on real-time estimation of material removal volume in micro-EDM,” *J. Mater. Process. Technol.*, vol. 210, no. 15, pp. 2292–2303, Nov. 2010.

[42] G. Bissacco, G. Tristo, H. N. Hansen, and J. Valentincic, “Reliability of electrode wear compensation based on material removal per discharge in micro EDM milling,” *CIRP Ann. - Manuf. Technol.*, vol. 62, no. 1, pp. 179–182, Jan. 2013.

[43] Z. Y. Yu and M. Fujino, “Micro-EDM for Three-Dimensional Cavities - Development of Uniform Wear Method -,” *CIRP Ann. - Manuf. Technol.*, vol. 47, no. 1, pp. 169–172, 1998.

[44] J. Narasimhan, Z. Yu, and K. P. Rajurkar, “Tool Wear Compensation and Path Generation in Micro and Macro EDM,” *J. Manuf. Process.*, vol. 7, no. 1, pp. 75–82, Jan. 2005.

[45] P. Bleys, J.-P. Kruth, B. Lauwers, A. Zryd, R. Delpretti, and C. Tricarico, “Real-time Tool Wear Compensation in Milling EDM,” *CIRP Ann. - Manuf. Technol.*, vol. 51, no. 1, pp. 157–160, Jan. 2002.

[46] P. Bleys, J.-P. Kruth, and B. Lauwers, “Sensing and compensation of tool wear in milling EDM,” *J. Mater. Process. Technol.*, vol. 149, no. 1–3, pp. 139–146, Jun. 2004.

[47] B. Lauwers, J.-P. Kruth, and K. Brans, “Development of Technology and Strategies for the Machining of Ceramic Components by Sinking and Milling EDM,” *CIRP Ann. - Manuf. Technol.*, vol. 56, no. 1, pp. 225–228, Jan. 2007.

[48] K. Liu, B. Lauwers, and D. Reynaerts, “Process capabilities of Micro-EDM and its applications,” *Int. J. Adv. Manuf. Technol.*, vol. 47, no. 1–4, pp. 11–19, Apr. 2009.

[49] F. Han, Y. Yamada, T. Kawakami, and M. Kunieda, “Experimental attempts of sub-micrometer order size machining using micro-EDM,” *Precis. Eng.*, vol. 30, no. 2, pp. 123–131, Apr. 2006.

[50] K. P. Rajurkar, G. Levy, a. Malshe, M. M. Sundaram, J. McGeough, X. Hu, R. Resnick, and a. DeSilva, “Micro and Nano Machining by Electro-Physical and Chemical Processes,” *CIRP Ann. - Manuf. Technol.*, vol. 55, no. 2, pp. 643–666, Jan. 2006.

[51] M. Kunieda, Y. Miyoshi, T. Takaya, N. Nakajima, Y. ZhanBo, and M. Yoshida, “High Speed 3D Milling by Dry EDM,” *CIRP Ann. - Manuf. Technol.*, vol. 52, no. 1, pp. 147–150, Jan. 2003.

[52] V. K. Jain, *Advanced machining processes*. Allied Publisher, 2005.

[53] J. Kozak, “Abrasive Electrodischarge Grinding (AEDG) of advanced materials,” *Arch. Civ. Mech. Eng.*, vol. II, no. 1, 2002.

[54] J. Kozak and K. E. Oczos, “Selected problems of abrasive hybrid machining,” vol. 109, pp. 360–366, 2001.

[55] E. Ya and Grodzinskii, “A new grinding process using metal-bonded wheels,” in *Proceedings of ISEM 7*, 1983.

[56] T. Masuzawa and H. K. Tönshoff, “Three-Dimensional Micromachining by Machine Tools,” *Ann. CIRP*, vol. 46, no. 2, pp. 621–628, 1997.

[57] K. Egashira and K. Mizutani, “EDM at Low Open-Circuit Voltage,” *J. Japan Soc. Electr. Mach. Eng.*, vol. 37, no. 85, pp. 18–23, 2003.

[58] K. Liu, “Micro Electrical Discharge Machining of Ceramic,” KU Leuven, 2011.

[59] TNO, *Introduction to MIPLAN*. 1981.

[60] D. Bedworth, M. Henderson, and P. Wolfe, *Computer Integrated Design and Manufacturing*. McGraw-Hill, 1991.

[61] H. Toenshoff, U. Beckendorf, N. Anders, and J. Detand, “A process description concept for process planning, scheduling and job shop control,” in *CIRP seminar on manufacturing systems*, 1990.

[62] C. Devireddy and K. Ghosh, “Feature-based modelling and neural networks-based CAPP for integrated manufacturing,” *Int. J. Comput. Integr. Manuf.*, vol. 12, no. 1, pp. 61–74, 1999.

[63] I. Rojek, “Neural Networks as performance Improvement Models in Intelligent CAPP Systems,” *Control Cybern.*, vol. 39, no. 1, pp. 55–68, 2010.

[64] A. S. Rana, R. Kumar, M. Singh, and A. Kumar, “Operation Sequencing in CAPP by using Artificial Neural Network,” *Int. J. Innov. Res. Sci. Eng. Technol.*, vol. 2, no. 4, pp. 1137–1141, 2013.

[65] “A first look at T.R.U.E Precision at GF Machining Solutions during the International Solution.” [Online]. Available: http://www.gfms.com/content/gfac/country_US/en/about-gf-machining-solutions/press-room/press-releases/2016/first-look-precision-at-gfms-during-the-international-solution.html. [Accessed: 10-Dec-2016].

[66] B. Verlinden, D. Cattrysse, and D. Van Oudheusden, “Integrated sheet-metal production planning for laser cutting and bending,” *Int. J. Prod. Res.*, vol. 45, no. 2, pp. 369–383, 2007.

[67] M. Geiger and J. Knoblach, “Cost Estimation of Sheet Metal Parts with Neural Networks,” in *SheMet 97*, 1997, vol. 5, pp. 69–78.

[68] J. Knoblach, “Beitrag zur rechnerunterstützten verursachungsgerechten Angebotskalkulation von Blechteilen mit Hilfe wissensbasierter Methoden,” Friedrich-Alexander-Universität Erlangen-Nürnberg, 1999.

[69] M. Cemal, O. Irfan, and K. Cavdar, “An Expert System Approach for Die and Mold Making Operations,” *Robot. Comput. Integr. Manuf.*, vol. 21, no. 2, pp. 175–183, 2005.

[70] B. Lauwers and J.-P. Kruth, “Computer-Aided Process Planning for EDM Operations,” *J. Manuf. Syst.*, vol. 13, no. 5, pp. 313–322, 1994.

[71] V. K. Jain, J. L. Batra, and A. K. Garg, “Computer Aided Process Planning (CAPP) for Electric Discharge Machining (EDM),” *J. Mater. Process. Technol.*, vol. 48, pp. 561–569, 1995.

[72] W. Meeusen, “Micro-electro-discharge machining: technology, computer aided design & manufacturing and applications,” KULeuven, 2003.

[73] Y. Watanabe, “Estimating machining time of Sinker EDM by EDcam,” *Int. J. Electr. Mach.*, vol. 9, pp. 59–61, 2004.

[74] R. Snoeys and F. S. Van Dijck, “Investigation of electro discharge machining operations by means of thermo-mathematical model,” *Ann. CIRP*, vol. 20, no. 1, pp. 35–37, 1971.

[75] S. H. Yeo, W. Kurnia, and P. C. Tan, “Critical assessment and numerical comparison of electro-thermal models in EDM,” *J. Mater. Process. Technol.*, vol. 203, no. 1–3, pp. 241–251, Jul. 2008.

[76] S. T. Jilani and P. C. Pandey, “Analysis and modelling of EDM parameters,” *Precis. Eng.*, vol. 4, no. 4, pp. 215–221, 1982.

[77] S. T. Jilani and P. C. Pandey, “Analysis of surface erosion in electrical discharge machining,” *Wear*, vol. 84, no. 3, pp. 275–284, 1983.

[78] P. C. Pandey and S. T. Jilani, “Plasma channel growth and the resolidified layer in EDM,” *Precis. Eng.*, vol. 8, no. 2, pp. 104–110, 1986.

[79] D. D. DiBitonto, P. T. Eubank, M. R. Patel, and M. A. Barrufet, “Theoretical models of the electrical discharge machining process,” *J. Appl. Phys.*, vol. 66, no. 9, pp. 4095–4103, 1989.

[80] K. Salonitis, a. Stournaras, P. Stavropoulos, and G. Chryssolouris, “Thermal modeling of the material removal rate and surface roughness for die-sinking EDM,” *Int. J. Adv. Manuf. Technol.*, vol. 40, no. 3–4, pp. 316–323, Jan. 2008.

[81] S. N. Joshi and S. S. Pande, “Thermo-physical modeling of die-sinking EDM process,” *J. Manuf. Process.*, vol. 12, no. 1, pp. 45–56, Jan. 2010.

[82] S. H. Yeo, W. Kurnia, and P. C. Tan, “Electro-thermal modelling of anode and cathode in micro-EDM,” *J. Phys. D. Appl. Phys.*, vol. 40, no. 8, pp. 2513–2521, Apr. 2007.

[83] Y. S. Tarng and L. K. Chung, “Determination of Optimal Cutting Parameters in Wire Electrical Discharge Machining,” *Science (80-.).*, vol. 35, no. 95, pp. 1693–1701, 1995.

[84] B. Y. Lee, H. S. Liu, and Y. S. Tarng, “Modeling and optimization of drilling process,” *J. Mater. Process. Technol.*, vol. 74, no. 1–3, pp. 149–157, 1998.

[85] D. Karayel, “Prediction and control of surface roughness in CNC lathe using artificial neural network,” *J. Mater. Process. Technol.*, vol. 209, no. 7, pp. 3125–3137, 2009.

[86] T. W. Liao and L. J. Chen, “A neural network approach for grinding processes: Modelling and optimization,” *Int. J. Mach. Tools Manuf.*, vol. 34, no. 7, pp. 919–937, 1994.

[87] İ. Asiltürk and M. Çunkaş, “Modeling and prediction of surface roughness in turning operations using artificial neural network and multiple regression method,” *Expert Syst. Appl.*, vol. 38, no. 5, pp. 5826–5832, 2011.

[88] A. M. Zain, H. Haron, and S. Sharif, “Prediction of surface roughness in the end milling machining using Artificial Neural Network,” *Expert Syst. Appl.*, vol. 37, no. 2, pp. 1755–1768, 2010.

[89] V. Cariapa, K. S. Akbay, and R. Rudraraju, “Application of neural networks for compliant tool polishing operations,” *J. Mater. Process. Technol.*, vol. 28, no. 1–2, pp. 241–250, 1991.

[90] H. S. Liu and Y. S. Tarng, “Monitoring of the Electrical Discharge Machining Process by Abductive Networks,” *Int. J. Manuf. Technol.*, vol. 13, pp. 264–270, 1997.

[91] D. K. Panda and R. K. Bhoi, “Artificial Neural Network Prediction of Material Removal Rate in Electro Discharge Machining,” *Mater. Manuf. Process.*, vol. 20, no. 4, pp. 645–672, Jul. 2005.

[92] J. C. Su, J. Y. Kao, and Y. S. Tarng, “Optimisation of the electrical discharge machining process using a GA-based neural network,” *Int. J. Adv. Manuf. Technol.*, vol. 24, pp. 81–90, Jun. 2003.

[93] K. Tsai and P. Wang, “Predictions on surface finish in electrical discharge machining based upon neural network models,” *Int. J. Mach. Tools Manuf.*, vol. 41, no. 10, pp. 1385–1403, 2001.

[94] K.-M. Tsai and P.-J. Wang, “Comparisons of neural network models on material removal rate in electrical discharge machining,” *J. Mater. Process. Technol.*, vol. 117, pp. 111–124, Nov. 2001.

[95] D. Mandal, S. K. Pal, “Modeling of electrical discharge machining process using back propagation neural network and multi-objective optimization using non-dominating sorting genetic algorithm-II,” *J. Mater. Process. Technol.*, vol. 186, no. 1–3, pp. 154–162, May 2007.

[96] K. Wang, H. L. Gelgele, Y. Wang, Q. Yuan, and M. Fang, “A hybrid intelligent method for modelling the EDM process,” *Int. J. Mach. Tools Manuf.*, vol. 43, no. 10, pp. 995–999, Aug. 2003.

[97] S. N. Joshi and S. S. Pande, “Development of an intelligent process model for EDM,” *Int. J. Adv. Manuf. Technol.*, vol. 45, no. 3–4, pp. 300–317, Mar. 2009.

[98] Y. Chen and S. . Mahdivian, “Analysis of electro-discharge machining process and its comparison with experiments,” *J. Mater. Process. Technol.*, vol. 104, no. 1–2, pp. 150–157, Aug. 2000.

[99] a Yahya and C. D. Manning, “Determination of material removal rate of an electro-discharge machine using dimensional analysis,” *J. Phys. D. Appl. Phys.*, vol. 37, no. 10, pp. 1467–1471, May 2004.

[100] I. Puertas, C. J. Luis, and L. Álvarez, “Analysis of the influence of EDM parameters on surface quality, MRR and EW of WC–Co,” *J. Mater. Process. Technol.*, vol. 153–154, pp. 1026–1032, Nov. 2004.

[101] A. Khan, “Electrode wear and material removal rate during EDM of aluminum and mild steel using copper and brass electrodes,” *Int. J. Adv. Manuf. Technol.*, vol. 39, no. 5–6, pp. 482–487, Oct. 2007.

[102] C. H. C. Haron, B. Deros, A. Ginting, and M. Fauziah, “Investigation on the influence of machining parameters when machining tool steel using EDM,” *J. Mater. Process. Technol.*, vol. 116, pp. 84–87, 2001.

[103] S. H. Lee and X. P. Li, “Study of the effect of machining parameters on the machining characteristics in electrical discharge machining of tungsten carbide,” *J. Mater. Process. Technol.*, vol. 115, pp. 344–358, 2001.

[104] C. H. Che Haron, J. a. Ghani, “Copper and graphite electrodes performance in electrical-discharge machining of XW42 tool steel,” *J. Mater. Process. Technol.*, vol. 201, no. 1–3, pp. 570–573, May 2008.

[105] S. Singh, S. Maheshwari, and P. C. Pandey, “Some investigations into the electric discharge machining of hardened tool steel using different electrode materials,” *J. Mater. Process. Technol.*, vol. 149, no. 1–3, pp. 272–277, Jun. 2004.

[106] K. Aas, “Performance of two graphite electrode qualities in EDM of seal slots in a jet engine turbine vane,” *J. Mater. Process. Technol.*, vol. 149, pp. 152–156, Apr. 2004.

[107] “Makino EDcam CAM system.” [Online]. Available: http://www.ffcam.makino.co.jp/EDcam/en/. [Accessed: 19-Aug-2014].

[108] T. Masuzawa, X. Cui, and N. Taniguchi, “Improved Jet Flushing for EDM,” *CIRP Ann. - Manuf. Technol.*, vol. 41, no. 1, pp. 239–242, 1992.

[109] C. Frei, D. Phil, and C. Hirt, “A New Approach for Contamination Measurements for EDM Dielectrics,” *Ann. CIRP*, vol. 36, no. 1, pp. 111–113, 1987.

[110] W. Koenig, R. Wertheim, and Jutzler W.I., “The Flow Fields in the Working Gap with Electro-Discharge Machining,” *Ann. CIRP*, vol. 25, no. 1, pp. 71–75, 1977.

[111] Y. S. Wong, L. C. Lim, and L. C. Lee, “Effects of Flushing on Electro-Discharge Machined Surfaces,” *J. Mater. Process. Technol.*, vol. 48, pp. 299–305, 1995.

[112] A. Erden, “Role of dielectric flushing on EDM performance,” in *Proceedings of Machine Tool Design Research Conference*, 1982, pp. 283–289.

[113] R. Kern, “Flushing Fundamentals: A primer for EDM machinists who seek clean die-sinking,” *European Tool & Mould Making*, vol. XI, no. 5, pp. 34–38, 2009.

[114] K. Y., Y. H., T. Toyonaga, and Shoda K., “Performance of Linear Motor Equipped Die-Sinking EDM,” *Int. J. Electr. Mach.*, vol. 5, pp. 59–64, 2000.

[115] S. Cetin, Y. Uno, A. Okada, and Y. Kawazoe, “Dielectric Fluid Flow in Die -Sinking EDM Gap,” vol. 4, no. 5, p. 2000, 2002.

[116] S. Cetin, A. Okada, and Y. Uno, “Electrode Jump Motion in Linear Motor Equipped Die-Sinking EDM,” *J. Manuf. Sci. Eng.*, vol. 125, no. 4, pp. 809–815, 2003.

[117] S. Cetin, A. Okada, and Y. Uno, “Effect of Debris Distribution on Wall Concavity in Deep-Hole EDM,” *JSME Int. J.*, vol. 47, no. 2, pp. 553–559, 2004.

[118] M. Ghoreishi and J. Atkinson, “A comparative experimental study of machining characteristics in vibratory, rotary and vibro-rotary electro-discharge machining,” *J. Mater. Process. Technol.*, vol. 120, no. 1–3, pp. 374–384, Jan. 2002.

[119] T. Masuzawa and C. J. Heuvelman, “A self-flushing method with Spark-Erosion Machining,” *Ann. CIRP*, vol. 32, no. 1, pp. 109–111, 1983.

[120] H. E. De Bruijn, T. H. Delft, and A. J. Pekelaring, “Effect of a magnetic field on the gap cleaning in EDM,” *Ann. CIRP*, vol. 27, no. 1, pp. 93–95, 1978.

[121] M. Kunieda and T. Masuzawa, “A Fundamental Study on a Horizontal EDM,” *Ann. CIRP*, vol. 37, no. 2, pp. 187–190, 1988.

[122] B. Lauwers, B. Boons, and W. Vanderauwera, “Questionnaire KnowEDM - Inputs for sinking EDM time estimation,” 2006.

[123] F. Kirchmann, “Entwicklung eines Modells zur Vorhersage der Erodierdauer bei der funkenerosiven Senkbearbeitung,” Technischen Universität Bergakademie Freiberg, 2013.

[124] M. Lonardo and A. Bruzzone, “Effect of flushing and electrode material on die-sinking EDM,” *Ann. CIRP*, vol. 48, no. 1, pp. 123–126, 1999.

[125] Charmilles Technologies, *Die Sinking Technologies Manual - ROBOFORM 350-550*. 2003.

[126] W. Natsu, S. Ojima, T. Kobayashi, and M. Kunieda, “Temperature distribution measurement in EDM arc plasma using spectroscopy,” *JSME Int. J.*, vol. 47, no. 1, pp. 384–390, 2004.

[127] A. Essiptchouk, L. Sharakhovsky, and A. Marotta, “The effect of surface electrode temperature on cold electrode erosion behaviour,” *Plasma Sources Sci. Technol.*, vol. 16, no. 1, pp. 1–6, Feb. 2007.

[128] F. L. Amorim and W. L. Weingaertner, “The Behavior of Graphite and Copper Electrodes on the Finish Die-Sinking Electrical Discharge Machining (EDM) of AISI P20 Tool Steel,” *J. Brazilian Soc. Mech. Sci. Eng.*, vol. 29, no. 4, pp. 366–371, 2007.

[129] J. R. Sasian Ramirez, E. A. Rodriguez Jara, W. Vanderauwera, W. Dewulf, and B. Lauwers, “Surface roughness modelling after the roughing step in die sinking EDM operations,” Leuven Engineering School Group T, 2008.

[130] F. Staelens, “Overall on-line optimization of planetary electro discharge machining,” PhD thesis, Katholieke Universiteit Leuven, 1990.

[131] F. Staelens and J.-P. Kruth, “An overall optimization strategy for planetary EDM,” in *Proceedings of the International Symposium for Electromachining*, 1989, pp. 317–320.

[132] B. Lauwers, “Report representing the system requirements for EDM machining time calculation,” 2007.

[133] R. B. Aronson, “Micromanufacturing is Growing,” *Manufacturing Engineering*, Apr-2004.

[134] T. Masuzawa, “State of the Art of Micromachining,” *Ann. CIRP*, vol. 49, no. 2, pp. 473–488, 2000.

[135] V. Piotter, W. Bauer, T. Benzler, and A. Emde, “Micro injection moulding of components for microsystems,” in *Euspen Topical Conference on Fabrication and Metrology in Nanotechnology*, 2000, vol. 1, pp. 182–189.

[136] E. W. Becker, W. Ehrfeld, P. Hagmann, A. Maner, and D. Münchmeyer, “Fabrication of microstructures with high aspect ratios and great structural heights by synchrotron radiation lithography, galvanoforming, and plastic moulding (LIGA process),” *Microelectron. Eng.*, vol. 4, no. 1, pp. 35–56, 1986.

[137] M. J. De Boer, J. G. E. Gardeniers, H. V. Jansen, E. Smulders, M. J. Gilde, G. Roelofs, “Guidelines for etching silicon MEMS structures using fluorine high-density plasmas at cryogenic temperatures,” *J. Microelectromechanical Syst.*, vol. 11, no. 4, pp. 385–401, 2002.

[138] H. Becker and U. Heim, “Hot embossing as a method for the fabrication of polymer high aspect ratio structures,” *Sensors Actuators, A Phys.*, vol. 83, no. 1, pp. 130–135, 2000.

[139] H. H. Gatzen and J. C. Maetzig, “Nanogrinding,” *Precis. Eng.*, vol. 21, no. 2–3, pp. 134–139, 1997.

[140] B. Lauwers, “Surface Integrity in Hybrid Machining Processes,” *Procedia Eng.*, vol. 19, pp. 241–251, 2011.

[141] J. Kozak, K. P. Rajurkar, and Y. Makkar, “Selected problems of micro-electrochemical machining,” *J. Mater. Process. Technol.*, vol. 149, no. 1–3, pp. 426–431, Jun. 2004.

[142] K. Li, J. J. Kim, and M. Shukor, “Grit blast assisted laser milling/grooving of metallic alloys,” *Ann. CIRP*, vol. 54, no. 1, pp. 155–158, 2005.

[143] A. W.-J. Hsue and Y.-F. Chang, “Toward Synchronous Hybrid Micro-EDM Grinding of Micro-Holes Using Helical Taper Tools Formed by Ni-Co/Diamond Co-deposition,” *J. Mater. Process. Technol.*, vol. 234, pp. 368–382, 2016.

[144] J.-C. Hung, S.-C. Lien, J.-K. Lin, F.-Y. Huang, and B.-H. Yan, “Fabrication of a micro-spherical tool in EDM combined with Ni-diamond co-deposition,” *J. Micromechanics Microengineering*, vol. 18, 2008.

[145] S. Campana and S. Miyazawa, “Micro EDM and ECM in DI water,” in *ASPE Proceedings 14th Annual Meeting*, 1999.

[146] S. Sakai, T. Masuzawa, and S. Ito, “ECM Finishing of Surface Products by EDM,” in *ISEM 9*, 1989, pp. 155–158.

[147] Z. Zeng, Y. Wang, Z. Wang, D. Shan, and X. He, “A study of micro-EDM and micro-ECM combined milling for 3D metallic micro-structures,” *Precis. Eng.*, vol. 36, no. 3, pp. 500–509, Jul. 2012.

[148] T. Masuzawa and S. Sakai, “Wire-ECM for finishing Surfaces produced by NC-wire EDM,” in *Proceedings of ISEM 7*, 1983, pp. 285–291.

[149] T. Kurita and M. Hattori, “A study of EDM and ECM/ECM-lapping complex machining technology,” *Int. J. Mach. Tools Manuf.*, vol. 46, no. 14, pp. 1804–1810, Nov. 2006.

[150] D. W. Rudorff, “Principles and applications of Spark Machining,” in *Proceedings of the Institution of Mechanical Engineers*, 1957, pp. 495–511.

[151] H. Langen, V. Fascio, R. Wüthrich, and D. Viquerat, “Three-Dimensional structuring of pyrex-glass devices - trajectory control,” in *EUSPEN*, 2002, pp. 435–438.

[152] R. Wüthrich and V. Fascio, “Machining of non-conducting materials using electrochemical discharge phenomenon—an overview,” *Int. J. Mach. Tools Manuf.*, vol. 45, no. 9, pp. 1095–1108, 2005.

[153] K. Furutani and M. Tomoto, “Combination Machining of Wire-sawing with Electro-chemical Discharge Machining,” in *ASPE Proceedings 23rd Annual Meeting*, 2008.

[154] I. M. Crichton, J. A. McGeough, W. Munro, and C. White, “Comparative studies of ECM, EDM and ECAM,” *Precis. Eng.*, vol. 3, no. 3, pp. 155–160, Jul. 1981.

[155] J. W. Liu, T. M. Yue, and Z. N. Guo, “An analysis of the discharge mechanism in electrochemical discharge machining of particulate reinforced metal matrix composites,” *Int. J. Mach. Tools Manuf.*, vol. 50, no. 1, pp. 86–96, 2010.

[156] M. Schöpf, “Electro Chemical Discharge Machining (ECDM) - New Method for Trueing and Dressing of Metal Bonded Diamond and CBN Grinding Wheels,” ETH Zürich, 2001.

[157] J. W. Liu, T. M. Yue, and Z. N. Guo, “Wire Electrochemical Discharge Machining of Al 2 O 3 Particle Reinforced Aluminum Alloy 6061,” *Mater. Manuf. Process.*, vol. 24, no. 4, pp. 446–453, Feb. 2009.

[158] S. Tandon, V. K. Jain, P. Kumar, and K. P. Rajurkar, “Investigations into machining of composites,” *Precis. Eng.*, vol. 12, pp. 227–238, 1990.

[159] S. K. Jui, A. B. Kamaraj, and M. M. Sundaram, “High aspect ratio micromachining of glass by electrochemical discharge machining (ECDM),” *J. Manuf. Process.*, no. 0, p. , 2013.

[160] W. Y. Peng and Y. S. Liao, “Study of electrochemical discharge machining technology for slicing non-conductive brittle materials,” *J. Mater. Process. Technol.*, vol. 149, no. 1–3, pp. 363–369, 2004.

[161] C. T. Yang, S. L. Song, B. H. Yan, and F. Y. Huang, “Improving machining performance of wire electrochemical discharge machining by adding SiC abrasive to electrolyte,” *Int. J. Mach. Tools Manuf.*, vol. 46, no. 15, pp. 2044–2050, 2006.

[162] V. K. Jain, S. K. Choudhury, and K. M. Ramesh, “On the machining of alumina and glass,” *Int. J. Mach. Tools Manufact.*, vol. 42, no. 2002, pp. 1269–1276, 2002.

[163] V. Schulze, P. Weber, and C. Ruhs, “Optical and Acoustical Process Control in Hybrid Micromachining Using a Picosecond Pulsed UV-laser and Micro EDM-milling,” no. c, pp. 978–981, 2011.

[164] J. Fleischer, J. Schmidt, “Combination of electric discharge machining and laser ablation in microstructuring of hardened steels,” *Microsyst. Technol.*, vol. 12, no. 7, pp. 697–701, Feb. 2006.

[165] V. Schulze, P. Weber, and C. Ruhs, “Increase of process reliability in the micro-machining processes EDM-milling and laser ablation using on-machine sensors,” *J. Mater. Process. Technol.*, vol. 212, no. 3, pp. 625–632, Mar. 2012.

[166] S. Kim, B. H. Kim, D. K. Chung, H. S. Shin, and C. N. Chu, “Hybrid micromachining using a nanosecond pulsed laser and micro EDM,” *J. Micromechanics Microengineering*, vol. 20, no. 1, 2009.

[167] L. Li, C. Diver, J. Atkinson, R. Giedl-Wagner, and H. J. Helml, “Sequential Laser and EDM Micro-drilling for Next Generation Fuel Injection Nozzle Manufacture,” *CIRP Ann. - Manuf. Technol.*, vol. 55, no. 1, pp. 179–182, Jan. 2006.

[168] D. Kremer, J. L. Lebrun, B. Hosari, and A. Moisan, “Effects of Ultrasonic Vibrations on the Performances in EDM,” *Ann. CIRP*, vol. 38, no. 1, pp. 199–202, 1989.

[169] D. Kremer, C. Lhiaubet, and A. Moisan, “A Study of the Effect of Synchronizing Ultrasonic Vibrations with Pulses,” *Ann. CIRP*, vol. 40, no. 1, pp. 211–214, 1991.

[170] S. H. Yeo and L. K. Tan, “Effects of Ultrasonic Vibrations in Micro Electro-Discharge Machining of Microholes,” *J. Micromechanics Microengineering*, vol. 9, pp. 345–352, 1999.

[171] H. Huang, H. Zhang, and H. Y. Zheng, “Ultrasonic vibration assisted electro-discharge machining of microholes in Nitinol,” *J. Micromechanics Microengineering*, vol. 13, no. 5, pp. 693–700, 2003.

[172] Z. Wansheng, W. Zhenlong, D. Shichun, C. Guanxin, and W. Hongyu, “Ultrasonic and electric discharge machining to deep and small hole on titanium alloy,” *J. Mater. Process. Technol.*, vol. 120, no. 1–3, pp. 101–106, Jan. 2002.

[173] Z. Y. Yu, Y. Zhang, J. Li, J. Luan, F. Zhao, and D. Guo, “High aspect ratio micro-hole drilling aided with ultrasonic vibration and planetary movement of electrode by micro-EDM,” *CIRP Ann. - Manuf. Technol.*, vol. 58, no. 1, pp. 213–216, Jan. 2009.

[174] Z. N. Guo, T. C. Lee, T. M. Yue, and W. S. Lau, “A Study of Ultrasonic-aided Wire Electrical Discharge Machining,” *J. Mater. Process. Technol.*, vol. 63, pp. 823–828, 1997.

[175] “Microfor HP4 EDM,” 2013. [Online]. Available: www.posalux.ch. [Accessed: 15-Jan-2013].

[176] T. C. Lee, J. H. Zhang, and W. S. Lau, “Machining of Engineering Ceramics by Ultrasonic Vibration Assisted EDM Method,” *Mater. Manuf. Process.*, vol. 13, no. 1, pp. 133–146, 1998.

[177] D. K. Aspinwall, R. C. Dewes, J. M. Burrows, M. A. Paul, and B. J. Davies, “Hybrid High Speed Machining (HSM): System Design and Experimental Results for Grinding/HSM and EDM/HSM,” *CIRP Ann. - Manuf. Technol.*, vol. 50, no. 1, pp. 145–148, 2001.

[178] S. Sakai, K. Tsuchino, and T. Masuzawa, “Development of an efficient finishing system of die and mould by electrochemical finishing using a mate electrode,” in *Proceedings of the 2nd International Conference on Mould an Die Technology*, 1992, pp. 104–115.

[179] A. Asad, T. Masaki, M. Rahman, H. Lim, and Y. Wong, “Tool-based micro-machining,” *J. Mater. Process. Technol.*, vol. 192–193, pp. 204–211, Oct. 2007.

[180] A. De Grave, H. N. Hansen, and G. Bissacco, “Integration of micro-milling high speed spindle on a micro-EDM milling machine set up,” in *International conference onMulti-Material Micro Manufacture (4M)*, 2009, pp. 355–358.

[181] Z. Y. Yu, K. P. Rajurkar, and H. Shen, “High Aspect Ratio and Complex Shaped Blind Micro Holes by Micro EDM,” *Ann. CIRP*, vol. 51, no. 1, pp. 359–362, 2002.

[182] C. R. Friedrich and M. J. Vasile, “Development of the Micromilling Process for High Aspect Ratio Microstructures,” *J. microelectromechanical Syst.*, vol. 5, no. 1, pp. 33–38, 1996.

[183] L. Uriarte, A. Herrero, A. Ivanov, H. Oosterling, L. Staemmler, P. T. Tang, and D. Allen, “Comparison between microfabrication technologies for metal tooling,” *J. Mech. Eng. Sci.*, vol. 220, no. 11, pp. 1665–1676, Jan. 2006.

[184] M. Garzon, “Report on Optimisation of Integrated Processing System,” 2011.

[185] “Westwind air bearing D1769.” [Online]. Available: http://www.westwind-airbearings.com/pcb/documents/TornadoD1769update08.pdf. [Accessed: 07-May-2016].

[186] Y. H. Jeong, B. HanYoo, H. U. Lee, B.-K. Min, D.-W. Cho, and S. J. Lee, “Deburring microfeatures using micro-EDM,” *J. Mater. Process. Technol.*, vol. 209, no. 14, pp. 5399–5406, Jul. 2009.

[187] A. Dhanorker, X. Liu, and T. Özel, “Micromilling Process Planning and Modeling for Micromold Manufacturing,” *ASME 2007 Int. Manuf. Sci. Eng. Conf.*, pp. 759–769, 2007.

[188] P. LI, “Micromilling of hardened tool steels,” TU Delft, 2009.

[189] X. D. Cao, B. H. Kim, and C. N. Chu, “Micro-structuring of glass with features less than 100μm by electrochemical discharge machining,” *Precis. Eng.*, vol. 33, no. 4, pp. 459–465, 2009.

Appendix A – Technology tables

Technology curve for the material combination copper-steel [125]

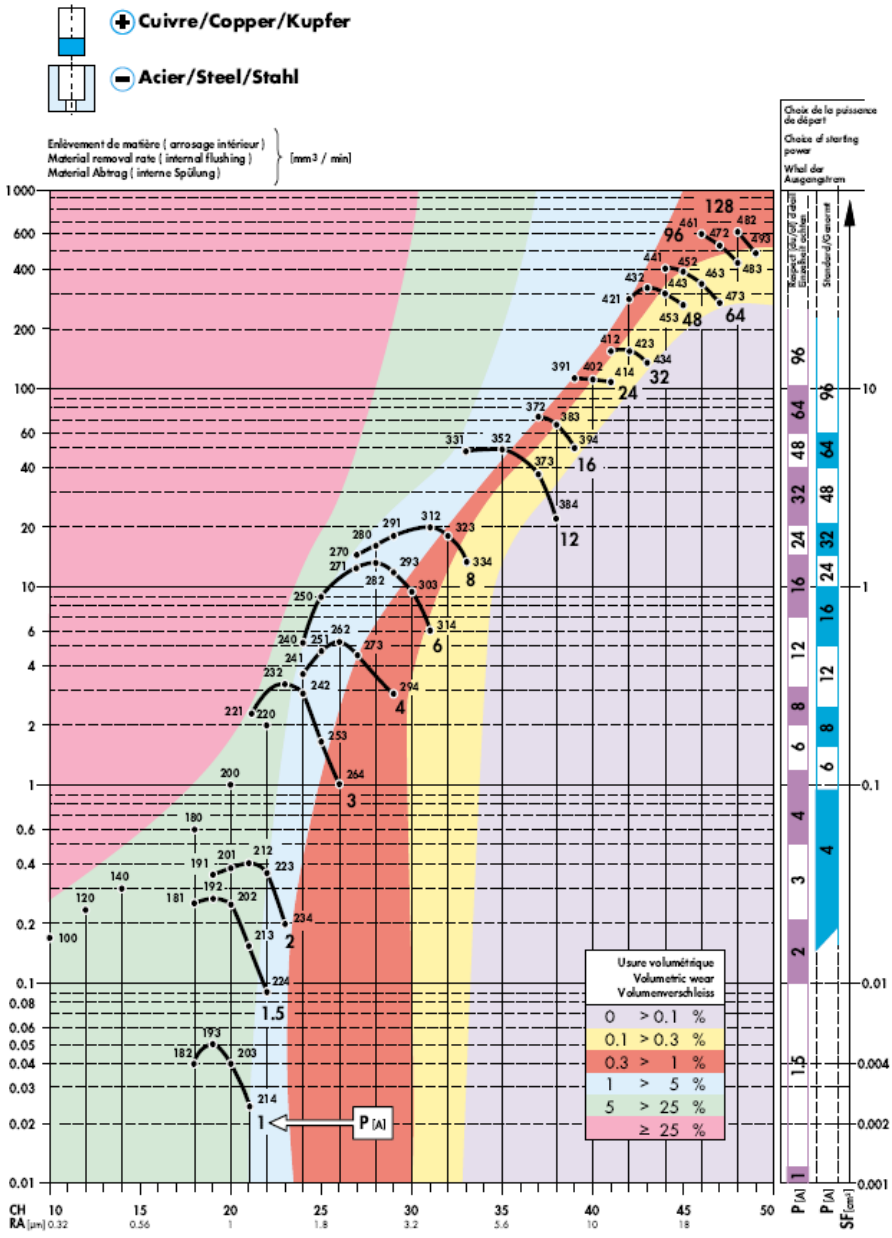

Overview of regimes and corresponding generator settings for material combination copper-steel.

Regime	i_e [A]	t_e [µs]	t_0 [µs]	SV [%]
E200	1.5	3.2	6.4	65
E220	2	6.4	6.4	65
E240	6	3.2	6.4	40
E250	6	6.4	6.4	40
E262	4	25	12.8	40
E270	8	6.4	3.2	30
E280	8	12.8	6.4	30
E293	6	50	25	40
E303	6	100	50	40
E312	8	50	25	35
E314	6	200	100	40
E323	8	100	50	35
E331	12	50	12.8	35
E334	8	200	100	35
E352	12	100	25	30
E372	16	100	25	35
E373	12	200	50	30
E383	16	200	50	30
E384	12	400	100	30
E391	24	100	50	30
E394	16	400	100	30
E402	24	200	50	30
E412	32	200	50	30
E414	24	400	100	30
E421	48	200	50	30
E423	32	400	50	30
E432	48	400	50	25
E434	32	800	100	30
E441	64	400	50	20
E443	48	800	100	25
E452	64	800	100	20
E453	48	1600	200	25
E463	64	1600	200	20

Appendix B – Pulse analysis system

In order to have a thorough understanding of the effect of certain parameters on the machining time or MRR, a pulse analysis system has been setup and elaborated in this work. By analysing the pulses the influence of certain process conditions on the debris density becomes clear. As the debris density and the amount of certain pulse types have a strong relation with the machining efficiency, a clear link with the machining speed can be established i.e. the amount of normal pulses is a measure for the machining efficiency hence machining speed.

The pulse analysis system is developed for the classification of iso-energetic pulses as these type of pulses are the most common type in sinking EDM. Three main pulse types can be distinguished in EDM applications:

- Short circuits: discharges with a very low discharge voltage u_e, nearly 0 (see Fig.B.1.c). These pulses do not contribute to the erosion process and damage both tool and workpiece.
- Arcs: discharges with a very short delay time t_d (see Fig.B.1.d) which tend to occur at the same spot on the workpiece at a high frequency.
- Normal pulses: discharges with long t_d and a moderate u_e (see Fig.B.1.a). These type of pulses are effectively contributing to the removal of material.

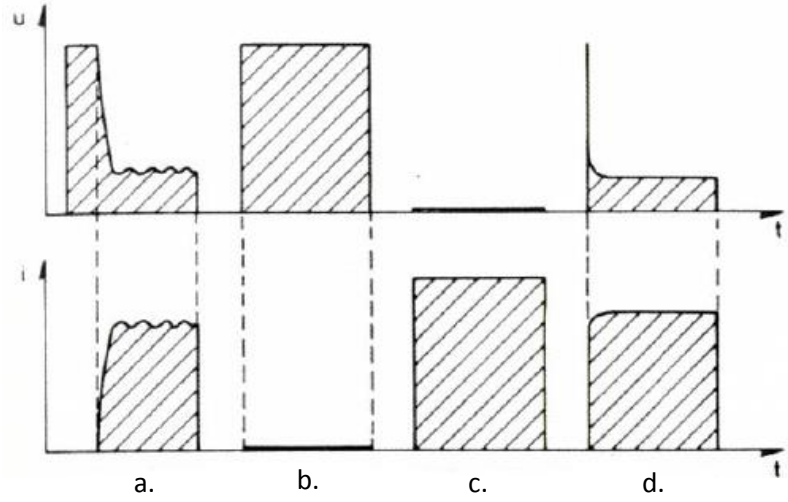

Fig. B.1: Voltage and current profiles of different pulse types.

System setup

In the developed system, the classification of pulses is based on two criteria namely the discharge delay time t_d and the average discharge voltage u_e. Input signals to the system are the gap voltage and the current signal measured during machining by means of a voltage and current probe. As the current signal is used for the detection of the beginning of the discharge, the voltage signal is used to determine u_e and serves as a measure for t_d. The delay time t_d is assessed by determining the average voltage during a time interval before the beginning of the discharge. A low average voltage reflects a short t_d whereas a high average voltage reflects a long t_d. On the other hand, the voltage signal during discharge is used to determine whether a low, normal or high voltage discharge is occurring. This is based on predefined threshold values U1, U2 and U3. A discharge with an average u_e larger than U3 is classified as a high voltage discharge. A discharge with an average u_e between U1 and U2 is defined as a low voltage discharge whereas a discharge with an average u_e between U2 and U3 is defined as a normal voltage discharge. Finally, discharges with an average u_e lower than U1 are defined as short circuits.

The classification logic is shown in Fig.B.2. This figure shows that pulses with different levels of average discharge voltage are grouped under one pulse type. Further classification regarding discharge voltage level can be done, if needed. It should also be noted that a fourth pulse type is defined for normal pulses with a shorter delay time, namely rapid discharges. As the discharge is more rapidly ignited after applying the open voltage, the presence of these type of pulses can indicate a higher debris density in the sparking gap. These pulses are not classified as arcs as these do contribute to a harmless machining operation.

The analysis and classification of the pulses is performed within LabView. The most important parameters are explained below:

- *Sampling frequency*: by default set at 20 MHz, can be extended to 50 MHz.
- *Record length*: number of data points during one measurement. This is chosen so that minimal 1500 pulses are always recorded.
- *Number of measurements*: defines the number of records that are performed during one measurement run.

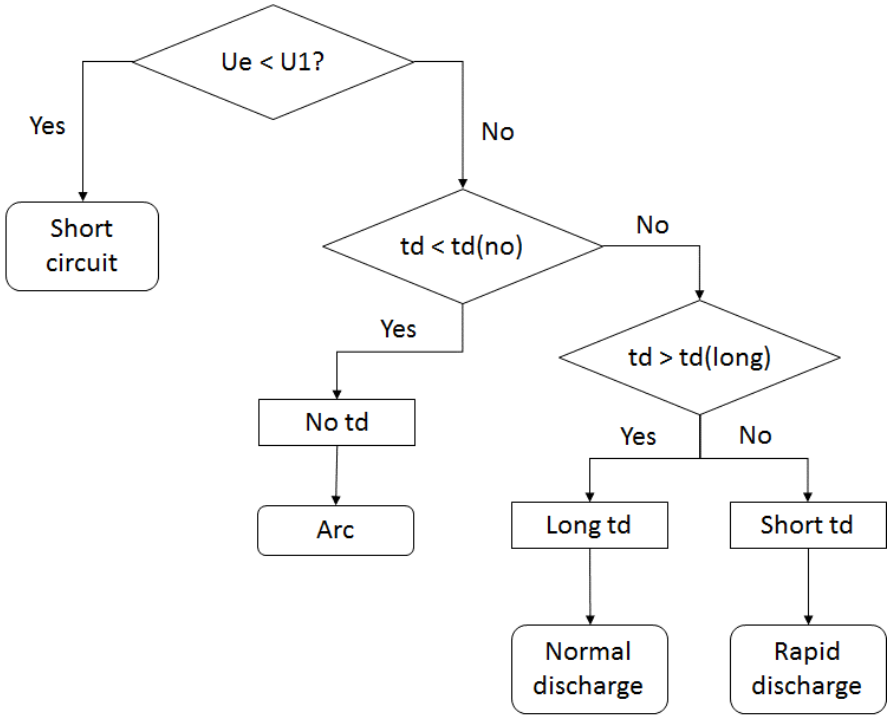

Fig. B.2. Pulse classification logic.

- *Current detection level*: crossing this current level indicates the beginning of a discharge.
- *Discharge duration:* this value is needed to determine the interval in which the average discharge voltage needs to be measured.
- *Pulse interval time:* during this interval no detection on the current value is performed.
- *Threshold values for the average discharge voltage*: these values are defined during calibration and are used to classify low, normal and high voltage level pulses and short circuits.
- *Pre-discharge interval*: period of time in which the gap voltage is measured. The average gap voltage during this period is an indication for the delay time.
- *Threshold values for the delay time*: these values are defined during calibration and are used to classify no, short and long delay times.

Measurement procedure

Prior to the actual measurement, the threshold values for the average u_e and t_d need to be determined. This is done by performing a calibration step consisting of two parts:

1. Definition of threshold values for discharge voltage. This is based on sampling of the average u_e during stable machining. For each pulse the average u_e is plotted. The major part of the data points should be between U2 and U3 as these reflect normal conditions. Points above U3 are classified as high voltage discharges whereas points between U1 and U2 are classified as low voltage discharges. U1 is used to differentiate short circuits from low voltage discharges.

2. Definition of threshold values for t_d. This is based on pulse images obtained with a small record length during different machining conditions and the corresponding average gap voltage in the period prior to the discharge. A low average gap voltage reflects a short t_d whereas a high average gap voltage reflects a long t_d. If the average gap voltage drops below a certain minimal value, this is an indication for short circuits.

The calibration procedure is performed for each generator regime.

During the actual measurement run several consecutive measurements are performed to have a solid base for the assessment of the machining conditions. Fig.B.3 shows a visualization of the systems output. The raw data is saved in a text file with the number of pulse arranged per pulse type. This text file serves for further analysis in for example Excel®.

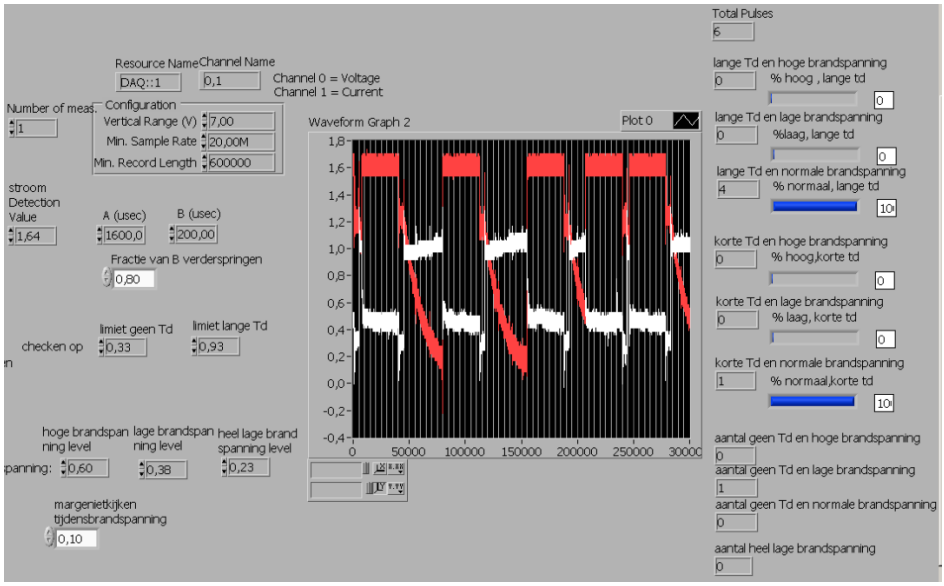

Fig. B.3: Visualization of pulse classification output.

Appendix C – Validation cases

1. Basis set roughing operation

For all listed cases 20 data points along the machining depth have been obtained.

#	Roughing regime	Frontal surfac e area per protrusion [mm²]	Number of protrusions	Current density [A/cm²]
1	E303	25	1	10
2	E303	50	1	4,8
3	E323	25	1	13,9
4	E323	50	1	7,6
5	E323	100	1	3,5
6	E373	25	1	28
7	E373	50	1	13,4
8	E373	100	1	6,7
9	E383	50	1	17,9
10	E383	100	2	4,5
11	E394	50	1	17,9
12	E394	100	2	4,5
13	E394	200	1	4,5
14	E414	50	6	4,5
15	E414	100	3	4,5
16	E414	100	2	6,7
17	E414	100	1	13,4
18	E414	150	2	4,5
19	E414	200	1	6,7
20	E414	300	1	4,5
21	E434	100	1	20
22	E434	100	2	10
23	E434	200	1	10
24	E434	200	2	5
25	E434	300	1	6,7
26	E453	50	6	10,7
27	E453	100	3	10,7
28	E453	100	2	16
29	E453	100	1	32
30	E453	150	2	10,7
31	E453	200	1	16
32	E453	300	1	10,7

2. Validation set roughing operation

For all listed cases 20 data points along the machining depth have been obtained.

Within model boundaries

#	Roughing regime	Frontal surfac e area per protrusion [mm²]	Number of protrusions	Current density [A/cm²]
1	E303	37	1	6,5
2	E373	75	1	4,5
3	E383	200	2	4,5
4	E434	300	1	6,7
5	E453	400	1	8
6	E463	200	1	22,8
7	E463	400	1	11,4

Outside model boundaries

#	Roughing regime	Frontal surfac e area per protrusion [mm²]	Number of protrusions	Current density [A/cm²]
8	E303	100	1	2,4
9	E303	300	1	0,8
10	E323	300	1	1,2
11	E373	200	1	3,3
12	E463	800	1	5,7

3. Validation set finishing operation

#	Finishing regime	Machining length [µm]	Total surface area [mm²]	Geometry
1	E200	20	750	Rectangular
2	E200	20	900	Rectangular
3	E200	60	1100	Rectangular
4	E220	60	1250	Rectangular
5	E220	20	750	Rectangular
6	E220	20	900	Rectangular
7	E240	60	1100	Rectangular
8	E240	60	1250	Rectangular
9	E240	20	750	Rectangular
10	E200	20	900	Rectangular
11	E200	60	1100	Rectangular
12	E200	60	1250	Rectangular
13	E220	20	750	Rectangular
14	E220	20	900	Rectangular
15	E220	60	1100	Rectangular
16	E240	60	1250	Rectangular
17	E240	20	750	Rectangular
18	E240	20	900	Rectangular
19	E200	60	1100	Rectangular
20	E200	60	1250	Rectangular
21	E200	20	750	Rectangular
22	E220	20	900	Rectangular
23	E220	60	1100	Rectangular
24	E220	60	1250	Rectangular
25	E240	20	750	Rib
26	E240	20	900	Rib
27	E240	60	1100	Rib
28	E200	60	1250	Rib
29	E200	20	750	Rib
30	E200	20	900	Rib
31	E220	60	1100	Rib
32	E220	60	1250	Rib
33	E220	20	750	Rib
34	E240	20	900	Rib
35	E240	60	1100	Rib
36	E240	60	1250	Rib

#	Finishing regime	Machining length [µm]	Total surface area [mm²]	Geometry
37	E200	20	750	Rib
38	E200	20	900	Rib
39	E200	60	1100	Rib
40	E220	60	1250	Rib
41	E220	20	750	Rib
42	E220	20	900	Rib
43	E240	60	1100	Rib
44	E240	60	1250	Rib
45	E240	20	750	Rib
46	E200	20	900	Rib
47	E200	60	1100	Rib
48	E200	60	1250	Rib
49	E220	20	750	Cylindrical
50	E220	20	900	Cylindrical
51	E220	60	1100	Cylindrical
52	E240	60	1250	Cylindrical
53	E240	20	750	Cylindrical
54	E240	20	900	Cylindrical
55	E200	60	1100	Cylindrical
56	E200	60	1250	Cylindrical
57	E200	20	750	Cylindrical
58	E220	20	900	Cylindrical
59	E220	60	1100	Cylindrical
60	E220	60	1250	Cylindrical
61	E240	20	750	Cylindrical
62	E240	20	900	Cylindrical
63	E240	60	1100	Cylindrical
64	E200	60	1250	Cylindrical
65	E200	20	750	Cylindrical
66	E200	20	900	Cylindrical
67	E220	60	1100	Cylindrical
68	E220	60	1250	Cylindrical
69	E220	20	750	Cylindrical
70	E240	20	900	Cylindrical
71	E240	60	1100	Cylindrical
72	E240	60	1250	Cylindrical

List of publications

W. Vanderauwera, B. Lauwers; Time Estimation for Sinking EDM Operations; Proceedings of the 16th International Symposium on Electro-Machining; 2010; p. 41-46.

B. Lauwers, H. Oosterling, W. Vanderauwera; Development of an Operations Evaluation System for Sinking EDM; CIRP Annals - Manufacturing Technology; 2010; Vol. 59; Issue 1; p. 223-226.

B. Lauwers, W. Vanderauwera, D. Plakhotnik, Y. Guo; Manufacturing Education and Research at KULeuven using a Mori Seiki NL2000Y/500 Mill-turn Centre; Proceedings of MTTRF 2011 Meeting; 2011; p. 139-156.

W. Vanderauwera, M. Garzon, T. Aerts, F. Klocke, B. Lauwers; Comparison of Micro-milling and Micro-EDM Operations; Proceedings of the 8th International Conference on Multi-Material Micro Manufacture, 2011; p. 285-289.

W. Vanderauwera, M. Vanloffelt, R. Perez, B. Lauwers; Investigation on the Performance of Macro Electrochemical Milling; Proceedings of the 17th International Symposium on Electro-Machining; 2013; p. 356–361.

O. Malek, J. González-Julián, J.Vleugels, W. Vanderauwera, B. Lauwers, M. Belmonte; Carbon Nanofillers for Machining Insulating Ceramics; Materials Today; 2011; Vol. 14; Issue 10; p. 496-501.